

Aus dem Bereich Physiologie
Theoretische Medizin und Biowissenschaften
der Medizinischen Fakultät
der Universität des Saarlandes, Homburg/Saar

**Oligodendrocyte progenitor cells shape the cortical inhibition
employing GABA_B receptors**

Dissertation

zur Erlangung des Grades eines Doktors der Naturwissenschaften

**der Medizinischen Fakultät
der Universität des Saarlandes**

2023

vorgelegt von: Lipao Fang

geb. am: 05. September.1992 in WenZhou, China

Date of oral examination: 19. December 2023

Dean of the faculty: **Prof. Dr. M. D. Menger**

Examinants: **Prof. F. Kirchhoff**

Prof. F. Schmitz

Prof. D. Hermann

This project has received funding from HOMFORexcellent Programm (2018-2021) and NanoBioMed Young Investigator Grant (2021-2024) of Saarland University.

Content

List of abbreviations	IV
List of figures	VI
List of tables	VIII
1. ABSTRACT	1
2. GRAPHICAL ABSTRACT	2
3. ZUSAMMENFASSUNG	3
4. INTRODUCTION	5
4.1 Cortical inhibition.....	5
4.2 Oligodendrocyte precursor cells.....	7
4.3 Interneuron-OPC communication.....	8
5. AIM OF THE STUDY	11
6. RESULTS	12
6.1 Successful deletion of GABA _B Rs in OPCs	12
6.2 GABA _B Rs of OPCs are essential for oligodendrogenesis in the cortex but not in the corpus callosum	13
6.3 GABA _B Rs of OPCs are pivotal for myelination in mPFC but not in MOp and corpus callosum.....	15
6.4 Conditional deletion of GABA _B Rs in mature oligodendrocytes do not affect oligodendrogenesis and myelination.....	18
6.5 Interneuron myelination deficits in cKO-mPFC.....	19
6.6 Attenuated inhibitory tone in cKO mPFC	21
6.6.1 Decreased interneuron activity in cKO mPFC during development.....	22
6.6.2 Less GABAergic-input to OPCs in cKO mPFC	23
6.7 Decreased OPC differentiation follows attenuated interneuron activity in the cKO-mPFC during development.....	24
6.7.1 Early deletion of GABA _B R in OPC affect myelination	24
6.7.2 Late deletion of GABA _B R in OPC do not affect myelination.....	26
6.8 Surplus PV interneurons present in cKO-mPFC.....	28
6.9 OPC-GABA _B R promote interneuron apoptosis	28
6.9.1 Interneuron apoptosis is attenuated in cKO-mPFC	28
6.9.2 OPC promotes interneuron apoptosis via TWEAK-GABA _B R signaling	30

6.10 Interrupted OPC-interneuron communication generates cognitive impairment	32
6.10.1 Gamma oscillations are altered by GABA _B R deletion in OPCs	32
6.10.2 Impaired short-term memory in mutant mice	32
6.10.3 Alteration of social novelty in mutant mice	34
7. DISCUSSION	36
7.1 Selective interneuron apoptosis induced by OPC-derived TWEAK	36
7.2 Attenuated cortical inhibition in mutant mice	37
7.2.1 Potential morphological change of PV interneurons in mutant mice	37
7.2.2 The interneurons myelin structure is altered in mutant mice	37
7.3 In OPCs the GABA _B R serves different functions in comparison to the GABA _A R	37
7.4 OPCs are the multitasker in brain function	38
7.5 The E/I imbalance in mPFC with cognition impairments	40
8. CONCLUSION	41
9. Materials and Methods	42
9.1 Materials	42
9.1.1 Reagents	42
9.1.2 Consumables	42
9.1.3 Kits	42
9.1.4 Devices	43
9.1.5 Antibodies	44
9.1.6 Primers	46
9.2 Animals	47
9.2.1 Ethics statement	47
9.2.2 Transgenic mice	47
9.3 Methods	48
9.3.1 Genotyping	48
9.3.2 Tamoxifen administration	48
9.3.3 Mouse perfusion	48
9.3.4 Immunohistochemistry	48
9.3.5 Bromodeoxyuridine assay	49
9.3.6 Magnetic-activated cell sorting (MACS) of OPCs	49
9.3.7 Western blot analysis	50
9.3.8 Quantitative real time PCR	50
9.3.9 Electrophysiology	51
9.3.10 EEG Telemetry and Analysis	53
9.3.11 Behavioral analysis	53
9.3.11.1 Nest building test	53

9.3.11.2 Open field test.....	53
9.3.11.3 New object recognition test.....	54
9.3.12 Cell culture	54
9.3.13 Image acquisition and analysis	55
9.3.14 Electron microscopy	55
9.4 Statistics	56
10. APPENDIX	57
11. REFERENCE	97
12. ACKNOWLEDGEMENT.....	104
13. CURRICULUM VITAE AND LIST OF PUBLICATIONS.....	105

Comments of thesis organization

Chapters 1-9 describe the main work during my PhD period, which has been published as one original article and one review. Chapter 10 (Appendix) presents four publications (two original study, one perspective and one review) related to this project.

List of abbreviations

ACSF	artificial cerebral spinal fluid
ANOVA	analysis of variance
APC	adenomatous polyposis coli
BAC	bacterial artificial chromosome
BrdU	bromodeoxyuridine
BSA	bovine serum albumin
cc	corpus callosum
CC1	adenomatous polyposis coli (APC) clone 1
CC-3	cleaved caspase-3
cKO	conditional knockout
CGE	caudal ganglionic eminence
CNS	central nervous system
CSPG-4	chondroitin sulfate proteoglycan 4
CTX	cortex
ctl	control
DNA	deoxyribonucleic acid
ECM	extracellular matrix
EEG	electroencephalography
FasL	Fas ligand
Fig	figure
GAD 67	glutamate decarboxylase 67
GFAP	glial fibrillary acidic protein
GFP	green fluorescent protein
HRP	horseradish peroxidase
IL	infralimbic
4-HT	4-OH tamoxifen
kb	kilo base pairs
kDa	Kilodalton
LGE	lateral ganglionic eminence
m	month
MOG	myelin oligodendrocyte glycoprotein
MOp	primary motor cortex
mPFC	medial prefrontal cortex
MACS	magnetic activated cell sorting
2-ME	β -mercaptoethanol
MBP	myelin basic protein
MGE	medial ganglionic eminence
n	number
NG2	nerve/glia antigen-2

NGF	Nerve Growth Factor
n.s.	not significant
OL	oligodendrocyte
OPC	oligodendrocyte precursor cell
p5	postnatal day 5
p7	postnatal day 7
p10	postnatal day 10
p14	postnatal day 14
PB	sodium phosphate buffer
PBS	phosphate buffered saline
PBS-T	PBS-tween-20
PCR	polymerase chain reaction
PDGFR	platelet-derived growth factor receptor
PLP	proteolipid protein
PL	prelimbic
pMN	motoneuron precursor domain
PV	parvalbumin
RT	room temperature
SDS	sodium dodecyl sulfate
SDS-PAGE	SDS-polyacrylamide gel electrophoresis
sEPSCs	spontaneous excitatory postsynaptic currents
SEM	standard error of the mean
sIPSC	spontaneous inhibitory postsynaptic current
TBR1	T-box brain transcription factor 1
TBST	TBS-tween-20
tdT	tdTomato
TgH	transgenic by homologous recombination
TgN	transgenic by non-homologous recombination
TNF	Tumor necrosis factor
TNF- α	Tumor necrosis factor alpha
TNFSF7	CD27 Ligand
Trp-53	Transformation related protein 53
TTX	tetrodotoxin
TWEAK	TNF-related weak inducer of apoptosis
WB	Western Blot
vGAT	vesicular GABA transporter

List of figures

Figure 1. Scheme of cortical interneuron apoptosis during development.	6
Figure 2. The morphology of oligodendrocyte precursor cells in white and grey matter.....	7
Figure 3. Scheme of the oligodendrocyte lineage progression.....	8
Figure 4. Onset of myelin generation at p12 in mPFC.....	8
Figure 5. The communication of OPC-Interneuron during development.....	9
Figure 6. The <i>Gabbr1</i> gene (GABA _B R subunit 1) is mainly expressed in astrocytes, OPCs and neurons.....	10
Figure 7. Conditional deletion of GABA _B R in cortical OPCs.	12
Figure 8. Alteration in oligodendrogenesis in mutant mice.	13
Figure 9. Oligodendrogenesis is slightly reduced in the primary motor cortex of cKO mice...	14
Figure 10. The densities of OPCs and oligodendrocytes are not altered in the corpus callosum of mutant mice.	15
Figure 11. GABA _B Rs of OPCs are pivotal for myelination in mPFC.....	16
Figure 12. Paranodal structures are altered in the cKO-mPFC.	17
Figure 13. Myelination remains unaltered in the cKO-corporum callosum.	18
Figure 14. Deletion of GABA _B R in oligodendrocytes does not alter the oligodendrogenesis or myelin formation in the mPFC and corpus callosum. .	19
Figure 15. Parvalbumin interneurons are abundant in MOp and mPFC.	20
Figure 16. Interneuron myelination deficits in cKO-mPFC.....	21
Figure 17. Attenuated inhibitory tone in cKO mPFC.....	22
Figure 18. GABAergic currents of OPCs are reduced by GABA _B R deletion.	24
Figure 19. Early deletion of GABA _B R in OPC affects myelination.....	25
Figure 20. Ablation of GABA _B R from OPCs does not affect apoptosis of oligodendrocytes...	26
Figure 21. GABA _B R expression of OPC reaches a plateau at 4 weeks age.	26
Figure 22. Late-phase deficiency of GABA _B R in OPCs (at 4 week of age) do not affect oligodendrogenesis.....	27
Figure 23. Surplus PV interneurons are found in the cKO-grey matter.	28
Figure 24. Interneuron apoptosis is attenuated in cKO-mPFC.	29

Figure 25. Cell death and survival of excitatory neurons are not affected by early ablation of OPC-GABA _B R	30
Figure 26. OPCs promote interneuron apoptosis via TWEAK-GABA _B R signaling.	31
Figure 27. OPC-GABA _B cKO mice exhibited altered EEGs.....	32
Figure 28. Gamma oscillations are altered by GABA _B R deletion in OPCs.....	33
Figure 29. Impaired short-term memory in mutant mice.....	33
Figure 30. Impaired social novelty in mutant mice.	34
Figure 31. No alteration of motor ability in mutant mice	35
Figure 32. OPCs are the multitaskers during brain function.	39
Figure 33. Procedure of magnetic-activated cell sorting of OPC.	49

List of tables

Table 1: Devices	43
Table 2: Primary antibodies for immunohistochemistry	44
Table 3: Secondary antibodies for immunohistochemistry.....	45
Table 4: Primary antibodies for Western blot.....	46
Table 5: Primers for genotyping	46
Table 6: Primer for qRT-PCR	46
Table 7: Mouse lines	47
Table 8: Primers for qRT-PCR	51

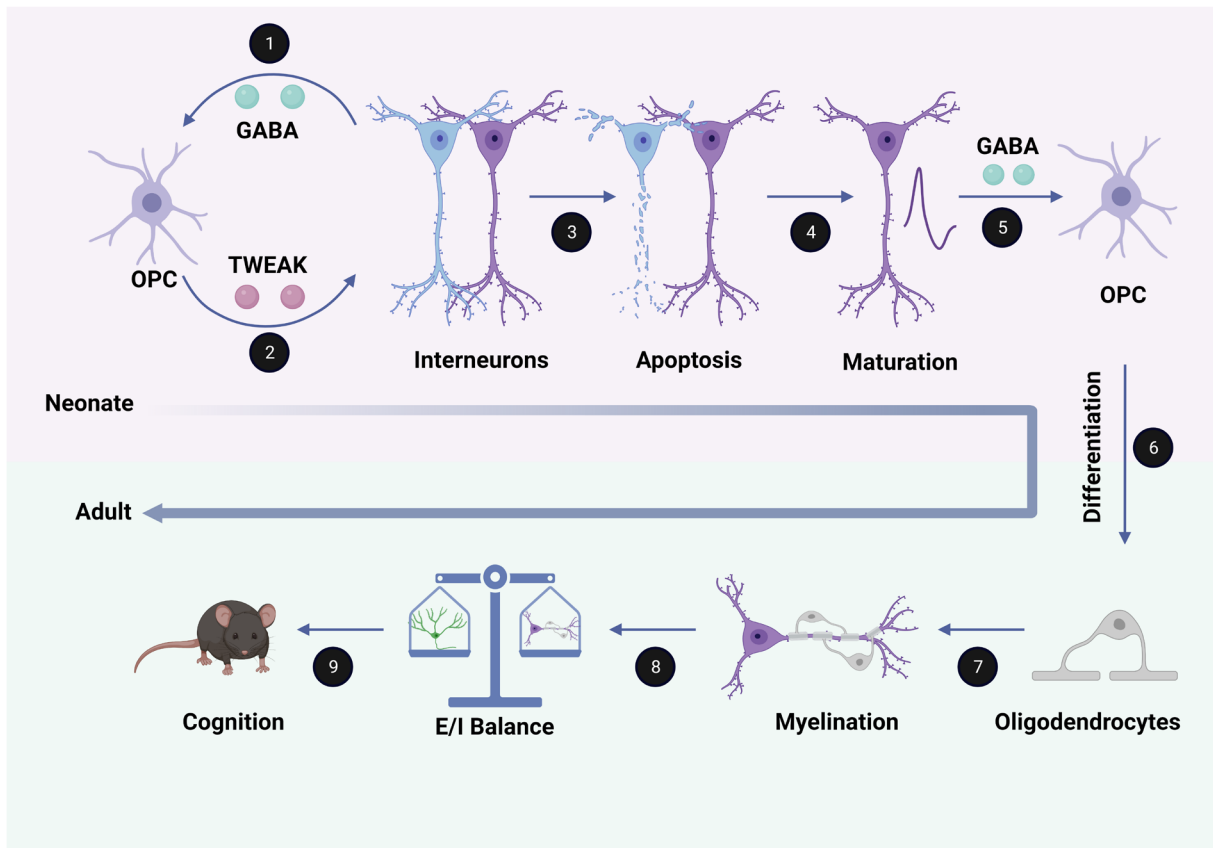
1. Abstract

The myelination of cortical inhibitory neurons plays a crucial role in facilitating fast and precise transmission of action potentials, which ultimately fine-tunes the activity of cortical circuits. The differentiation of oligodendrocyte precursor cells (OPCs) into oligodendrocytes, which myelinate interneurons, is regulated by GABAergic signaling from interneurons to OPCs.

To investigate the role of OPC GABA_B receptors in this process, we generated conditional knockout (cKO) of GABA_B receptors subunit 1 (GABA_{B1}R) specifically in OPCs and their descendants using NG2-CreERT2 knock-in mice and GABA_{B1}R floxed mice. We induced cKO at postnatal days 7 and 8, and analyzed the medial prefrontal cortex (mPFC) at 9 weeks of age. In the mPFC of cKO mice, we observed a reduction in OPC differentiation, decreased expression of myelin basic protein (MBP), and changes in paranodal loops. Double immunostaining of parvalbumin (PV) and MBP showed that hypomyelination predominantly occurred in PV interneurons. Additionally, we detected reduced levels of the vesicular GABA transporter (vGAT) in postnatal mice and attenuated spontaneous inhibitory postsynaptic currents (sIPSCs) in young adult mice, as well as reduced GABAergic current in OPCs, indicating that GABA_B receptor-deficient OPCs received significantly less GABAergic input and their differentiation was suppressed. Our data also revealed an overpopulation of PV neurons in the mutant mPFC of adult mice. Further analysis of interneuron programmed cell death during development showed that OPCs release TWEAK (Apo3I), a weak apoptotic factor of the TNF superfamily, which contributes to the removal of surplus interneurons in the normal central nervous system (CNS) development. Our results suggest that interneuron-OPC signaling via GABA_B receptors is crucial for regulating TWEAK and is essential for interneuron myelination and network function in the mPFC. Lastly, a subsequent behavioral analysis revealed significant impairments in social cognitive behavior in the cKO mice.

In conclusion, our findings reveal a bidirectional communication pathway between interneurons and OPCs, where OPCs sense GABA through GABA_B receptors and release TWEAK to optimize interneuron population and function, which is vital for interneuron myelination and network function in the mPFC.

2. GRAPHICAL ABSTRACT



3. ZUSAMMENFASSUNG

Die Myelinisierung kortikaler hemmender Neuronen spielt eine entscheidende Rolle bei der schnellen und präzisen Übertragung von Aktionspotentialen, die letztendlich die Aktivität kortikaler Schaltkreise feinabstimmen. Die Differenzierung von Oligodendrozyten-Vorläuferzellen (OPCs) zu Oligodendrozyten, die die Interneuronen myelinisieren, wird durch GABAerge Signalgebung von Interneuronen zu OPCs reguliert.

Um die Rolle von GABA_B-Rezeptoren in diesem Prozess zu untersuchen, erzeugten wir konditionelle Knockouts (cKO) von GABA_B-Rezeptor-Untereinheit 1 (GABA_{B1}R) spezifisch in OPCs und deren Nachkommen unter Verwendung von NG2-CreERT2-Knock-in-Mäusen und GABA_{B1}R-Flox-Mäusen. Wir induzierten das cKO an postnatalen Tagen 7 und 8 und analysierten den medialen präfrontalen Cortex (mPFC) im Alter von 9 Wochen. Im mPFC von cKO-Mäusen beobachteten wir eine Verringerung der OPC-Differenzierung, eine verminderte Expression des Myelin Basic Protein (MBP) und Veränderungen in den paranodalen Anteilen der Ranvierschen Schnürringe. Eine Doppel-Immunfärbung von Parvalbumin (PV) und MBP zeigte, dass die Hypomyelinisierung vorwiegend in PV-Interneuronen auftrat. Zusätzlich konnten wir reduzierte Mengen des vesikulären GABA-Transporters (vGAT) bei postnatalen Mäusen und abgeschwächte spontane inhibitorische postsynaptische Ströme (sIPSCs) bei jungen erwachsenen Mäusen sowie reduzierte GABAerge Ströme in OPCs nachweisen, was darauf hindeutet, dass GABA_B-Rezeptor-defiziente OPCs signifikant weniger GABAergen Input erhielten und ihre Differenzierung unterdrückt wurde. Unsere Daten zeigten auch eine Überpopulation von PV-Neuronen im mutierten mPFC adulter Mäuse. Eine weitere Analyse des programmierten Zelltods von Interneuronen während der Entwicklung zeigte, dass OPCs TWEAK (Apo3l), einen schwachen apoptotischen Faktor der TNF-Superfamilie, freisetzen, der zur Beseitigung überschüssiger Interneuronen bei der normalen Entwicklung des Zentralnervensystems beiträgt. Unsere Ergebnisse legen nahe, dass die Signalgebung zwischen Interneuronen und OPCs über GABA_B-Rezeptoren entscheidend für die Regulation von TWEAK ist und für die Myelinisierung und Netzwerkfunktion von Interneuronen im mPFC unerlässlich ist. Schließlich zeigte eine nachfolgende Verhaltensanalyse signifikante Beeinträchtigungen des sozialen kognitiven Verhaltens bei den cKO-Mäusen.

Zusammenfassend zeigen unsere Ergebnisse einen bidirektionalen Kommunikationsweg zwischen Interneuronen und OPCs, bei dem OPCs GABA über GABA_B-Rezeptoren wahrnehmen und TWEAK freisetzen

ZUSAMMENFASSUNG

4. INTRODUCTION

Cognitive impairment is a condition where a person experiences difficulty in remembering, learning new things, concentrating, or making decisions (Morley 2018). In Europe, about 6 - 8 % of the population suffer from cognitive impairment per year (Pais et al. 2020). Recently, the COVID-19 pandemic has further increased this number (Soysal et al. 2022), as the SARS-CoV-2 patients with severe symptoms experience cognitive issues, especially in memory and attention, even after their recovery (Daroische et al. 2021). Cognitive impairment limits one's independency by making even the easiest daily task arduous and challenging (Eshkoo et al. 2015). However, the cellular and molecular mechanisms involved in cognitive impairment are still far from being understood.

In mammals, the prefrontal cortex (PFC) is responsible for cognition by orchestrating thoughts and actions, highly relying on the exquisite activity of neural circuits and balanced excitation and inhibition (E/I balance) (Arnsten 2009). Disrupting the E/I balance induces brain dysfunctions, e.g., cognitive deficits. Many neuropsychiatric disorders including schizophrenia and autism are accompanied with an E/I imbalance (Sohal and Rubenstein 2019). Intriguingly, the major cause of E/I imbalance is often attributed to the disorder in inhibitory circuits.

4.1 Cortical inhibition

γ -aminobutyric acid (GABA) is the main inhibitory neurotransmitter in the forebrain (Meldrum 1982). GABA exerts inhibition by acting on ionotropic GABA A receptors and metabotropic GABA B receptors which induces hyperpolarization of the cells. In the brain, the major cellular source of GABA is inhibitory neurons. Hence, correct cell density, firing activity and myelination of inhibitory neurons are critical for the inhibition. GABA is mainly synthesized from glutamate by glutamate decarboxylase 65 and 67 (GAD65 and GAD67) (Pinal and Tobin 1998; Deidda, Bozarth, and Cancedda 2014). Therefore, GAD65 and GAD67 are often used as markers of inhibitory neurons.

Cortical inhibitory neurons are also called as interneurons since they act as 'intermediaries' between two target neurons. The heterogeneity of cortical interneurons is manifested in their distinct synaptic connections, firing properties and molecular marker expressions. The majority of cortical interneurons can be categorized into three subgroups based on the expression of calcium-binding proteins: ionotropic 5-hydroxytryptamine receptor (5-HT receptors), neuropeptide somatostatin (SST) and parvalbumin (PV) (Hu, Gan, and Jonas 2014). In neocortex, PV interneurons count for up-to 40-50 % of all interneurons and exhibit a distinctive fast-spiking electrophysiological properties. PV neurons can be further classified into basket and chandelier cells based on their morphology (Klausberger and Somogyi 2008; Gonchar, Wang, and Burkhalter 2007). Both subtype PV interneurons extensively integrate into local circuits by targeting excitatory neurons in soma/proximal dendrites and axon initial segment, respectively (Freund and Buzsaki 1996).

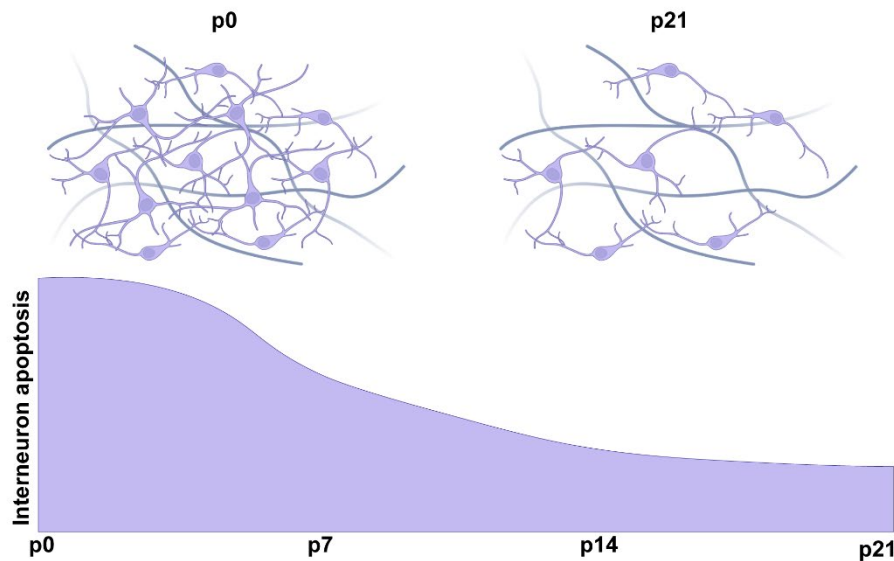


Figure 1. Scheme of cortical interneuron apoptosis during development.

Surplus cortical interneurons are generated during development, but eliminated through apoptosis at the first two postnatal weeks. Compare to p0, around 20-40 % of interneurons are eliminated through apoptosis (Priya et al. 2018; Wong et al. 2018; Southwell et al. 2012; Velez-Fort et al. 2010).

Developmentally, super numerous interneurons are generated from the subpallial region (the medial and caudal ganglionic eminences (MGE-CGE) and the preoptic area (POA)), and migrate to the dorsal cortex (Tricoire et al. 2011). Subsequently, 20-40 % interneurons are eliminated through apoptosis during the first two postnatal weeks (Figure. 1) (Priya et al. 2018; Wong et al. 2018; Southwell et al. 2012). It should be noted that interneurons with higher activity are prone to survive than those with lower activities (Wong et al. 2018). The activity of interneuron is highly dependent on their target cells, such as pyramidal neurons or glial cells, with which they form connection and receive the neurotrophic signals (Davies 2003; Mercau et al. 2022). After determination of proper density by apoptosis, interneurons gradually mature and subsequently integrate into the local neural circuit. When the interneuron apoptosis is intervened, the local inhibition alters (Orduz et al. 2019; Wang et al. 2021). Abnormal density as well as altered firing activity of interneurons are frequently observed in neuropsychiatric disorders (Orduz et al. 2019; Lin et al. 2021). Therefore, proper density and activity of interneurons are crucial for precise function of inhibitory circuits.

Myelination is a vital event for the brain function as myelin optimizes the propagation of action potentials and supplies energy to the neurons (Fields 2015; Saab et al. 2016). Myelination of excitatory neurons is extensively studied, while the mechanism of interneuron myelination is just starting to emerge. Myelination of interneurons was first reported in the visual cortex of cat more than 35 years ago, but it had gone unnoticed for decades (Somogyi and Soltesz 1986). Till 2016, Micheva et al. has described that a substantial amount of myelin wrapping inhibitory axons in mouse cerebral cortex, reaching even beyond 80 % in hippocampal area (Micheva et al. 2016). Of note, most myelinated interneurons are PV interneurons (Stedehouder et al. 2017). PV interneurons with proper myelin sheath guarantee a suitable inhibitory circuit (Dubey et al. 2022), while deficits in PV interneuron myelination disrupts the E/I balance (Benamer et

al. 2020). Thus, interneuron myelination, especially of PV interneurons could be a putative target for refining inhibitory circuit in the brain.

4.2 Oligodendrocyte precursor cells

In the central nervous system (CNS), myelin is exclusively formed by oligodendrocyte, which is generated from their precursors, oligodendrocyte precursor cells (OPCs). The fate-mapping studies showed that OPCs in the mouse forebrain originate from three successive streams of progenitor cells that begin in the ventral region and then shift to a dorsal region in the second and third waves of OPCs: the first wave arises from $Nkx2.1^+$ medial ganglion cells (MGEs) at E12.5; the second wave of OPCs originate from the $Gsx2^+$ lateral and caudal ganglion cells (LGE/CGE) around E15.5; the final wave of OPCs arises from the $Emx1^+$ dorsal cortical ventricular zone after birth (Ong and Levine 1999; Bergles et al. 2000; Zawadzka et al. 2010; Tabata 2015). Due to their specific expression of NG2 (chondroitin sulfate 4, *cspg4*) and PDGFR α protein (platelet-derived growth factor receptor α), NG2 and PDGFR α is often used as cell specific marker and *cspg4* and *pdgfra* for cell specific gene editing.

OPCs constitute about 5-8 % of the brain cell population and ubiquitously tile the brain parenchyma sharing only about 5 % of their territories. Morphologically, OPCs are characterized by small cell bodies, approximately 10-15 μm in diameter, and multiple processes with several levels of branches. The processes of OPCs tend to be radially oriented in the grey matter (Figure. 2) (Levine, Reynolds, and Fawcett 2001; Sakry and Trotter 2016; Ong and Levine 1999), while more elongated in the white matter (Figure. 2) (Butt et al. 1999). Nevertheless, in both grey and white matter, the processes consist of lamellipodia and filopodia, and numerous OPC processes are in contact with the nodes of Ranvier (Fernandez-Castaneda and Gaultier 2016) and presynapse (Kukley et al. 2008), suggesting a close contact of OPCs with neurons.

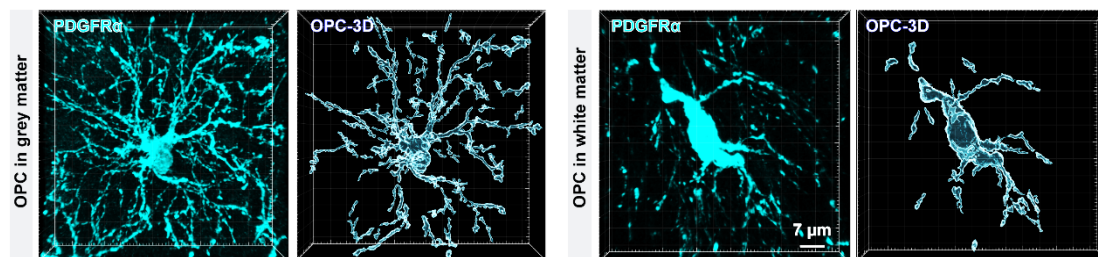


Figure 2. The morphology of oligodendrocyte precursor cell in white and grey matter.

Immunostaining of oligodendrocyte precursor cells (OPCs) specific marker (PDGFR α) in gray matter (cortex, right) and white matter (corpus callosum, left).

During development, OPCs differentiate into oligodendrocytes, which are responsible for myelin generation. Oligodendrogenesis is a process of gradual differentiation through three stages: OPCs initially yield pre-myelinating oligodendrocytes, followed by a further differentiation into myelinating oligodendrocytes (Hughes and Stockton 2021). Throughout the processes, *Olig2* and *Sox10* are constantly expressed, thereby they are often used as the markers of oligodendrocyte lineage cells (Figure. 3).

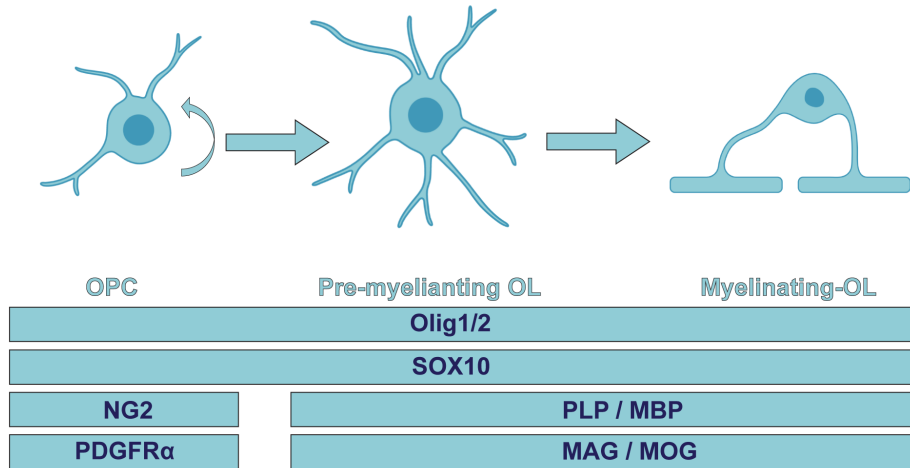


Figure 3. Scheme of the oligodendrocyte lineage progression.

Three stages of oligodendrocyte lineage cells. OPCs are proliferative and express NG2 and PDGFR α . OPCs differentiate into pre-myelinating oligodendrocytes (OL) that subsequently become myelin forming OLs. Both pre-myelinating OLs and myelin forming OLs express myelin associated proteins, including PLP, MBP, MAG and MOG. Transcription factor Sox10 and Olig1/2 are expressed throughout the lineage (Hughes and Stockton 2021).

Cortical oligodendrocytes are generated already from the first postnatal week and their density reaches peak around 90 weeks after birth in mouse brain (Trapp et al. 1997; Baracskey et al. 2002; Hill, Li, and Grutzendler 2018; Orduz et al. 2015). Likewise, myelination is initiated from p12 in mPFC (Figure. 4).

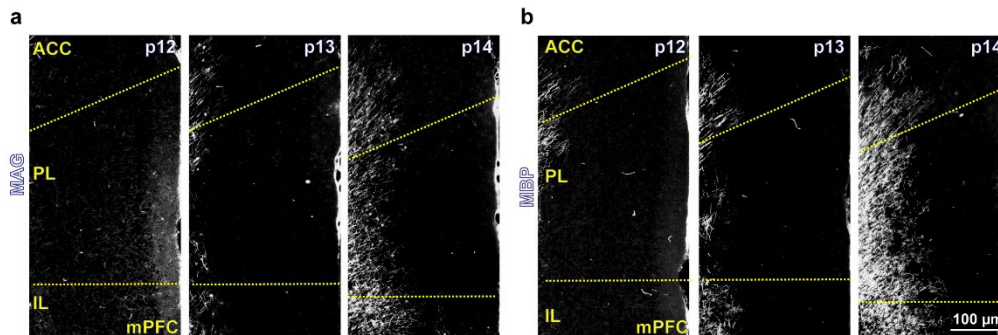


Figure 4. Onset of myelin generation at p12 in mPFC.

a b Immunostaining of MBP (myelin basic protein) and MOG (myelin oligodendrocyte glycoprotein) at the onset of myelination in mPFC of c57bl/6 mice.

4.3 Interneuron-OPC communication

OPCs are the unique glial cell type forming direct synapses with neurons. In 2004, the group of Dwight Bergles first described that OPCs innervate the synaptic inputs from interneurons in the hippocampus (Lin and Bergles 2004). Subsequently, successive articles reported the existence of interneuron-OPC synapses in cortex and cerebellum (Velez-Fort et al. 2010; Zonouzi et al. 2015). In the cortex, synapses between interneurons and OPCs are formed

around p4 - p5 (Figure. 5) and this connection peaks at p10 (Velez-Fort et al. 2010). Interestingly, the incidence of interneuron apoptosis increases from p5 and stays at high level till p11 (Southwell et al. 2012). Since the apoptosis of interneurons is linked to the communication with their target cells, it is possible that also OPCs are involved in interneuron apoptosis during development.

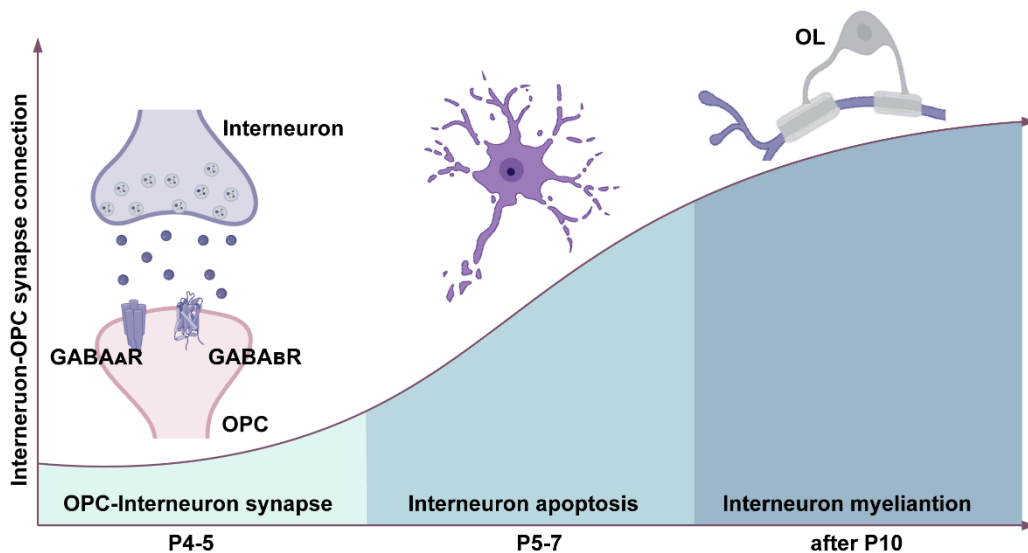


Figure 5. The communication of OPC-Interneuron during development.

OPCs form synaptic connections with interneurons starting at p4, the peak of interneuron apoptosis is at p5 to p7, while interneuron myelination occurs from p10 in mPFC (Orduz et al. 2015).

Meanwhile, the connection between interneurons and OPCs accelerates till p10, which prompts vigorous generation of oligodendrocytes and myelination of interneurons (Figure. 5) (Orduz et al. 2015). OPCs receive GABAergic inputs from interneurons via GABA receptors. OPCs express both ionotropic GABA_AR and metabotropic GABA_BR. GABA_AR mediates fast responds to inhibitory signals, while GABA_BR transduces signals rather slowly through coupled G proteins (Bettler et al. 2004). GABA_ARs are heteropentameric complexes. By far, 19 subunits of GABA_ARs are reported (Olsen and Sieghart 2008). Postsynaptic GABA_ARs of OPCs primarily consists of α 1, α 2, β 3, γ 1, and γ 2 subunits. γ 2 subunits is an interacting partner of the scaffolding protein gephyrin (Essrich et al. 1998) and are involved in early postnatal interneuron-OPC synaptic communication (Balía et al. 2015). Deletion of the γ 2 of the GABA_ARs in cortical OPCs reduced the myelination and activity of PV interneurons, which subsequently causes decreased activity of inhibitory circuit (Benamer et al. 2020). However, the absence of the γ 2-subunit in OPCs does not affect their proliferation and differentiation (Balía, Benamer, and Angulo 2017), possibly due to compensation by GABA_BR. GABA_BRs are heterodimers. The functional GABA_BRs are composed by GABA_{B1} and GABA_{B2} subunit: GABA_{B1} subunit for ligand binding through its Venus fly trap domain located extracellularly and GABA_{B2} subunit for intracellular signaling transduction (Marshall et al. 1999). *Gabbr1* gene (GABA_BR subunit 1) are mainly expressed in astrocytes, OPC and neurons (Figure. 6) (La Manno et al. 2021). In 2007, Luyt et al. has shown that activation of GABA_BR promoted

INTRODUCTION

proliferation and migration of OPC cell line CG4 (Luyt et al. 2007). Till 2020, a second study confirmed the contribution of GABA_BR in oligodendrocyte differentiation and myelination *in vitro* (Serrano-Regal et al. 2020; Pudasaini et al. 2022). Moreover, systemic application of baclofen, selective GABA_BR agonist, promoted remyelination in a lysolecithin induced demyelination model (Serrano-Regal et al. 2022). However, whether and how OPC-GABA_BRs are involved in myelination, especially for interneurons, is not clear.

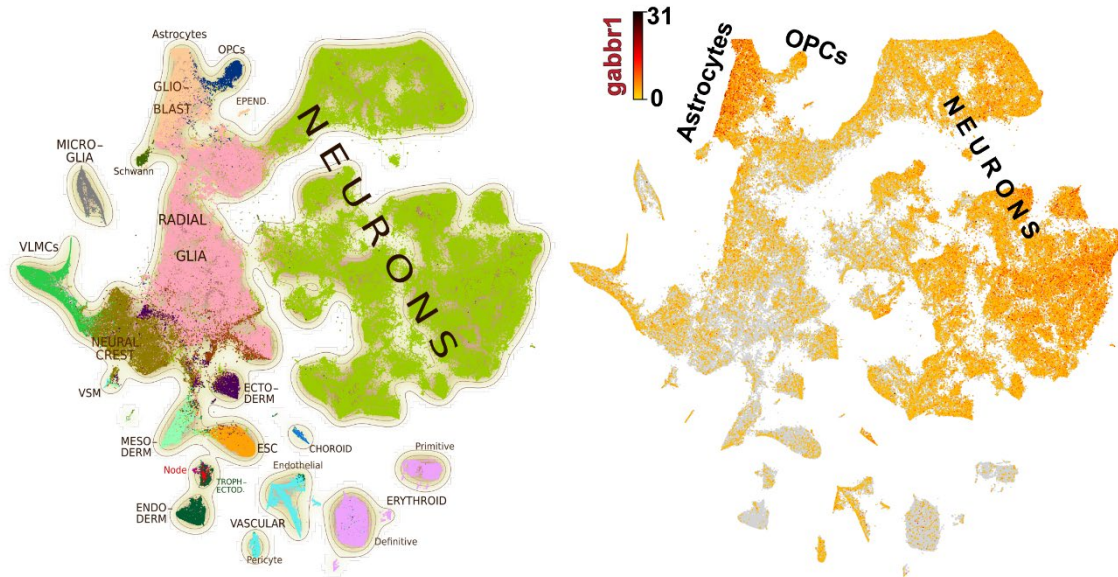


Figure 6. The *Gabbr1* gene (GABA_BR subunit 1) are mainly expressed in astrocytes, OPCs and neurons.

Single-cell RNA sequencing data demonstrated *gabbr1* gene is expressed in various cells, mainly in astrocytes, OPC and neurons. Modified from La Manno et al., Nature, 2021.

5. AIM OF THE STUDY

To investigate the role of OPC-GABA_BRs in interneurons myelination and apoptosis

To address this question, we devised the following work packages:

- **Verify the cell-specific deletion of GABA_BRs in OPCs**

To conditional knockout GABA_B receptors in OPCs, we will utilize transgenic mice with OPCs inducible GABA_BRs deletion (GABA_BRs cKO) and expression of the genetic reporter tdTomato. The expression of OPC-GABA_BRs will be quantified by Western blot with cortical OPCs, which will employ a magnetically activated cell sorting (MACs) method to isolate OPCs of 9 weeks age mice.

- **Identify the contribution of OPC-GABA_BRs in the myelination of interneurons**

To assess the role of OPC-GABA_BRs in myelination, we will employ immunostaining of oligodendrocyte-lineage cell markers to quantify the myelin-related cell density, using qRT-PCR and Western blot and to measure the myelin-related genes and proteins, using electron microscopy to check the myelin structure, and will utilize the Imaris software to assess the interneurons myelination.

- **Characterize the role of OPC-GABA_BRs for the apoptosis of interneurons**

We will examine the role of OPC-GABA_BRs during the first two postnatal weeks when excess interneurons are eliminated by apoptosis, and screen the molecular factors by qRT-PCR on cortical tissue and MACs-OPCs, then will be confirmed by the primary neuron culture with pharmacology.

- **Evaluate the impact of OPC-GABA_BRs for inhibitory circuits and behavior**

To assess the effect of OPC-GABA_BRs in neural circuits, we will record the cortical circuits and brain oscillation *in vivo*. Cortical circuits will be recorded by patch clamp and brain oscillation will be captured by electroencephalography (EEG). To investigate the behavioral impact of OPC-GABA_BR deletion, general behavior tests and cognitive related behavior tests will be performed.

6. RESULTS

6.1 Successful deletion of GABA_BR in OPCs

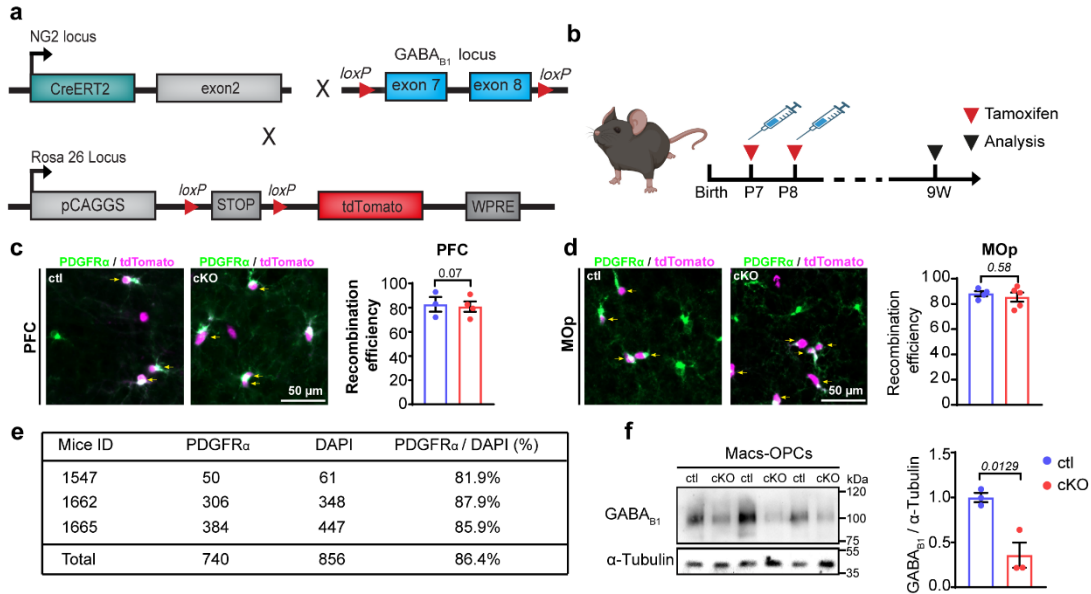


Figure 7. Conditional deletion of GABA_BR in cortical OPCs.

a Breeding strategy of transgenic mice. **b** Scheme of experimental plan. **c-d** Coronal section of the prefrontal cortex (PFC) and primary motor cortex (MOp) stained for PDGFR α (P α). Expression of tdTomato⁺ (tdT⁺) indicates recombined cells. PFC (ctl=86.2, n=3 mice vs cKO=80.5, n=4 mice, unpaired t-test); MOp (ctl=88.0, n=4 mice vs cKO=85.4, n=5 mice unpaired t-test). **e** Quantification of OPCs purity after MACs (PDGFR α ⁺/DAPI⁺). **f** Western blot analysis of GABA_BR subunit 1 expression in MACs -OPCs of control and cKO mice. (ctl=1.0, n=3 mice vs cKO=0.36, n=3 mice, unpaired t-test).

To assess the function of GABA_BR in OPC-neuron communication, we took advantage of NG2-CreERT2: GABA_{B1}R^{fl/fl} mice (Figure. 7a) to conditionally and specifically knock out (cKO) the GABA_BR subunit 1 in OPCs and their progeny. To visualize the recombined cells, we introduced the Rosa26-fSf-tdTomato reporter line to the double transgenic mice (Figure. 7a). Since OPC-interneurons connection begin on postnatal (p) day 4, and oligodendrocytes formation is initiated on p10-11 in cortex (Orduz et al. 2015), we induced cKO with tamoxifen injection at p7 and 8 (p7/8) (Figure. 7b). At the age of 9 weeks, around 80 % of OPCs were recombined with tdTomato in mPFC and 85 % in primary motor cortex (MOp), respectively (Figure. 7c-d).

To confirm and quantify the loss of GABA_BR in OPCs, firstly, we isolated OPCs from the cortex with magnetic-activated cell sorting (MACS) (see Materials and Methods section). By performing Western blot analysis with these sorted OPCs, we found that the expression of GABA_BR subunit 1 was decreased by 64 % compared to the controls (Figure. 7f). Considering the purity of MACS OPCs (86 %, Figure. 7e) and recombination efficiency (83 %), theoretically about 74 % (64 % / 86 % (purity of MACS)) of GABA_BR was deleted in OPCs *in vivo*. These

RESULTS

results confirm the majority of GABA_BRs on OPCs were successfully deleted and also suggest that the recombination efficiency of reporter (83 %) and the degree of receptor deletion (74 %) are similar in our transgenic mice, which is consistent with previous study (Jahn et al. 2018).

6.2 GABA_BRs of OPCs are essential for oligodendrogenesis in the cortex but not in the corpus callosum

Next, we investigated the impact of GABA_BR on OPC differentiation by analyzing the density of OPCs and oligodendrocytes. OPCs and oligodendrocytes were identified by the expression of PDGFR α and CC1 respectively, together with Olig2, the transcription factor expressed over the lineage (Figure. 8b). In mPFC and MOp, the density of OPCs (PDGFR α ⁺Olig2⁺) was not altered in cKO mice (Figure. 8c), implying GABA_BR did not affect OPC pool maintenance. However, the number of mature oligodendrocytes (CC1⁺Olig2⁺) was reduced by 26 % (Figure. 8c), indicating the formation of oligodendrocytes decreased by GABA_BR deletion (Figure. 8d).

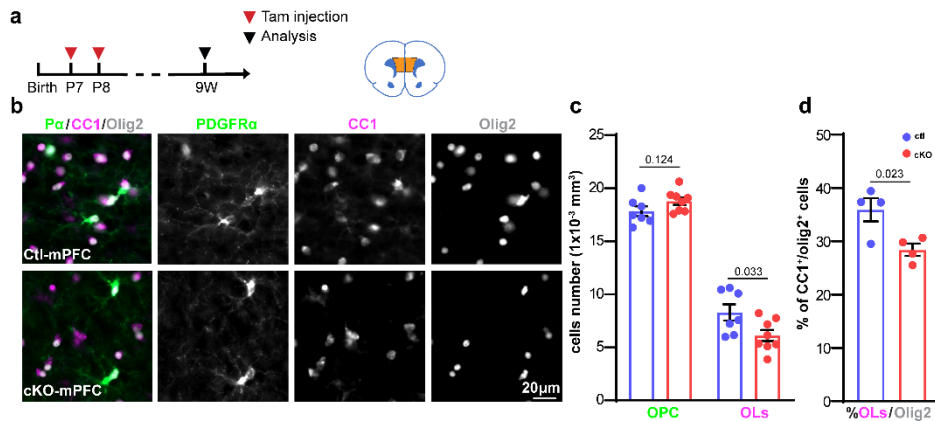


Figure 8. Alteration in oligodendrogenesis in mutant mice.

a Experimental schedule for **b-d** and the scheme of analyzed brain region (orange). **b** Immunostaining of PDGFR α (green), CC1 (magenta), Olig2 (grey) in adult ctl and cKO mPFC. **c** Quantification of OPC (ctl=17.8, n=7 mice vs cKO=18.8, n=8 mice, multiple t-tests) and oligodendrocyte (OL) (ctl=8.3, n=7 mice vs cKO=6.1, n=8 mice, multiple t-tests) densities in mPFC. **d** Quantification of the oligodendrocyte proportion among the total lineage (ctl=35.9, n=4, cKO=28.4, n=4, multiple t-tests).

In the MOp, a similar result has been observed, i.e. oligodendrocyte density was reduced while the number of OPCs remained stable both at 2-week and 9-week of age (Figure. 9b and Figure. 9d), further confirming that GABA_BRs are required for oligodendrocytes formation in the grey matter. It is worth noting that the relative proportion of mature oligodendrocyte was significantly reduced at the 9-week cKO group, whereas it showed slight tendency of reduction at the 2w-cKO group (Figure. 9b and Figure. 9f).

RESULTS

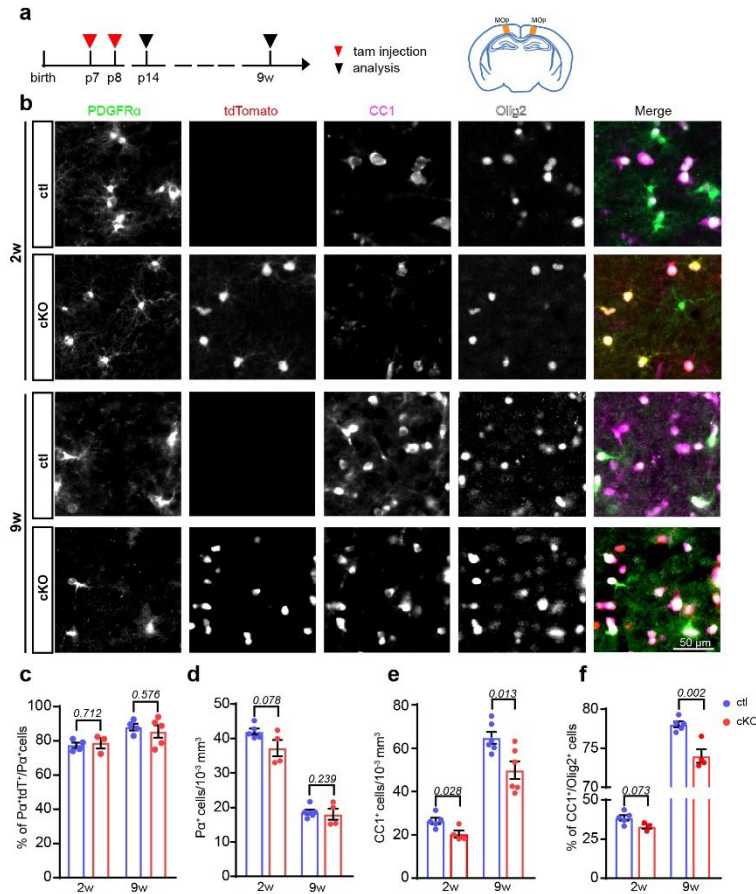


Figure 9. Oligodendrogenesis is slightly reduced in the primary motor cortex of cKO mice.

a Schedule of experiments and brain regions analyzed (orange), i.e., the primary motor cortex region at the hippocampal level (MOP). **b** Immunostaining of OPCs (PDGFR α , green), oligodendrocytes (CC1, magenta) and olig2 (lineage cell marker, grey) in MOP at 2 and 9 weeks of age, respectively. Recombinant cells were indicated by tdTomato expression. **c** Quantification of OPC recombination efficiency. **d** Quantification of OPCs density in MOP of 2w (ctl=42.0, n=5 vs cKO=37.2, n=4, unpaired t-test) and 9w old mice (ctl=16.6, n=6 vs cKO=13.5, n=4, unpaired t-test), respectively. **e** Quantification of oligodendrocytes in the MOP at the age of 2w (ctl=26.4, n=5 vs cKO=20.4, n=4, unpaired t-test) and 9w (ctl=64.8, n=6 vs cKO=49.8, n=6, unpaired t-test), respectively. **f** OPC differentiation rate were indicated by percentage of oligodendrocytes in the whole lineage cells at 2w (ctl=38.5, n=5 vs cKO=33, n=3, unpaired t-test) and 9w (ctl=78.0, n=5 vs cKO=74.0, n=4, unpaired t-test), respectively.

Corpus callosum is white matter with enriched myelin and oligodendrocyte. However, in corpus callosum, neither the OPC nor the oligodendrocyte exhibited density alteration by the deletion of GABA_BR at both 2-week and 9-weeks of age (Figure. 10), revealing the OPC-GABA_BR mediated mature oligodendrocyte formation is brain region-dependent. In addition, in corpus callosum, about 80 % of recombination efficiency of OPCs showed that the similar extent of GABA_BR subunit 1 deletion compare to cortex (83 %, recombination efficiency) (Figure. 10).

RESULTS

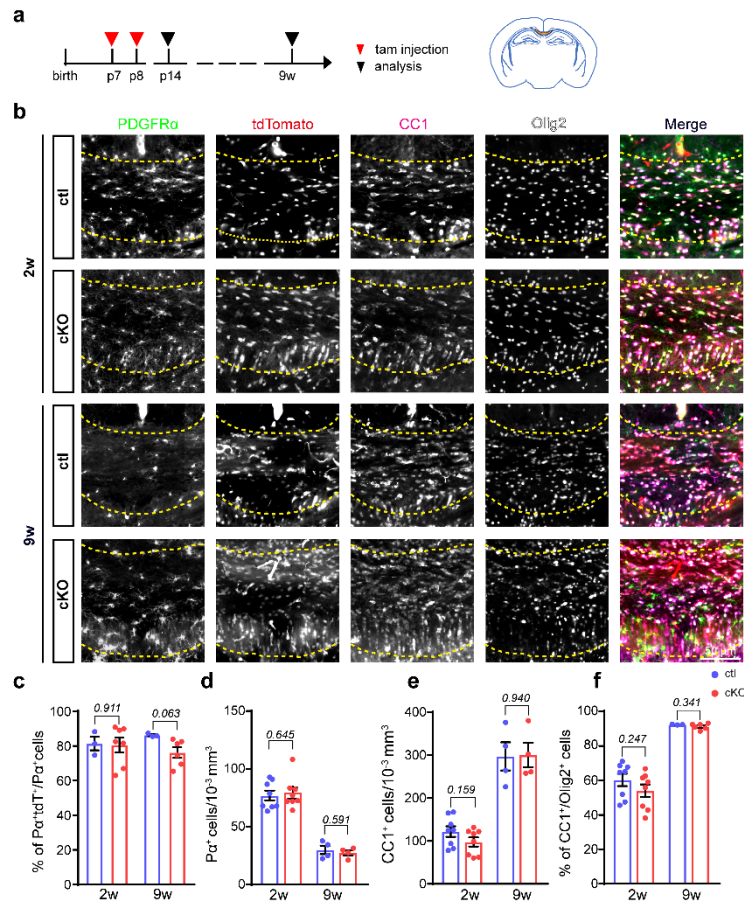


Figure 10. The densities of OPCs and oligodendrocytes are not altered in the corpus callosum of mutant mice.

a Schedule of experiments and brain regions analyzed (orange), i.e. corpus callosum. **b** Immunostaining of OPCs (PDGFR α , green), oligodendrocytes (CC1, magenta) and Olig2 (lineage cell marker, grey) in corpus callosum at 2 and 9 weeks of age, respectively. Recombinant cells were indicated by tdTomato expression. **c** Quantification of OPCs recombination efficiency in ctl and cKO. **d e** Quantification cell density of OPCs and oligodendrocytes of 2-week (OPC: ctl=77.0, n=8 vs cKO=80.0, n=8, unpaired t-test; oligodendrocytes: ctl=121.7, n=8 vs cKO=97.6, n=8, unpaired t-test) and 9-week (OPC: ctl=30.0, n=4 vs cKO=27.6, n=4, unpaired t-test; oligodendrocytes: ctl=296.9, n=4 vs cKO=300, unpaired t-test), respectively. **f** OPC differentiation rate were indicated by percentage of oligodendrocytes of the whole lineage cells at 2w (ctl=60.3, n=8 vs cKO=54.0, n=8, unpaired t-test) and 9w (ctl=92.4, n=3, cKO=91.3, n=6, unpaired t-test).

All these data indicate that OPC-GABA β Rs are required for the mature oligodendrocytes' formation in mPFC and MOP but not in corpus callosum.

6.3 GABA β Rs of OPCs are pivotal for myelination in mPFC but not in MOP and corpus callosum

Oligodendrocytes extend their processes to wrap the axon to form myelin. To further investigate whether the reduction in mature oligodendrocytes alters myelination in mutant mice, we performed Western blot and qRT-PCR with lysate of mPFC, MOP and corpus callosum.

RESULTS

Myelin basic protein (MBP) expression was reduced in the cKO mPFC both at protein (Figure. 11b-c) and mRNA levels (Figure. 11d). However, the expression of other myelin related proteins, including proteolipid protein (PLP) and myelin oligodendrocyte glycoprotein (MOG) did not change (Figure. 11d), which may be due to the different expression degree in various oligodendrocyte lineage-stage. In the MOp and corpus callosum of cKO mice, MBP expression remained unchanged (Figure. 11e-h). These data demonstrated that deletion of GABA_BR in OPCs reduces myelination in mPFC.

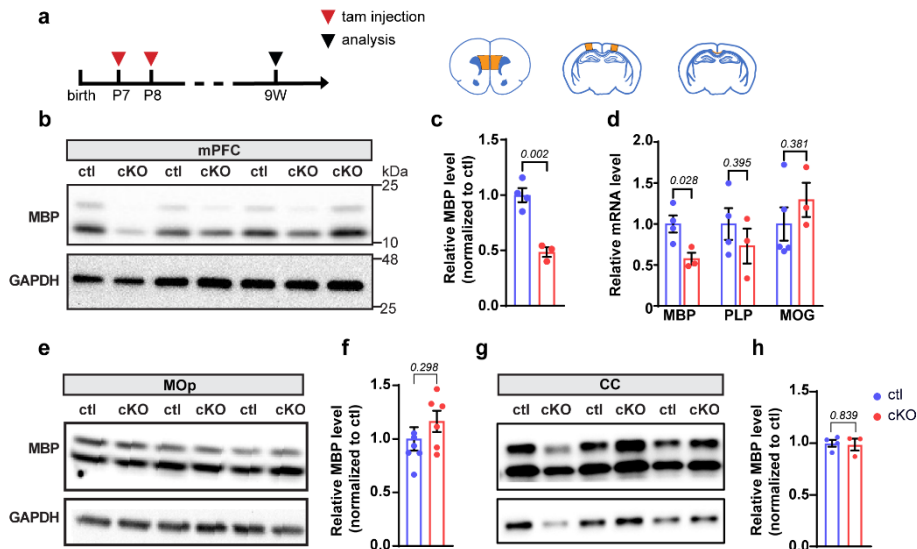


Figure 11. GABA_BRs of OPCs are pivotal for myelination in mPFC.

a Schedule of experiments and brain regions analyzed (orange), i.e. mPFC and primary motor cortex (MOp) as well as corpus callosum (cc). **b-h** myelin basic protein (MBP) was only reduced in mPFC of cKO; not in the MOp and cc. **b-c** Western blot analysis of MBP expression (ctl=1.0 n=4 vs cKO=0.48 n=3, multiple t-tests) in mPFC. **d** Relative mRNA expression of MBP (ctl=1, n=4 vs cKO=0.6, n=3, unpaired t-test) was reduced in the cKO mPFC, while proteolipid protein (PLP) (ctl=1, n=4 vs cKO=0.7, n=3, unpaired t-test) and oligodendrocyte glycoprotein (MOG) (ctl=1, n=4 vs cKO=1.3, n=3, unpaired t-test) mRNA were not affected. **e-f** Western blot analysis of MBP expression (ctl=1.0 n=7, cKO=1.2 n=6, multiple t-tests) in MOp. **g-h** Western blot analysis of MBP expression in corpus callosum (ctl=1.0 n=4 mice, cKO=0.74 n=3, multiple t-tests).

The unmyelinated axons between the myelin sheath are the nodes of Ranvier, and Caspr is specifically expressed on the paranode axons (Figure. 12a). To further investigate the structural change of myelin in cKO mice, we performed Caspr and MBP double immunostaining (Figure. 12b). In cKO-mPFC, a significantly increased proportion of longer paranode was observed (Figure. 12c-e). Moreover, the mean paranode length of cKO mice was significantly greater than that of ctl mice (Figure. 12c-d). The distribution and the average length of node did not differ between cKO and ctl mice (Figure. 12f-g). The density of paranodes and nodes were also not altered in the cKO mPFC (Figure. 12e and 12h). Additionally, we did not observe changes in nodal and paranodal length and density neither in the MOp (Figure. 12i-o) nor the corpus callosum (Figure. 13b-e).

However, in the corpus callosum, myelination was not altered in cKO, which as showed by no alteration of MBP expression between ctl and cKO (Figure. 11g). Electron microscopy data

RESULTS

showed that the myelin sheath did not differ between ctl and cKO mice, as indicated by the g ratio data (Figure. 13f-h). The speed of action potential transmission in the central nervous system is mainly influenced by the diameter of the axon and myelin sheath, which can act as an insulating membrane to increase resistance and decrease membrane capacitance (Bolino 2021). The patch clamp data also showed that the action potential in the corpus callosum was not affected in cKO, revealing that myelin structure was not altered by GABA_BR deletion in the OPCs in corpus callosum (Figure. 13i).

These results indicated that deletion GABA_BR_s in OPCs does not alter the myelination in MOP and corpus callosum, and OPC-GABA_BR_s may promote myelination only in mPFC.

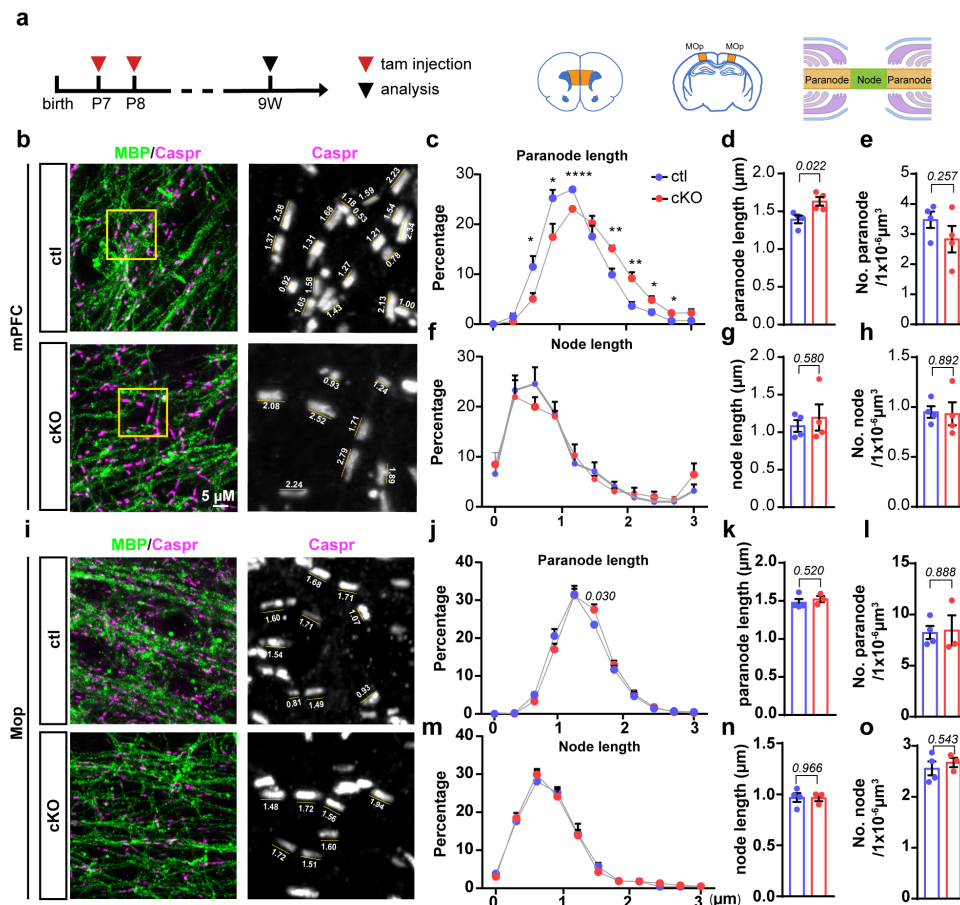


Figure 12. Paranodal structures are altered in the cKO-mPFC.

a The schedule of experiments for b-o and the brain region analyzed (orange). **b** Immunostaining of paranode (Caspr, magenta) and myeline (MBP, green). **c-e** Quantification of paranode length (ctl=1.4 n=4 mice vs cKO=1.6 n=4, multiple t-tests) and paranode density (ctl=3.5 n=4 mice, cKO=2.8 n=4, multiple t-tests) in mPFC. **f-h** Quantification of node length (ctl=1.0 n=4, cKO=1.2 n=4, multiple t-tests) in mPFC. **i** Immunostaining of paranode (Caspr, magenta) and myelin (MBP, green) in MOp. **j-o** In MOp Quantification of paranode length (ctl=1.5, n=4, cKO=1.5, n=4, unpaired t-test) and density (ctl=8.2, n=4, cKO=1.5, n=3), and quantification of node length (ctl=1.0, n=4 vs cKO=1.0, unpaired t-test) and node density (ctl=2.6, n=4, cKO=2.7, n=4, unpaired t-test)

RESULTS

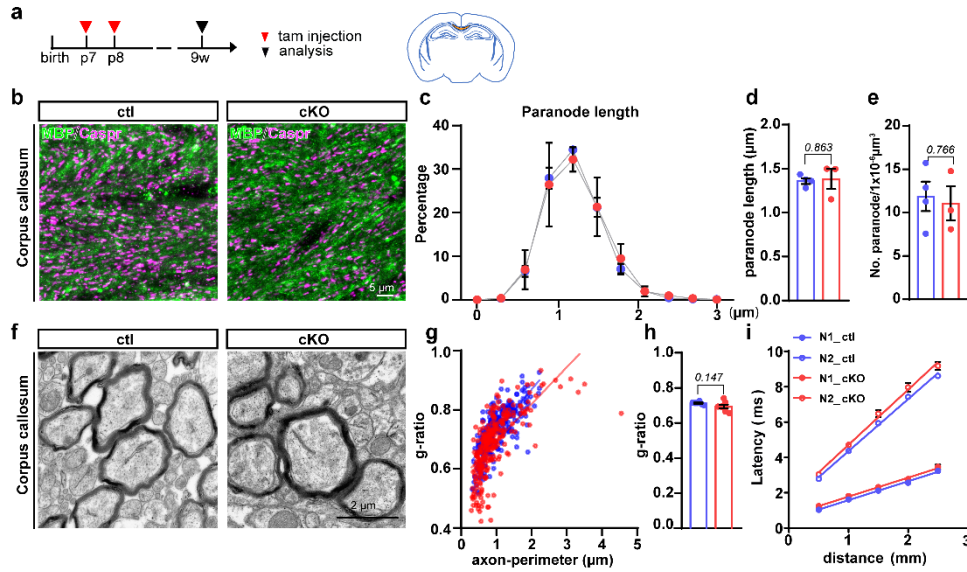


Figure 13. Myelination remains unaltered in the corpus callosum of cKO mice.

a the schedule of experiment and the brain region analyzed (orange), i.e. corpus callosum. **b** Immunostaining of paranode (Caspr, magenta) and myelin (MBP, green). **c-e** Quantification of paranode length (ctl=1.4, n=4 vs cKO=1.4, n=3, unpaired t-test) and density (ctl=11.9, n=4 vs cKO=11.1, n=3, unpaired t-test). **f-h** Electron microscopic analysis of myelin ultrastructure in sagittal section of corpus callosum and the quantification of g-ratios (the ratio between the inner and the outer diameter of the myelin sheath) (ctl=0.7, n=3 vs cKO=0.7, n=2 unpaired t-test). **i** According to the extracellular field recordings, the conduction velocity of the compound action potential was not altered. N1 indicates the conduction velocity of non-myelinated axons, N2 myelinated axons (ctl=35 cells from 3 mice; cKO=10 cells from 3 mice; unpaired t-test).

In summary, all of results demonstrated that OPC-GABA_BRs are specifically involved in the myelination of mPFC via mature oligodendrocyte formation.

6.4 Conditional deletion of GABA_BRs in mature oligodendrocytes do not affect oligodendrogenesis and myelination

Since OPCs can differentiate into oligodendrocytes throughout their lifetime (Huang et al. 2014; Kang et al. 2010; Zhu et al. 2011), the cKO OPCs will also generate a portion of oligodendrocytes depleted of GABA_BR when we induce cKO at p7/8. To exclude the observed phenotype was attributed to the loss of GABA_BRs in oligodendrocytes, we specifically deleted GABA_B receptor in oligodendrocytes utilizing PLP-CreERT2 x GABA_B1^{fl/fl} mice (Figure. 14a). GABA_BR deletion was achieved by intraperitoneal administration of tamoxifen at either p7/8 or 4 weeks and the mice were analyzed at the age of 9 week (Figure. 14b). Immunostaining results elucidated that the density of OPCs as well as oligodendrocytes did not alter in cKO mouse brain, regardless of the mPFC or in corpus callosum (Figure. 14c-f). As well, MBP expression remained unchanged in both brain regions (Figure. 14g). These results indicated that the observed myelin deficit in mPFC of OPC-cKO mice was attributable to elimination of GABA_BR from OPCs rather than oligodendrocytes.

RESULTS

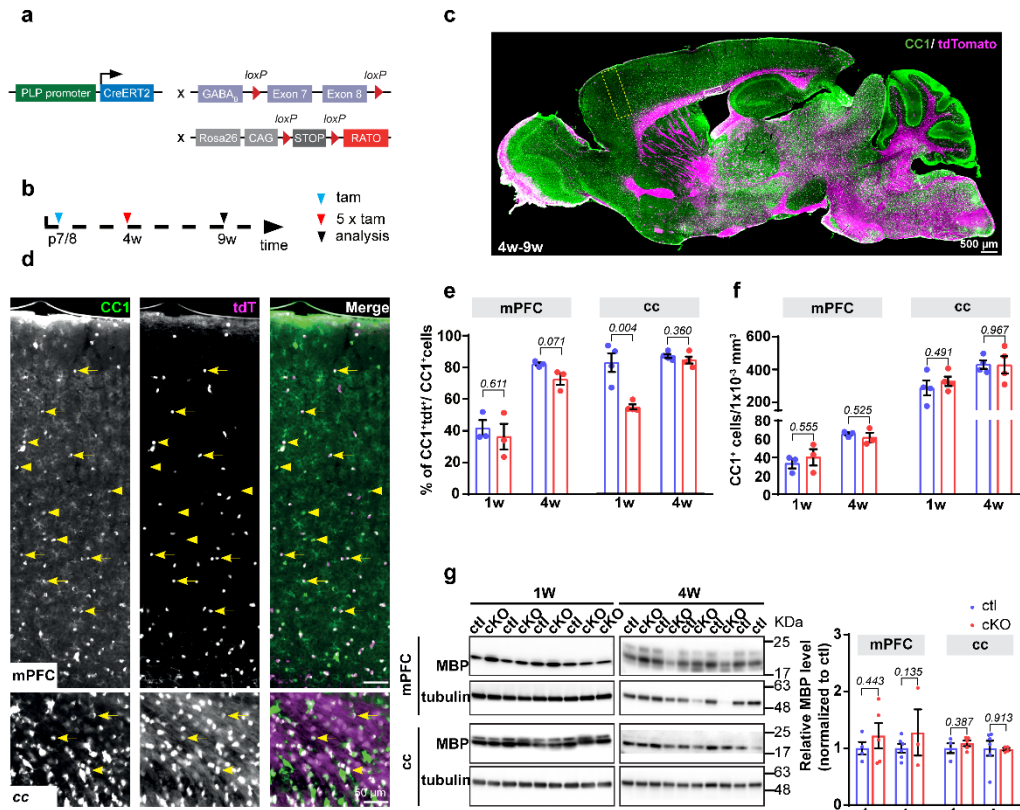


Figure 14. Deletion of GABA_BR in oligodendrocytes does not alter the oligodendrogenesis or myelin formation in the mPFC and corpus callosum.

a Transgenic mouse lines. **b** The schedule of experiments. **c** The immunostaining of oligodendrocytes (CC1, green) in 9w old ctl mouse. The recombined cell is indicated by the expression of tdTomato (magenta). **d** Enlarged micrographs of the PFC (yellow frame in **c**) and corpus callosum (white frame in **c**). **e** Quantification of oligodendrocytes recombination efficiency in mPFC (ctl=44, n=4 vs cKO=32, n=4, unpaired t-test) and cc (ctl=82, n=4 vs cKO=54, n=4, unpaired t-test). **f** Quantification of oligodendrocytes density in both PFC and cc. arrows: recombined OL; triangles: non-recombined oligodendrocytes. mPFC: (1w-ctl=38.4 vs 1w-cKO=38.9, unpaired t-test; 4w-ctl=51.2 vs 4w-cKO=38.3, unpaired t-test); cc: (1w-ctl=292.1 vs 1w-cKO=330.5 unpaired t-test; 4w-ctl=430.1 vs 4w-cKO=427.7 unpaired t-test). **g** The MBP expression in mPFC and cc of ctl and cKO mice showed by Western blot, in 1week and 4week-age groups, respectively. mPFC: (1w-ctl=1 vs 1w-cKO=1.2, unpaired t-test; 4w-ctl=1 vs 4w-cKO=1.27 unpaired t-test); cc: (1w-ctl=1 vs 1w-cKO=1.1, unpaired t-test; 4w-ctl=1 vs 4w-cKO=0.98 including one outlier, only 3 mice were analyzed), unpaired t-test).

In conclusion, our data suggest that the function of OPC-GABA_BRs are brain region-specific and GABA_BRs are required for mPFC-oligodendrocytes formation and subsequent myelination.

6.5 Interneuron myelination deficits in cKO-mPFC

In the cortex, including MOp and mPFC, numerous inhibitory neurons are present shown by immunostaining (Figure. 15), and axons of interneurons are mainly localized in cortical areas of the same hemisphere. In contrast, the majority of myelinated axons in corpus callosum are pyramidal neurons, i.e. excitatory (Hines et al. 2015). Thereby, we hypothesized that the myelin deficit in cKO-mPFC is mainly attributed to inhibitory axons. Among inhibitory neurons, the

RESULTS

fast-spiking PV expressing interneurons are predominantly myelinated ones (Stedehouder et al. 2017). The cell bodies of PV interneurons are mainly located in layers IV and V of the mPFC, but their axons can project to layers II / III and V (Scala et al. 2019). Hence, we speculate that deletion of GABA_BRs in OPCs leads to a reduction in PV neuron myelination in the mPFC.

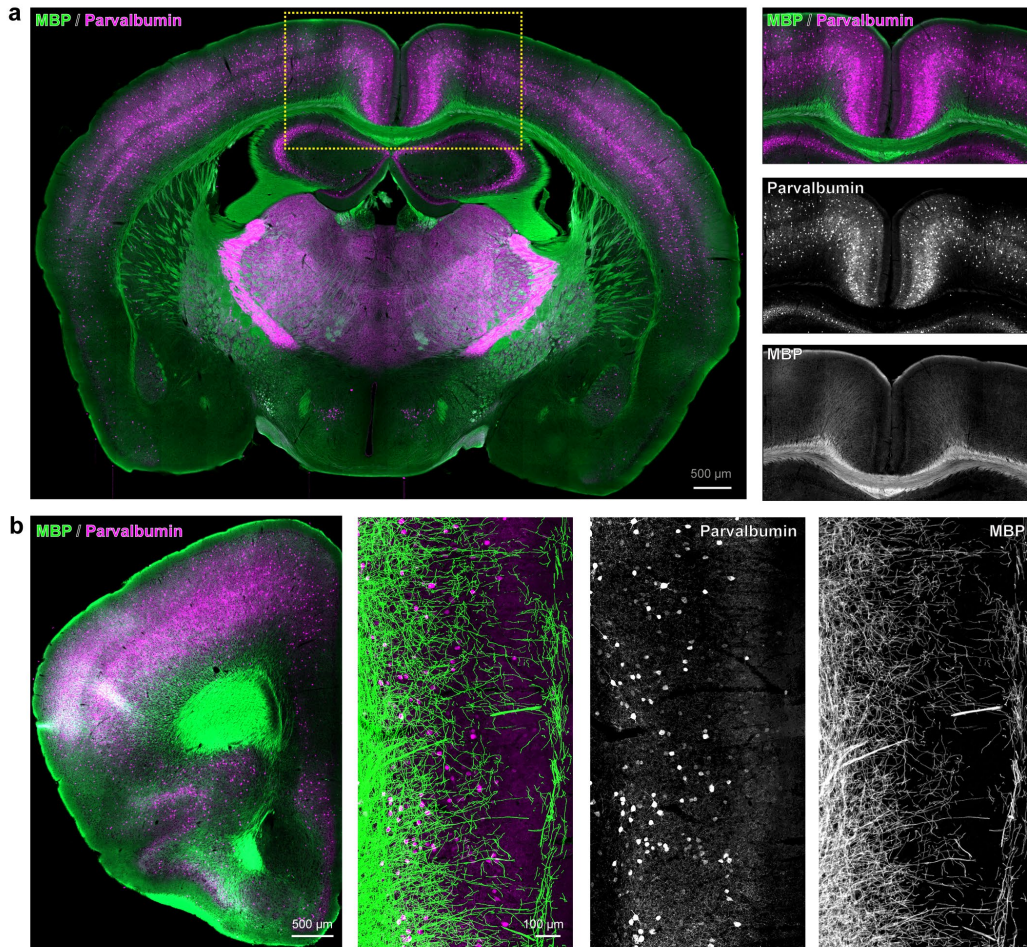


Figure 15. Parvalbumin interneurons are abundant in MOp and mPFC.

a-b immunostaining of MBP (green) and parvalbumin (magenta) in somatosensory cortex of C57BL/6N mouse.

To evaluate the myelination of PV interneurons, we labeled axons by using PV and SIM312 (pan axonal marker) antibodies. In the cKO mPFC, MBP expression was decreased while MOG stayed unchanged. To better visualize the myelin sheath, we labeled myelin with MOG antibodies (Figure. 16b). Using Imaris software, we rebuilt 3D structure of myelin sheaths wrapping PV axons and analyzed the relative volume of myelin sheath (MOG⁺) of PV axons (PV⁺SIM312⁺) (Figure. 16c). In the cKO mouse mPFC, the total myelin volume wrapping all axons (SMI 312⁺) was comparable between ctl and cKO mice (Figure. 16d). However, the volume of myelin sheaths wrapping PV interneurons (PV⁺SMI 312⁺) was reduced by around 60 %, indicating GABA_BR may specifically promote interneuron myelination (Figure. 16d). In contrast, excitatory neuron myelination was not changed as the g ratio (the ratio between the inner and outer diameters of the myelin sheath) of callosal axons were comparable between

RESULTS

ctl and cKO mouse (Figure. 13f-h). As well, the conduction velocity of compound action potential was not compromised in the cKO mouse corpus callosum (Fields 2015; Saab et al. 2016) (Figure. 13i). Therefore, knockout of GABA_BR in OPCs specifically suppress inhibitory neuron myelination in mPFC.

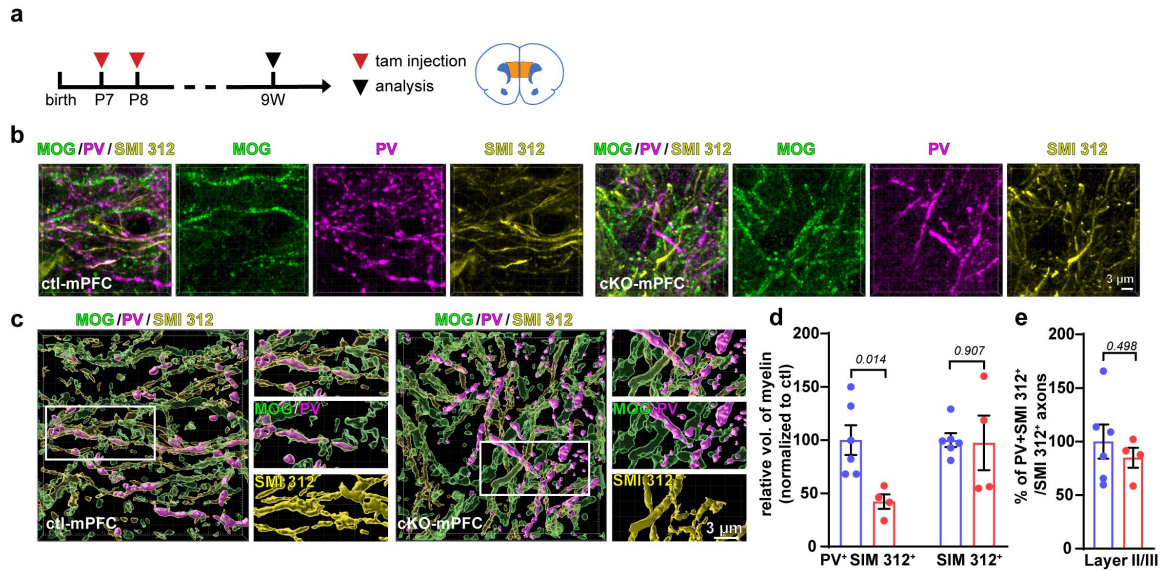


Figure 16. Interneuron myelination deficits in cKO-mPFC.

a The schedule of experiments for **b-e** and the brain region analyzed (orange). **b** The immunostaining of myelin (MOG, green), interneurons (Parvalbumin, magenta) and neuronal axons (SMI 312) in layers II/III (L^oII/III). **c** The 3D reconstruction and analysis were performed by Imaris. **d** The relative myelin volume (MOG) of PV axons (PV⁺SMI 312⁺) and total axons (SMI 312⁺) (ctl= 100.0, n=6 mice vs cKO= 42.3, n=4 mice, unpaired t-test). **e** Relative of PV interneuron axons to all axons. (ctl=100, n=6 mice vs cKO=84.9, n=4 mice, unpaired t-test).

6.6 Attenuated inhibitory tone in cKO mPFC

The interneuron hypomyelination is intimately associated with local neural circuits (Benamer et al. 2020). Hence, we recorded spontaneous inhibitory postsynaptic currents (sIPSCs) and spontaneous excitatory postsynaptic currents (sEPSCs) of the pyramidal neurons in layer V/VI of mPFC (Figure. 17a), because in these layers, a substantial interneurons form connections with pyramidal neurons. Despite of the increased number of PV interneurons, the pyramidal neurons received mitigated inhibitory tone as the frequency of sIPSCs was decreased about 40 % in cKO mPFC compared to ctl group (Figure. 17c). The amplitude of sIPSCs was slightly reduced in the cKO mPFC (Figure. 17d). All these data indicated that the activity of PV interneurons was perturbed by GABA_BR deletion in OPCs. The amplitude and frequency of sEPSCs were comparable between cKO and ctl groups (Figure. 17e and f), indicating deletion of GABA_BRs in OPCs specifically affect the local inhibitory circuits.

RESULTS

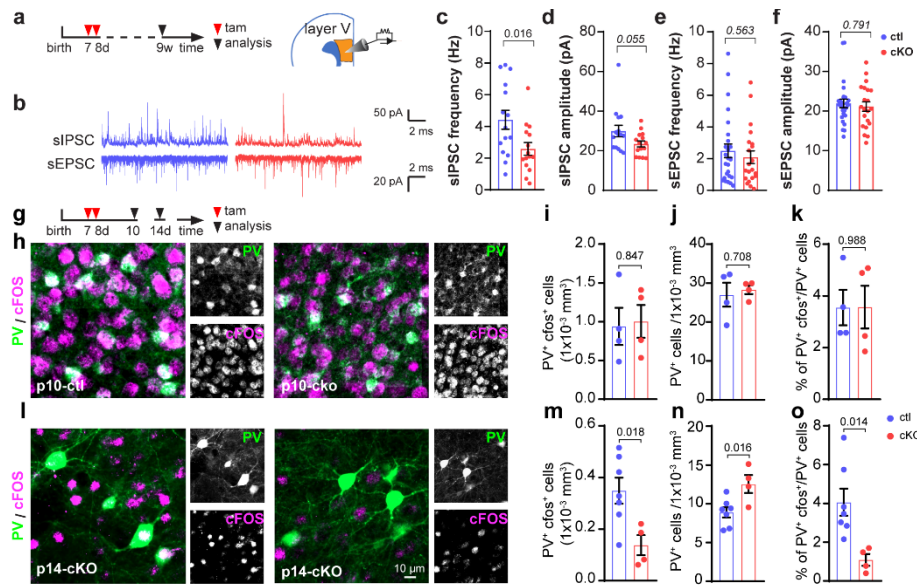


Figure 17. Attenuated inhibitory tone in cKO mPFC.

a The schedule of experiments for **b-f**. **b** Patch-clamp recordings of sIPSCs and sEPSCs in pyramidal neurons of layer V of mPFC. **c-f** Quantification of frequencies and amplitudes of sIPSC and sEPSC (sIPSC: ctl=15 cells from 4 mice, cKO=15 cells from 5 mice; sEPSC: ctl=26 cells from 4 mice, cKO=21 cells from 5 mice; sIPSC frequency with unpaired t-test, others with Mann Whitney test). **g-o** Interneuron activity was altered in the mPFC of mutant mice. **g** The schedule of experiments for **h-o** and the brain region analyzed (orange). **h-i** Immunostaining and quantification of PV (Parvalbumin) interneurons expressing c-Fos (magenta) in the mPFC of p10 and p14. The PV interneuron activity is suppressed at p14 (**l-o**) but not affected at p10 (**h-k**). p10: PV+cFos+ cells: (ctl=0.9, n=4 mice vs cKO=1.0, n=4 mice, unpaired t-test); PV+ cells: (ctl=27, n=4 mice vs cKO=28.3, n=4 mice, unpaired t-test); % of PV+cFos+ cells: (ctl=3.6, n=4 mice vs cKO=3.6, n=4 mice, unpaired t-test). p14: PV+cFos+ cells: (ctl=0.35, n=7 mice vs cKO=0.1, n=4 mice, unpaired t-test); PV+ cells: (ctl=9.5, n=7 mice vs cKO=12.5, n=4 mice, unpaired t-test); % of PV+cFos+ cells: (ctl=4.4, n=7 mice vs cKO=1.1, n=4 mice, unpaired t-test).

6.6.1 Decreased interneuron activity in cKO mPFC during development

OPCs form synaptic connection with interneurons from the first postnatal week and receive GABAergic signals for further differentiation (Bai, Kirchhoff, and Scheller 2021). On the other hand, hypomyelination of PV neurons attenuates spiking frequency of PV neurons (Benamer et al. 2020). Given the decreased interneurons myelination and inhibitory signaling in the cKO mPFC, we wondered whether the decrease in myelination was due to attenuated neuronal activity. To understand the causal link, we analyzed the interneuron activity and OPC differentiation at the second postnatal week (Figure. 18a), before and after the onset of myelination in the mPFC (p12) (Figure. 4).

To assess interneuron activity, we adapted the double staining of OPCs and vesicular GABA transporter (vGAT) with PDGFR α and vGAT antibodies, respectively (Figure. 18b). Since vGAT is potentially releasing GABA-containing transmitter vesicles, the density and volume of vGAT can be considered as an indicator of inhibitory neuronal activity (Bai, Kirchhoff, and Scheller 2021). Only three days after tamoxifen injection, i.e., at p10 (approximately 50 % of OPCs are recombined), the density and volume of vGAT was already decreased by 25 % in cKO mice

compared to ctl (Figure. 18c, d), suggesting a decreased inhibitory tone before myelination in local cKO mPFC.

cFos is a proto-oncogene whose expression can be induced in neurons after depolarization (Pan-Vazquez et al. 2020; Denaxa et al. 2018). Neuronal activity is closely linked to expression of the immediate early gene (cFos). Therefore, we further assessed interneuron activity with cFos and PV double immunostaining. At p10, PV interneuron density and cFos⁺PV⁺ population did not differ between ctl and cKO mice (Figure. 17h-k), although vGAT was already altered at this time point (Figure. 18c-e). However, at p14, cFos⁺PV⁺ population in the cKO-mPFC dramatically decreased by approximately 60 %, and the density of PV interneurons began to increase in the cKO mice (Figure. 17n), which further caused the decrease in the ratio of PV⁺cFos⁺ cells in total PV interneurons (Figure.17i and o). Thus, these data illuminated that deletion of GABA_BR in OPCs leads to a reduction in inhibitory neuronal activity during development and the in mPFC.

6.6.2 Less GABAergic-input to OPCs in cKO mPFC

The distance between presynaptic vGAT and postsynaptic GABA_AR/Gephyrin is around 270 nm (Crosby et al. 2019). To further investigate whether OPCs also integrate down tuned GABAergic signal, we further classified the vGATs into two subgroups according to their distance to OPCs (PDGFRa⁺) surface: we defined the vGAT puncta with a 'the distance to OPCs surface < 200 nm as vesicles possibly targeting on OPCs (magenta, pOPCs, Figure. 18b), and vGAT puncta with a distance > 200 nm to OPC surface are targeting other cells (grey, other, Figure. 18b). Both the 'pOPC' and 'other' subgroups, the density and volume of vGAT were reduced, implying OPCs as well as other cells (likely neurons) receive less inhibitory input (Figure. 18c and d). To quantify the capability of OPC reception, we adapted the index between density of vGAT and OPC surface. Again, the vGAT density targeting on per OPC unit surface was drastically reduced in cKO, suggesting OPCs receive less GABAergic input (Figure. 18).

To further confirm these findings, we recorded spontaneous postsynaptic current (sPSC) in OPCs with patch clamp recording at p10-14 (Figure. 18h). The frequency of OPC- sPSC was reduced by about 64 % in cKO mice (Figure. 18i), while the amplitude did not change (Figure. 18j). These data suggest that OPCs indeed receive less GABAergic signal in cKO mPFC, but no change in vesicle loading. When the interneurons are stimulated by Carbachol, muscarin receptor agonist which is shown to activate interneuron activity (Lin and Bergles 2004), the sPSC frequency in OPCs of both control and cKO mPFC was increased (Figure. 18i and j), but still it was about 40 % less in cKO OPCs (Figure. 18i). The amplitudes of OPC-sIPSC were slightly increased in cKO mice compared with ctl mice, which may be due to the changes in vesicle loading upon stimulation by carbachol (Figure. 18j). To exclude the reduced GABAergic input in OPCs was due to change in GABA_AR function, we administered GABA in brain slices and measured the evoked current in OPCs. The amplitudes of OPCs were not altered in cKO mice (Figure. 18k), suggesting that GABA_A receptor function was not affected by deletion of GABA_BR in OPCs.

RESULTS

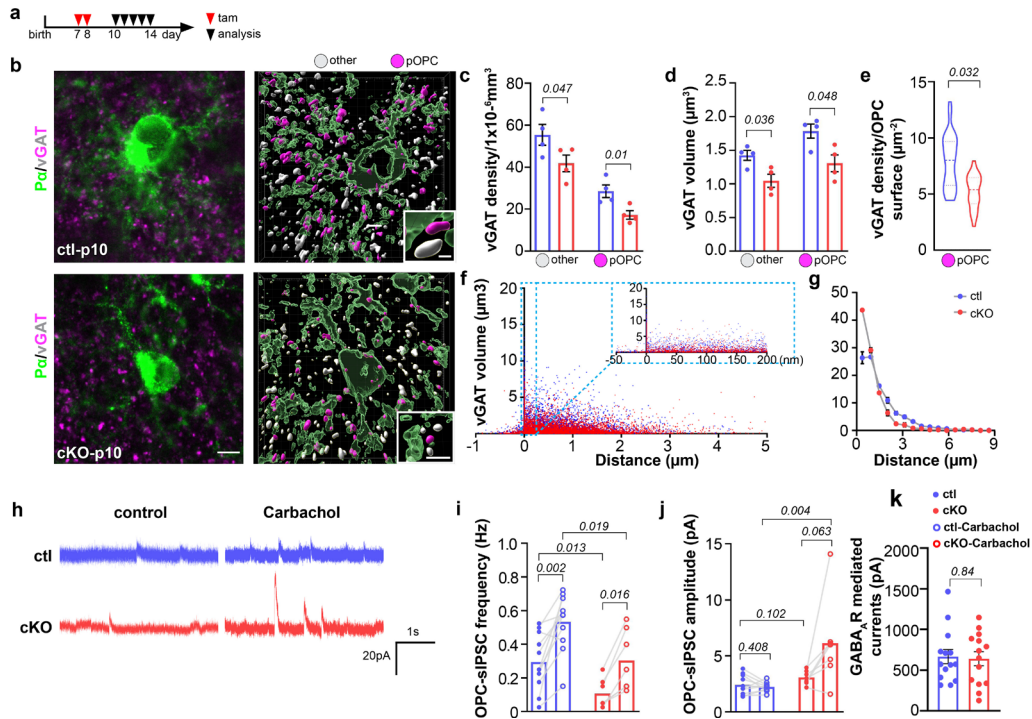


Figure 18. GABAergic currents of OPCs are reduced by GABA_BR deletion.

a The schedule of experiments for **b** The immunostaining of OPC (PDGFR α , green) and vesicular GABA transporter (vGAT, magenta and grey) in mPFC. **b-e** Quantification of vGAT density (**c**) and volume (**d**) in mPFC, (ctl=4 mice, cKO=4 mice; multiple t-tests). **e** Quantification of synaptic vGAT (< 200 nm, based on the distance between presynaptic vGAT and postsynaptic GABA_AR/gephyrin) density per μm^2 of OPC surface. (ctl=7.9, n=4 mice vs cKO=5.2, n=4 mice, unpaired t-test). **f** Quantitative analysis of vGAT puncta volume and distance to OPC surfaces. ctl=4 mice, cKO=4 mice. **g** The volume of vGAT in cKO mPFC was smaller than that in ctl group. ctl=4 mice, cKO =4 mice. **h** Patch-clamp recordings of OPC- sIPSC. **i-k** The frequency and amplitude of OPC-sIPSC in mPFC without and with carbachol treatment (ctl=14 cells from 3 mice, cKO=14 cells from 3 mice, unpaired t-tests). **k** Electrophysiological recordings indicated that GABA_AR mediated currents in cKO-OPCs were not altered (ctl=665.5 \pm 87.6 pA, n=14 cells from 4 mice, cKO=639.9 \pm 86.1 pA, n=14 cells from 4 mice).

Taken together, all of results demonstrated that OPC-GABA_BRs are required for interneuron activity during development.

6.7 Decreased OPC differentiation follows attenuated interneuron activity in the cKO-mPFC during development

6.7.1 Early deletion of GABA_BR in OPC affects myelination

To understand whether attenuated GABAergic input affects OPC proliferation and differentiation, we analyzed OPC and oligodendrocyte density at p10 and p14 (Figure. 19a). At p10, the density of both OPCs and oligodendrocytes were comparable between ctl and cKO mice (Figure. 19b and c), as well as the oligodendrocyte proportions in all oligodendrocyte lineage cells. However, at p14, oligodendrocyte density and their proportion in total oligodendrocyte lineage were greatly reduced in mutant mPFC (Figure. 19b-d), as well as the

RESULTS

mRNA level of MBP (Figure. 19e). To rule out the reduction in oligodendrocyte density was due to an increase in oligodendrocyte apoptosis or reduction of OPC proliferation, we assessed oligodendrocyte differentiation with Bromodeoxyuridine (BrdU) assay and apoptosis with CC-3 immunostaining. BrdU was intraperitoneally administered at p13 and mice were analyzed at p14. BrdU will label all proliferating OPCs and also oligodendrocytes derived from BrdU incorporated OPCs (Figure. 19a). The density of CC1⁺BrdU⁺ cells was significantly reduced by 85 %, but the density of Pd⁺BrdU⁺ cells was comparable, implying that OPC differentiation is reduced in cKO mice (Figure. 19f-h). Moreover, CC1⁺ CC3⁺ cells were barely visible at p14 of both ctl and cKO mice (Figure. 20). We also did not observe any changes in OPCs and oligodendrocyte population in the corpus callosum in cKO mice. In cKO-mPFC, since the vGAT and OPC-sPSC results showed a mitigated inhibitory activity at p10 (Figure. 18), OPC differentiation is unaltered at p10 but change at p14, it is highly possible that interneuron activity is decreased before OPC differentiation changes, and attenuated inhibitory tone reduces OPC differentiation.

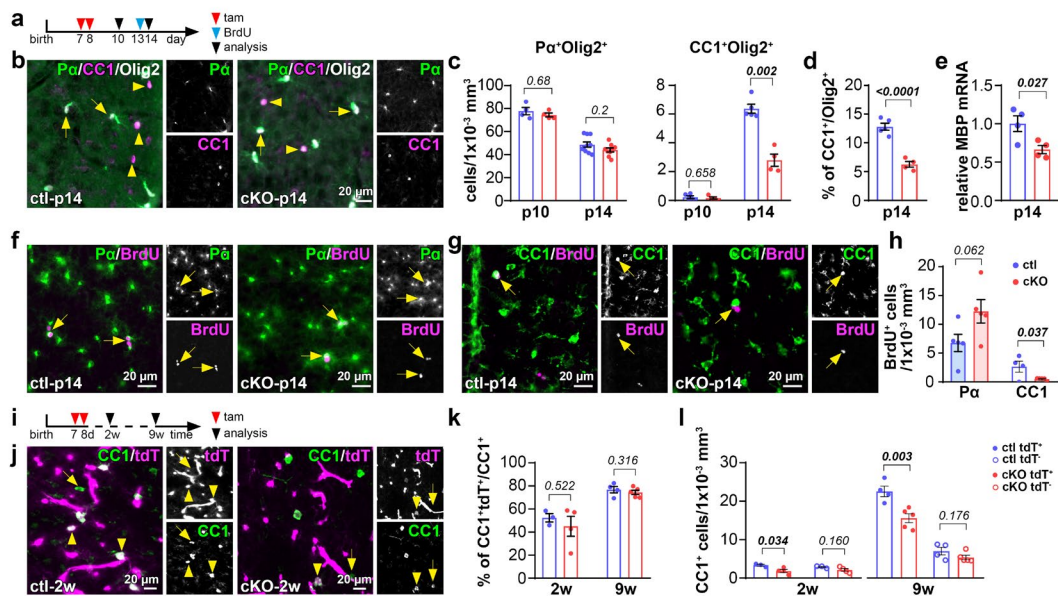


Figure 19. Early deletion of GABA_BR in OPC affects myelination.

a The schedule of experiment for **b-d**. **b** Immunostaining of apoptosis vesicle (CC3, magenta) and oligodendrocytes (CC1, green). **c** Quantification of oligodendrocytes apoptosis (CC1⁺CC3⁺) in the mPFC of p14 mice. (ctl=2.2, n=8 mice vs cKO=1.3 n=8 mice, unpaired t-test). **d-e** Immunostaining of OPCs (PDGFR α , green) and oligodendrocytes (CC1, magenta) as well as BrdU. **f** Quantification of OPCs and oligodendrocytes incorporated with BrdU (Pd α : ctl=6.7, n=5 vs cKO=12.3, n=5; CC1: ctl=2.7, n=4 vs cKO=0.5, n=5, unpaired t-test). **g** The schedule of experiment for **h-j**. **h** Immunostaining of oligodendrocytes (CC1⁺, green) combined with tdTomato (tdT, magenta) expression in the mPFC at 2 week. **i** Recombination efficiency of oligodendrocytes 2w: (ctl=52.3, n=3 vs cKO=45.1, n=4, two-sided unpaired t-test); 9w: (ctl=76.8, n=4 vs cKO=74.4, n=5, two-sided unpaired t-test). **j-l** Quantification of recombined and non-recombined oligodendrocytes densities (with or without tdT expression). 2w: (ctl-tdt⁺=22.6 n=4 vs ctl-tdt⁻=15.6 n=5, two-sided unpaired t-test); 9w: (ctl-tdt⁻=7.0 n=4 vs ctl-tdt⁻=5.4 n=5, two-sided unpaired t-test).

Furthermore, the total mature oligodendrocytes (CC1⁺Olig2⁺, Figure. 8c and Figure. 19c) and recombined oligodendrocytes (CC1⁺tdT⁺, Figure. 19l) both were decreased at 2w and 9w,

RESULTS

suggesting the lower density of total oligodendrocytes was due to the reduced oligodendrocytes of early generation instead of later/newly formed, which was confirmed by the no alteration in non-recombined oligodendrocytes (CC1⁺tdt⁻ oligodendrocytes) between ctl and cKO mice (Figure. 19I), indicating that OPC-GABA_BR does not directly regulate OPC differentiation.

Taken together, early elimination of GABA_BR in OPC leads to deficits in communication between OPC and inhibitory neurons. The inhibitory tone altered by early deletion GABA_BR in OPC, which in turn impairs OPC differentiation and myelination.

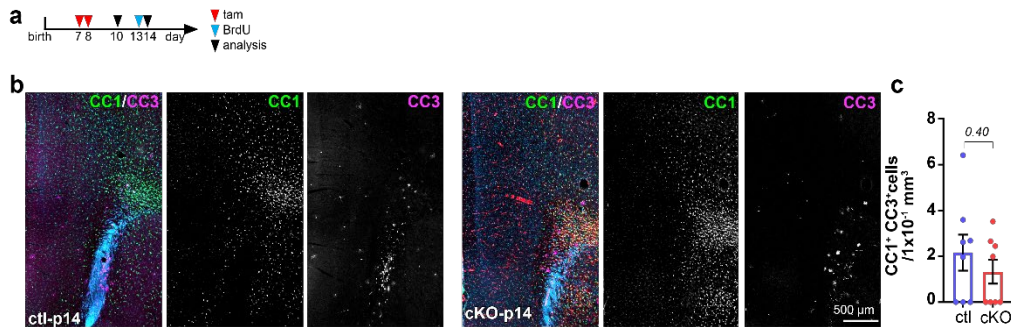


Figure 20. Ablation of GABA_BR in OPCs does not affect apoptosis of oligodendrocytes.

a Experimental schedule and analyzed brain region (orange), i.e. mPFC (medial prefrontal cortex).

b Immunostaining and quantification of oligodendrocytes (CC1) and the apoptotic marker cleaved Caspase 3 (CC-3) in the mPFC of p14 mice. ctl=2.2±0.8 (n=8 mice), cKO=1.3±0.5 (n=8 mice), two-sided unpaired t-test.

6.7.2 Late deletion of GABA_BR in OPC do not affect myelination

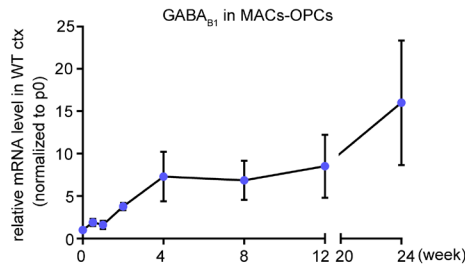


Figure 21. GABA_BR expression of OPC reaches a plateau at 4 weeks age.

All data were acquired from MACs-OPC of C57BL/6N: p0=4 mice, p3=7 mice, p7=7 mice, p14=3 mice, 4w=7 mice, 8w=7 mice, 12w=4 mice, 24w= 3 mice.

To investigate whether GABA_BR is involved in OPC differentiation or not, we induced knockout at the age of 4 weeks and analyzed the mice at 9 weeks of age, because of two reasons: the expression of GABA_BR in OPC reaches a plateau at the age of 4 weeks (Figure. 21); and, cortical inhibition is well established after the third postnatal week. The density of OPCs and oligodendrocytes, as well as the MBP expression remained unchanged in the cKO mouse mPFC (Figure. 22), indicating OPC-GABA_BR is not directly engaged in OPC differentiation and

RESULTS

myelination, further confirmed that deletion $GABA_B R$ in OPCs modulate myelination via the inhibitory tone.

In summary, these data strongly suggest that OPC- $GABA_B R$ s mediate the local inhibitory tone which subsequently regulates myelination.

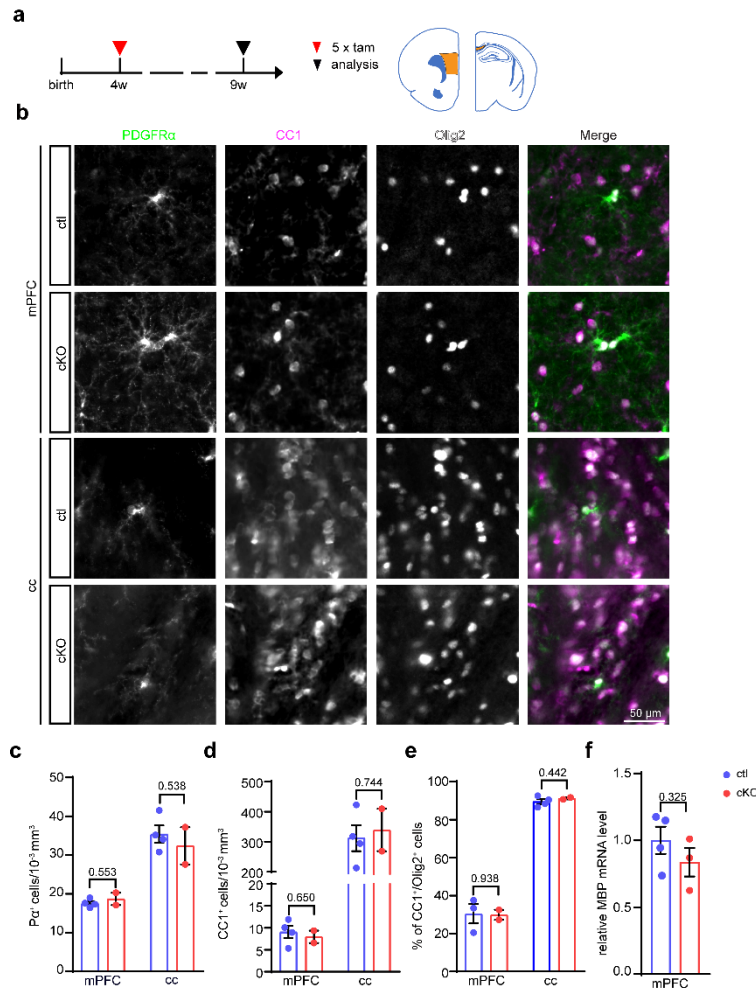


Figure 22. Late-phase deficiency of $GABA_B R$ in OPCs (at 4 week of age) do not affect oligodendrogenesis.

a The schedule of experiment for b-f and the brain regions analyzed (mPFC and corpus callosum). **b** Immunostaining of OPCs (PDGFR α , green) and oligodendrocytes (CC1, magenta) with Olig2 (white) in ctl and cKO mPFC and corpus callosum (cc) at the age of 9w. **c-d** Quantification the density of OPCs (PDGFR α^+) and oligodendrocytes (CC1 $^+$) in the mPFC (OPC: (ctl=17.6, n=4 mice vs cKO=18.7, n=2 mice, two-sided unpaired t-test); oligodendrocytes: (ctl=9.1, n=4 mice vs cKO=8.0, n=2 mice two-sided unpaired t-test)) and cc (OPC: (ctl=35.4, n=4 mice vs cKO=32.4, n=2 mice, two-sided unpaired t-test); oligodendrocytes: (ctl=311.8, n=4 mice vs cKO=339.2, n=2 mice, two-sided unpaired t-test)) of ctl and cKO mice. **e** The ratio of oligodendrocytes of all lineage cells did not change, in the mutant mouse mPFC (ctl=30.5, n=3 mice vs cKO=29.9, n=2 mice, two-sided unpaired t-test); and cc (ctl=89.5, n=3 mice vs cKO=91.2, n=2 mice, two-sided unpaired t-test). **f** MBP (Myelin Basic Protein expression) was not altered in the cKO mPFC at mRNA level.

6.8 Surplus PV interneurons present in cKO-mPFC

Correct cortical inhibition are affected by the proper interneuron density (Wang et al. 2021). Interestingly, by analyzing the PV neuron myelination, we observed an increased density of PV interneurons in the mPFC of cKO mice as well as in MOp (Figure. 23). Especially in mPFC, higher density of PV interneurons was observed in each cortical layers (layer II /III and layer V/ VI, Figure. 23a and c), except in layer I (only few interneurons are present). Remarkably, the volume of PV axons was not altered in the cKO mPFC (Figure. 16e). Therefore, it is possible that the PV interneurons may be morphological simpler and less mature in the cKO mouse mPFC.

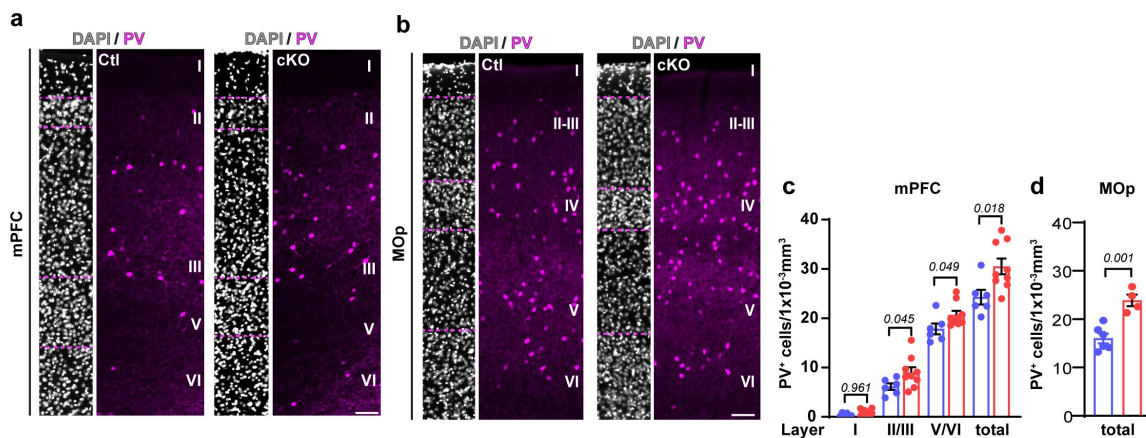


Figure 23. Surplus PV interneurons are found in cKO-grey matter.

a-b Immunostaining of interneurons in media prefrontal cortex and primary motor cortex (MOp) (PV, magenta; DAPI, grey). **c-d** Quantification of PV interneurons cell density in mPFC (**c**) and MOp (**d**) at the age of 9 weeks (ctl=16.0 n=6 mice vs cKO=23.9 n=9 mice, unpaired t-tests).

6.9 OPC-GABA_BR promote interneuron apoptosis

6.9.1 Interneuron apoptosis is attenuated in cKO-mPFC

Aberrant inhibitory neuronal activity may be a consequence of an overabundance of interneurons (Duan et al. 2020). Interneuron density is mainly determined during development via programmed cell death between p1 to p15 (with peak at p7) and around 20-40 % interneurons are eliminated by the apoptosis (Wong et al. 2018). Therefore, we hypothesized that the interneuron apoptosis might have been diminished in the cKO mPFC. To address this question, we immunostained apoptotic cells with cleaved caspase 3 (CC-3) and examined apoptosis of interneurons at p10 (before myelination) and p14 (onset of myelination) (Figure. 24a).

RESULTS

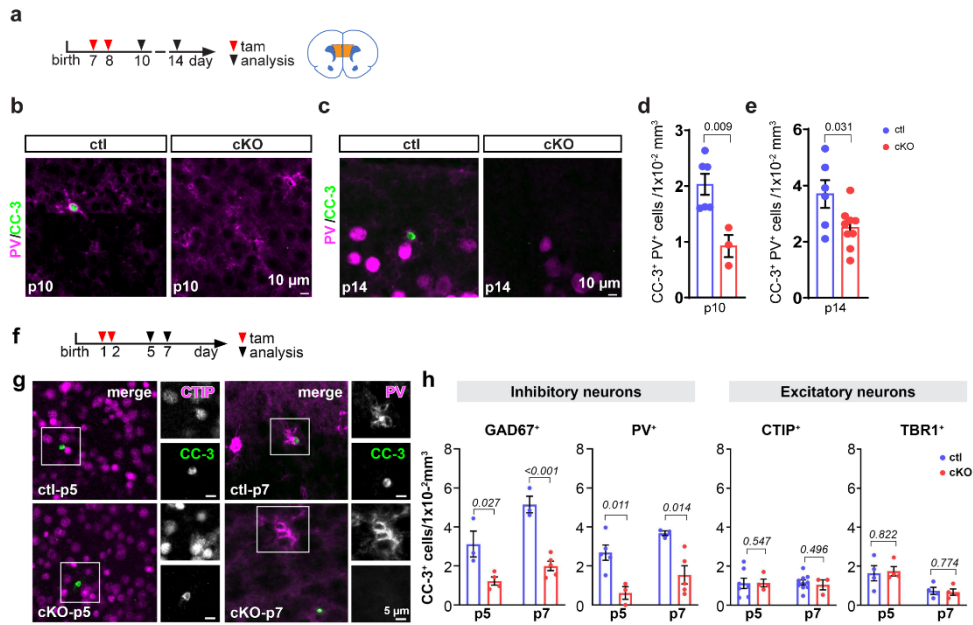


Figure 24. Interneuron apoptosis is attenuated in cKO-mPFC.

a The schedule of experiment for **b-e** and the brain region analyzed (orange). **b-c** Immunostaining of PV (parvalbumin, magenta) interneurons with the apoptotic marker (CC-3, green) at the p10 and p14 in ctl and cKO mPFC. **d-e** Quantification of apoptotic PV interneurons at p10 and p14 revealed a reduced apoptosis of PV interneurons in the cKO mPFC (p10: ctl=2.0, n=6 mice vs cKO=0.9, n=3 mice, unpaired t-test; p14: ctl=3.7, n=6 mice vs cKO=2.5, n=9 mice, unpaired t-test). OPCs specifically promote apoptosis of inhibitory neurons during development. **f** The schedule of experiment for **g-h**. **g** Immunostaining of inhibitory neurons (parvalbumin, magenta) and excitatory neurons (CTIP, magenta) with the apoptotic marker (CC-3, green) at the p5 and p7, respectively. **h** Quantification of apoptosis of inhibitory neurons (GAD67 and PV) and excitatory neurons (CTIP and TBR1). (GAD67: p5-ctl=3.1, n=3 mice vs p5-cKO=1.2, n=4 mice; p7-ctl=5.2, n=3 mice vs p7-cKO=2.0, n=5 mice); (PV: p5-ctl=2.7, n=5 mice vs p5-cKO=0.62, n=3 mice; p7-ctl=3.7, n=3 mice vs p7-cKO=1.5, n=5 mice); (CTIP: p5-ctl=1.1, n=7 mice vs p5-cKO=1.1, n=4 mice; p7-ctl=1.2, n=9 mice vs p7-cKO=1.0, n=3 mice) (TBR1: p5-ctl=1.6, n=4 mice vs p5-cKO=1.7, n=4 mice; p7-ctl=0.7, n=4 mice vs p7-cKO=0.7, n=4 mice, multiple t-tests).

Indeed, at both time points (p10 and p14) the interneuron apoptosis in cKO mice were reduced compared to the ctl mice, especially at p10 the number of PV⁺CC⁺ cells were only half of that in ctl mice (Figure. 24d), implying that plenty of interneurons escaped apoptotic process in cKO mice. These results suggest that GABA_BR deletion in OPC diminish the neuronal apoptosis in mPFC during development.

To understand whether the apoptosis induced by OPC-GABA_BR is general to all neurons or specific to interneurons, we further tested excitatory and inhibitory neuronal apoptosis. The time window for apoptosis of excitatory neurons is quite narrow, around from p2 to p5 (Wong et al. 2018), and p7 is the peak of apoptosis of inhibitory neurons (Southwell et al. 2012). We induced cKO as early as postnatal day 1 and day 2 and analyzed neuronal apoptosis at P5 and P7, respectively (Figure. 24f). The apoptosis of total inhibitory neurons (GAD67⁺CC-3⁺) as well as PV interneurons (PV⁺CC-3⁺) in cKO-mPFC was decreased both at P5 and P7

RESULTS

(Figure. 24g and h). However, the apoptosis of excitatory neurons was not affected in cKO mPFC (CTIP⁺CC-3⁺, TBR1⁺CC-3⁺, Figure. 24g and h, Figure. 25).

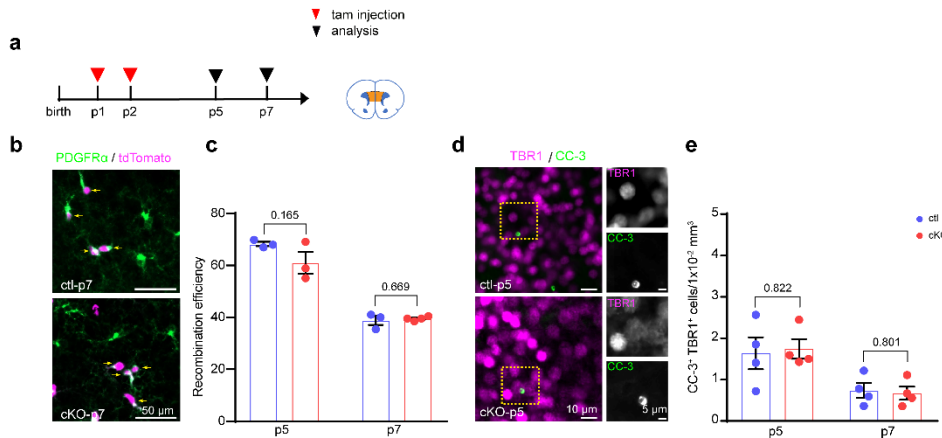


Figure 25. Cell death and survival of excitatory neurons are not affected by early ablation of OPC-GABA_BR

a The schedule of experiments for b-c and the brain region analyzed (orange). **b-c** Immunostaining of OPCs (PDGFR α ⁺, green) and tdT (tdTomato, magenta)⁺ indicated that around 62 % and 39 % of OPCs are recombined cell at p5 and p7, respectively. (ctl=4 mice, cKO=4 mice). **d e** Immunostaining and quantification of excitatory neurons (TBR1⁺) with the apoptotic marker CC-3 at p5 (**d**) and p7 (**e**). (p5: ctl=1.6, n=4 mice vs cKO=1.7 n=4 mice, p10: ctl=0.7 n=4 mice vs cKO=0.7 n=4 mice, unpaired t-test)

In summary, these results indicate that OPC-GABA_BR are specifically involved in interneuron apoptosis.

6.9.2 OPCs promotes interneuron apoptosis via TWEAK-GABA_BR signaling

To address how OPC-GABA_BR is involved in interneuron apoptosis, we next assessed the expression of apoptotic factors as well as the neurotrophic factors in early OPCs. We sampled p7 mPFC tissues since p7 is the peak of inhibitory neuron apoptosis (Figure. 26a). Among the tests, we observed a significant change in the mRNA level of TWEAK (tumor necrosis factor-like weak inducer of apoptosis, also known as Apo3l or TNF superfamily member 12, TNFSF12) was reduced about 30 % in cKO mPFC (Figure. 26b). To further validate this observation, we assessed the TWEAK expression in MACs-OPCs as well as in Oli-neu cells (OPC cell line) treated with GABA_BR antagonist (CGP 55845). In all three different levels, when GABA_BRs were inactivated, the TWEAK expression was reduced (Figure. 26c).

To confirm that the OPC derived TWEAK is the molecular inducing interneuron apoptosis, we first checked the expression of TWEAK receptor (TWEAKR or fibroblast growth factor-induced 14 (FN14), TNF receptor superfamily member 12A, TNFRSF12A) on interneurons (Chicheportiche et al. 1997). In mPFC, we observed that FN14/TWEAKR were very well co-localized with PV interneuron processes at the age of p5 (Figure. 26e).

Next, we treated primary cortical neurons with conditioned medium from Oli-neu cells to evaluate the interneuron apoptosis. Here we have noted that the cultured neurons included a large population of PV interneurons and these PV neurons also express TWEAKR

RESULTS

(Figure. 26d). As expected, considerable apoptosis of primary interneurons occurred following the incorporation of Oli-neu CM (Figure. 26f-h). However, at the presence of FN14 / TWEAKR antagonist, triazolylthione L524-0366 (20 μ M), interneuron apoptosis was reduced (Figure. 26f-h). These results suggest that OPCs selectively induce interneuron apoptosis by secreting TWEAK.

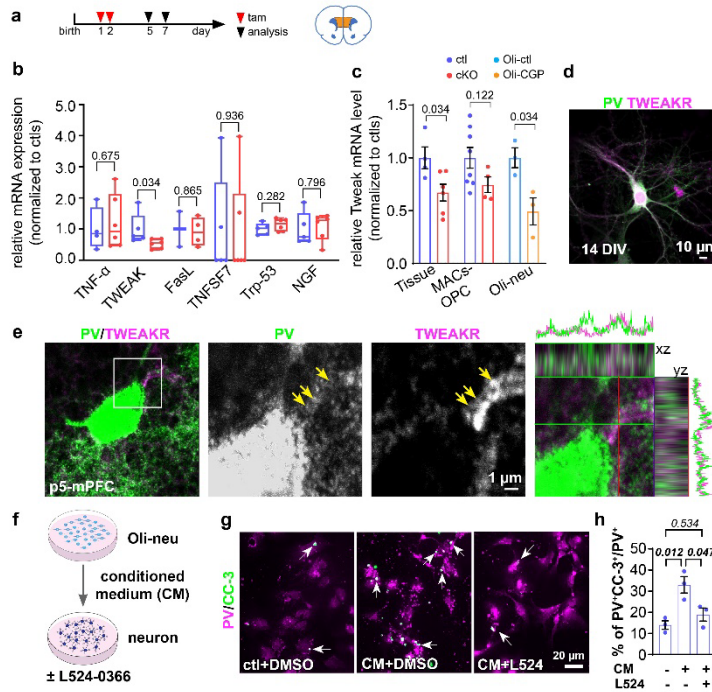


Figure 26. OPCs promote interneuron apoptosis via TWEAK-GABA_B signaling.

a The schedule of experiment for **b-c**. **b** Relative mRNA level of cell death-related protein in the mPFC at p7. (TNF- α : ctl=1, n=4 mice vs cKO=1.2, n=6 mice, unpaired t-test); (TWEAK: ctl=1, n=4 mice vs cKO=0.7, n=6 mice, unpaired t-test); (FasL: ctl=1, n=2 mice vs cKO=0.9, n=4 mice, unpaired t-test); (TNFSF7: ctl=1, n=4 mice vs cKO=0.9, n=6 mice, unpaired t-test); (Trp53: ctl=1, n=4 mice vs cKO=1.1, n=6 mice, unpaired t-test); (NGF: ctl=1, n=5 mice vs cKO=1.1, n=6 mice, unpaired t-test). **c** Quantification of TWEAK expression in the mPFC and MACs-OPCs from ctl and cKO mice as well as Oli-neu cells treated with or without 20 μ M CGP 55845 (tissue-ctl=1, n=4 mice vs tissue-cKO=0.67, n=6 mice; MACs-ctl=1, n=8 mice vs MACs-cKO=0.74, n=3 mice; Oli-neu-ctl=1 vs Oli-neu-CGP=0.49; n=3 independent experiments; multiple t-tests). **d-e** Interneuron express the specifically TWEAK receptor (FN14). The immunostaining of FN14 (TWEAKR, magenta) and interneuron (parvalbumin, green) in the primary cortical neurons at day 14 (**d**) and control mPFC at p5 (**e**). **f-h** Quantification of PV interneurons apoptosis in conditioned medium and treated with a competitive TWEAKR inhibitor (ctl+DMSO=13.9 vs CM+DMSO=33.02 vs CM+L524=18.9, n=3 independent experiments, one-way ANOVA, multiple comparison).

Taken together, our results suggest that OPCs regulate inhibitory neuronal apoptosis via the GABA_BR-TWEAK pathway. In the absence of GABA_BR, OPCs secrete insufficient TWEAK, allowing more PV interneurons to escape from programmed cell death, ultimately leading to attenuated inhibitory tone and consequent attenuation of myelination in mPFC.

6.10 Interrupted OPC-interneuron communication generates cognitive impairment

6.10.1 Gamma oscillations are altered by GABA_BR deletion in OPCs

The E/I balance in mPFC is crucial determinant for cognition (Grossmann 2013). Our electrophysiological recordings have shown the attenuated inhibition in the cKO mPFC (Figure. 17f-h). To detect the inhibitory tone in the mPFC *in vivo*, we recorded intracerebral electroencephalography (EEG) in the adult mice (Figure. 27). The gamma oscillations (30-80 Hz) represent the GABAergic signaling in the brain, and are responsible for the cognition, especially low gamma oscillations (30-50 HZ) (Lewis, Hashimoto, and Volk 2005; Sohal et al. 2009). As expected, both the gamma oscillation and low gamma oscillation were reduced in cKO mouse brain, implying reduced inhibition in the cKO mouse brain and mutant mice might exhibit cognitive impairment (Figure. 27, Figure. 28a-d).

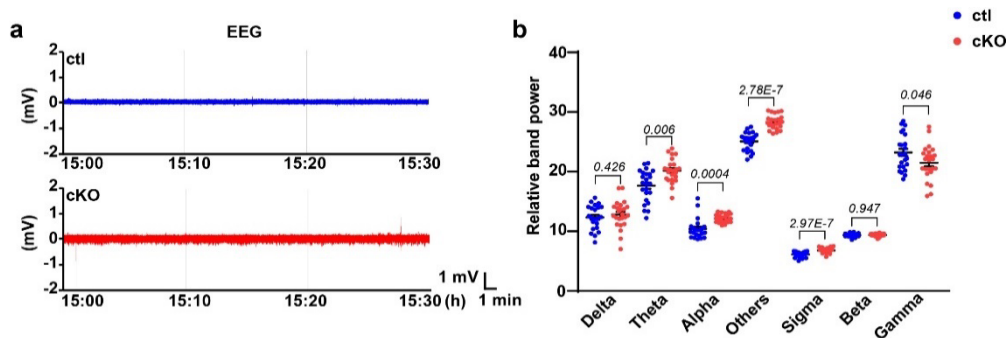


Figure 27. OPC-GABA_B cKO mice exhibited altered EEGs

a b EEG recordings indicated that the power of EEG frequency bands related to cognition and sleep were altered in mutant mice, including theta, alpha and gamma (n=24 h from 4 ctl mice and 4 cKO mice). Delta: ctl=12±0.4 vs cKO=13±0.5; Theta: ctl=18±0.5 vs cKO=20±0.4; Alpha: ctl=10.4±0.3 vs cKO=12.2±0.1; Others: ctl=25±0.3 vs cKO=28±0.2; Sigma: ctl=6±0.1 vs cKO=7±0.1; Beta: ctl=9±0.06 vs cKO=9±0.05; Gamma: ctl=23±0.6 vs cKO=22±0.6; unpaired t-tests for individual band power.

6.10.2 Impaired short-term memory in mutant mice

Next, we assessed the general well-being of the mice, by observing their nest building activity. Nest-building is often considered as an early indicator of cognitive decline (Neely et al. 2019). Compared to the elaborated nests built by ctl mice, the nest of cKO mice was simpler and cruder, not even achieving half of the performance score of ctl mice, suggesting cKO mice may exhibit cognitive impairment (Figure. 28e and f).

RESULTS

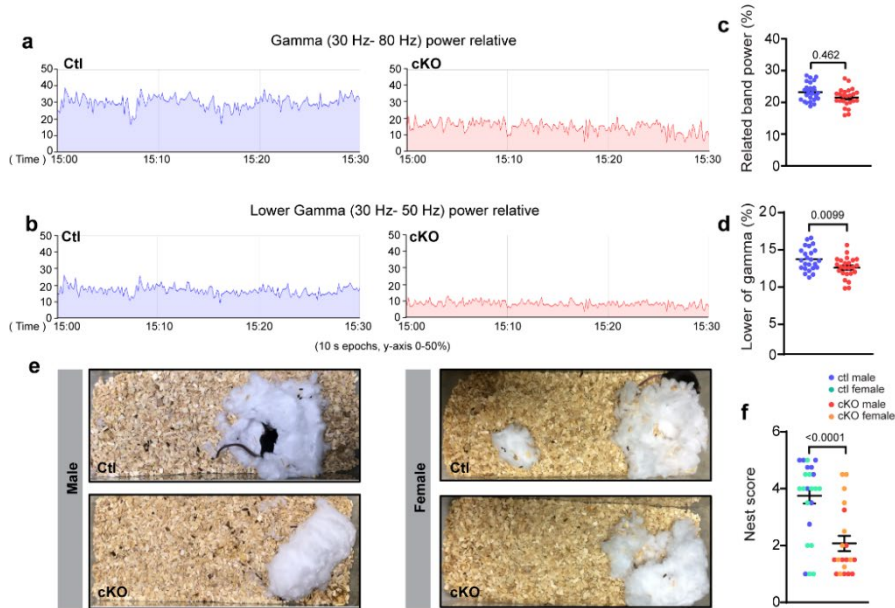


Figure 28. Gamma oscillations are altered by GABA_BR deletion in OPCs.

a-b Gamma band and lower gamma band acquired by EEG recordings. **c-d** Quantification of gamma and lower gamma oscillation in the mouse brain. (gamma-ctl=23.2 n=24 h from 4 mice vs gamma-cKO=21.5, n=24 h from 4 mice, unpaired t-test); (lower gamma-ctl=11.3, n=24 h from 4 mice vs lower gamma-cKO=9.8, n=24 h from 4 mice, unpaired t-test). **e-f** Impaired nest building ability of mutant mice. **e** The imaging of nest built. **f** score of nest (male: ctl=4.0 vs n=10 mice vs cKO=1.5, n=10; female: ctl=3.8, n=15 vs cKO=2.6, n=9, unpaired t-test).

To explore the cognition of the mice, we assessed the ability of new object recognition and social cognition which are closely associated with mPFC (Bicks et al. 2015) (Figure. 29 and Figure. 30). In the “new object recognition” test, after confirming that both ctl and cKO mice exhibited no preference for a specific object, we replaced one of the objects with a new object in different shape (Figure. 29b and c). The ctl mice showed a robust exploration of the novel object, whereas the cKO mice behaved more aberrantly, seemingly unable to effectively distinguish between familiar and new object (Figure. 29).

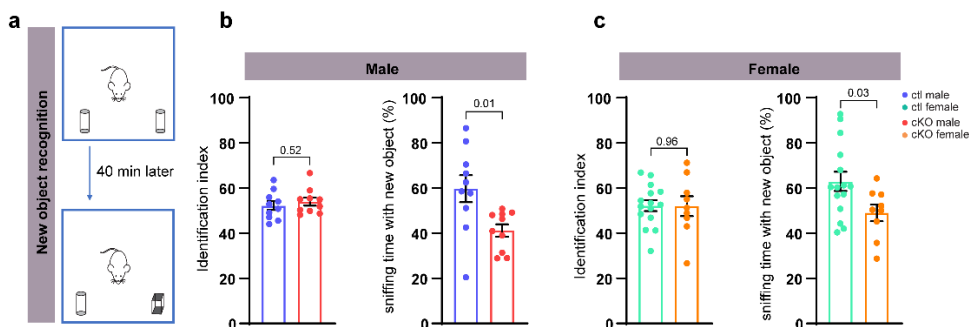


Figure 29. Impaired short-term memory in mutant mice.

a The scheme of experiment for new object recognition. **b-c** Quantification of mice (male and female) sniffing time with new object among total sniffing time. Identification index (male-ctl=52.3, n=10 mice vs male-cKO=53.9, n=10 mice, unpaired t-test; female-ctl=52.2, n=15 mice vs female-cKO=52.0, n=9 mice, unpaired t-test); sniffing time with new object (male-ctl=59.7, n=10 mice vs male-cKO=41.2, n=10 mice, unpaired t-test; female-ctl=63.0, n=15 mice vs female-cKO=49.0, n=9 mice, unpaired t-test).

6.10.3 Alteration of social novelty in mutant mice

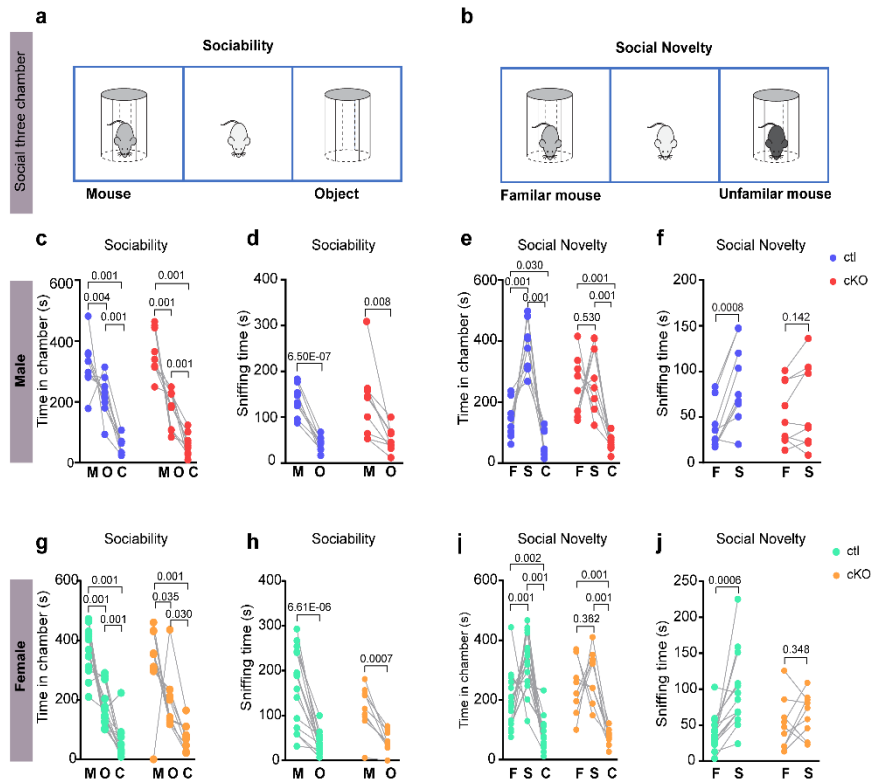


Figure 30. Impaired social novelty in mutant mice.

a-b The scheme of experiment for social three chamber test. **c-f** Both control and mutant mice prefer to stay in the chamber with a mouse rather than object, but mutant mice show cognitive impairment in social novelty test. **(c)** ctl: mouse chamber=326±27, object chamber=220±21, center=54±9, (n=9 mice), Ordinary one-way ANOVA; cKO: mouse chamber=362±24, object chamber=178±20, center=60±12, (n=9 mice), Ordinary one-way ANOVA. **d** ctl: sniffing with mice =137±10, sniffing with object=41.9±5, (n=9 mice), paired t-test.; cKO: sniffing with mouse=131±26, sniffing with object=52±8, (n=9 mice), paired t-test. **e** ctl: familiar mouse chamber=143±19, stranger chamber=395±28, center=62±14, (n=9 mice), Ordinary one-way ANOVA; cKO: familiar mouse chamber =246±32, stranger chamber=289±36, center=65±9, (n=9 mice), Ordinary one-way ANOVA. **f** ctl: sniffing with familiar mouse=38±8, sniffing with stranger=88±15, (n=9 mice), paired t-test.; cKO: sniffing with familiar mouse=53±11, sniffing with stranger=64±16, (n=9 mice), paired t-test. **g-j** Both control (female) and mutant mice (female) prefer to stay in the chamber with a mouse rather than object, but mutant mice show cognitive impairment in social novelty test. **g** ctl: mouse chamber=380±21, object chamber=166±2, center=54±14, (n=15 mice), Ordinary one-way ANOVA; cKO: mouse chamber=327±46, object chamber=201±21, center=72±15 (n=9 mice), Ordinary one-way ANOVA. **h** ctl: sniffing with mice=166±22, sniffing with object=39±6, (n=15 mice), paired t-test.; cKO: sniffing with mouse =116±17, sniffing with object=43±8, (n=9 mice), paired t-test. **i** ctl: familiar mouse chamber=197±14, stranger chamber=323±26, center=80±15, (n=15 mice), Ordinary one-way ANOVA; cKO: familiar mouse chamber=237±30, stranger mouse chamber=285±28, center=78±9, (n=9 mice), Ordinary one-way ANOVA. **j** ctl: sniffing with familiar mouse=38±6, sniffing with stranger=99±14 (n=15 mice), paired t-test.; cKO: sniffing with familiar mouse=52±12, sniffing with stranger=65±10, (n=9 mice), paired t-test.

The social three-chamber test was applied to assess social cognition by evaluating the general sociability of the mice and their interest in social novelties (Figure. 30a and b). In the first phase of sociability test, the cKO mice did not show difference from the ctl mice, both group of mice

RESULTS

showed greater interest (longer sniffing times) in the mice than in the objects (Figure. 30c, d, g, h). However, in the second phase of social novelty assessment, the cKO mice cannot effectively discriminate between familiar mice and stranger (Figure. 30e, f, i, j). All the behavioral tests demonstrated that OPC-GABA_BRs are required for cognition.

It is worth noting that the cKO mice do not have mobility deficit as shown by the results of open field (speed, Figure. 31a-b). In contrast, the cKO mice exhibited slightly enhanced motility (Figure. 31c).

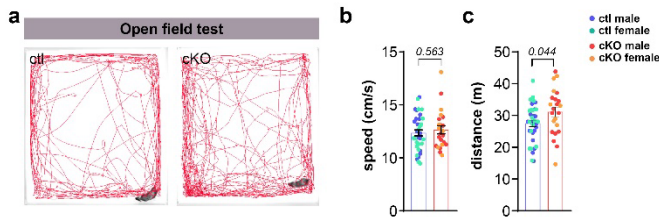


Figure 31. No alteration of motor ability in mutant mice

a The map of mice movement in open field. **b** Quantification of mice speed in the open field (male: ctl=7.6, n=17 mice vs cKO=7.4, n=14; female: ctl=7.1, n=18 mice vs cKO=8.0, n=9, unpaired t test). **c** Quantification of mice distance in the open field. (male: ctl=2645, n=17 mice vs cKO=3066, n=14; female: ctl=2855, n=18 mice vs cKO=3190, n=9, unpaired t-test)

In conclusion, deletion GABA_BR in OPCs disrupt the fine-tuning of inhibitory circuits in the mPFC, leading to cognitive impairment.

7. Discussion

7.1 Selective interneuron apoptosis induced by OPC-derived TWEAK

The TWEAK protein has two isoforms, membrane-bound and cleaved, both are capable of initiating apoptosis in cells by binding to TWEAK receptor (TWEAKR/FN14). Our results demonstrate that GABA_BR-TWEAK apoptotic signaling specifically targets interneurons, suggesting that this process is a highly localized 'kill me' signal. TWEAK is preferentially recruited to synapses that express TWEAKR/FN14 on the neuronal membrane (Cheadle et al. 2020). OPCs sense GABAergic signals via GABA_BRs at the contact site (eg. at the interneuron-OPC synapse). As a result, our work suggests that following signaling events in OPCs, TWEAK synthesis and translocation occur towards the contact site where it can interact with interneuronal TWEAKR/FN14. Another possibility is that the TWEAK ectodomain undergoes proteolytic cleavage, enabling it to function as a soluble factor. This process may also take place at soma-somatic contact sites between OPCs and interneurons (Mangin et al. 2008).

TWEAK can also be derived from microglia. RNA sequencing studies suggest that both OPCs and microglia can express TWEAK during development (Zhang et al. 2014). The impact of microglia-TWEAK on interneurons is unknown. In addition, whether TWEAK release from microglia is compensated by the deletion of the GABA_BR in OPCs needs to be further demonstrated by future studies. Nevertheless, in the pure Oli-neu cell system, a TWEAK receptor inhibitor could rescue the interneuron apoptosis induced by conditioned medium of Oli-neu cells, suggesting that OPC derived TWEAK can induce interneuron apoptosis. Of note, in the mPFC of autism spectrum disorder (ASD) patients, the TWEAK expression in OPCs was reduced, while that in microglia remained unchanged as revealed by the single-cell RNA-seq data (Velmeshev et al. 2019). Whether and how OPC-TWEAK participate in the ASD brain requires further experiments. Our study contributes to our knowledge by providing novel insight for developing potential therapeutic interventions for ASD patients.

GABA_BR is G protein-coupled receptor that negatively regulates adenylate cyclase and the cAMP levels in OPCs (Luyt et al. 2007). This results in decreased transfer of cAMP response element binding protein (CREB) to the nucleus, affecting the expression of various genes that regulate neuronal function, including metabolism and survival, as well as modulation of transcription factors and growth factors (Middei et al. 2013; Tao et al. 1998). G_{βγ} subunits can also activate the phosphatidylinositol-3 kinases (PI3K) pathway, generating phosphatidylinositol (3,4,5)-trisphosphate (PtdIns(3,4,5)P₃) lipid units. This pathway modulates various signaling cascades and perinuclear effectors such as PLC. Yet, it needs to be determined which subunit of G proteins (G_{αi} or G_{βγ}) are involved in GABA_BR mediated TWEAK expression.

7.2 Attenuated cortical inhibition in mutant mice

7.2.1 Potential morphological change of PV interneurons in mutant mice

In the context of neuronal surplus, a reduction in activity is commonly observed (Wang et al. 2021). Our investigation of OPC-GABA_BR cKO mice demonstrated a notable increase in PV interneurons to approximately 125 % of control levels. However, these interneurons exhibited a decrease in immunolabel for vGAT within their presynaptic terminals, indicating a substantial reduction in both GABA release and activity. More precisely, the decrease in vGAT puncta to 75 % corresponds to a reduction of about 60 % for PV interneurons (i.e., 75 % of 125 %). This same reduction was observed in the density of PV⁺cFos⁺ cells (63 %) as well as the frequency of sIPSCs (64 %). Based on these findings, it is plausible that the supernumerary PV interneurons in the cKO mPFC are physiologically less mature (Miyamae et al. 2017). However, these are only speculative ideas and further experiments are necessary to validate them, such as investigating the potential reduction in the number of interneuron axons, the density of dendrites and spines, the diameter of axons, and/or the spacing between dendrites and axons in cKO mice. Chandelier cells (ChCs) are a specialized interneuron subtype that a single ChC can innervate hundreds of pyramidal neurons via its candlesticks-like branches. The maturation of ChCs is performed by dendrites and synapse elimination during development. Recently, it was demonstrated that OPCs participate in the pruning of synapses (Auguste et al. 2022). Hence, the morphology of ChCs is potential to be altered in mutant mice.

7.2.2 The interneurons myelin structure is altered in mutant mice

Our results suggest that the hypomyelination of interneurons is due to a reduction in myelin sheaths encasing interneuronal axons and alteration in paranodal structures in cKO-mPFC mice. These alterations to the paranodal structures have the potential to impede the conduction of action potentials (Arancibia-Carcamo and Attwell 2014). The extension of paranodes is associated with a redistribution of Kv1 channels from under the juxtaparanode towards the paranode in the brains (Arancibia-Carcamo and Attwell 2014). Therefore, these exposed Kv1 channels are more active, ultimately leading to a decline in action potential propagation and synaptic communication. It should be emphasized that the observed morphological deterioration was limited to the mPFC, but not the corpus callosum, which mainly consists of excitatory neuron axons (Fame, MacDonald, and Macklis 2011). Our RT-qPCR data also revealed reduced levels of MBP mRNA expression, but not PLP or MOG, in the mutant mPFC at both postnatal day 14 and 9 weeks of age. Notably, the expression of myelin proteins in inhibitory and excitatory axons varies, with MBP being the primary component of myelin in inhibitory axons (Micheva et al. 2016).

7.3 In OPCs the GABA_BR serves different functions in comparison to the GABA_AR

The loss of the ionotropic GABA type A receptor (GABA_AR) γ 2 subunit in OPCs has been found to reduce the firing rate of presynaptic PV interneurons and result in similar myelin defects

(Benamer et al. 2020). This suggests that both ionotropic and metabotropic GABA receptors can impact PV interneuron activity and myelin gene expression. However, the effects on myelin structures were distinct. Deletion of GABA_AR resulted in prolonged lengths of nodes and internodes with decreased density of paranodes, while deletion of GABA_BR in OPCs only extended the length of paranodes. Additionally, GABA_ARs have been found to aid interneuron maturation in the juvenile somatosensory cortex, while GABA_BRs are involved in the apoptosis of interneurons during development. Both receptors are involved in optimizing the activity of PV interneurons, but employ different mechanisms at different developmental stages.

The primary function of the GABA_AR-γ2 subunit is to preserve the density of OPCs without impacting the formation of oligodendrocytes (Balia, Benamer, and Angulo 2017). Nonetheless, the involvement of GABA_BRs in OPC differentiation is intricate. Our study showed that GABA_BR played a crucial role in oligodendrocyte formation during the early stages of development, but diminishes in later stages. Additionally, an *in vitro* study demonstrated that the activation of GABA_BR with the selective agonist (baclofen) can induce the differentiation of cortical OPCs obtained from newborn pups aged between 0 and 2 days (Serrano-Regal et al. 2022).

7.4 OPCs are the multitasker in brain function

OPCs exhibit heterogeneity and play diverse region-specific roles throughout brain development (Spitzer et al. 2019; Marisca et al. 2020). Interestingly, when OPC somata are located in areas enriched with neuronal somatas, high calcium activity was observed in their processes. But these OPCs are in a "quiescent" state rarely differentiating into oligodendrocytes (Marisca et al. 2020), suggesting OPCs may play other roles in brain circuits instead of oligodendrogenesis. Additionally, OPCs monitor the extracellular K⁺ with their Kir4.1 channels (Maldonado et al. 2013; Timmermann et al. 2021). Given that glial cells, such as microglia, monitor neuronal activity by extending their processes to neuronal somata (Davalos et al. 2005; Nimmerjahn, Kirchhoff, and Helmchen 2005; Cserep et al. 2020), we can hypothesize that OPC may also be involved in this process.

Our data demonstrate that OPCs promote interneuron apoptosis via TWEAK release. Recent evidences suggest that OPCs participate in axon engulfment (Buchanan et al. 2022) or synaptic pruning (Auguste et al. 2022). These findings collectively suggest that OPCs may play a role in neuronal plasticity under physiological conditions. In pathological conditions such as amyotrophic lateral sclerosis (ALS) and chronic stress, the density of OPCs increase along with motor neuron death (Kang et al. 2010) or in the locus coeruleus of rats, respectively (Seifi et al. 2014; Saul et al. 2015). When OPCs are depleted, mice develop a depression-like behavior (Birey et al. 2015), and this was linked to loss of fibroblast growth factor 2, (FGF2) from OPCs (Nagy et al. 2020). Collectively, these findings suggest that OPCs may play a critical role in neuronal plasticity, and alterations in OPC function could potentially lead to neuronal dysfunction.

Moreover, OPCs play a crucial role in the maintenance of the blood-brain barrier (BBB), a physical barrier that separates the brain from the blood circulation and maintains homeostasis

Discussion

within the brain. The initial wave of OPCs originates from $Nkx2.1^+$ progenitors and migrates to the dorsal area along blood vessels (Lepiemme et al. 2022; Tsai et al. 2016). These $Nkx2.1^+$ OPCs are also essential for blood vessel formation during development. A reduction in the number of $Nkx2.1^+$ OPCs leads to a decrease in blood vessel density and branching (Minocha et al. 2015). In addition, OPCs release tumor growth factor β (TGF β), which promotes the expression of tight junction proteins (ZO1) in *vitro* (Seo et al. 2014). Furthermore, transplantation of OPCs into a mouse brain with artery occlusion has been shown to enhance functional angiogenesis and improve neurological outcomes (Wang et al. 2022).

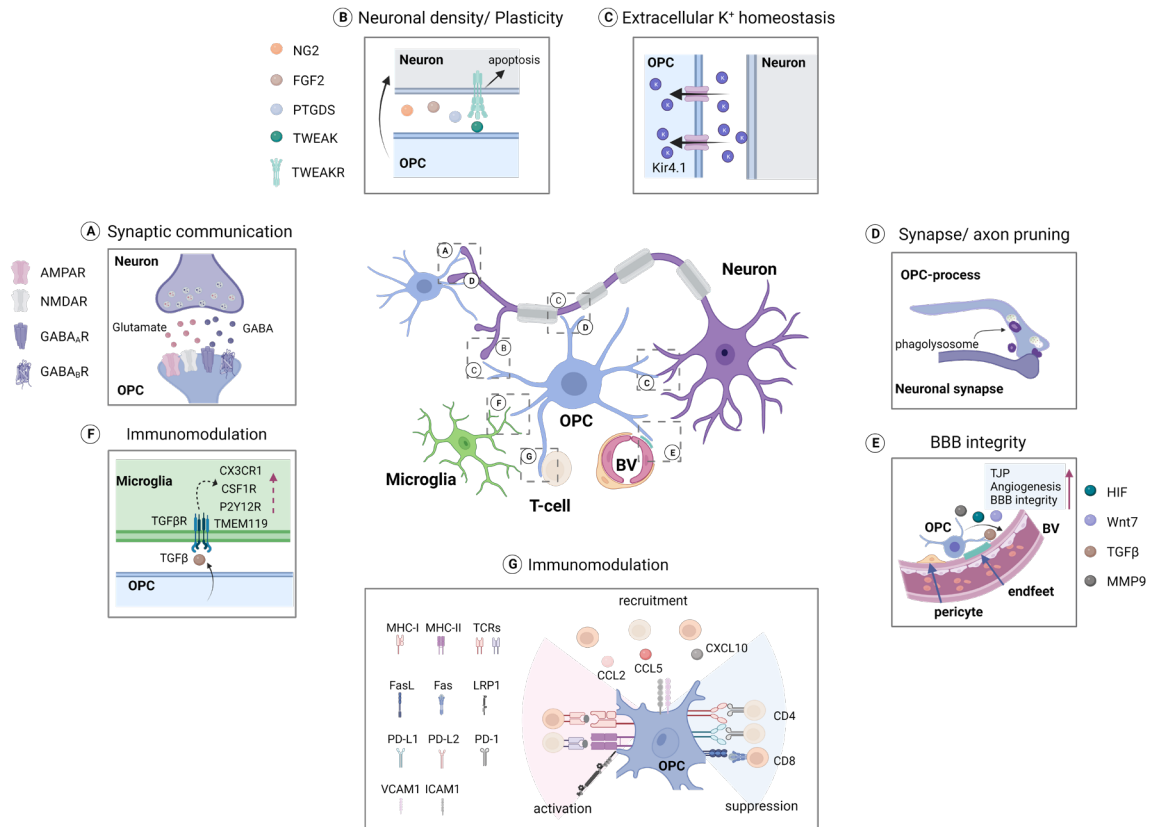


Figure 32. OPCs are the multitaskers during brain function.

A OPCs receive synaptic input from interneurons via glutamate (AMPA_R; NMDAR) and GABA receptors (GABA_AR; GABA_BR). **B** OPC modulate neuronal density and plasticity via releasing TWEAK (TNF Superfamily Member 12), NG2 (chondroitin sulfate proteoglycan 4), FGF2 (Fibroblast growth factor 2), PTGDS (prostaglandin D2 synthase). **C** OPCs monitor extracellular K⁺ with their Kir4.1 channels. **D** OPCs are involved in synapse and axon pruning during development. **E** OPCs participate in BBB integrity by promoting blood vessel formation during development. **F-G** OPCs participate in neuroinflammation. **(F)** OPCs promote microglial immune response through TGF β secreting. **(G)** OPCs recruit T cells via (C-C motif) ligand 2 (CCL2), and are targeted by T cells (CD4/8⁺) by histocompatibility complex class (MHC) I.

Neuroinflammation and neural circuit alterations are commonly observed in many neuropathological conditions. In response to neuroinflammation, OPCs play a crucial role. For instance, OPCs promote CX3CR1-mediated microglial immune response through Tumor growth factor β (TGF β) secreting (Zhang, Wang et al., 2019). Additionally, OPCs recruit T cells

to lesion site via secreting (C-C motif) ligand 2 (CCL2) (Moyon, Dubessy et al., 2015). Moreover, the expression of major histocompatibility complex class (MHC) I in OPCs are targeted by CD8⁺ and CD4⁺ T cells, which inhibiting the differentiation of OPCs, further contributing to neuroinflammation (Falcão, van Bruggen et al., 2018; Kirby, Jin et al., 2019; Zveik, Fainstein et al., 2022) (Reviewed by Cabeza-Fernández et al., 2023).

In summary, OPCs perform multiple functions (Figure. 32) in the brain and represent a promising target for treatment of diverse neurodegenerative diseases.

7.5 The E/I imbalance in mPFC with cognition impairments

The GABA signaling of OPCs is crucial for interneuron myelination, essential for the fine-tuning of local neural circuits (Arancibia-Carcamo et al. 2017). Our study in OPC-GABA_BR cKO mice showed that excessive interneurons in the mPFC resulted in reduced activity and myelination, contributing to cognitive impairment. This was also observed in early socially isolated mice, which experienced a hypomyelination in the mPFC and cognitive decline (Makinodan et al. 2012). The proper E/I ratio in the PFC, especially in the developing mPFC, is essential for social cognition (Grossmann 2013; Bitzenhofer et al. 2021). Enhancing pyramidal neuron activity in the mPFC during early p7-11 caused severe cognitive dysfunction in adulthood (Bitzenhofer et al. 2021). Myelination of cortical interneurons, particularly PV neurons, is crucial for fine-tuning local activity in the mPFC and cortex, ensuring proper behavioral performance (Wang et al. 2021; Maas et al. 2020). It should be noted that the genetic manipulation is not limited to the PFC, and other brain regions may also contribute to the behavioral phenotype, which requires further investigation.

8. CONCLUSION

Our study highlights a non-canonical function of OPCs in brain circuits. During early postnatal weeks, OPCs sense GABA from interneurons via GABA_BRs and release TWEAK to induce interneuron apoptosis. Deletion of GABA_BRs induces survival of super numerous interneurons that exhibited declined activity and hypomyelination, and concomitant impairment of social cognition. (Fang *et al. Nat Communications*, (2022)).

Recent studies have highlighted OPCs are more than precursors (Reviewed by Fang *et al. Pflügers Arch*, 2023, *in press*). When neuronal plasticity is enhanced, OPCs concomitantly turn down the expression of oligodendrocyte transcription factor Olig2 (Fang *et al. Glia*, 2023; Fang *et al. Neural Regen Res*, 2023; see in the appendix) and exhibit rather quiescent feature, i.e. rarely proliferating and differentiating. Human brain organoids represent a promising platform for modeling neural disorders, providing an opportunity to investigate the role of OPCs in greater detail. (Chen *et al., Frontiers in Cellular Neuroscience*, 2020; see in the appendix). Further experiments using human brain organoids can be conducted to explore and validate the contribution of OPCs in shaping brain circuits.

9. Materials and Methods

9.1 Materials

9.1.1 Reagents:

Standard chemicals were purchased from customary companies including Serva, Thermo Fisher Scientific (Karlsruhe), Sigma Aldrich (Taufkirchen), Eppendorf (Hamburg), Merck (Darmstadt), BioRad (München), Invitrogen (Karlsruhe), Roche (Penzberg), Carl Roth (Karlsruhe), Amersham Biosciences (Freiburg), and BD Falcon.

9.1.2 Consumables

Pipette tips (10/200/1000 µl, Sarstedt, Nümbrecht); glass pipettes, VWR International (Darmstadt); RT-PCR-96-well-plates, Axon (Kaiserslautern); 24 well culture plates, Sarstedt (Nümbrecht); 12 well culture plates, Sarstedt (Nümbrecht); 96-well-PCR-reaction-tubes, 4titude (Berlin); object slides, Karl Hecht Glaswarenfabrik (Sondheim); Falcontubes, Greiner Bio-One (Frichenhausen); Cover slips, Menzel-Gläser (Braunschweig); Eppendorf reaction tubes, Eppendorf (Hamburg); Venomix cannulas, Braun (Meksungen)

9.1.3 Kits

Precellys homogenizing tubes, Precellys Ceramic Kit, peqlab (Erlangen);

All prep DNA/RNA Mini and Micro kit, Qiagen (Hilden);

REDExtract-N-Amp™ Tissue PCR Kit, Sigma-Aldrich (Taufkirchen);

Adult Brain Dissociation Kit, Anti-CD140-MicroBead Kit (130-101-502), Anti-NG2- MicroBead Kit (130-097-170) and Anti-O4-MicroBead Kit (130-096-670);

Super Signal West Pico Chemiluminescent Substrate and Pierce BCA Protein Assay Kit, Thermo Scientific (Rockford, USA);

9.1.4 Devices

Table 1: Devices

Device	Producer	City
AxioScan.Z1	Zeiss	Oberkochen
BioSpectrometer	Eppendorf	Hamburg
Centrifuges 5418,5804,5430R	Eppendorf	Hamburg
CFX96 Real-Time PCR Detection System	BioRad	München
Confocal microscope LSM 710	Zeiss	Oberkochen
Electrophoresis power supply	Consort	Turnhout
Gel chambers and supplies for agarose gels	Workshop of the CIPMM	Homburg
Gel chambers for SDS-PAGE	Serva	Heidelberg
IKA MAG HS 7dital (magnetic mixer)	ChemLabz	Benzheim
Infinite PRO 200 microplate reader	Tecan	Crailsheim
Intelli Mixer	neoLab	Hedelburg
PeqSTAR Thermo Cycler	Peqlab Biotechnologie GMBH	Erlangen
Pipettes	Brand	Wertheim
Precellys 24 (Homogenizer)	Peqlab Biotechnologie GMBH	Erlangen
Preparations- and perfusion instruments	F.S.T., Biotechnologie GMBH	Erlangen
Thermomixer comfort	Eppendorf	Hamburg
Vacuum pump	Integra Biosciences	Biebertal
Vibratome VT1000S, VT1200S	Leica	Wetzlar
Western blotting system	Biorad	München
Water facility Milli-Q	Merck	Darmstadt

9.1.5 Antibodies

9.1.5.1 Primary antibodies for immunohistochemistry

Table 2: Primary antibodies for immunohistochemistry

Antibodies	Host	Dilutions	Cat.No.	Company	PRID
PDGFR α	goat	1:500	AF1062	R&D Systems	AB_2236897
adenomatous polyposis coli clone 1(CC1)	mouse	1:200	OP80	Calbiochem	AB_2057371
Olig2	rabbit	1:500	AB9610	Millipore	AB_570666
MBP	mouse	1:500	SMI99	Biolegend	AB_10120130
Parvalbumin	rabbit	1:1000	PV 25	Swant	AB_10000344
Parvalbumin	mouse	1:500	P3088	Sigma	AB_477329
Caspr	rabbit	1:500	ab34151	abcam	AB_869934
DsRed	rabbit	1:1000	632496	Clontec	AB_10013483
BrdU	rat	1:1000	ab6326	abcam	AB_305426
Cleaved Caspase-3	rabbit	1:200	9661	Cell Signaling Technology	AB_2341188
Cleaved Caspase-3	mouse	1:100	STJ9744	St. John's Laboratory	
GAD67	mouse	1:500	MAB5406	Millipore	AB_2278725
NeuN	mouse	1:500	MAB377	Millipore	AB_2298772
CTIP2	rat	1:200	650601	Biolegend	AB_10896795
TBR1	rabbit	1:500,	49661	Cell Signaling Technology	AB_2799364
vGAT	mouse	1:500	13002	Synaptic Systems	AB_887871
FN14	mouse	1:50	314108	Biolegend	AB_2810477

9.1.5.2 Secondary antibodies for immunohistochemistry

Table 3: Secondary antibodies for immunohistochemistry

Antibodies	Fluorophore	Cat. No.	Company
Donkey anti-mouse	Alexa Fluor® 488	A21202	Thermofischer
	Alexa Fluor® 546	A10036	
	Alexa Fluor® 647	A31571	
	DyLight® 755	SA5-10171	Invitrogen
Donkey anti-rabbit	Alexa Fluor® 488	A21206	Thermofischer
	Alexa Fluor® 546	A10040	
	Alexa Fluor® 647	A31573	
	Alexa Fluor® 790	A11374	
Donkey anti-goat	Alexa Fluor® 488	A11055	Thermofischer
	Alexa Fluor® 546	A11056	
	Alexa Fluor® 647	A21447	
	Alexa Fluor® 750	ab175744	abcam
Donkey anti-rat	DyLight-755	SA5-10031	Thermofischer
DAPI (25ng/ml)		A10010010	biochmica

Note: Secondary antibodies were diluted 1:1000 with the blocking buffer.

9.1.5.3 Primary antibodies for Western blot

Table 4: Primary antibodies for Western blot

Antibodies	Host	Dilutions	Cat.No.	Company	PRID
GABA _B R subunit 1	mouse	1:500	ab55051	abcam	AB_941703
GAPDH	mouse	1:2000	G8795	Sigma	AB_1078991
MBP	mouse	1:1000	SMI99	Biolegend	AB_10120130
Tubulin- α	rabbit	1:2000	T6074	Sigma	AB_477582

9.1.6 Primers

Table 5: Primers for genotyping

Name	Serial number		Sequence
Gabbr1	24391	KI	5'-TGGGGTGTGTCTTACATGCAGCGGACGG-3'
Gabbr1	24392	WT	5'-GCTCTTCACCTTTCAACCCAGCCTCAGGCAGGC-3'
tdTomato	27490	KI	5'-GGCATTAAAGCAGCGTATCC-3'
tdTomato	27491	KI	5'-CTGTTCTGTACGGCATGG-3'
tdTomato	27488	WT	5'-AAGGGAGCTGCAGTGGAGTA-3'
tdTomato	27489	WT	5'-CCGAAAATCTGTGGGAAGTC-3'
CSPG4	19398	WT	5'-GGCAAACCCAGAGCCCTGCC-3'
CSPG4	19399	WT	5'-GCTGGAGCTGACAGCGGGTG-3'
CreERT2	19400	KI	5'-GCCCGGACCGACGATGAAGC-3'

Table 6: Primers for qRT-PCR

Name	Type	Sequence
Gabbr1	forward	5'-CGAAGCATTTCCAACATGAC-3'
Gabbr1	reverse	5'-CAAGGCCAGATAGCATCATA-3'
β -actin	forward	5'-CTTCTCCCTGGAGAAGAGC-3'
β -actin	reverse	5'-ATGCCACAGGATTCCATACC-3'
TNF- α	forward	5'-GACGTGGAAGTGGCAGAAGAG-3'
TNF- α	reverse	5'-TTGGTGGTTTGTGAGTGTGAG-3'
TWEAK	forward	5'-CCGCCAGATTGGGGAATTTAC-3'
TWEAK	reverse	5'-AGTCCAAAGTAGGTTAGGAAGGG-3'
FasL	forward	5'-TCCGTGAGTTCACCAACCAAA-3'
FasL	reverse	5'-GGGGGTTCCCTGTAAATGGG-3'
TNFSF7	forward	5'-TGTAGCGGACTACTCAGTAAGC-3'
TNFSF7	reverse	5'-TGGGGTCCTCCGAGGAAC-3'
Trp53	forward	5'-CTCTCCCCCGCAAAGAAAAA-3'
Trp53	reverse	5'-CGGAACATCTCGAAGCGTTTA-3'
NGF	forward	5'-TGATCGGCGTACAGGCAGA-3'
NGF	reverse	5'-GCTGAAGTTTAGTCCAGTGGG-3'

9.2 Animals

9.2.1 Ethics statement

All animal husbandry were conducted at the animal facility of CIPMM, University of Saarland, in accordance with European and German regulations for the protection and welfare of experimental animals. Animal experimental protocols were reviewed and approved by the "Landesamt für Gesundheit und Verbraucherschutz" in Saarbrücken/Germany (with animal license numbers 65/2013, 12/2014, 34/2016, 36/2016 and 08/2021).

9.2.2 Transgenic mice

To induce conditional knockout (cKO) of GABA_B receptor subunit 1 in oligodendrocyte precursor cells (OPCs), TgH(NG2-Cre^{ERT2}) mice (Huang et al. 2014) were bred with GABA_{B1}^{Lox511/lox511} mice (which harbor loxP sites flanking exons 7 and 8 of the *gabbr1* gene) (Haller et al. 2004). Mice with genotypes of NG2^{ct2/wt} x GABA_{B1}R^{fl/fl} were used as cKO, while the littermates NG2^{wt/wt} x GABA_{B1}R^{fl/fl} or NG2^{ct2/wt} x GABA_{B1}R^{wt/wt} were used as controls after tamoxifen administration. To visualize recombined cells, the double transgenic mice were further bred with TgH(Rosa26-CAG-^{fl}STOP^{fl}-tdTomato) mice (Rosa26-tdTomato) (Madisen et al. 2010). For oligodendrocyte-specific deletion of GABA_{B1} subunit, the TgN(PLP-Cre^{ERT2}) mice (Leone et al. 2003) were bred with GABA_{B1}^{lox511/lox511} mice. The PLP^{ct2/wt} x GABA_{B1}R^{fl/fl} mice were used as cKO, while the PLP^{wt/wt} x GABA_{B1}R^{fl/fl} or PLP^{ct2/wt} x GABA_{B1}R^{wt/wt} were used as controls after tamoxifen administration. The ages of the mice used in the experiments are indicated in the main text and figure legends. In all experiments, data from males and females were pooled.

Table 7: Mouse lines

Mouse line	Brief	Reference
TgH (NG2-Cre ^{ERT2})	OPC-specific- Cre ^{ERT2} -driver line	(Huang et al. 2014)
TgN (PLP -Cre ^{ERT2})	Oligodendrocytes-specific- Cre ^{ERT2} -driver line	(Leone et al. 2003)
TgH (Rosa26-CAG- ^{fl} STOP ^{fl} -tdTomato)	tdTomato reporter expression	(Madisen et al. 2010)
TgH (GABA _{B1} R ^{fl/fl})	GABA _B R intervention	(Haller et al. 2004)

9.3 Methods

9.3.1 Genotyping

Mouse tail biopsy was collected at the age of 2-3 weeks and genomic DNA was extracted from the tails using the REDextract-N-Amp PCR KIT with some modifications. The tail tissue was incubated with 62.5 µl of extraction solution (Sigma-Aldrich, T3073) for 10 minutes with agitation. The extraction reaction was terminated by incubation at 95°C for 20 minutes, followed by addition of 50 µl of neutralization solution (3% BSA in PBS). Genotyping PCR was conducted with primers listed in Table 6: Genotyping primers. PCR products were determined by electrophoresis and the gel was documented using the Quantum gel documentation system.

9.3.2 Tamoxifen administration

Tamoxifen dissolved in Miglyol (10mg/ml, 3274, Caesar & Loretz GmbH) was intraperitoneally injected to the mice according to the body weight (100 mg/kg body weight). The time points of injection are indicated in the figures. Only for the pups treated at postnatal day 1 (p1) and 2, tamoxifen was injected to the lactating mother with the same protocol (Huang et al. 2018). For 4-week-old mice, tamoxifen was injected once per day for five consecutive days (Jahn et al. 2018).

9.3.3 Mouse perfusion

Mice were deeply anesthetized with the mixture of Ketamine and Xylacin (Ketamine, 100 mg/ml, Xylacin, 10 mg/ml, in 0.9% NaCl, 100 µl/10 µg body weight). The abdomen was opened from caudal to cranial, up to the sternum, and the peritoneum was incised from medial to lateral. The diaphragm was divided longitudinally, and the pericardium was carefully released from the peritoneum by severing the costal up to the sternum. A butterfly needle was inserted into the left ventricle, and the perfusion was initiated with 1x PBS using a pump. Simultaneously, the superior concave vein was incised, allowing for drainage of blood. The animal was then perfused with 4% paraformaldehyde (FA), following which the brain was removed, post-fixed overnight in 4% FA at 4°C, and stored in PBS the following day.

For RNA, DNA, protein, and magnetic-activated cell sorting (MACS) extraction, the animals were perfused only with cold Hank's balanced salt solution (HBSS, H6648, Gibco). The brains were removed and divided into three regions (cortex, corpus callosum, and medial prefrontal cortex), which were immediately frozen on dry ice and stored at -80°C.

9.3.4 Immunohistochemistry

Free-floating brain slices in 40 µm thickness were prepared in either coronal or sagittal sections using a Leica VT1000S vibratome. For immunocytochemistry, cells on coverslips were fixed with ice-cold 4% PFA for 15 minutes. The slices or coverslips were then incubated with a blocking solution containing 5% horse serum and 0.5% Triton X-100 for 1 hour at room temperature (RT), followed by overnight incubation with primary antibodies at 4°C and 2-hour

incubation with secondary antibodies at RT, both in the blocking solution. The primary and secondary antibodies used are listed in Table 3 and 4, respectively.

9.3.5 Bromodeoxyuridine assay

Adult mice received oral administration of 1 mg/ml bromodeoxyuridine (BrdU) (Sigma-Aldrich, St. Louis, MO) in their drinking water for a duration of seven consecutive days. In the case of juvenile mice, a single dose of 10 mg/ml BrdU dissolved in 0.9% NaCl was administered intraperitoneally to p13 pups and analyzed at p14. BrdU IHC

9.3.6 Magnetic-activated cell sorting (MACS) of OPCs

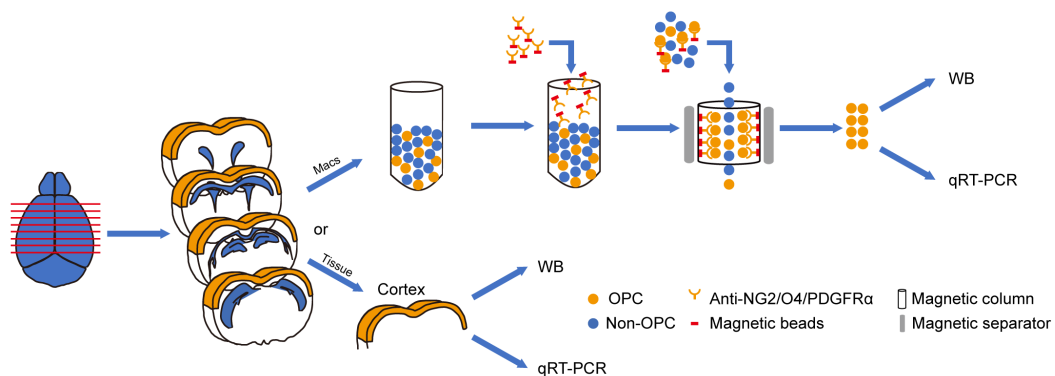


Figure 33. Procedure of Magnetic-activated cell sorting of OPC.

The magnetic-activated cell sorting (MACS) of OPCs was conducted according to the guidelines provided by the manufacturer (Miltenyi Biotec) with slight modifications. Mice were perfused with cold HBSS without calcium and magnesium, and the cortices were dissected in ice-cold HBSS. After debris removal, cells were resuspended with re-expression medium, containing NeuroBrew-21(1:50 in MACS neuro Medium) (130-093-566 and 130-093-570, Miltenyi Biotec), 200 mM L-glutamine (1:50 in MACS neuro Medium), and incubated for 30 minutes at 37°C. Cells were incubated with Fc-receptor blocker for 10 minutes at 4°C, followed by an incubation with mixture of microbeads conjugated to the antibodies of CD140 (130-101-502), NG2 (130-097-170), and O4 (130-096-670) for 15 minutes at 4°C.

For the purity assessment, cells were re-suspended in re-expression medium and seeded on poly-L-lysine (P2533, Sigma) coated coverslip, and incubated for 2 hours at 37°C in 5% CO₂ before being processed for immunocytochemistry against PDGFRα and DAPI.

For quantitative RT-PCR or Western blot analysis, the MACS-sorted OPCs were lysed using RIPA buffer (89900, Thermo Scientific).

9.3.7 Western blot analysis

Tissue Preparation: Samples of different brain regions (cortex, corpus callosum and medial prefrontal cortex) were transferred into Precellys tubes containing 300 or 600 μ L of homogenization buffer or RIPA buffer, both of which were supplemented with 1X protease inhibitors (05892970001 Roche) and 1X phosphatase inhibitors (04906837001, Roche). The homogenate was utilized for the preparation of RNA and protein. The protein concentration was determined using the Pierce BCA Protein Assay Kit and Infinte M 200pro plate reader (Tecan) according to the manual.

Protein Separation: Each protein samples were diluted into a final volume of 20 μ L with dd H₂O and loading buffer containing 2-mercaptoethanol. Proteins were loaded to discontinuous SDS-PAGE gel (SERVAGel™ TG PRiME™ 10%) and Precision Plus Protein™ Dual Color Standard was used as the indicator of molecular weights. The gel was run in a BlueVertical™ PRiME™ chamber (Serva) filled with running buffer at 120 V (50 mA, 150 W) for 90 minutes.

Western Blot and Immunodetection: Proteins were transferred onto polyvinylidene difluoride (PVDF) membrane with semidry blotter (Bioenzym), followed by incubation with blocking buffer (5% milk powder or 5 % BSA in PBS) for 1 hour at room temperature (RT). The membrane was then cut into stripes corresponding to the predicted molecular weight of the analyzed proteins and incubated overnight with primary antibodies in 5 % milk powder in PBS at 4°C. The list of primary antibodies used for Western blot is provided in the Table 5. After washing, the corresponding HRP-conjugated secondary antibody was diluted in TBS-T and applied to the membrane for 2 hours at RT. After additional washing, the membrane was incubated for 2 minutes in enhanced chemiluminescent detection solution (ECL) (541015, Biozym) and documented with ChemiDoc-MP. Protein bands were quantified by densitometric analysis using ImageJ.

9.3.8 Quantitative real time PCR

Brain tissue or MACS-sorted OPCs were homogenized using a previously described method (9.3.6). Total RNA was extracted using the NucleoSpin RNA Plus XS Kit (740990.50, Macherey-Nagel) and reverse transcribed using Omniscript Kit (205113, QIAGEN). Quantitative RT-PCR was then performed using the EvaGreen (27490, Axon) with primers listed in Table 7.

Table 8: Primers for qRT-PCR

Name	type	Sequence
Gabbr1	forward	5'-CGAAGCATTTCCTCAACATGAC-3'
Gabbr1	reverse	5'-CAAGGCCAGATAGCATCATA-3'
β -actin	forward	5'-CTTCTCCCTGGAGAAGAGC-3'
β -actin	reverse	5'-ATGCCACAGGATTCCATACC-3'
TNF- α	forward	5'-GACGTGGAAGTGGCAGAAGAG-3'
TNF- α	reverse	5'-TTGGTGGTTTGTGAGTGTGAG-3'
TWEAK	forward	5'-CCGCCAGATTGGGGAATTTAC-3'
TWEAK	reverse	5'-AGTCCAAAGTAGGTTAGGAAGGG-3'
FasL	forward	5'-TCCGTGAGTTCACCAACCCAAA-3'
FasL	reverse	5'-GGGGGTTCCCTGTAAATGGG-3'
TNFSF7	forward	5'-TGTAGCGGACTACTCAGTAAGC-3'
TNFSF7	reverse	5'-TGGGGTCCTCCGAGGAAC-3'
Trp53	forward	5'-CTCTCCCCCGCAAAGAAAAA-3'
Trp53	reverse	5'-CGGAACATCTCGAAGCGTTTA-3'
NGF	forward	5'-TGATCGGCGTACAGGCAGA-3'
NGF	reverse	5'-GCTGAAGTTTAGTCCAGTGGG-3'

9.3.9 Electrophysiology

Slice Preparation

Mice were anesthetized with isoflurane prior to decapitation and the brain was immediately removed and immersed in an ice-cold, oxygenated cutting solution (NaCl, 87 mM; KCl, 3 mM; Na₂HPO₄, 1.25 mM; NaHCO₃, 25 mM; Glucose, 25 mM; Sucrose, 75 mM; MgCl₂, 3 mM; CaCl₂, 0.5 mM; HEPES, 5 mM, Ph 7.4) with carbogen (5% CO₂/ 95% O₂, pH 7.4). Coronal or semi-sagittal slices (300 μ m thickness) were prepared using a vibratome (Leica VT 1200S, Nussloch, Germany) and transferred to a nylon basket slice holder for incubation in incubating solution (NaCl, 126 mM; KCl, 3 mM; Na₂HPO₄, 1.25 mM; NaHCO₃, 25 mM; glucose, 15 mM; sucrose, 75 mM; MgCl₂, 1 mM; CaCl₂, 2.5 mM; pH 7.4) at 32°C for 30 minutes. Slices were then removed from the water bath and kept at room temperature with continuous oxygenation before use.

IPSCs and EPSCs recordings

Recordings of IPSCs and EPSCs in pyramidal neurons: Semi-sagittal brain slices were transferred to a recording chamber and continuously perfused with oxygenated artificial cerebrospinal fluid (ACSF) containing 1 mM MgCl₂ and 2.5 mM CaCl₂ at a flow rate of 2-5 mL/min. To block inhibitory synaptic transmission during EPSC recordings, 50 μ M strychnine and 50 μ M picrotoxin were added to the ACSF. Pyramidal neurons were morphologically identified using an Axioskop 2 FS mot microscope (Zeiss, Jena, Germany) with a 40x water immersion objective and a QuantEM 512SC camera (Photometrics, Tucson, USA). Whole-cell membrane currents were recorded using an EPC 10 USB amplifier (HEKA, Lambrecht,

Germany), and data acquisition was controlled by Patchmaster software (v2x90.5, HEKA). The signals were low-pass filtered at 3 kHz. Patch pipettes with resistances ranging from 7-9 Ω were prepared from borosilicate capillaries (outer diameter: 1.5 mm; Sutter, USA) using a Micropipette Puller (Model P-97, Sutter Instrument Co., CA). The pipettes were filled with an internal solution containing (in mM): 125 cesium gluconate, 20 tetraethylammonium (TEA), 2 mM $MgCl_2$, 0.5 mM $CaCl_2$, 1 mM EGTA, 10 mM HEPES, and 5 mM Na_2ATP (pH = 7.2). Spontaneous excitatory (sEPSCs) and inhibitory (sIPSCs) postsynaptic currents in pyramidal neurons in the medial prefrontal cortex (mPFC) were recorded for 40 s in voltage-clamp mode, with a holding potential of -70 mV and +30 mV, respectively. Only currents exceeding 10 pA were analyzed using MATLAB.

Whole-cell Patch Clamp Recordings of OPCs

Semi-sagittal slices with a thickness of 300 μm were obtained from mice at postnatal day 11 to 14 (p11-14). To record GABA-A receptor ($GABA_A$ R) currents in OPCs, cells were held at a membrane potential of -70 mV in the whole-cell configuration. GABA (Tocris, 100 μM , 56-12-2) was focally applied to patched OPCs in the presence of CNQX (Tocris, 20 μM , 115066-14-3) and DAP5 (Tocris, 118876-58-7, 30 μM), Non-competitive picrotoxin (Tocris, 50 μM , 83-79-4) and the selective $GABA_A$ R antagonist SR95503 (Tocris, 20 μM , 104104-50-9), were added to the bath solution to verify $GABA_A$ R currents. To record GABAergic spontaneous postsynaptic currents (sPSCs) of OPCs (OPC-sPSC), CNQX (Tocris, 20 μM , 115066-14-3) and DAP5 (Tocris, 118876-58-7, 30 μM) were added to inhibit excitatory signals. To improve the signal-to-noise ratio, a Matlab tool, the Savitzky-Golay filter (Sgolay), was used. This smoothing technique uses a quadratic polynomial fit over each window of the original trace and is particularly effective at fast variations of recorded data. After filtering, currents larger than 1 pA were selected for further analysis. In some experiments, carbachol (Tocris, 50 μM , 51-83-2) was added to stimulate inhibitory neurons.

Compound action potential recordings

The compound action potentials in the corpus callosum were recorded as previously described by Crawford et al. (2009). A micropipette with 1-3 M Ω resistance was filled with ACSF and used to record inward responses elicited by varying the intensity of current-clamp mode stimulus pulses (0.2-4.0 mA) at a distance of 1 mm between recording and stimulation electrodes. The stimulus duration was 200 μs , and sample sweeps were acquired every 5 seconds. The conduction velocity was estimated by changing the distance between recording and stimulation electrodes from 2.5 mm to 0.5 mm with a constant stimulus intensity. To improve the signal-to-noise ratio, at least 15 successive sweeps were averaged. Data analysis was performed using Igor Pro 6.3.7.2 (WaveMetrics, Oregon, USA). The experiments were performed at room temperature (22-24°C).

Data analysis

Data analysis was performed using MATLAB (Mathworks, MA, USA) and custom written routines. The evoked EPSCs and IPSCs were manually checked, and the traces from the same cells were pooled. The average EPSC/IPSC trace from each cell was used for analysis.

Note: The electrophysiology experiments were performed by Dr. Na Zhao.

9.3.10 EEG Telemetry and Analysis

Implantation of telemetric EEG transmitters was performed in mice aged between 8-10 weeks using a procedure adapted from Bedner and colleagues (Bedner et al. 2015). The animals were placed in a stereotaxic frame (Robot Stereotaxic, Neurostar, Tübingen, Germany) and depth electrodes were implanted bilaterally, 3.4 mm posterior to bregma and 1.6 mm from the sagittal suture. After post-operative care, the cages were placed on individual radio receiving plates (DSI PhysioTel® RPC-1, Data Sciences International, St. Paul, USA) for synchronized EEG and video recording (MediaRecorder Software, Noldus Information Technology, Wageningen, Netherlands) for a period of 24 hours. EEG traces were analyzed using the Neuroscore software (Version 3.3.1, Data Sciences International, St. Paul, USA). After applying a 50 Hz band stop Notch filter, relative power band values were determined using an order 13 fast Fourier transform applied in 10-second epochs and then averaged per hour of recording. Statistical analysis was performed using GraphPad Prism 8.0.

Note: The EEG experiments were performed by Dr. Laura C. Caudal.

9.3.11 Behavioral analysis

Behavioral assessments were conducted on a cohort of male and female mice (9 weeks of age). To minimize the potential impact of prior testing on subsequent assessments, the order of testing was arranged in ascending order of invasiveness. Before each behavioral test, the testing chamber or square was thoroughly disinfected with 75 % ethanol to eliminate any residual odors.

9.3.11.1 Nest building test

The nest building test was conducted following the procedure described previously in (Deacon 2006). Mice were housed in individual cages in the behavior testing room for a 24-hour habituation period. A piece of pressed cotton (7x5 cm²) was placed in each cage. After 14 hours, the shape and weight of the cotton were recorded and scored using the criteria outlined in (Deacon 2006).

9.3.11.2 Open field test

The open field test was performed in a square arena in 50 cm (length) x 50 cm (width) x 38 cm (height). Each mouse was placed in the center of the arena and allowed to freely move and explore for 10 minutes, during which their behavior was recorded using a USB webcam and analyzed using EthoVision XT 11.5 (Noldus Technology). The duration of time spent in the center area (seconds), total distance traveled (cm), and average speed (cm/s) were calculated based on the criteria described in (Seibenhener and Wooten 2015).

9.3.11.3 New object recognition test

New object recognition test was performed by placing two identical objects in opposite corners of the apparatus, 8.5 cm from the side walls. Each mouse was allowed to freely explore the objects for 10 minutes. After 40 minutes, one of the objects was replaced with a novel one, and the mouse was again allowed to explore both objects for 10 minutes. The preference index (the sniffing time with object of right or left / total sniffing time with objects) was calculated as the percentage of time spent exploring one of the identical objects, relative to the total time spent exploring both objects. The recognition index was calculated as the percentage of time spent exploring the novel object, relative to the total time spent exploring both objects.

9.3.11.4 Three chamber social behavior test

The three-chamber box was used to evaluate social behavior (Kaidanovich-Beilin et al. 2011). The box is consisted of three equally sized chambers separated by two walls, each with a square door at the bottom center that allowed free movement between chambers. The side chambers contained empty wire cages, while the center chamber was empty. The mice were first habituated to the center chamber for 10 minutes, followed by a 10-minute habituation session with access to all three chambers. During the sociability test, the test mouse was placed in the center chamber, while a familiar mouse was housed under the wire cage in one of the side chambers, and the other side chamber contained an empty cage. The test mouse was then allowed to freely explore all three chambers for 10 minutes. During the social novelty test, a novel mouse was placed under the other empty cage, and the test mouse was again allowed to explore both familiar and novel mice for 10 minutes. The experiment was recorded using a video camera, and the time spent in each chamber and the sniffing time were analyzed.

9.3.12 Cell culture

9.3.12.1 Cell line Oli-neu

The murine OPC cell line Oli-neu (Jung et al. 1995) was kindly provided by Professor Jacqueline Trotter (University of Mainz). The cells were cultured in Sato medium, consisting of DMEM high glucose medium (Fisher Scientific) supplemented with various growth factors and hormones (10 µg/ml transferrin (Sigma), 10 µg/ml insulin (Santa Cruz), 100 µM putrescine (Sigma), 200 nM progesterone (Sigma), 500 nM tri-iodo-thyrodine (Sigma), 220 nM sodium selenite (Sigma), 520 nM L-thyroxine (Sigma) and 1.5 % normal horse serum (Fisher Scientific)), at 37°C and 5% CO₂ in poly-L-lysine (Merck) coated flasks or dishes (Greiner Bio one). For experiments, 2x10⁵ cells were seeded in a 60 mm Petri dish and treated with or without the compound CGP 55845 (50 µM) for 24 hours. The cells were then lysed and analyzed via qRT-PCR. The conditioned medium of control cells was collected for further neuronal treatment.

9.3.12.2 Primary culture of cortical neurons

Primary cortical neurons were isolated from neonatal mice of C57BL/6 strain. The procedure began with the dissection of the cortex from the whole brain using ice-cold Earle's Balanced

Salt Solution (EBSS; Gibco). The cortex was then subjected to enzymatic digestion using 35 units of papain (Worthington, NJ) for 45 minutes at 37°C, followed by gentle mechanical trituration. Subsequently, 1×10^5 cells were seeded on 25 mm glass coverslips in 24-well culture plates for further immunostaining. The glass coverslips were pre-coated with a mixture of coating solution consisting of 17 mM acetic acid, poly-D-Lysine (Sigma, P6407), and collagen I (Gibco, A1048301). The neurons were cultured in a neurobasal (NBA) medium that comprised of 10% fetal calf serum (FCS), 1% penicillin-streptomycin, 1 % GlutaMAX, and 2 % B-27 supplement (Gibco) for 7 days at 37°C in a 5 % CO₂ incubator prior to experimentation.

To investigate the effect of TWEAK on the neurons, the conditioned Oli-neu culture medium supernatant or Sato medium was added to the NBA medium for the neurons, resulting in a 1:2 ratio of the conditioned medium to NBA (1 mL per 24-well and 2 mL per 6-well). The cells were then collected after 6 hours of culture under different conditions, either with or without the TWEAKR inhibitor L524-0366 (Calbiochem, 509374) at a concentration of 20 µM, for further analysis.

Note: The primary neurons culture experiments were performed by Ching-Hsin Lin.

9.3.13 Image acquisition and analysis

Brain slices were imaged using the AxioScan.Z1 fully automated slide scanner (Zeiss, Jena) and the LSM 710 confocal microscope (Zeiss, Jena). Cell counting was performed in a blinded manner using manual techniques with ZEN software (Zeiss, Jena). The lengths of nodes and paranodes were measured using the "Straight" tool in Fiji software. vGAT and myelin volume were analyzed with Imaris software version 9.6.

9.3.14 Electron microscopy

Mice were anesthetized using a ketamine/xylazine solution in 0.9% NaCl (Bayer, Leverkusen, Germany) and subjected to intracardial perfusion with buffered heparin (B. Braun, Melsungen, Germany) at a concentration of 50 IU/mL. The mice were then perfused with a fixative solution of 4 % paraformaldehyde and 0.5 % glutaraldehyde in 0.1M cacodylate buffer and the solutions were cooled gradually from 37 °C to ice-cold temperatures. Whole brains were dissected, immersed in the fixative solution for 24 hours, and stored in 0.1M cacodylate buffer at 4°C for further use.

For vibratome slicing, the brains were embedded in 10 % gelatin and sliced into 500 µm frontal sections using a vibratome (VT1000S, Leica Microsystems, Wetzlar, Germany) at a frequency of 80 Hz and 0.1 mm/s speed. The slices were examined using a mouse brain atlas (Franklin and Paxinos 2007) to determine the regions of interest and particular brain areas (e.g. corpus callosum) were cut out using a scalpel.

The specimens of different brain regions were prepared for electron microscopy (1975) (Glauert 1975). The samples were rinsed in 0.1 M cacodylate buffer, osmicated in 2 % osmium tetroxide in 0.1 M cacodylate buffer for 1 hour, washed in distilled water, and dehydrated in ascending series of ethanol (70 % to 100 %) and acetone (100 %, water-free). The samples

were then embedded in Epon resin (EMS, Hatfield, PA, USA). After polymerization, ultra-thin (65 nm) sections were cut using an ultra-microtome (EM UC7, Leica Microsystems, Wetzlar, Germany). Ultra-thin sections were contrasted with 5 % lead citrate for 5 minutes, examined with a transmission electron microscope (Tecnai G2, FEI, Hillsboro, OR, USA), and randomly selected areas were documented with a digital camera (MegaView III, Olympus, Shinjuku, Japan).

9.4 Statistics

Before statistical analysis, outliers were identified and the Gaussian distribution of the data was tested using GraphPad Prism 8. Statistical differences were reported in the figures and legends. Each data point in the graphs represents a biological individual, unless specified otherwise in the figure legends. The data are presented as the mean \pm SEM, except for violin plots where the median and quartiles are indicated by thick and thin dashed lines, respectively.

Comments of appendix

Throughout the duration of my PhD studies, I have authored and submitted a review (2023) and a perspective (2023) concerning this work (2022) and other associated articles (2023 and 2021). Kindly find them in appendix. As of now, the review is in press and awaits publication, pending its official release.

10. APPENDIX

Fang LP, et al., *Neural Regen Res*, 2023

Perspective

Implications of Olig2 silencing in oligodendrocyte precursor cells

Li-Pao Fang, Xianshu Bai*

Oligodendrocytes (OLs) are the only myelin-forming cells in the central nervous system. Their differentiation from OL precursor cells (OPCs) occurs throughout life and is mediated by numerous intrinsic and extrinsic factors. OL transcription factor 2 (Olig2), a basic helix-loop-helix transcription factor, is one of the intrinsic factors that specify the OL lineage. It is expressed by both OPCs and OLs, and no variant of Olig2 has yet been identified in rodents. Although the function of Olig2 in OL maturation and myelination is still under debate, Olig2 is essential for OPC differentiation in health and disease. Because of its broad expression throughout the OL lineage, Olig2 is often used as a lineage marker. However, in the healthy perinatal and adult brain, a small population of NG2-positive (NG2^{POS}) cells were found to be Olig2-negative (Olig2^{NEG}), and stab wound injury increased the population of NG2^{POS}Olig2^{NEG} cells. NG2 is a protein specifically expressed by OPCs and pericytes in the healthy brain and additionally by microglia after acute brain injury. Therefore, it remained unclear whether these NG2^{POS}Olig2^{NEG} cells are OPCs or other cell types, such as pericytes or microglia? If these cells are OPCs, are they functionally different from the Olig2^{POS} OPCs? By immunostaining for platelet-derived growth factor receptor alpha (PDGFR α), the established marker of OPCs, we confirmed that a subset of OPCs does indeed not express Olig2. This population of OPCs could be detected throughout life, from the embryonic stage (embryonic day 14.5) to the aged mouse (44 weeks old). Fate mapping studies provided strong evidence that Olig2^{NEG} OPCs are derived from pre-existing Olig2^{POS} OPCs (Fang et al., 2023). Therefore, it is conceivable that Olig2^{NEG} OPCs do not represent a separate cell type, but rather a distinct functional stage of OPCs in which Olig2 expression is transiently downregulated in response to microenvironmental changes. In other words, OPCs may dynamically up- and downregulate Olig2 expression in response to changes in brain activity.

Integration of OPCs into local neural circuits:

However, the main question remains: why do OPCs downregulate Olig2 upon changes in brain activity? Are they functionally and physiologically different from Olig2^{POS} OPCs? Olig2 is known to be a pro-differentiating transcription factor for OPCs, accompanied by an increase in morphological complexity with more processes and branches. Indeed, Olig2^{NEG} OPCs are morphologically simpler than Olig2^{POS} OPCs. Therefore, it is tempting to speculate that Olig2^{NEG} OPCs may have less differentiation potential. Olig2 ensures the

differentiation of OPCs into OLs by repressing a number of genes involved in general pathways of neuronal differentiation and brain development (Zhang et al., 2022). OPCs could downregulate or turn off Olig2 expression to maintain their progenitor status. In the adult brain, OPCs are also referred to as NG2 glia (based on the specific expression of the *cspg4* gene encoding NG2), particularly when their acute physiological function is addressed. OPCs receive synaptic inputs and are active components of neural circuits. Notably, Olig2^{NEG} OPCs were enriched in the juvenile brain (approximately 10–26% of total OPCs), but decreased in the adult brain (approximately 1–2% of OPCs). The appearance of Olig2^{NEG} OPCs in the postnatal brain coincided with the development of neuron-OPC connectivity, starting at postnatal days 4–5 and peaking at postnatal day 10 for cortical interneurons (Orduz et al., 2015). In addition, the size of this cell population could be increased by modulation of brain activity, such as acute brain injury or complex motor learning tasks. These observations link neuron-OPC communication to Olig2 silencing in OPCs. Apparently, when neurons are challenged, they increase their firing rate, which could keep OPCs in a progenitor state and feed back to the innervating neuron (Figure 1). Indeed, OPCs could tune the activity of neuronal circuits through several pathways. First, OPCs receive direct γ -aminobutyric acid (GABA)-ergic and glutamatergic input that induces differentiation into OLs and subsequent myelination. As OPCs differentiate, they lose their synapses and reprogram their transcriptional profile, including changes in α -amino-3-hydroxy-

NEURAL REGENERATION RESEARCH
www.nrronline.org

5-methyl-4-isoxazole-propionic acid-type and GABA_A receptors. The GABA_A receptor $\gamma 2$ subunit is expressed exclusively in OPCs, not in OLs, and is essential for interneuron-OPC communication. Its genetic inactivation in OPCs during early postnatal weeks results in attenuated activity and myelination of parvalbumin interneurons (Benamer et al., 2020). Similarly, the L-type voltage-gated calcium channels Cav1.2 and Cav1.3 of OPCs, which facilitate long-term potentiation and N-methyl-D-aspartic acid-mediated long-term depression in the hippocampus, are downregulated in mature OLs (Zhao et al., 2021). In addition, OPCs can set the inhibitory tone in the medial prefrontal cortex by adjusting interneuron density, activity, and myelination. In the first two postnatal weeks, depending on interneuronal GABA release and activation of GABA_A receptors on OPCs, OPCs adjust interneuron density by releasing the weak apoptosis factor TWEAK (tumor necrosis factor-like weak inducer of apoptosis) (Fang et al., 2022). Reduced TWEAK release from GABA_A receptor-deficient OPCs induces an increase in interneuron density but a decrease in interneuron activity and myelination. In addition, OPCs form synapse-like inputs on inhibitory neurons and modulate the network. Using optogenetic stimulation in the juvenile mouse hippocampus, OPCs could be induced to release GABA in a synaptobrevin 2/vascular associated membrane protein 2-dependent mechanism, further demonstrating another pathway of potent OPC-to-interneuron communication (Zhang et al., 2021). Third, OPCs can modulate axonal and cortical development. In the zebrafish optic tectum, ablation of OPCs impairs the arborization of retinal ganglion cell axons (Xiao et al., 2022). In the developing mouse visual cortex, numerous phagolysosomes containing axonal fragments were found in OPC processes, suggesting an involvement of OPCs in axonal pruning (Buchanan et al., 2022). More recently, Auguste et al. (2022) reported

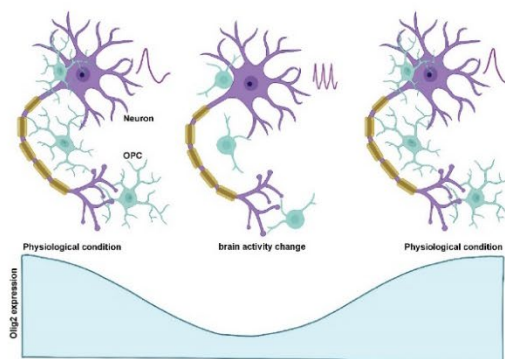


Figure 1 | Dynamic expression of Olig2 in OPCs.

OPCs are innervated into neural circuits by forming pre- and postsynaptic structures with neurons. Changes in brain activity induced by acute brain injury or complex motor learning tasks transiently suppress Olig2 expression in OPCs. Thus, OPCs remain in their progenitor state. Olig2: oligodendrocyte transcription factor 2; OPC: oligodendrocyte precursor cell. Created with BioRender.com.



that OPCs engulf and eliminate thalamocortical synapses in the developing and adult mouse visual cortex, with a beneficial effect on sensory experience during neural circuit refinement. Taken together, OPCs may temporarily shut down Olig2 and regulate various circuit functions as required by brain development and neural network activity. This hypothesis can be tested in the double transgenic Olig2-DsRed × PDGFRα-EGFP mouse line by *in vivo* imaging of DsRed^{pos}EGFP^{pos} cells (indicating Olig2^{pos} OPCs) using two-photon laser scanning microscopy. Accordingly, after acute brain injury, a DsRed^{pos}EGFP^{pos} cell would lose its red fluorescence and transform into a cell expressing only EGFP, i.e., an Olig2^{neg} OPC that could eventually reexpress DsRed and EGFP.

It appears that Olig2^{neg} OPCs are not restricted to the mouse brain. Olig2^{neg} OPCs rarely express Ki67 and exhibit less proliferative properties than Olig2^{pos} cells. Interestingly, single cell transcriptomic studies of zebrafish spinal cord and mouse brain suggest a subset of PDGFRα^{pos} OPCs that appear to lack expression of Olig2 as well as the mitotic marker Ki67. In the zebrafish spinal cord, 'cluster #1' OPCs were also found to be negative for Ki67 and considered to be 'quiescent' OPCs as they lacked proliferation and differentiation-related markers (Marisca et al., 2020). Instead, these cells were enriched for mRNAs involved in axon guidance and synaptic communication and preferentially remained in the progenitor stage. If these are the same cell types, then Olig2^{neg} OPCs may represent these quiescent cells in the mouse brain. However, further studies are needed to determine how Olig2^{neg} OPCs are functionally different from Olig2^{pos} cells, for example by patch-clamp recordings of DsRed^{neg}EGFP^{pos} in Olig2-DsRed × PDGFRα-EGFP mice. The basic electrophysiological properties as well as the postsynaptic current of Olig2^{neg} (DsRed^{neg}EGFP^{pos}) and Olig2^{pos} OPCs (DsRed^{pos}EGFP^{pos}) will be compared after stimulation of neighboring neurons. Furthermore, single cell Patch-Seq analysis of these two cell types will be performed to compare their transcriptomic profiles.

Prospects: Two major questions remain: (1) how do OPCs regulate Olig2 expression, and (2) what is the underlying molecular mechanism? *In silico* analysis of published single-cell RNA sequencing data revealed several differentially expressed genes in Olig2^{pos} and Olig2^{neg} OPCs. In Olig2^{pos} cells, myelination-facilitating factors such as *Mbp* or *Egr2* genes were enriched, while Olig2^{neg} cells were found to express higher levels of the adenosine A1 receptor (*Adora1*), suggesting a putative purinergic signaling pathway involved in Olig2 suppression. Notably, elevated levels of extracellular adenosine has been observed in many neuropathologic context. Alternatively, suppression of the Olig2 gene may be due to

upregulation of bone morphogenetic protein 4 during development and after brain injury. Not only is bone morphogenetic protein 4 known to repress Olig2, but it is also involved in synaptic plasticity. Further studies are needed to fully elucidate the molecular mechanisms by which OPCs regulate Olig2 expression.

Olig2 may participate in the progress of many neurological disorders. Overexpression of Olig2 is observed in disorders of neural development such as Down syndrome and autism spectrum disorder. However, clinical treatment of these disorders targets neurons and the therapeutic effect of such perturbation is still quite limited. The molecular mechanism of OPC function in controlling neural circuits is just beginning to be understood. Additional studies are needed to further elucidate the function and molecular mechanism of Olig2 involved in OPC control of neural circuits. Such studies focusing on myelinating glia would not only provide new insights into the regulation of neural circuits, but also offer alternative ways to modify central brain functions without targeting neurons. In the future, promising therapeutic approaches for neurodevelopmental disorders may be on the horizon.

This work was supported by a NanoBioMed Young Investigator grant from the University of Saarland (to XB).

Li-Pao Fang, Xianshu Bai*

Molecular Physiology, Center for Integrative Physiology and Molecular Medicine, University of Saarland, Homburg, Germany

*Correspondence to: Xianshu Bai, PhD, xianshu.bai@uks.eu.

<https://orcid.org/0000-0002-4758-1645> (Xianshu Bai);

<https://orcid.org/0000-0002-7973-9523> (Li-Pao Fang)

Date of submission: January 17, 2023

Date of decision: March 2, 2023

Date of acceptance: March 7, 2023

Date of web publication: April 10, 2023

<https://doi.org/10.4103/1673-5374.373666>

How to cite this article: Fang LP, Bai X (2023) Implications of Olig2 silencing in oligodendrocyte precursor cells. *Neural Regen Res* 18(12):2649-2650.

Open access statement: This is an open access journal, and articles are distributed under the terms of the Creative Commons AttributionNonCommercial-ShareAlike 4.0 License, which allows others to remix, tweak, and build upon the work non-commercially, as long as appropriate credit is given and the new creations are licensed under the identical terms.

References

- Auguste YSS, Ferro A, Kahng JA, Xavier AM, Dixon JR, Vrudhula U, Nichitiiu AS, Rosado D, Wee TL, Pedmale UV, Cheadle L (2022) Oligodendrocyte precursor cells engulf synapses during circuit remodeling in mice. *Nat Neurosci* 25:1273-1278.

Perspective

- Benamer N, Vidal M, Balia M, Angulo MC (2020) Myelination of parvalbumin interneurons shapes the function of cortical sensory inhibitory circuits. *Nat Commun* 11:5151.
- Buchanan J, Elabbady L, Collman F, Jorstad NL, Bakken TE, Ott C, Glatzer J, Bleckert AA, Bodor AL, Brittain D, Bumbarger DJ, Mahalingam G, Seshamani S, Schneider-Mizell C, Takeno MM, Torres R, Yin W, Hodge RD, Castro M, Dorkenwald S, et al. (2022) Oligodendrocyte precursor cells ingest axons in the mouse neocortex. *Proc Natl Acad Sci U S A* 119:e2202580119.
- Fang LP, Zhao N, Caudal LC, Chang HF, Zhao R, Lin CH, Hainz N, Meier C, Bettler B, Huang W, Scheller A, Kirchhoff F, Bai X (2022) Impaired bidirectional communication between interneurons and oligodendrocyte precursor cells affects social cognitive behavior. *Nat Commun* 13:1394.
- Fang LP, Liu Q, Meyer E, Welle A, Huang W, Scheller A, Kirchhoff F, Bai X (2023) A subset of OPCs do not express Olig2 during development which can be increased in the adult by brain injuries and complex motor learning. *Glia* 71:415-430.
- Marisca R, Hoche T, Agirre E, Hoodless LJ, Barkey W, Auer F, Castelo-Branco G, Czopka T (2020) Functionally distinct subgroups of oligodendrocyte precursor cells integrate neural activity and execute myelin formation. *Nat Neurosci* 23:363-374.
- Orduz D, Maldonado PP, Balia M, Vélez-Fort M, de Sars V, Yanagawa Y, Emiliani V, Angulo MC (2015) Interneurons and oligodendrocyte progenitors form a structured synaptic network in the developing neocortex. *Elife* 4:e06953.
- Xiao Y, Petrucco L, Hoodless LJ, Portuguez R, Czopka T (2022) Oligodendrocyte precursor cells sculpt the visual system by regulating axonal remodeling. *Nat Neurosci* 25:280-284.
- Zhang K, Chen S, Yang Q, Guo S, Chen Q, Liu Z, Li L, Jiang M, Li H, Hu J, Pan X, Deng W, Xiao N, Wang B, Wang ZX, Zhang L, Mo W (2022) The oligodendrocyte transcription factor 2 Olig2 regulates transcriptional repression during myelinogenesis in rodents. *Nat Commun* 13:1423.
- Zhang X, Liu Y, Hong X, Li X, Meshul CK, Moore C, Yang Y, Han Y, Li WG, Qi X, Lou H, Duan S, Xu TL, Tong X (2021) NG2 glia-derived GABA release tunes inhibitory synapses and contributes to stress-induced anxiety. *Nat Commun* 12:5740.
- Zhao N, Huang W, Cătălin B, Scheller A, Kirchhoff F (2021) L-type Ca²⁺ channels of NG2 glia determine proliferation and NMDA receptor-dependent plasticity. *Front Cell Dev Biol* 9:759477.

C-Editors: Zhao M, Liu WJ, Yu J; T-Editor: Jia Y



ARTICLE

<https://doi.org/10.1038/s41467-022-29020-1>

OPEN

Impaired bidirectional communication between interneurons and oligodendrocyte precursor cells affects social cognitive behavior

Li-Pao Fang¹, Na Zhao¹, Laura C. Caudal¹, Hsin-Fang Chang², Renping Zhao³, Ching-Hsin Lin², Nadine Hainz⁴, Carola Meier⁴, Bernhard Bettler⁵, Wenhui Huang¹, Anja Scheller¹, Frank Kirchhoff^{1,6}✉ & Xianshu Bai¹✉

Cortical neural circuits are complex but very precise networks of balanced excitation and inhibition. Yet, the molecular and cellular mechanisms that form the balance are just beginning to emerge. Here, using conditional γ -aminobutyric acid receptor B1- deficient mice we identify a γ -aminobutyric acid/tumor necrosis factor superfamily member 12-mediated bidirectional communication pathway between parvalbumin-positive fast spiking interneurons and oligodendrocyte precursor cells that determines the density and function of interneurons in the developing medial prefrontal cortex. Interruption of the GABAergic signaling to oligodendrocyte precursor cells results in reduced myelination and hypoactivity of interneurons, strong changes of cortical network activities and impaired social cognitive behavior. In conclusion, glial transmitter receptors are pivotal elements in finetuning distinct brain functions.

¹Molecular Physiology, Center for Integrative Physiology and Molecular Medicine (CIPMM), University of Saarland, 66421 Homburg, Germany. ²Cellular Neurophysiology, CIPMM, University of Saarland, 66421 Homburg, Germany. ³Biophysics, CIPMM, University of Saarland, 66421 Homburg, Germany. ⁴Department of Anatomy and Cell Biology, University of Saarland, 66421 Homburg, Germany. ⁵Department of Biomedicine, University of Basel, 4056 Basel, Switzerland. ⁶Experimental Research Center for Normal and Pathological Aging, University of Medicine and Pharmacy of Craiova, 200349 Craiova, Romania. ✉email: frank.kirchhoff@uks.eu; xianshu.bai@uks.eu

The inhibition of cortical network activity is performed by interneurons that release the inhibitory transmitter γ -aminobutyric acid (GABA) which acts on ionotropic GABA_A and metabotropic GABA_B receptors (GABA_BR)^{1,2}. Alterations of interneuron cell density as well as concomitant changes of firing activity are often observed in several neuropsychiatric conditions^{3–6}. In the mouse cortex, higher frequencies of spontaneous inhibitory postsynaptic currents (sIPSCs) were observed after increasing the interneuron density by transplantation of precursor cells⁷. Similarly, blocking of interneuron apoptosis caused a decrease of the excitation/inhibition (E/I) ratio^{6,8}. Interneuron density is a pivotal determinant of correct inhibitory circuits in the central nervous system (CNS). During development, a surplus of interneurons is generated that populates the cortical plate⁹. Subsequently, about 40% of cortical inhibitory neurons are eliminated by programmed cell death during the first two postnatal weeks⁷. One hypothesis links the apoptosis of supernumerary neurons with the onset of first neuron–neuron connections¹⁰. Only the neurons that receive sufficient neurotrophic signals from their target cells will survive^{10,11}.

Oligodendrocyte precursor cells (OPCs) receive synapses from interneurons as early as postnatal day (p) 4–5¹². Concomitantly, the incidence of interneuron apoptosis increases drastically after p5 and reaches its peak at p7⁷. Right after, the interneuron–OPC connectivity accelerates till p10, which drives an immediate oligodendrocyte (OL) boom with subsequent myelination of interneurons regulated by OPC–GABA_A and GABA_B receptors^{13–15}. Despite relatively short axons, myelination of cortical interneurons (mainly parvalbumin (PV)⁺ fast-spiking interneurons¹⁶) contributes significantly to the fine-tuning of local activity in the cortex, including the medial prefrontal cortex (mPFC), ensuring correct behavioral performance^{4,17}. However, how the early communication between interneurons and OPC affects inhibitory network activity still remains unknown.

To assess the function of OPC GABA_BRs for cortical inhibition, we conditionally deleted the GABA_B receptor subunit *gabbr1* selectively in OPCs at the end of the first postnatal week. Focusing on the mPFC, we found that OPCs shape the inhibitory network by GABA_B receptors and the cytokine tumor necrosis factor-like weak inducer of apoptosis (TWEAK) signaling pathways, thereby regulating interneuron cell death and survival as well as its myelination onset. The functional and morphological changes of PV⁺ interneurons observed in the adult mPFC of mutant mice resulted in reduced inhibitory tone, which finally caused impaired cognition and perturbed social behavior.

Results

GABA_BRs of OPCs are required for oligodendrogenesis in the mPFC. To assess the function of GABA_BRs for OPC–interneuron communication, we generated Tg(NG2-CreERT²):GABA_{B1}R^{fl/fl} mice (Fig. 1a) to conditionally knockout (cKO) GABA_BR from OPCs and their progeny. We induced the cKO at postnatal day 7 and 8 (p7/8) (Fig. 1a) before the onset of OL formation at p10–11¹³. When analyzed at the age of 9 weeks (w), about 76% of OPCs (platelet-derived growth factor receptor α^+ (PDGFR α^+ , Pa $^+$)) were found reporter recombined in the cKO medial prefrontal cortex (mPFC), based on tdTomato (tdT) gene expression (Pa $^+$ tdT $^+$ /Pa $^+$, Fig. 1b, c).

To confirm and quantify the deletion of GABA_BR in OPCs, we performed Western blot analysis with OPCs purified by magnetic-activated cell sorting (MACs, Supplementary Fig. 1a). In cKO OPCs, GABA_BR expression was reduced by about 64.2% compared to controls (ctl) (Fig. 1d). Considering the substantial purity of MACs OPCs (85%, Supplementary Fig. 1b) and recombination efficiency (80%, Fig. 1c), we concluded that a vast majority of GABA_BRs had been ablated from OPCs. In addition,

as suggested by the previous study¹⁸, the reporter recombination efficiency (76%) faithfully indicated the extent of GABA_{B1} deletion in our mice (64.2%/85% (MACs–OPC purity) = 75.5% of GABA_{B1} ablation).

Next, we focused on the oligodendrocyte lineage and evaluated the contribution of GABA_BRs for OPC differentiation in the mPFC by immunostaining of PDGFR α , CC1 and Olig2 (Fig. 1e), established markers for OPCs, OLs and the whole lineage, respectively. In cKO mice, the density of OPCs (PDGFR α^+ Olig2 $^+$) did not change (Fig. 1f), while that of mature OLs (CC1 $^+$ Olig2 $^+$) was strongly reduced by 26% (Fig. 1g, 8.3 to 6.1 cells/ 1×10^{-3} mm³), indicative of decreased OPC differentiation to OLs (Fig. 1h). A similar reduction was observed in the primary motor cortex (MOp) (Supplementary Fig. 2a), where OPC–GABA_BR deletion induced a decrease of OL density without affecting the OPC population (Supplementary Fig. 2). Notably, in the corpus callosum the densities of OLs and OPCs, as well as their relative proportions did not differ between ctl and cKO mice (Fig. 1f–h, Supplementary Fig. 3). These data suggested that OPC–GABA_BRs were involved in OPC differentiation in gray matter regions such as mPFC and MOp, but not in the white matter corpus callosum.

We further analyzed structural aspects of myelination with impact on axonal conductivity, i.e., the lengths of nodes (the non-insulated gaps between paired contactin-associated protein-positive (Caspr $^+$) segments) or paranodes (single Caspr $^+$ segments indicating uncompacted myelin lamellae), by immunostaining (Fig. 1i). In cKO mPFC, the paranodal length was increased by 17% (Fig. 1j, Supplementary Fig. 4a–c) while the density and the uninsulated length of nodes were not affected (Supplementary Fig. 4d–f). In parallel, we observed a reduction of myelin basic protein (MBP) expression at mRNA (Supplementary Fig. 4g) and protein levels (Fig. 1k) in cKO mPFC, while the mRNA levels of other myelin proteins such as proteolipid protein (PLP) and myelin oligodendrocyte glycoprotein (MOG) were not changed (Supplementary Fig. 4g). Although we had observed an impaired OPC differentiation in MOp (Supplementary Fig. 2), the length and density of paranodes and nodes as well as the MBP expression were unaffected in the mutant mice (Supplementary Fig. 4h–o). Similarly, in the corpus callosum, myelination was unperturbed as indicated by unchanged paranode length and density (Supplementary Fig. 5a–e) or MBP expression (Fig. 1k). Thereby, our data showed that OPC–GABA_BRs were involved in organizing nodal structures of OLs in the mPFC, but not in the MOp or corpus callosum.

Since OPCs continuously differentiate^{19–21}, cKO mice will also have OLs lacking GABA_BRs. To evaluate the cell-specific role of GABA_BR and to distinguish between OPCs and mature OLs, we selectively targeted OLs using TgN(PLP-Cre^{ERT2}):GABA_{B1}R^{fl/fl} mice (Supplementary Fig. 6a). The gene deletion was induced by tamoxifen injections either at p7/8 or at 4w (Supplementary Fig. 6b). At the age of 9w, we did not observe differences in the OPC and OL population between ctl and cKO mice (Supplementary Fig. 6c–f), neither in the mPFC nor in the corpus callosum. In addition, MBP expression was not altered neither in mPFC nor in corpus callosum (Supplementary Fig. 6g). These data suggested that the phenotypic changes observed in OPC–GABA_BR cKO mice resulted from the functional loss of GABA_BRs in OPCs rather than OLs.

In summary, our data strongly suggest that GABA_BR was specifically required for early OPC differentiation and subsequent myelination in the mPFC, but not in the MOp or corpus callosum.

Increased density of PV neurons with deteriorated myelination in cKO mPFC. Since callosal axons are primarily excitatory²² and

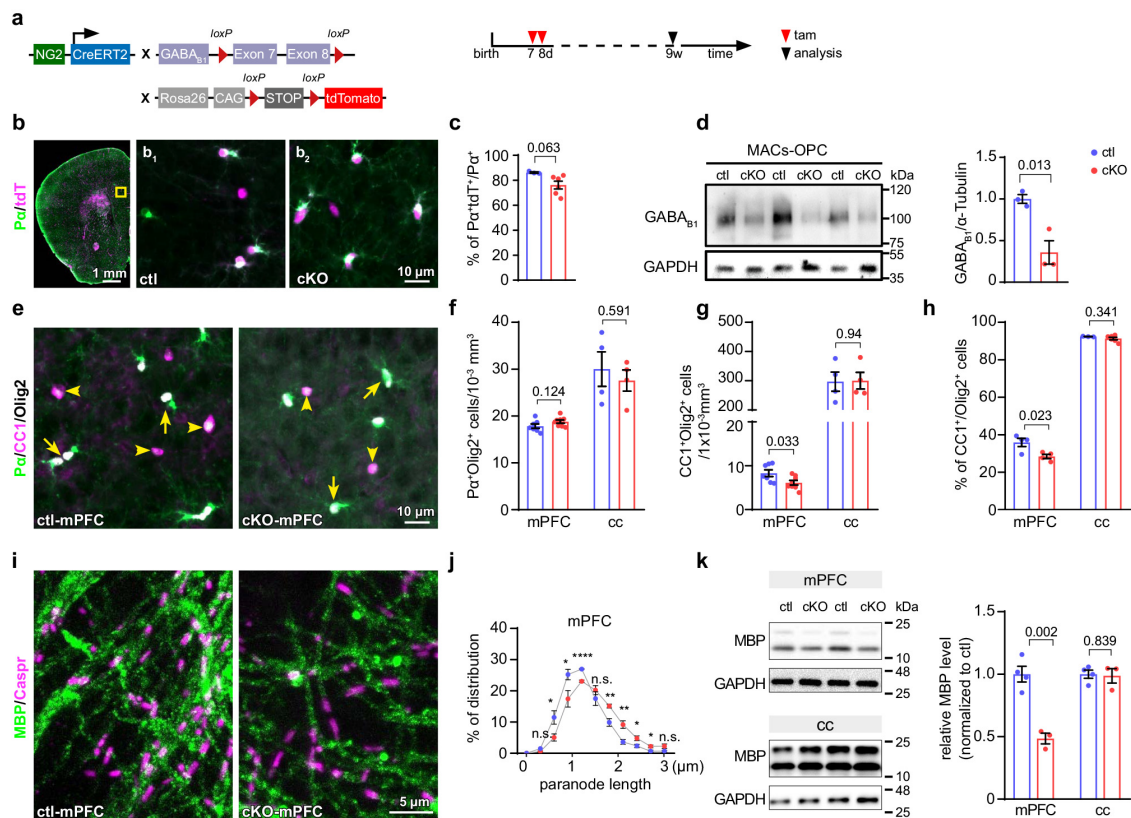


Fig. 1 Ablation of $GABA_B$ Rs in OPCs attenuates oligodendrocyte differentiation and alters myelination in the medial prefrontal cortex. **a** Mouse line and experimental schedule for OPC-specific and temporal control of $GABA_B$ deletion. **b** Coronal section of the prefrontal cortex immune-stained for PDGFR α (P α , green). Expression of tdTomato⁺ (tdT⁺, magenta) indicates recombined cells. **b₁**, **b₂** Magnified micrographs of medial prefrontal cortex (mPFC, highlighted in **b**) of control (ctl) and conditional knockout (cKO) mice. **c** Recombination efficiency of OPCs in ctl and cKO mPFC. (ctl = 3 mice, cKO = 6 mice, two-sided unpaired *t*-test). **d** Western blot analysis of $GABA_B$ subunit 1 in magnetic-activated cell sorted (MACs) OPCs from cortex. (ctl = 3 mice, cKO = 3 mice, two-sided unpaired *t*-test). **e** Olig2 (white), P α (green) and CC1 (magenta) immunostaining in adult ctl and cKO mPFC. **f**, **g** Quantification of OPC and oligodendrocyte (OL) densities in mPFC and corpus callosum (cc). (mPFC: ctl = 7 mice, cKO = 8 mice; cc: ctl = 4 mice, cKO = 4 mice, two-sided unpaired *t*-tests). **h** Quantification of the OL proportion among the total lineage (mPFC: ctl = 4 mice, cKO = 4 mice; cc: ctl = 3 mice, cKO = 6 mice, two-sided unpaired *t*-tests). **i** Immunostaining of Caspr (magenta) and MBP (green) in ctl and cKO mPFC. **j** Quantitative analysis of paranode length in mPFC (ctl = 4 mice, cKO = 4 mice, two-sided unpaired *t*-tests: *p* = 0.193 (n.s.), 0.038 (*), 0.048 (*), 7.67E-05 (****), 0.34 (n.s.), 0.009 (**), 0.008 (**), 0.044 (*), 0.03 (*), 0.092 (n.s.), respectively). **k** Western blot analysis of MBP expression in mPFC and cc. (ctl = 4 mice, cKO = 3 mice, two-sided unpaired *t*-tests). Data are shown as mean \pm SEM in **c**, **d**, **f**, **j** and **k**. Source data are provided as a Source Data file.

axons of inhibitory interneurons are largely restricted to cortical areas of the same hemisphere (including mPFC, Fig. 2a–c), we hypothesized that the observed myelin deficits were restricted to mPFC interneurons. Parvalbumin (PV)⁺ interneurons, the fast-spiking interneurons, are the most abundantly myelinated interneurons of the cortex^{16,23–25}. These neurons are most prominent at layers IV and V with a majority of their axons projecting to layers II/III and V²⁶. To evaluate their myelination, we performed PV, neurofilament (SMI 312, pan axonal marker) and MOG triple immunostaining (Fig. 2d). We volume-rendered the MOG immunolabel as indicator of myelin sheaths and normalized the volume of MOG⁺ fragments that covered the PV⁺ axons (PV⁺SMI 312⁺) to the total volume of PV⁺ axons at the cortical layers II/III of mPFC. Indeed, the volume of myelin sheaths wrapping PV axons was reduced by 60% in the cKO mPFC (Fig. 2e). However, the total volume of MOG immunolabel covering all SMI 312⁺ axons was not affected (Fig. 2e), in agreement with the unchanged MOG mRNA levels in control and

mutant mice (Supplementary Fig. 4g). Also the myelination of excitatory neurons (in the corpus callosum) was not affected as indicated by an unaltered g-ratio (the ratio between the inner and the outer diameter of the myelin sheath) or unchanged conduction velocity of compound action potentials (Supplementary Fig. 5f–i). Thus, we concluded that $GABA_B$ of OPCs were preferentially involved in the myelination of inhibitory rather than excitatory neurons.

While investigating the interneuronal myelination, we recognized that early ablation of $GABA_B$ R in OPCs was associated with a 25% increase of interneuron density (Fig. 2f, g, 24.3 to 30.5 cells/ 1×10^{-3} mm³) in the adult mPFC as revealed by immunostaining for PV (Fig. 2f). A detailed analysis of PV neuron density in three sub-regions of the mPFC (layer I, layer II/III and layer V/VI, Fig. 2f, g) showed a general overpopulation of PV interneurons in all cortical layers of the adult mPFC. However, the proportion of PV⁺SMI 312⁺ axons to all axons in layer II/III was identical between the cKO and ctl groups (Fig. 2h). These data suggested a

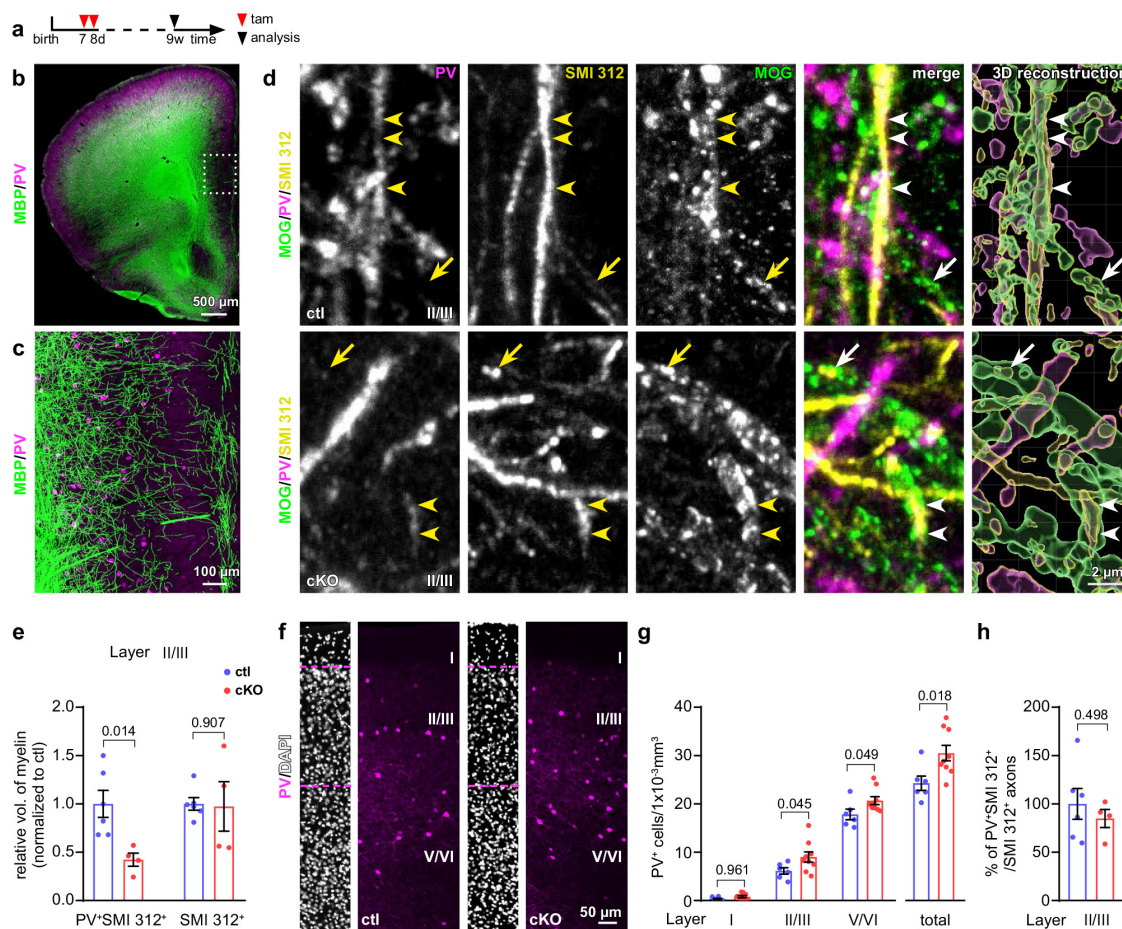


Fig. 2 Reduced myelination and increased cell density of interneurons in OPC-GABA_B cKO mice. **a** Experimental schedule. **b, c** Overview of coronal brain slices immunostained for parvalbumin (PV, magenta) and MBP (green). PV⁺ neurons are abundantly myelinated in the mPFC. **d** Magnified micrographs of myelinated PV axons immunostained for PV (magenta), neurofilament (with SMI 312 antibody, yellow) and myelin-oligodendrocyte glycoprotein (MOG, green) in layers II/III (II/III) *ctl* and *cKO*. The 3D reconstruction was performed using Imaris. Arrows: myelinated PV+SMI 312⁺ axons; arrowheads: myelinated PV+SMI 312⁺ axons. **e** Relative volume of MOG immunolabel around PV⁺ axons (PV+SMI 312⁺) and total axons (SMI 312⁺) (normalized to *ctl*) (*ctl* = 6 mice, *cKO* = 4 mice, two-sided unpaired *t*-tests). Immunostaining (**f**) and quantification (**g**) of PV⁺ interneurons in different layers of mPFC at the age of 9 weeks (*ctl* = 6 mice, *cKO* = 9 mice; two-way Anova, Sidak's multiple comparison for different layers; two-sided unpaired *t*-tests for total). **h** Ratio of PV⁺ interneuron axons to all axons. (*ctl* = 6 mice, *cKO* = 4 mice, two-sided unpaired *t*-test). Data are shown as mean \pm SEM in **e, g** and **h**. Source data are provided as a Source Data file.

potential morphological changes of PV axons, e.g., thinner axonal caliber and/or shortened axons in the *cKO* mPFC.

Together, our results demonstrated that OPC-GABA_BR were essential for the correct cell density and myelination of interneurons in the mPFC.

Surplus of interneurons display suppressed activity in the *cKO* mPFC. To investigate the impact of the supernumerous interneurons detected in the mutant mPFC for the local network activity, we recorded spontaneous inhibitory postsynaptic currents (sIPSCs) and sEPSCs of the pyramidal neurons in layer V of the mPFC (Fig. 3a, b), where interneurons are abundantly located (Fig. 2f, g). In contrast to our expectation, the increase of PV interneuron density did not result in a concomitant increase of inhibitory input. In contrast, the frequency of sIPSCs was reduced by 40% (Fig. 3c) while simultaneously the amplitude of sIPSCs

remained unaffected in the mutant mPFC (Fig. 3d), as well as the firing rate and amplitude of sEPSCs (Fig. 3e, f).

Neuronal activity can regulate myelination^{23,27}. Therefore, considering the attenuated interneuron myelination and decreased inhibitory tone in the *cKO* mPFC, we asked whether such morphological and physiological changes could already be initiated during early development and before myelination onset at p14 in mPFC (Supplementary Fig. 7). To answer this question, we assessed the density of the vesicular GABA transporter (vGAT) (Fig. 3g, h) as a readout of inhibitory neuron activity²⁸. Indeed, already at p10, i.e., only 3 days after the first tamoxifen injection, the density and the volume of vGAT immunopuncta were reduced to 75% in the *cKO* mPFC (55.4 to 41.8 puncta/ $1 \times 10^{-3} \text{mm}^3$ and 1.42 to 1.05 μm^3 , respectively) (Fig. 3h–j, Supplementary Fig. 8a–d), suggesting a reduced interneuron activity in the *cKO* mPFC. Since the expression of immediate early genes has been correlated with the electrical activity of

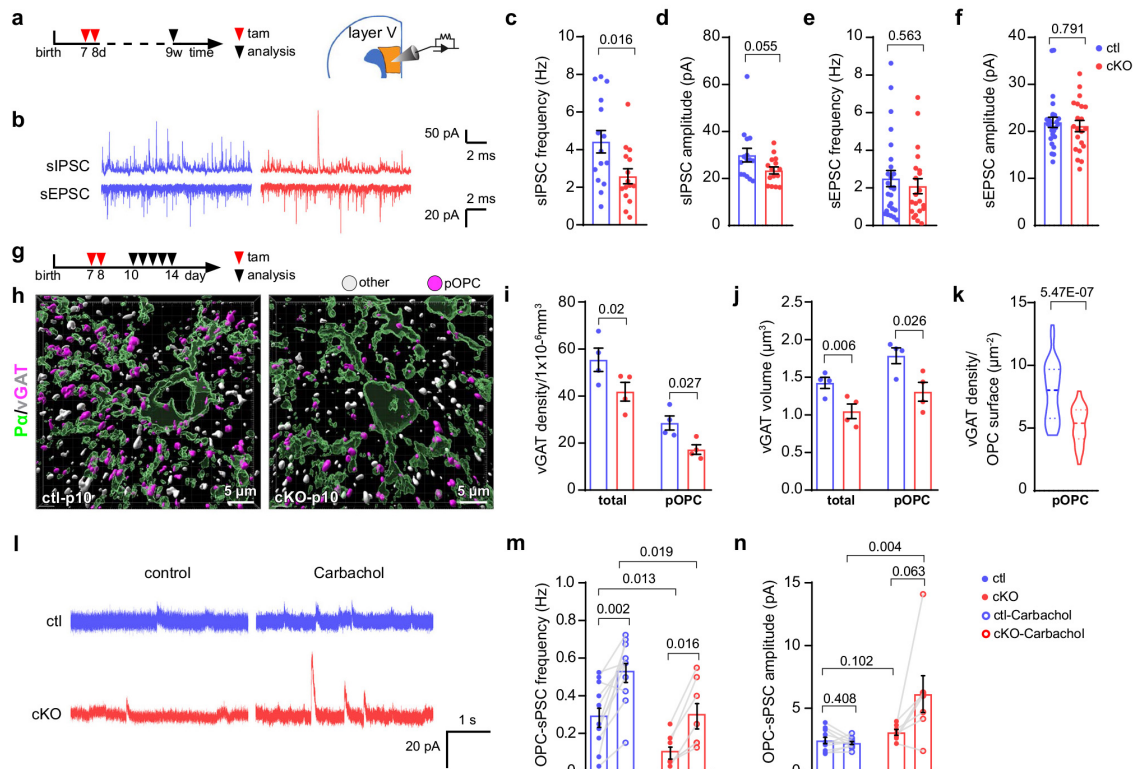


Fig. 3 Interneuron activity is impaired in the mPFC of OPC-GABA_B cKO mice. **a** Experimental schedule for **b–f** and the scheme of analyzed brain region (orange). **b** Patch-clamp recordings of sIPSCs and sEPSCs in pyramidal neurons of layer V of medial prefrontal cortex (mPFC). **c–f** Quantification of frequencies and amplitudes of spontaneous inhibitory and excitatory postsynaptic currents (sIPSC and sEPSC, respectively) (sIPSC: ctl = 15 cells from 4 mice, cKO = 15 cells from 5 mice; sEPSC: ctl = 26 cells from 4 mice, cKO = 21 cells from 5 mice; sIPSC frequency was analyzed with two-sided unpaired *t*-test, **d–f**: two-sided unpaired Mann–Whitney test). **g** Experimental schedule for **h–n**. **h** Surface renderings of OPCs and inhibitory presynapses based on PDGFR α (P α , green) and vGAT (vesicular GABA transporter, white and magenta) immunostaining in ctl and cKO mPFC at p10 using Imaris software. vGAT was classified into two subgroups: on putative OPC synapses (pOPC, magenta vGATs with less than 200 nm distance from the OPC surface) and other synapses (other, gray vGATs more than 200 nm). Density (**i**) and volume (**j**) of vGAT in ctl and cKO mPFC. (ctl = 4 mice, cKO = 4 mice; two-sided unpaired *t*-tests). **k** Quantification of synaptic vGAT (<200 nm) density per μm^2 of OPC surface. (ctl = 4 mice, cKO = 4 mice, two-sided unpaired *t*-tests). **l** Patch-clamp recordings of spontaneous postsynaptic currents (sPSCs) of OPCs at the layer V of mPFC at p11–14. **m, n** Quantification of sPSC frequency and amplitude of OPCs before and after addition of carbachol. (ctl = 11 cells from 3 mice, cKO = 7 cells from 3 mice, two-sided unpaired *t*-tests). Data are shown as mean \pm SEM in **c–f, i, j, m** and **n**. In **k**, data are shown with indications of median and quartiles in thick and thin dashed lines, respectively. Source data are provided as a Source Data file.

neurons^{29,30}, we investigated the expression of cFos in PV interneurons at p10 and p14. Although at p10, we observed already a reduction of vGAT in the cKO mPFC (Fig. 3i, j), the proportions of PV⁺cFos⁺ cells were comparable in the cKO and ctl mPFC (Supplementary Fig. 8f). However, at p14, the density and the percentage of PV⁺ interneurons with cFos expression was reduced by 60–75% in the cKO mPFC (0.35 to 0.14 PV⁺cFos⁺ cells/ $1 \times 10^{-3} \text{ mm}^3$; 4.4% to 1.1% PV⁺cFos⁺/PV⁺ cells; Supplementary Fig. 8g). These results suggested that the activity of inhibitory neurons was impaired in the cKO mPFC during development.

To demonstrate whether such a change of interneuron activity could affect GABAergic communication between interneurons and OPCs, we further analyzed the vGAT density on OPCs. For that purpose, we classified the puncta of the vGAT immunolabel into two subgroups based on the distance between the vGAT label and the OPC surface using the image analysis software Imaris (Fig. 3h). We defined the vGAT puncta with a ‘distance < 200 nm’ as vesicles to be potentially released to OPCs (magenta, pOPCs),

and vGAT puncta with a ‘distance > 200 nm’ as vesicles targeted to other cells (gray, other cells), based on the assumption of about 270 nm as the distance of presynaptic vGAT and postsynaptic GABA_AR/gephyrin³¹. The density and the volume of vGAT immunolabel close to OPCs were decreased (Fig. 3i, j), including less puncta at the OPC surface in cKO mPFC (Fig. 3k), suggesting a reduction of GABAergic input to OPCs in the cKO mPFC. To confirm this observation, we took advantage of the GABA_A receptor expression (in addition to GABA_BR) of OPCs and evaluated the frequency of spontaneous GABAergic currents in OPCs (OPC-sPSC) of p11–14 mice (Fig. 3l). Our results showed that the OPC-sPSC frequency was reduced by about 64% (0.3 to 0.1 Hz) in the cKO mPFC (Fig. 3m), while the amplitude remained unaffected (Fig. 3n), indicating OPCs receive less GABAergic signals in the mutant mouse brain. In this context, it is important to remind that GABAergic currents of OPCs are depolarizing (due to high intracellular Cl⁻) with the potential to activate voltage-gated Ca²⁺ channels in OPCs^{32,33}. In addition, we increased the neuronal firing by muscarinic stimulation

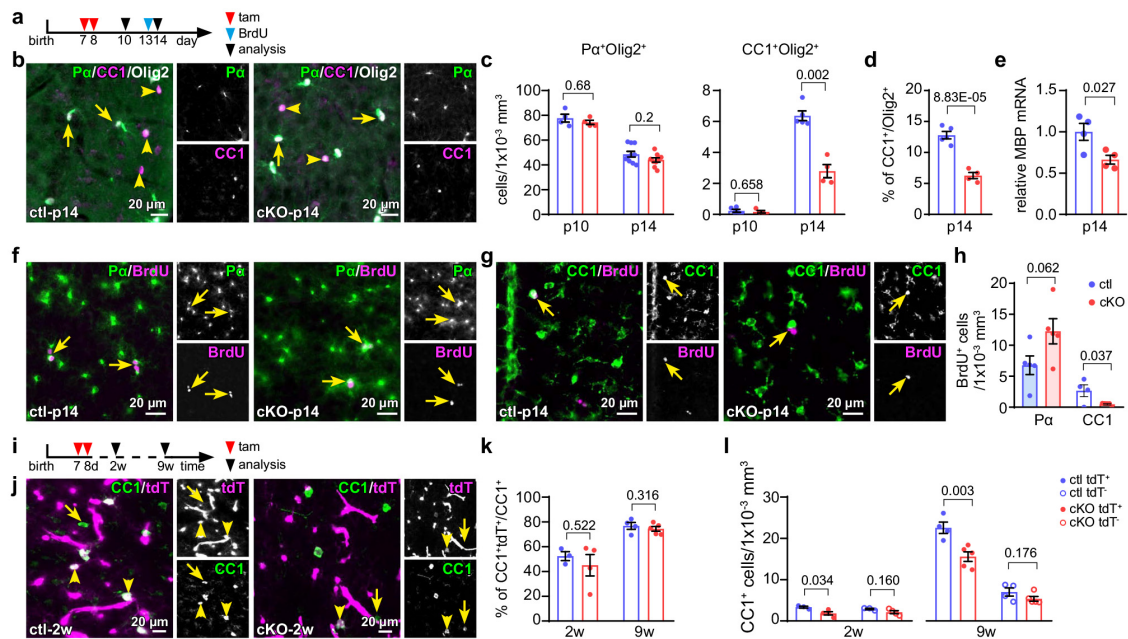


Fig. 4 Reduced oligodendrocyte differentiation and myelin gene expression at the onset of myelination in the mutant mPFC. **a** Experimental plan. **b** Immunostaining of OPCs and oligodendrocytes (OLs) for PDGFR α (P α , green), Olig2 (white) and CC1 (magenta) in p14 medial prefrontal cortex (mPFC). **c** Density of OPCs and OLs in ctl and cKO mPFC at p10 and p14. (OPC: p10: ctl = 4 mice, cKO = 4 mice; p14: ctl = 10 mice, cKO = 9 mice; OL: p10: ctl = 5 mice, cKO = 4 mice; p14: ctl = 5 mice, cKO = 4 mice, two-sided unpaired *t*-tests). **d** Percentage of OLs of the complete lineage at p14 (ctl = 5 mice, cKO = 4 mice, two-sided unpaired *t*-tests). **e** Quantitative analysis of MBP mRNA level in ctl and cKO mPFC at p14. (ctl = 4 mice, cKO = 4 mice, two-sided unpaired *t*-test). **f, g** Immunostaining of OPCs (P α , green in **f**) and OLGs (CC1, green in **g**) incorporated with BrdU (magenta). (OPC: ctl = 5 mice, cKO = 5 mice, two-sided unpaired *t*-test; OL: ctl = 4 mice, cKO = 5 mice, two-sided unpaired *t*-test). **i** Experimental design of **j-l**. **j** Immunostaining of OLGs (CC1, green) combined with tdTomato (tdT, magenta) expression in the mPFC at 2w. **k** Recombination efficiency of OLGs. (2w: ctl = 3 mice, cKO = 4 mice, two-sided unpaired *t*-test; 9w: ctl = 4 mice, cKO = 5 mice, two-sided unpaired *t*-test). **l** Comparison of recombined and non-recombined OLG densities (with or without tdT expression). (2w: ctl = 3 mice, cKO = 4 mice, two-sided unpaired *t*-tests; 9w: ctl = 4 mice, cKO = 5 mice, two-sided unpaired *t*-tests). Data are shown as mean \pm SEM in **c-e**, **h**, **k** and **l**. Source data are provided as a Source Data file.

using carbachol³⁴ and observed a rise in OPC-sPSC frequency (Fig. 3l, m). Also under these conditions, we still recorded a 40% lower frequency in the cKO OPCs. In addition, with carbachol treatment, we observed more variability of slightly higher current amplitudes in cKO OPC (Fig. 3n), which we attributed to putative changes of vesicle loading upon presynaptic muscarinic stimulation. Since the current amplitudes evoked by application of GABA were unperturbed in the cKO OPCs (Supplementary Fig. 8e), the expression of GABA_A receptors appeared unaffected by the GABA_BR ablation. Therefore, our data strongly suggested an impairment of interneuron activity in the mutant mouse mPFC.

In summary, we concluded that interneurons exhibit lower activity and transmit less GABAergic signals to OPCs in the cKO mPFC during development.

Decreased OPC differentiation in the cKO mPFC during development. Next, we asked whether the reduced inhibitory tone could contribute to the observed changes in OPC differentiation and whether it could correlate with the onset of myelination specifically. For that purpose, we compared the densities of OPCs and OLs populations at p10 and p14 (Fig. 4a-c). At p10, the densities of both were still comparable in the cKO and ctl mPFC. However, at p14, the differentiation and cell numbers of OLs dropped strongly in the mutant mPFC (Fig. 4c, d), as did the MBP expression (Fig. 4e). As the PV/cFos immunostaining

results had shown, the interneuron activities of the cKO mPFC was still comparable to the ctl mPFC at p10 while it was suppressed at p14 (Supplementary Fig. 8f, g), thereby suggesting that interneuron activity and OPC differentiation are co-regulated during development. To confirm that the reduction of the OL density was attributed to the OPC differentiation but not to OL apoptosis, we performed a BrdU proliferation/differentiation assay and immunostaining for cleaved caspase-3 (CC-3, a well established marker for apoptosis) at p14. BrdU was administered at p13 to label proliferating cells, and we analyzed the population of cells incorporated with BrdU at p14 (Fig. 4a). The density of P α ⁺BrdU⁺ cells did not change at p14, however, the number of CC1⁺BrdU⁺ cells was drastically reduced by 85% (2.7 to 0.5 cells/ 1×10^{-3} mm³, Fig. 4f-h). In contrast, the CC-3 staining showed a similarly low apoptosis rate of OLs in both groups at p14 (Supplementary Fig. 9). Again, in the corpus callosum, the populations of OPCs and OLs were not affected by the deletion of GABA_BRs at p14 (Supplementary Fig. 3). These results suggested that reduced GABAergic input gave rise to attenuated OPC differentiation in the cKO mPFC during development.

When we induced GABA_BR deletion in the young adult mice at the age of 4 weeks, representing the peak of OPC-GABA_BR expression during development (Supplementary Fig. 1c), the density of OLs as well as the MBP expression were not affected in the cKO mice both in the mPFC and corpus callosum (Supplementary Fig. 10). These data strongly suggested that the

OPC-GABA_BR was not directly involved in OPC differentiation, at least during early postnatal weeks. In addition, the percentage of recombined tdT⁺ OLs of all OLs in both cKO and ctl mPFC did not differ at 2w and 9w (Fig. 4i–k), despite decreased densities of mature CC1⁺ OLs (Figs. 4c and 1g) or CC1⁺tdT⁺ OLs (Fig. 4l) in the cKO mPFC. Thereby, it implied that the reduced OPC differentiation during development was rather due to the impaired interneuron-OPC communication.

In summary, our data demonstrated that during early development of the mPFC, deletion of GABA_BR in OPCs affected the inhibitory tone of interneurons, feeding back onto OPC differentiation and interneuron myelination.

OPCs induce interneuron apoptosis via GABA_BR-TWEAK signaling. As we had seen a surplus of interneurons in the mutant mPFC which could explain the abnormal neuronal activity^{8,35}, we tested whether the interneuron numbers would be accurately controlled by programmed cell death early during development. After induction of GABA_BR in OPCs at p7 and 8, the extent of interneuron apoptosis was determined at p10 and p14 by immunostaining for PV and CC-3 (Supplementary Fig. 11). As expected by the earlier experiments, we found a 50% reduction of PV⁺/CC-3⁺ interneurons at p10 suggestive of a strongly reduced apoptosis of PV⁺ interneurons in the mutant mPFC (Supplementary Fig. 11). These results indicated a defective apoptotic process of the interneurons in the mPFC of OPC-GABA_BR cKO mice during development.

To confirm the selective cell death of interneurons, we already induced the OPC-GABA_BR deletion as early as p1 and p2 and compared the apoptosis of inhibitory neurons with that of excitatory ones at p5 and p7 (Fig. 5a). The interneuron apoptosis lasted from p1 till p15 with a peak at p7⁷, while the time window for the excitatory neuron apoptosis was rather narrow, between p2–5³⁶. The apoptosis of total interneurons (GAD67⁺CC-3⁺) as well as of PV interneurons (PV⁺CC-3⁺, Fig. 5b) were significantly reduced in cKO mPFC at p5 and p7 (Fig. 5c), while that of the excitatory neurons (CTIP⁺CC-3⁺, Fig. 5b; TBRI⁺CC-3⁺, Fig. 5c) did not change at both time points (Fig. 5c, Supplementary Fig. 12). Therefore, we concluded that OPCs sent pro-apoptotic signals back to interneurons at the early postnatal weeks.

To molecularly identify the critical apoptotic factor released by OPCs, we tested the expression levels of six peptides which had previously been associated with cell survival or cell death. Gene deletion was induced at p1 and 2, and mPFC was collected at p7, the peak of interneuron apoptosis (Supplementary Fig. 13a). Out of the six cytokines, only the expression of TWEAK (tumor necrosis factor-like weak inducer of apoptosis, also known as Apo3l or TNF superfamily member 12, TNFSF12) was significantly changed with a reduction of about 30% in cKO mPFC (Fig. 5d, Supplementary Fig. 13b). Subsequently, we tested MACs-purified OPCs (collected from cKO and ctl cortices at p7) (Fig. 5d) as well as Oli-neu cells (an OPC cell line) treated with GABA_BR antagonist CGP 55845 for TWEAK expression. Also here, we observed a downregulation of TWEAK (Fig. 5d). In three independent experiments, including genetic deletion or pharmacological inhibition of OPC GABA_BR signaling, we consistently observed reduced levels of TWEAK (Fig. 5d, Supplementary Fig. 13).

To confirm that OPC-derived TWEAK can indeed induce neuronal apoptosis after binding to its cognate TWEAK receptor (TWEAKR; TNF Receptor Superfamily Member 12A, TNFRSF12A; also known as Fibroblast Growth Factor-inducible 14 or FN14)³⁷, we first verified the expression of TWEAKR on the PV neurons in the mPFC at p5 by immunohistochemistry

(Fig. 5e). Then, we treated primary cortical neurons with conditioned medium obtained from OPC Oli-neu cultures (Fig. 5f). The selective TWEAKR antagonist, a triazolylthiomorpholinyl-methanone L524-0366, was added to the conditioned medium at 20 μM competing for the binding of TWEAK to the TWEAKR on interneurons (Fig. 5f, g). While conditioned medium harvested from the OPC cell line increased the interneuron apoptosis, blocking TWEAKR signaling by co-incubation with the antagonist L524-0366 prevented cell death (Fig. 5h, i). These results further substantiated that OPCs could induce interneuron apoptosis via TWEAK secretion.

In summary, our results demonstrated that OPCs induced interneuron apoptosis by releasing TWEAK upon GABA_BR activation. Blocking this pathway prevented the apoptosis of interneurons. In the mPFC, the concomitant dysregulation of interneuron density resulted in reduced inhibitory GABAergic tone and altered myelination.

Interrupted OPC-interneuron communication generates cognitive impairment. The mPFC is responsible for cognitive processes and their regulatory finetuning is guaranteed by the E/I balance³⁸. To test whether the selectively reduced interneuron apoptosis and the associated structural myelin alterations could generate defects in neural circuits and cognition, we performed *in vivo* electroencephalographical (EEG) recordings and behavioral tests in 9w old mice after gene ablation (induced at p7 and 8, Fig. 6a).

Our patch-clamp recordings had already revealed a reduced interneuron activity suggesting an imbalance of E/I in the mutant mPFC (Fig. 3b–f). And indeed, an impaired cortical network activity of the mutant mice was also detected in EEG recordings. The relative contribution of the gamma band power (30–80 Hz) to the total brain oscillatory pattern, in particular, the lower gamma wave band (30–50 Hz) was slightly, but significantly decreased by about 10% in cKO mice (Fig. 6b, c, Supplementary Fig. 14a, b).

To evaluate the impact of the circuit dysregulation in the mutant mPFC for the living animal, we challenged mice for their cognitive performance employing tasks of social cognitive behavior which had been associated with mPFC function, i.e., social novelty and new object recognition³⁹. In addition, nest building behavior is often introduced as an indicator of general well-being, and its alteration as an early sign of cognitive decline⁴⁰. We observed that the mutant mice built significantly less elaborated nests, even not reaching half the performance score of ctl mice, indicating putative cognitive deficits (Fig. 6d). The three-chamber test was used to assess social cognition by analyzing mice for a form of general sociability and their interest in social novelty (Fig. 6e). First, the three-chamber test was used to monitor general social behavior, i.e., preference of other mice over objects. Both, ctl and cKO mice exhibited more interest (i.e., longer sniffing times) into the mouse rather than the object during the first test phase, indicating no disorder in sociability of the mutant mice (Fig. 6f, Supplementary Fig. 14c, d, g, h). At the second phase, a social novelty preference was assessed. While control animals explored the unfamiliar mouse longer than the familiar one, the cKO mice could not discriminate stranger and familiar mouse (Fig. 6g, Supplementary Fig. 14e, f, i, j). Also, when we employed the novel object recognition test (Fig. 6h), the cKO mice did not recognize a new object when it was replaced after a 40 min break from the habituation (Fig. 6i, j). The general motor activity appeared only mildly affected. In the open-field the motor activity of the cKO mice was slightly increased based on the total distance run in the cage (Fig. 6k–m).

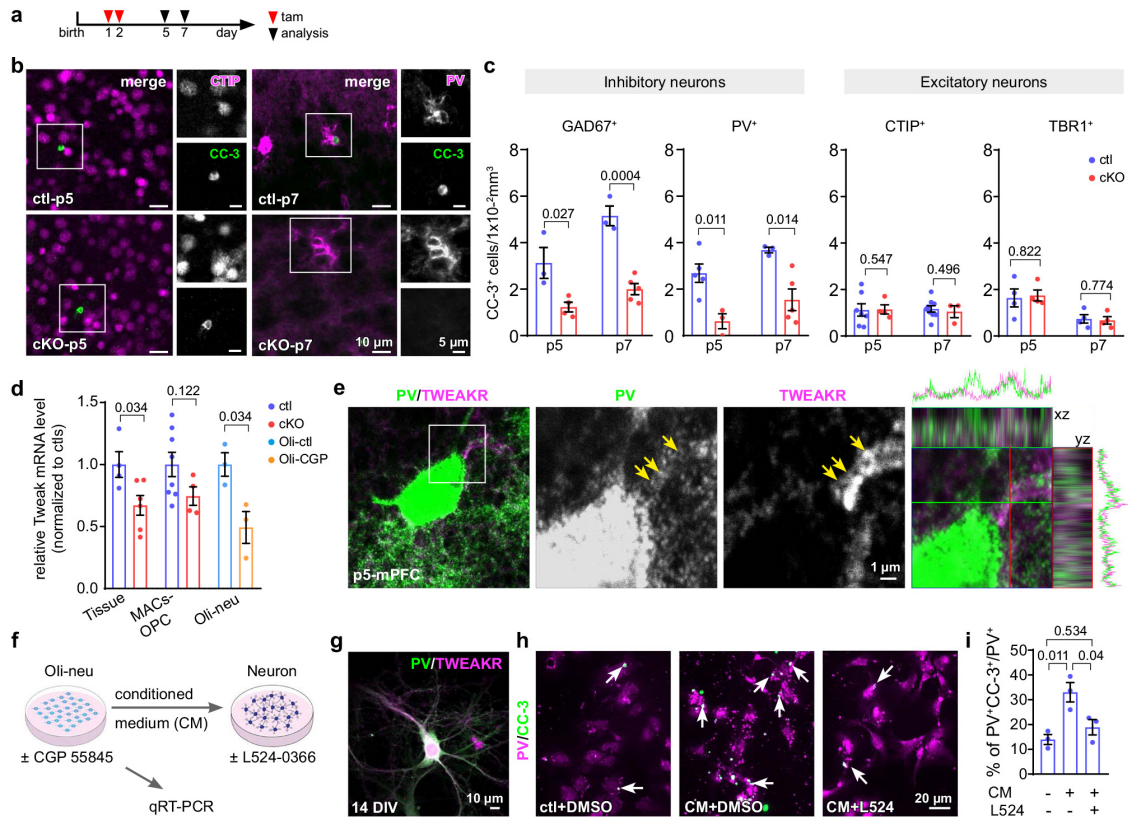


Fig. 5 During early CNS development impaired release of TWEAK from GABA_B-deficient OPCs mitigated programmed cell death of interneurons. **a** Experimental schedule. **b** Fluorescent micrographs of excitatory (CtBP-interacting protein (CTIP)⁺, magenta) and inhibitory (parvalbumin (pv)⁺, magenta) interneurons co-stained with the apoptotic marker cleaved caspase 3 (CC-3, green) in p5 and p7 mPFC. **c** Quantification of apoptotic neurons (CC-3⁺) co-expressing the interneuron marker glutamate decarboxylase 67 (GAD67) and PV or CTIP and T-box brain transcription factor 1 (TBR1) as markers for excitatory neurons. (GAD67: p5-ctl = 3 mice, p5-cKO = 4 mice; p7-ctl = 3 mice, p7-cKO = 5 mice) (PV: p5-ctl = 5 mice, p5-cKO = 3 mice; p7-ctl = 3 mice, p7-cKO = 5 mice) (CTIP: p5-ctl = 7 mice, p5-cKO = 4 mice; p7-ctl = 9 mice, p7-cKO = 3 mice) (TBR1: p5-ctl = 4, p5-cKO = 4; p7-ctl = 4, p7-cKO = 4 mice) (two-sided unpaired t-tests). **d** Relative mRNA level of TNF like weak inducer of apoptosis (TWEAK) in the medial prefrontal cortex (mPFC), magnetic-activated cell sorted (MACs)-OPCs from ctl and cKO mice as well as Oli-neu cells treated with or without 20 μM CGP 55845 (tissue-ctl = 4 mice, tissue-cKO = 6 mice; MACs-ctl = 8 mice, MACs-cKO = 4 mice; Oli-neu: n = 3 independent experiments; two-sided unpaired t-tests). **e** Double-immunostaining of TWEAK receptor (TWEAKR, magenta) and PV (green) in the control mPFC at p5. Arrows indicate co-expression of TWEAKR and PV. **f** Experimental design for in vitro studies. **g** Immunolabeling of TWEAKR (magenta) on 14 days in vitro (DIV) PV⁺ interneurons (green). **h** Immunostaining of apoptotic primary PV⁺ neurons with CC-3 (green) and PV (magenta) after being treated with conditional medium (CM) of Oli-neu cells co-treated with or without TWEAKR antagonist L524-0366 (L524, 20 μM). White arrows indicate PV⁺ cells co-expressing CC-3. **i** Percentage of apoptotic PV⁺ interneurons of all PV⁺ interneurons in conditioned medium and treated with a competitive TWEAKR inhibitor (n = 3 independent experiments from distinct samples, one-way ANOVA, Turkey's multiple comparison). Data are shown as mean ± SEM in **c**, **d**, and **i**. Source data are provided as a Source Data file.

Hence, we conclude that GABA_BRs of OPCs are essential for the fine-tuning of inhibitory circuits in the mPFC, and thereby for distinct cognitive behavior.

Discussion

A balance of excitation and inhibition (E/I) in the medial prefrontal cortex (mPFC) is of key importance for mammalian cognition. Establishing correct cell densities and subsequent myelination have been identified as pivotal elements during CNS development^{35,41}. This has been well documented for fast-spiking parvalbumin-positive (PV⁺) interneurons^{6,17}. Here, we highlight OPCs as indispensable regulators of the interneuron population and its myelination in the mPFC. We provide a molecular explanation and can demonstrate how impaired

bidirectional OPC-interneuron signaling affects social cognitive behavior. At the first two postnatal weeks OPCs sense the interneuron activity via expression of GABA_B receptors and concomitantly adjust interneuron cell density by releasing TNF-like weak inducer of apoptosis (TWEAK) limiting interneuron survival. When the interneuron-OPC signaling is interrupted by genetic ablation of GABA_BR in OPCs and attenuated release of TWEAK, the population of fast-spiking, parvalbumin-positive interneurons builds up. However, despite their increased cell numbers, the interneurons appear hypoactive, have less contacts with OPCs during development and exhibit deteriorated myelin structures in the adulthood. Notably, the mutant mice exhibit severe cognitive defects in their social behavior.

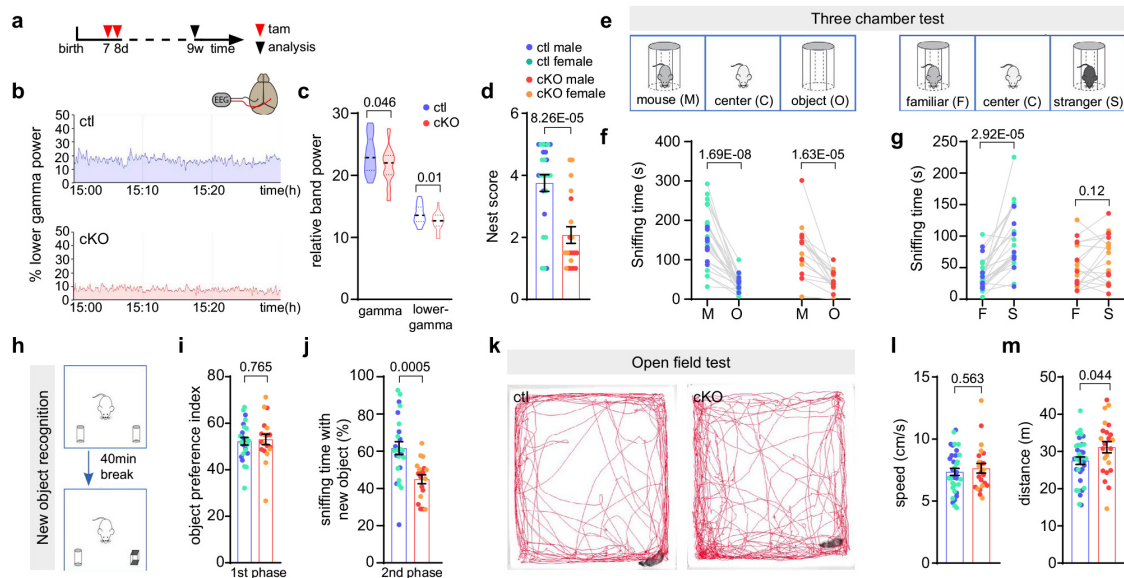


Fig. 6 In OPC-GABA_B cKO mice a perturbed neuronal firing translates into deficits of social behavior. **a** Experimental schedule. **b** Lower gamma band acquired by electroencephalogram recordings. **c** Violin plot shows decreased gamma oscillation in the cKO mouse brain. (ctl = 24 h from 4 mice, cKO = 24 h from 4 mice, two-sided unpaired *t*-tests). **d** Impaired nest building ability of mutant mice. (male: ctl = 10 mice, cKO = 10 mice; female: ctl = 15 mice, cKO = 10 mice, two-sided unpaired *t*-test). **e** Scheme of the three-chamber behavior test. **f** Quantification of the sniffing time with mouse (M) and object (O) (male: ctl = 9 mice, cKO = 9 mice, two-sided paired *t*-tests; female: ctl = 15 mice, cKO = 9 mice, two-sided paired *t*-tests). **g** Quantification of the sniffing time with familiar (F) and stranger (S) mouse (male: ctl = 9 mice, cKO = 9 mice, two-sided paired Wilcoxon test; female: ctl = 15 mice, cKO = 9 mice, two-sided paired *t*-test). **h** Scheme of new object recognition test. **i** Assessment of object preference (male: ctl = 10 mice, cKO = 10 mice; female: ctl = 15 mice, cKO = 9 mice, two-sided unpaired *t*-test). **j** Percentage of sniffing time with new object among total sniffing time. (male: ctl = 10 mice, cKO = 10 mice; female: ctl = 15 mice, cKO = 9 mice, two-sided unpaired *t*-test). **k** Representative trajectory charts of the animals during the open field test. **l, m** Both ctl and cKO mice exhibited similar motor activities shown by the speed and distance analysis. (male: ctl = 17 mice, cKO = 14 mice; female: ctl = 18 mice, cKO = 9 mice, two-sided unpaired *t*-test). Data are shown as mean ± SEM in **d, i, j, l** and **m**. In **c**, data are shown with indications of median and quartiles in thick and thin dashed lines, respectively. Source data are provided as a Source Data file.

During development, large populations of immature interneurons invade the cortex where their cell density is adjusted by programmed cell death^{9,10}. For assuring their survival, these neurons form connections with adjacent cells and receive retrograde signals from their targets^{10,11}. Interneuron apoptosis drastically increases at p7⁷, shortly after formation of interneuron-OPC synapses at p4–5¹², and it stays elevated till p11⁷, right after the peak of interneuron-OPC connectivity at p10¹³. Based on this established knowledge, we hypothesized that OPCs could exert an apoptotic impact to their presynaptic partners. Indeed, our data provide strong evidence that, starting from postnatal day 5, OPCs elicit an apoptotic cascade of adjacent interneurons to adjust their density. In OPCs, the regulatory process employs a GABA_B-TWEAK signaling pathway. TWEAK, TNF super family member 12 (TNFSF12), is TNF-like weak apoptotic factor. Membrane-bound and cleaved isoforms of TWEAK are both able to induce cell apoptosis by binding to the TWEAK receptor (TWEAKR, also known as fibroblast growth factor-inducible 14 or FN14) on the neuronal side^{37,42,43}. According to our data GABA_B-TWEAK signaling preferentially affects interneurons, suggesting this ‘kill me’ signal acting highly localized. Indeed, TWEAK is specifically recruited to synapses where TWEAKRs are expressed at the neuronal membrane⁴⁴. OPCs directly sense GABAergic signals at their interneuron-OPC synapse. We suggest that subsequent signaling triggers TWEAK synthesis and translocation to the OPC surface, where it can directly bind interneuronal TWEAKRs. Alternatively, the TWEAK ectodomain could be proteolytically cleaved and act as a

soluble factor. However, this scenario could also happen at somatosomatic contact sites between OPCs and interneurons^{2,45,46}. Overall, the regulatory impact appears to be highly specific since the OPC-induced interneuron apoptosis was restricted to the first two postnatal weeks, a well-established time window of interneuron apoptosis^{7,36}. This also explains why the cKO induction at the age of 4w did not affect OPC differentiation and myelination, although GABA_BR expression peaks in OPCs at 4w (Supplementary Fig. 1c). Please note, instead of a gradual decline, we found a slight increase of PV⁺CC3⁺ cells at p14 compared to p10 in both control and mutant mice, probably due to the age-dependent increase of PV expression described for fast spiking interneurons⁴⁷.

GABA_BRs are G-protein coupled receptors. In cultures of OPCs, activation of GABA_BR negatively regulates adenylyl cyclase and reduces cAMP levels⁴⁸. Subsequently, protein kinase A activity is suppressed, followed by impeded nuclear translocation of cAMP response element binding protein (CREB) affecting gene expression, e.g., the expression of brain derived neurotrophic factor (BDNF) or AMPA (α-amino-3-hydroxy-5-methyl-4-isoxazolepropionic acid)-type glutamate receptor GluA1 subunit^{49,50}. A recent study suggested that activation of GABA_BR in cultured OPCs can also activate Akt/Src kinases required for OPC differentiation¹⁴. Additional studies are necessary to elucidate which class of G proteins (G_{ai} and/or G_{βγ}) transmit GABA_BR signaling in OPCs to elicit TWEAK expression and release. As shown by RNA sequencing, microglia express rather high levels of TWEAKR during development in the cortex⁵¹. However, whether

or not a TWEAK-based OPC-microglial crosstalk contributes to the elimination of interneurons during development is not clear yet. At this point, we can not exclude a contribution of TWEAKR-expressing microglia, which requires future experiments. So far, our *in vitro* data show that in a pure culture system, TWEAKR antagonist can interfere with interneuron apoptosis induced by TWEAK from conditioned medium of OPCs (Oli-neu cell line).

A neuronal surplus is often accompanied with reduced activity^{6,8}. In the OPC-GABA_BR cKO mice, we observed a strong increase of PV⁺ interneurons to about 125% of ctl levels. However, their presynaptic terminals contained less immunolabel for the vesicular GABA transporter (vGAT) and implying a significant reduction in activity and GABA release. The reduction of vGAT puncta to 75% represents a reduction of about 60% for PV interneurons (i.e., 75% of 125%), as observed for the PV⁺cFos⁺ cell density (63%) or the sIPSC frequency (64%). It is quite conceivable that the surviving, supernumerous PV interneurons are physiologically less mature in the cKO mPFC⁵². Additionally, a potential change in the PV interneuron morphology is detected since the relative axon volumes of PV interneurons in cKO and ctl mice were identical despite a larger population of PV⁺ interneurons in the mPFC of mutant mice, e.g., thinner axonal caliber, shortened axons or less arborized axons in the cKO mPFC. However, such a detailed anatomical analysis is beyond the scope of this study.

Interestingly, also the early loss of the ionotropic GABA_AR γ 2 subunit in OPCs reduced the firing rate of presynaptic PV⁺ interneurons as well as a similar myelin defect⁴. The very different signal pathways of ionotropic and metabotropic GABA receptors merge and similarly affect PV interneuron activity, OPC-axon contacts and myelin gene expression. However, the impact on myelin structures was rather distinct. GABA_AR deletion resulted in prolonged lengths of nodes and internodes with a decreased density of paranodes⁴, while only an extended length of paranodes was detected in the OPC-GABA_BR cKO mPFC of our study. In addition, GABA_ARs facilitated interneuron maturation in the juvenile (p24) somatosensory cortex, while GABA_BRs regulate the elimination of interneurons during the first two postnatal weeks. Apparently, both receptors optimize the density and activity of PV interneurons, cooperating jointly but employing different machineries at distinct time points.

The GABA_AR signaling between interneurons and OPCs is relatively well established^{4,15,53,54}. E.g., the γ 2 subunit of GABA_AR contributes to the maintenance of the OPC, but has no impact on OL formation¹⁵. However, the role of GABA_BRs for OPC differentiation is complex. We observed that GABA_BR was essential for formation of OLs at the early development but not at later stages. Similarly, an *in vitro* study showed that activation of GABA_BR by the selective agonist baclofen could stimulate the differentiation of cortical OPCs prepared from p0–2 pups¹⁴. Since OPCs are heterogeneous with age⁵⁵, GABA_BR of OPCs could contribute to the developmental diversity. Differentiation of OLs and subsequent myelination are strongly affected by neuronal activity and axonal caliber^{23,27,56}. Indeed, we observed a suppression of the inhibitory tone in the mPFC at p10 followed by a change in oligodendrocyte density detected at p14. Concomitantly, the oligodendrocytes formed less myelin (only 40% of control) around the interneuronal axons and altered paranodal structures in the adult mPFC, which are essential for precise action potential propagation. The elongation of paranode will be accompanied with redistribution of Kv1 channels from under juxtapanode towards paranode in the brain of multiple sclerosis and aging⁵⁷. These exposed Kv1 channels are more active. As a result, these changes hinder the action potential propagation, which in turn reduces the synaptic communication. Regardless, the morphological deterioration was only observed in the mPFC,

but not in the corpus callosum, largely composed axons of excitatory neurons only²². In line with these neuron-type specific observations, the qRT-PCR results indicated reduced levels of MBP, but neither PLP nor MOG mRNA expression in the mutant mPFC, both at p14 and 9w of age. Myelin proteins of inhibitory and excitatory axons are differently expressed, e.g., MBP is preferentially expressed in the myelin of inhibitory axons¹⁶.

The GABAergic signaling of OPCs plays pivotal roles for the myelination of interneurons, which ensures precise finetuning of the local neural circuitry⁵⁸. As seen in chandelier cells⁶, excessive number of interneurons in the OPC-GABA_BR cKO mice exhibited suppressed activity and reduced myelination in the mPFC. All these physiological and morphological abnormalities certainly contribute to the cognitive impairment. In early socially isolated mice the observed cognitive impairment is also accompanied by a strong hypomyelination in the mPFC^{59,60}. A proper E/I ratio in the prefrontal cortex, especially the E/I balance in the postnatally developing mPFC, is extremely important for social cognition^{38,61}. When the pyramidal neuron activity was enhanced in the mPFC at early p7–11 caused a severe cognitive dysfunction in the adulthood⁶¹. In addition, despite relatively short axons, myelination of cortical interneurons (mainly PV⁺ neurons¹⁶) contributes significantly to the finetuning of local activity in the mPFC and cortex, insuring proper behavior performance^{4,6,17}. *Nota bene*, since the genetic manipulation is not selective to the PFC, we cannot rule out contributions of other brain regions to the behavioral phenotype, which has to be left for future studies.

In conclusion, our study demonstrates that OPCs regulate inhibition in the mPFC via GABA_BR/TWEAK signaling. During development, OPCs determine the density of interneurons by adjusting their apoptosis. Subsequently, correct myelination of interneurons, as an essential component of the network activity in the mPFC, determines the cognition and social behavior.

Methods

Ethics statement. Animal husbandry and procedures were performed at the animal facility of CIPMM, University of Saarland according to European and German guidelines for the welfare of experimental animals. Animal experiments were approved by the Saarland state's "Landesamt für Gesundheit und Verbraucherschutz" in Saarbrücken/Germany (animal license number: 65/2013, 12/2014, 34/2016, 36/2016, 03/2021 and 08/2021).

Animals. To conditionally knock out (cKO) GABA_B receptor subunit1 in oligodendrocyte precursor cells (OPCs), TgH(NG2-Cre^{ERT2})¹⁹ mice were crossed to GABA_{B1}^{lox511/lox511} mice (flanking exon 7 and 8 of *gabrb1*)⁶². Mice with genotypes of NG2^{ct2/wt} x GABA_{B1}R^{fl/fl} were used as cKO and the littermates NG2^{wt/wt} x GABA_{B1}R^{fl/fl} or NG2^{ct2/wt} x GABA_{B1}R^{wt/wt} were controls after tamoxifen application. To visualize the recombined cells, we crossed the double transgenic mice with TgH(Rosa26-CAG- β STOP^{fl}-tdTomato) (Rosa26-tdTomato)⁶³. Mouse strains were maintained in C57Bl/6N background. Mice were kept at the animal facility of the CIPMM in a 12 h light/dark cycle at 20 °C with humidity at 55–70% and fed a breeding diet (V1125, Sniff) *ad libitum*.

Mouse numbers and ages are indicated in the main text and figure legends. Behavioral tests were carried out at the age of 9 weeks. Both genders were used in all experiments.

Tamoxifen administration. Tamoxifen was dissolved in Miglyol (3274, Caesar&Loretz GmbH, Hilden, Germany) to a final concentration of 10 mg/ml. Tamoxifen was intraperitoneally injected to the mice depending on the body weight (100 mg/kg body weight). The time points of injections are indicated in the figures. Only for the pups treated at postnatal day 1 (p1) and 2, tamoxifen was injected to the lactating mother with the same protocol⁶⁴. For 4-week-old mice, tamoxifen was injected once per day for five consecutive days¹⁸.

Immunohistochemistry. Mice were perfused with PBS and 4% paraformaldehyde (PFA). Dissected mouse brains were post fixed with 4% PFA at 4 °C overnight. Free floating brain slices (40 μ m thickness) were prepared as coronal or sagittal sections using a Leica VT1000S vibratome. For immunocytochemistry, cells on coverslips were fixed with ice cold 4% PFA for 15 min. Slices or coverslips were incubated with blocking solution containing 5% horse serum and 0.5% Triton X-100 at room temperature (RT) for 1 h, followed by primary antibody incubation at 4 °C

overnight and secondary antibody incubation at RT for 2 h in blocking solution. Primary and secondary antibodies are listed in the Supplementary Tables 1 and 2, respectively.

Magnetic cell separation (MACs) of OPCs. MACs sorting of OPCs was performed according to the manufacturer's instruction (Miltenyi Biotec) with some modifications. Mice were perfused with cold Hank's balanced salt solution without calcium and magnesium (HBSS, H6648, Gibco) and cortices were dissected in ice cold HBSS. After the removal of debris (130-107-677, Miltenyi Biotec), cells were resuspended with 1 mL "re-expression medium" containing NeuroBrew-21 (1:50 in MACS neuro Medium) (130-093-566 and 130-093-570, Miltenyi Biotec) and 200 mM L-glutamine (1:100, G7513, Sigma) at 37 °C for 30 min. Cells were then incubated with Fc-receptor blocker for 10 min at 4 °C (provided with CD140 microbeads kit), followed by a 15 min incubation with 10 μ L microbeads mixture containing antibodies directed against CD140 (130-101-502), NG2 (130-097-170) and O4 (130-096-670) in 1:1:1 at 4 °C.

For qRT-PCR or Western blot analysis, MACs-sorted OPCs were lysed by RIPA buffer (89900, Thermo Scientific).

Western blot analysis. Deeply anesthetized mice were perfused with cold PBS. Medial prefrontal cortices (mPFC) and corpus callosa (cc) were dissected in ice cold PBS. Tissues were homogenized with sucrose lysis buffer (320 mM sucrose, 10 mM Tris-HCl, 1 mM NaHCO₃ (pH = 7.4); 1 mM MgCl₂), and MACs-sorted OPCs were lysed with RIPA buffer. Both buffers were supplemented with 1 X protease inhibitors (05892970001 Roche) and 1 X phosphatase inhibitor (04906837001, Roche). Protein (5 μ g) was blotted onto nitrocellulose transfer membranes (QP0907015, qpor). Membrane was blocked with 5% non-fat milk or 5% BSA (A7906, Sigma) diluted in 0.1% TBST. Primary antibodies were diluted with corresponding blocking buffer. Primary antibodies used for Western blot are listed in the Supplementary Table 3.

Secondary antibodies were: HRP anti-mouse (1:2000, A9044, Sigma) and anti-rabbit (1:2000, 111-035-045, Dianova). Membranes were illuminated with WesternBright Chemilumineszenz Substrat Quantum kit (541015, Biozym) and documented with ChemiDoc-MP. Complete and unprocessed original blots are provided in the Source Data file.

Quantitative real time PCR. Brain tissue or the MACs OPCs and Oli-neu cells were homogenized as described above. NucleoSpin RNA Plus XS kit (740990.50, Macherey-Nagel) was used to extract mRNA and Omniscript kit (205113, QIAGEN) was used for reverse transcription. RT-PCR was performed using EvaGreen (27490, Axon) kit with CFX96 Real Time System (BioRad). Primer sequences for qRT-PCR are listed in Supplementary Table 4.

Electrophysiology. Slice preparation: Mice were anesthetized by isoflurane before decapitation, and the brain was quickly prepared and immersed in an ice-cold, oxygenated (5% CO₂/95% O₂, pH = 7.4) solution containing (in mM) 87 NaCl, 3 KCl, 25 NaHCO₃, 1.25 NaH₂PO₄, 3 MgCl₂, 0.5 CaCl₂, 75 sucrose and 25 glucose. Coronal or semi-sagittal slices in 300 μ m thickness were prepared with a vibratome (Leica VT 1200S, Nussloch, Germany) and transferred to a nylon basket slice holder for incubation in artificial cerebral spinal fluid (ACSF) containing (in mM) 126 NaCl, 3 KCl, 25 NaHCO₃, 15 glucose, 1.2 NaH₂PO₄, 2 CaCl₂, and 2 MgCl₂ at 32 °C for 0.5 h. Subsequently, slices were removed from the water bath and kept at RT with continuous oxygenation prior to use.

IPSCs and EPSCs recordings of neurons: Semi-sagittal slices were transferred to the recording chamber that was continuously perfused with oxygenated ACSF containing 1 MgCl₂ and 2.5 CaCl₂ at a flow rate of 2–5 mL/min. During sEPSC recordings, 50 μ M strychnine and 50 μ M picrotoxin were added to block inhibitory synaptic transmission. Pyramidal neurons were identified morphologically (Axioskop 2 FS mot, Zeiss, Jena, Germany) with a 40x water immersion objective and a QuantEM 512SC camera (Photometrics, Tucson, USA). Whole-cell membrane currents were recorded by an EPC 10 USB amplifier (HEKA, Lambrecht, Germany), low pass filtered at 3 kHz and data acquisition was controlled by Patchmaster software (v2x90.5, HEKA). The patch pipettes (7–9 Ω M) were prepared from borosilicate capillaries (OD: 1.5 mm; Sutter, USA) using a Micropipette Puller (Model P-97, Sutter Instrument Co., CA). Patch pipettes were filled with the solution containing (in mM) 125 cesium gluconate, 20 tetraethylammonium (TEA), 2 MgCl₂, 0.5 CaCl₂, 1 EGTA, 10 HEPES and 5 Na₂ATP (pH = 7.2). Spontaneous excitatory and inhibitory postsynaptic currents (sEPSCs, sIPSCs) of pyramidal neurons in mPFC were recorded for 40 s in voltage-clamp mode at a holding potential of -70 mV and +30 mV, respectively. Currents above 10 pA were analyzed with MATLAB.

Whole-cell patch clamp recordings of OPCs: Semi-sagittal slices in 300 μ m thickness were prepared from p11–14 mice. To record GABA_AR current in OPCs, cells were clamped at -70 mV in whole-cell mode. 100 μ M GABA (Tocris) was focally applied to patched OPCs in the presence of 20 μ M CNQX and 30 μ M DAP5. Non-competitive picrotoxin (50 μ M, Tocris) and selective GABA_AR antagonist SR95503 (20 μ M, Tocris) were applied in the bath as well used to verify GABA_AR currents. To record GABAergic sPSCs of OPCs (OPC-sPSC), 20 μ M CNQX (Tocris) and 30 μ M DAP5 (Tocris) were added to inhibit excitatory signals.

To improve the signal to noise ratio, the Matlab tool 'Sgolay' was used. Sgolay is a Savitzky-Golay filter, which smoothes according to a quadratic polynomial that is fitted over each window of the original trace. This method is particular effective at fast variations of recorded data. After filtering, currents larger than 1 pA were selected for further analysis. In some experiments, 50 μ M carbachol (Tocris) was added to stimulate inhibitory neurons.

Data analysis. Data generated by PatchMaster were loaded into MATLAB (Mathworks, MA, USA) with a module adapted from sigTOOL⁶⁵. Evoked EPSC and IPSC traces from the same cells were manually checked and pooled. The average of EPSC/IPSC traces from each cell was used for analysis. Data analysis was performed using routines that were custom written in Matlab.

EEG telemetry and analysis. Telemetric EEG transmitter implantation was adapted from Bedner and colleagues⁶⁶. Mice were implanted with telemetric EEG transmitters (DSI PhysioTel ETA-F10, Harvard Biosciences, Inc. Holliston, Massachusetts, USA) between 8 and 10 weeks of age. The animals were placed in a stereotaxic frame (Robot stereotaxic, Neurostar, Tübingen, Germany) for implantation of depth electrodes at 3.4 mm posterior to bregma and bilaterally 1.6 mm from the sagittal suture. After post-surgical care and recovery, cages were placed on individual radio receiving plates (DSI PhysioTel RPC-1, Data Sciences International, St. Paul, USA) for synchronized EEG and video recording (MediaRecorder Software, Noldus Information Technology, Wageningen, Netherlands). EEG and video recording were performed for 24 h.

Data analysis of EEG recordings: EEG traces were analyzed with the Neuroscore software (Version 3.3.1., Data Sciences International, St. Paul, USA). After applying a general Notch filter (50 Hz band stop), relative power band values were determined with a order 13 fast-Fourier transform in 10^s epochs and later averaged per hour of recording. Statistical analysis was performed with GraphPad Prism 8.0.1.

Behavioral analysis. Several behavioral tests were performed with the same cohorts of mice (male and female, 9-week-old). The order of tests was arranged from low to high invasiveness to reduce the interference from the prior tests. The chamber or tested square was wiped with 75% ethanol before tests to remove odors.

Nest building test. Mice were moved into new single cages in the behavior testing room for habituation. After 24 h, a piece of pressed cotton in size of 7 × 5 cm² was placed in the cage. After 14 h, the shape and weight of the cotton was recorded and unbiasedly scored according to the criteria⁶⁷.

Open field test. The mice were put in the open field maze, which measured 50 cm (length) × 50 cm (width) × 38 cm (height). Mice could move and explore freely for 10 min in the open field square. In each test, the single mouse was put in the center of the square arena. The videos of these 10 min were recorded (USB webcam) and analyzed (EthoVision XT 11.5, Noldus Technology). Duration time in the center area (s), moved distance (cm) and speed (cm/s) were determined⁶⁸.

New object recognition test. The mice could freely explore the two identical objects placed at a distance of 8.5 cm from the side walls in two opposite corners of the apparatus for 10 min. After 40 min, one of the objects was replaced by a novel one, and the test mouse was allowed to explore again. Preference index was defined as the percentage of the time exploring one identical object within the total time exploring both objects. Recognition index was defined as the percentage of the time exploring the novel object among the total time of exploring both objects.

Three chamber social behavior test: The three-chamber box was employed for social behavioral studies⁶⁹. Three chambers were equally sized and separated by two walls evenly distributed in the box. A square door at the bottom center of each door allowed free running of the mice within the three chambers. Two empty wire cages were placed at the side chambers, leaving the center chamber empty. For habituation, mice were kept in the center chamber for 10 min, followed by a 10 min-habituation session with access to all three chambers. For the sociability test, the test mouse was placed in the center chamber, while a mouse of similar age was kept under the stainless wire cage in one of the side chambers. The other chamber contained an empty wire cage. For 10 min, the test mouse could select freely all three chambers. For the social novelty test, a novel mouse was placed under the other empty cage being an unfamiliar mouse, and the prior mouse as familiar one. The test mouse was again allowed to freely explore both animals for 10 min. The experiment was video-recorded and the time that the test mouse spent in each chamber and the time of sniffing was analyzed.

Cell culture

Cell line Oli-neu. The murine oligodendroglial precursor cell line Oli-neu⁷⁰ was kindly provided by Professor Jacqueline Trotter (University of Mainz). Undifferentiated Oli-neu cells were incubated at 37 °C and 5% CO₂ in poly-L-lysine (Merck) coated cell culture flasks (Greiner Bio one) for expansion or cell culture dishes (Greiner Bio one) for experiments. Sato medium consisting of DMEM high glucose medium (Fisher Scientific) with supplementation of 10 μ g/ml transferrin (Sigma), 10 μ g/ml insulin (Santa Cruz), 100 μ M putrescine (Sigma), 200 nM progesterone (Sigma), 500 nM tri-iodo-thyrodine (Sigma), 220 nM sodium selenite (Sigma), 520 nM L-thyroxine (Sigma) and 1.5% normal horse serum (Fisher

Scientific) was used for culturing and proliferation of cells. For each independent experiment, 2×10^5 cells from the same passage were seeded in a 60 mm Petri dish. 48 h later, the medium was changed to fresh, with or without (2S)-3-[[[(1S)-1-(3,4-Dichlorophenyl)ethyl]amino]-2-hydroxypropyl](phenylmethyl)phosphinic acid (CGP 55845, 50 μM , Tocris) for 24 h. Cells were lysed with Qiazol (Qiagen) for qRT-PCR in a blind manner. Conditional medium of control cells was collected for further neuronal treatment. In total, three independent experiments were performed.

Primary culture of cortical neurons. Cortical neurons were isolated from p0 pups (C57BL/6N mouse strain). Briefly, the cortex was dissected from the whole brain in ice cold Earle's Balanced Salt Solution (EBSS, Gibco). The cortex was then digested with 35 units papain (Worthington, NJ) for 45 min at 37 °C, followed by gentle mechanical trituration. 1×10^5 cells were seeded on 25 mm glass coverslips in 24-well culture plates for further immunostaining. Each mouse brain was independently prepared for one 24-well plate, considered as one independent experiment. The glass coverslips were pre-coated with a mixture of coating solution containing 17 mM acetic acid, poly-D-Lysine (Sigma, P6407) and collagen I (Gibco, A1048301). Neurons were cultured in NBA culture medium that contained 10% FCS, 1% penicillin-streptomycin, 1% GlutaMAX and 2% B-27 supplement (Gibco) for 7d at 37 °C with 5% CO₂ before the experiment. To examine the effect of TWEAK on neurons, conditioned Oli-neu culture medium supernatant or Sato, was applied to neuron NBA culture medium, with a ratio of 1:2 to NBA resulting in 1 ml medium per 24-well and 2 ml medium per 6-well. Cells were collected after 6 h with different culture condition with or without 20 μM TWEAKR inhibitor L524-0366 (509374, Calbiochem) for further analysis.

Image acquisition and analysis. Brain slices were scanned with the fully automated slide scanner AxioScan.ZI (Zeiss, Jena) and LSM 710 and 780 confocal microscope (Zeiss, Jena). Cell counting was manually performed by using ZEN software (Zeiss, Jena). The lengths of nodes and paranodes were measured using the 'straight' tool of Fiji software. The Imapris (version 9.6) with surface tracking functions of volume analysis and vesicle classification were used for the analysis of MOG (Fig. 2d, e, h) and vGAT immunostainings (Fig. 3h–k, Supplementary Fig. 8b–d). Briefly, for the MOG/PV/SMI312 immunolabel analysis, after background subtraction a surface of the axonal SMI312 immunostaining was rendered and respective volumes estimated. All the immunoreactive fragments, of which the volume was larger than 0.6 μm^3 , were selected for analysis. To specifically select the axons of PV⁺ interneurons, a filter with 'Minimum intensity' of the PV channel was applied and only double positive fragments were selected for volume analysis. On this surface, an additional filter 'Minimum intensity' of the MOG channel was applied to quantify the myelination of PV⁺ interneurons. For the myelination of all axons (inhibitory and excitatory), the MOG channel filter was directly applied to the SMI 312 surface. For the vGAT analysis, background subtraction was followed by 'Surface' mode in Imapris. On this surface, the distance between vGAT puncta and OPCs was analyzed and classified in '<200 nm' and '>200 nm', as putative presynapses on OPCs or on other cells, respectively. The volume of each vGAT punctum and total number of vGAT puncta were analyzed by Imapris. Cell counting and Imapris analysis were carried out in a blind manner.

Bromodeoxyuridine assay. Adult animals received 1 mg/ml bromodeoxyuridine (BrdU) (B5002, Sigma-Aldrich, St. Louis, MO) dissolved in drinking water for seven consecutive days. For juvenile mice, single shots of 10 mg/ml BrdU dissolved in 0.9% NaCl were intraperitoneally injected to the p13 pups and analyzed at p14.

Statistics and reproducibility. The statistical analyses of all data were performed with GraphPad Prism 8.0.1. For all immunostainings, four brain hemispheres from randomly selected brain slices of each mouse were studied. In addition, for the analysis of vGAT and PV/SMI312/MOG, at least 6 OPCs or 8 regions of interests per mouse was analyzed, respectively. For the in vitro study, three independent primary cell preparations or 6 independent experiments of the Oli-neu cell line were performed. Within one independent experiment, cells from the same passage (Oli-neu cells) or the same preparation (primary neurons) were randomly distributed to different experimental groups prior to the treatment. In the PV/CC-3 immunostaining experiments, each group had two replicates. Prior to statistical analysis, data were tested for normal distribution with the Anderson-Darling test and outlier identification using the Rout method (Q = 1%). Outliers were excluded from the statistical analysis. For the normally distributed dataset, unpaired *t*-tests, paired *t*-test (for studies of behavior), one-way ANOVA and two-way ANOVA were used (indicated in each figure legend), while the Mann-Whitney test was used for non-normally distributed datasets. *P*-values are indicated in the figures and legends. For the in vivo experiments, each data point represents the data obtained from a single mouse (except for electrophysiology and EEG recordings). The total mouse numbers are given in the figure legends. For electrophysiology and EEG recordings, each data point refers to a single cell or single recording unit (hour), respectively, and the numbers of cells and mice are given in the figure legends. Data are shown as mean \pm SEM, except for the violin plots (Figs. 3k and 6c), where the median and quartiles are indicated as thick and thin dashed lines, respectively.

Reporting summary. Further information on research design is available in the Nature Research Reporting Summary linked to this article.

Data availability

Source data are provided with this paper. Further data to support the findings can be obtained upon request to the corresponding authors.

Code availability

Custom codes used for electrophysiology analysis are available at GitHub⁷¹ (<https://github.com/XianshuBai/OPC-GABABR-interneuron>).

Received: 5 May 2021; Accepted: 23 February 2022;

Published online: 16 March 2022

References

- Douglas, R. J. & Martin, K. A. Inhibition in cortical circuits. *Curr. Biol.* **19**, R398–R402 (2009).
- Bai, X., Kirchhoff, F. & Scheller, A. Oligodendroglial GABAergic signaling: more than inhibition! *Neurosci. Bull.* **7**, 1039–1050 (2021).
- Marin, O. Interneuron dysfunction in psychiatric disorders. *Nat. Rev. Neurosci.* **13**, 107–120 (2012).
- Benamer, N., Vidal, M., Balia, M. & Angulo, M. C. Myelination of parvalbumin interneurons shapes the function of cortical sensory inhibitory circuits. *Nat. Commun.* **11**, 5151 (2020).
- Ferguson, B. R. & Gao, W. J. PV interneurons: critical regulators of E/I balance for prefrontal cortex-dependent behavior and psychiatric disorders. *Front. Neural Circuits* **12**, 37 (2018).
- Wang, B. S. et al. Retinal and callosal activity-dependent chandelier cell elimination shapes binocularity in primary visual cortex. *Neuron* **109**, 502–515.e507 (2021).
- Southwell, D. G. et al. Intrinsically determined cell death of developing cortical interneurons. *Nature* **491**, 109–113 (2012).
- Orduz, D. et al. Developmental cell death regulates lineage-related interneuron-oligodendroglia functional clusters and oligodendrocyte homeostasis. *Nat. Commun.* **10**, 4249 (2019).
- Lim, L., Mi, D., Llorca, A. & Marin, O. Development and functional diversification of cortical interneurons. *Neuron* **100**, 294–313 (2018).
- Davies, A. M. Regulation of neuronal survival and death by extracellular signals during development. *EMBO J.* **22**, 2537–2545 (2003).
- Oppenheim, R. W. Cell death during development of the nervous system. *Annu. Rev. Neurosci.* **14**, 453–501 (1991).
- Vélez-Fort, M., Maldonado, P. P., Butt, A. M., Audinat, E. & Angulo, M. C. Postnatal switch from synaptic to extrasynaptic transmission between interneurons and NG2 cells. *J. Neurosci.* **30**, 6921–6929 (2010).
- Orduz, D. et al. Interneurons and oligodendrocyte progenitors form a structured synaptic network in the developing neocortex. *Elife* **4**, e06953 (2015).
- Serrano-Regal, M. P. et al. Oligodendrocyte differentiation and myelination is potentiated via GABA. *Neuroscience* **439**, 163–180 (2020).
- Balia, M., Benamer, N. & Angulo, M. C. A specific GABAergic synapse onto oligodendrocyte precursors does not regulate cortical oligodendrogenesis. *Glia* **65**, 1821–1832 (2017).
- Micheva, K. D. et al. A large fraction of neocortical myelin ensheathes axons of local inhibitory neurons. *Elife* **5**, e15784 (2016).
- Maas, D. A. et al. Interneuron hypomyelination is associated with cognitive inflexibility in a rat model of schizophrenia. *Nat. Commun.* **11**, 2329 (2020).
- Jahn, H. M. et al. Refined protocols of tamoxifen injection for inducible DNA recombination in mouse astroglia. *Sci. Rep.* **8**, 5913 (2018).
- Huang, W. et al. Novel NG2-CreERT2 knock-in mice demonstrate heterogeneous differentiation potential of NG2 glia during development. *Glia* **62**, 896–913 (2014).
- Kang, S. H., Fukaya, M., Yang, J. K., Rothstein, J. D. & Bergles, D. E. NG2+ CNS glial progenitors remain committed to the oligodendrocyte lineage in postnatal life and following neurodegeneration. *Neuron* **68**, 668–681 (2010).
- Zhu, X. et al. Age-dependent fate and lineage restriction of single NG2 cells. *Development* **138**, 745–753 (2011).
- Fame, R. M., MacDonald, J. L. & Macklis, J. D. Development, specification, and diversity of callosal projection neurons. *Trends Neurosci.* **34**, 41–50 (2011).
- Stedehouder, J. et al. Fast-spiking parvalbumin interneurons are frequently myelinated in the cerebral cortex of mice and humans. *Cereb. Cortex* **27**, 5001–5013 (2017).
- Stedehouder, J. et al. Local axonal morphology guides the topography of interneuron myelination in mouse and human neocortex. *Elife* **8**, e48615 (2019).

25. Zonouzi, M. et al. Individual oligodendrocytes show bias for inhibitory axons in the neocortex. *Cell Rep.* **27**, 2799–2808.e2793 (2019).
26. Scala, F. et al. Layer 4 of mouse neocortex differs in cell types and circuit organization between sensory areas. *Nat. Commun.* **10**, 4174 (2019).
27. Miteew, S. et al. Pharmacogenetic stimulation of neuronal activity increases myelination in an axon-specific manner. *Nat. Commun.* **9**, 306 (2018).
28. Chaudhry, F. A. et al. The vesicular GABA transporter, VGAT, localizes to synaptic vesicles in sets of glycinergic as well as GABAergic neurons. *J. Neurosci.* **18**, 9733–9750 (1998).
29. Pan-Vazquez, A., Wefelmeyer, W., Gonzalez Sabater, V., Neves, G. & Burrone, J. Activity-dependent plasticity of axo-axonic synapses at the axon initial segment. *Neuron* **106**, 265–276.e266 (2020).
30. Denaxa, M. et al. Modulation of apoptosis controls inhibitory interneuron number in the cortex. *Cell Rep.* **22**, 1710–1721 (2018).
31. Crosby, K. C. et al. Nanoscale subsynaptic domains underlie the organization of the inhibitory synapse. *Cell Rep.* **26**, 3284–3297.e3283 (2019).
32. Kirchhoff, F. & Kettenmann, H. GABA triggers a [Ca²⁺]_i increase in murine precursor cells of the oligodendrocyte lineage. *Eur. J. Neurosci.* **4**, 1049–1058 (1992).
33. Zhao, N., Huang, W., Cătălin, B., Scheller, A. & Kirchhoff, F. L-Type Ca²⁺ channels of NG2 glia determine proliferation and NMDA receptor-dependent plasticity. *Front Cell Dev. Biol.* **9**, 759477 (2021).
34. Lin, S. C. & Bergles, D. E. Synaptic signaling between GABAergic interneurons and oligodendrocyte precursor cells in the hippocampus. *Nat. Neurosci.* **7**, 24–32 (2004).
35. Fang, W. Q. et al. Overproduction of upper-layer neurons in the neocortex leads to autism-like features in mice. *Cell Rep.* **9**, 1635–1643 (2014).
36. Wong, F. K. et al. Pyramidal cell regulation of interneuron survival sculpts cortical networks. *Nature* **557**, 668–673 (2018).
37. Chicheportiche, Y. et al. TWEAK, a new secreted ligand in the tumor necrosis factor family that weakly induces apoptosis. *J. Biol. Chem.* **272**, 32401–32410 (1997).
38. Grossmann, T. The role of medial prefrontal cortex in early social cognition. *Front Hum. Neurosci.* **7**, 340 (2013).
39. Bicks, L. K., Koike, H., Akbarian, S. & Morishita, H. Prefrontal cortex and social cognition in mouse and man. *Front Psychol.* **6**, 1805 (2015).
40. Neely, C. L. C., Pedemonte, K. A., Boggs, K. N. & Flinn, J. M. Nest building behavior as an early indicator of behavioral deficits in mice. *J. Vis. Exp.* **152**, 60139 (2019).
41. Magno, L. et al. Transient developmental imbalance of cortical interneuron subtypes presages long-term changes in behavior. *Cell Rep.* **35**, 109249 (2021).
42. Winkles, J. A. The TWEAK-Fn14 cytokine-receptor axis: discovery, biology and therapeutic targeting. *Nat. Rev. Drug Disco.* **7**, 411–425 (2008).
43. Brown, S. A., Ghosh, A. & Winkles, J. A. Full-length, membrane-anchored TWEAK can function as a juxtacrine signaling molecule and activate the NF- κ B pathway. *J. Biol. Chem.* **285**, 17432–17441 (2010).
44. Cheadle, L. et al. Sensory experience engages microglia to shape neural connectivity through a non-phagocytic mechanism. *Neuron* **108**, 451–468.e459 (2020).
45. Mangin, J. M., Kunze, A., Chittajallu, R. & Gallo, V. Satellite NG2 progenitor cells share common glutamatergic inputs with associated interneurons in the mouse dentate gyrus. *J. Neurosci.* **28**, 7610–7623 (2008).
46. Boulanger, J. J. & Messier, C. Oligodendrocyte progenitor cells are paired with GABA neurons in the mouse dorsal cortex: Unbiased stereological analysis. *Neuroscience* **362**, 127–140 (2017).
47. Larsen, R., Proue, A., Scott, E. P., Christiansen, M. & Nakagawa, Y. The Thalamus Regulates Retinoic Acid Signaling and Development of Parvalbumin Interneurons in Postnatal Mouse Prefrontal Cortex. *eNeuro* **6** (2019).
48. Luyt, K. et al. Developing oligodendrocytes express functional GABA(B) receptors that stimulate cell proliferation and migration. *J. Neurochem.* **100**, 822–840 (2007).
49. Middei, S. et al. CREB is necessary for synaptic maintenance and learning-induced changes of the AMPA receptor GluA1 subunit. *Hippocampus* **23**, 488–499 (2013).
50. Tao, X., Finkbeiner, S., Arnold, D. B., Shaywitz, A. J. & Greenberg, M. E. Ca²⁺ influx regulates BDNF transcription by a CREB family transcription factor-dependent mechanism. *Neuron* **20**, 709–726 (1998).
51. Zhang, Y. et al. An RNA-sequencing transcriptome and splicing database of glia, neurons, and vascular cells of the cerebral cortex. *J. Neurosci.* **34**, 11929–11947 (2014).
52. Miyamae, T., Chen, K., Lewis, D. A. & Gonzalez-Burgos, G. Distinct physiological maturation of parvalbumin-positive neuron subtypes in mouse prefrontal cortex. *J. Neurosci.* **37**, 4883–4902 (2017).
53. Balia, M. et al. Postnatal down-regulation of the GABAA receptor γ 2 subunit in neocortical NG2 cells accompanies synaptic-to-extrasynaptic switch in the GABAergic transmission mode. *Cereb. Cortex* **25**, 1114–1123 (2015).
54. Passlick, S. et al. Expression of the γ 2-subunit distinguishes synaptic and extrasynaptic GABA(A) receptors in NG2 cells of the hippocampus. *J. Neurosci.* **33**, 12030–12040 (2013).
55. Spitzer, S. O. et al. Oligodendrocyte progenitor cells become regionally diverse and heterogeneous with age. *Neuron* **101**, 459–471.e455 (2019).
56. Nagy, B., Hovhannisyian, A., Barzan, R., Chen, T. J. & Kukley, M. Different patterns of neuronal activity trigger distinct responses of oligodendrocyte precursor cells in the corpus callosum. *PLoS Biol.* **15**, e2001993 (2017).
57. Arancibia-Carcamo, I. L. & Attwell, D. The node of Ranvier in CNS pathology. *Acta Neuropathol.* **128**, 161–175 (2014).
58. Arancibia-Carcamo, I. L. et al. Node of Ranvier length as a potential regulator of myelinated axon conduction speed. *Elife* **6**, e23329 (2017).
59. Swire, M., Kotelevsev, Y., Webb, D. J., Lyons, D. A. & Ffrench-Constant, C. Endothelin signalling mediates experience-dependent myelination in the CNS. *Elife* **8**, e49493 (2019).
60. Makinodan, M., Rosen, K. M., Ito, S. & Corfas, G. A critical period for social experience-dependent oligodendrocyte maturation and myelination. *Science* **337**, 1357–1360 (2012).
61. Bitzenhofer, S. H., Pöpplau, J. A., Chini, M., Marquardt, A. & Hanganu-Opatz, I. L. A transient developmental increase in prefrontal activity alters network maturation and causes cognitive dysfunction in adult mice. *Neuron* **109**, 1350–1364.e6 (2021).
62. Haller, C. et al. Floxed allele for conditional inactivation of the GABAB(1) gene. *Genesis* **40**, 125–130 (2004).
63. Madisen, L. et al. A robust and high-throughput Cre reporting and characterization system for the whole mouse brain. *Nat. Neurosci.* **13**, 133–140 (2010).
64. Huang, W. et al. During development NG2 glial cells of the spinal cord are restricted to the oligodendrocyte lineage, but generate astrocytes upon acute injury. *Neuroscience* **385**, 154–165 (2018).
65. Lidieth, M. sigTOOL: a MATLAB-based environment for sharing laboratory-developed software to analyze biological signals. *J. Neurosci. Methods* **178**, 188–196 (2009).
66. Bedner, P. et al. Astrocyte uncoupling as a cause of human temporal lobe epilepsy. *Brain* **138**, 1208–1222 (2015).
67. Deacon, R. M. Assessing nest building in mice. *Nat. Protoc.* **1**, 1117–1119 (2006).
68. Seibenhener, M. L. & Wooten, M. C. Use of the Open Field Maze to measure locomotor and anxiety-like behavior in mice. *J. Vis. Exp.* **96**, e52434 (2015).
69. Kaidanovich-Beilin, O., Lipina, T., Vukobradovic, I., Roder, J. & Woodgett, J. R. Assessment of social interaction behaviors. *J. Vis. Exp.* **48**, 2473 (2011).
70. Jung, M. et al. Lines of murine oligodendroglial precursor cells immortalized by an activated neu tyrosine kinase show distinct degrees of interaction with axons in vitro and in vivo. *Eur. J. Neurosci.* **7**, 1245–1265 (1995).
71. Zhao, N., Tian, Q., Fang, L. P., Kirchhoff, F., Bai, X. OPC-GABABR-interneuron. Zenodo <https://doi.org/10.5281/zenodo.6127555> (2022).

Acknowledgements

We thank Daniel Schauenburg for excellent animal husbandry and Frank Rhode, Alexander Grissmer and Samantha Bechet for experimental assistance, Qinghai Tian for technical support. We are also grateful to Prof. Jacqueline Trotter (University of Mainz, Mainz, Germany) for providing the Oli-neu cell line and Prof. Leda Dimou (University of Ulm, Ulm, Germany) for sharing MACs sorting protocols of OPCs. This work was supported by grants from the Deutsche Forschungsgemeinschaft (SPP 1757, DFG-237267101; SFB 894, DFG-157660137 to F.K.; FOR2289, DFG-262890264 to F.K. and A.S.; SPP1757 Young Investigator grant to X.B.), the BMBF (EraNet-Neuron, JTC2014: BrIE to F.K.), the European Commission (H2020-MSCA-ITN-2016 EU-GliaPhD #722053 to F.K.), the Romanian UEFISCDI (PCE 227; PN-III-P4-ID-PCE-2020-2477 to F.K.) and University of Saarland (HOMFORzellent2017 and NanoBioMed Young Investigator grant 2021 to X.B.).

Author contributions

X.B. initiated and designed the project. L.F., X.B., N.Z., L.C., H.C., N.H., C.L. and A.S. performed experiments. L.F., X.B., N.Z., L.C. and R.Z. analyzed data. B.B., W.H., and C.M. provided materials. X.B. and F.K. supervised the study and wrote the manuscript with comments of the other authors.

Funding

Open Access funding enabled and organized by Projekt DEAL.

Competing interests

The authors declare no competing interests.

Additional information

Supplementary information The online version contains supplementary material available at <https://doi.org/10.1038/s41467-022-29020-1>.

Correspondence and requests for materials should be addressed to Frank Kirchoff or Xianshu Bai.

Peer review information *Nature Communications* thanks Alexandria Hughes, Najate Benamer and the other anonymous reviewer(s) for their contribution to the peer review of this work. Peer review reports are available.

Reprints and permission information is available at <http://www.nature.com/reprints>

Publisher's note Springer Nature remains neutral with regard to jurisdictional claims in published maps and institutional affiliations.



Open Access This article is licensed under a Creative Commons Attribution 4.0 International License, which permits use, sharing, adaptation, distribution and reproduction in any medium or format, as long as you give appropriate credit to the original author(s) and the source, provide a link to the Creative Commons license, and indicate if changes were made. The images or other third party material in this article are included in the article's Creative Commons license, unless indicated otherwise in a credit line to the material. If material is not included in the article's Creative Commons license and your intended use is not permitted by statutory regulation or exceeds the permitted use, you will need to obtain permission directly from the copyright holder. To view a copy of this license, visit <http://creativecommons.org/licenses/by/4.0/>.

© The Author(s) 2022

A subset of OPCs do not express Olig2 during development which can be increased in the adult by brain injuries and complex motor learning

Li-Pao Fang¹  | Qing Liu¹  | Erika Meyer^{1,2}  | Anna Welle³  |
Wenhui Huang¹  | Anja Scheller¹  | Frank Kirchhoff^{1,4}  | Xianshu Bai¹ ¹Molecular Physiology, Center for Integrative Physiology and Molecular Medicine, University of Saarland, Homburg, Germany²Laboratory of Brain Ischemia and Neuroprotection, Department of Pharmacology and Therapeutics, State University of Maringá, Maringá, Brazil³Department of Genetics and EpiGenetics, University of Saarland, Saarbrücken, Germany⁴Experimental Research Center for Normal and Pathological Aging, University of Medicine and Pharmacy of Craiova, Craiova

Correspondence

Frank Kirchhoff and Xianshu Bai, Molecular Physiology, Center for Integrative Physiology and Molecular Medicine, Building 48, University of Saarland, 66421 Homburg, Germany.
Email: frank.kirchhoff@uks.eu and xianshu.bai@uks.eu

Funding information

Deutsche Forschungsgemeinschaft, Grant/Award Numbers: FOR 2289, HU2614/1-1(ProjectID, 462650276), SPP1757; Unitatea Executiva pentru Finantarea Invatamantului Superior, a Cercetarii, Dezvoltarii si Inovarii, Grant/Award Number: PCE 227; Universität des Saarlandes, Grant/Award Numbers: HOMFORExzellenz2018, Young Investigator Grant

Abstract

Oligodendrocyte precursor cells (OPCs) are uniformly distributed in the mammalian brain; however, their function is rather heterogeneous in respect to their origin, location, receptor/channel expression and age. The basic helix–loop–helix transcription factor Olig2 is expressed in all OPCs as a pivotal determinant of their differentiation. Here, we identified a subset (2%–26%) of OPCs lacking Olig2 in various brain regions including cortex, corpus callosum, CA1 and dentate gyrus. These Olig2 negative (Olig2^{neg}) OPCs were enriched in the juvenile brain and decreased subsequently with age, being rarely detectable in the adult brain. However, the loss of this population was not due to apoptosis or microglia-dependent phagocytosis. Unlike Olig2^{pos} OPCs, these subset cells were rarely labeled for the mitotic marker Ki67. And, accordingly, BrdU was incorporated only by a three-day long-term labeling but not by a 2-hour short pulse, suggesting these cells do not proliferate any more but were derived from proliferating OPCs. The Olig2^{neg} OPCs exhibited a less complex morphology than Olig2^{pos} ones. Olig2^{neg} OPCs preferentially remain in a precursor stage rather than differentiating into highly branched oligodendrocytes. Changing the adjacent brain environment, for example, by acute injuries or by complex motor learning tasks, stimulated the transition of Olig2^{pos} OPCs to Olig2^{neg} cells in the adult. Taken together, our results demonstrate that OPCs transiently suppress Olig2 upon changes of the brain activity.

Abbreviations: BrdU, bromodeoxyuridine; CA1, cornu ammonis 1; Cspg4, chondroitin sulfate proteoglycan 4; CC, corpus callosum; CCA, common carotid artery; ctl, control; DG, dentate gyrus; CTX, cortex; dpi, days post injury; E, embryonic day; FI, fluorescence intensity; GFAP, glial fibrillary acidic protein; GS, glutamine synthetase; hp, hippocampus; KA, kainate; MCAO, middle cerebral artery occlusion; MOp, primary motor cortex; mPFC, medial prefrontal cortex; neg, negative; NG2, neural/glia antigen 2; Olig2, oligodendrocyte transcription factor 2; OPCs, oligodendrocyte precursor cells; p, postnatal day; pos, positive; PDGFR α /P α , platelet derived growth factor receptor alpha; R26, Rosa26; SEM, standard error of the mean; SO, stratum oriens; SP, stratum pyramidale; SR, stratum radiatum; SWI, stab wound injury; tdT, tdTomato; w, week.

This is an open access article under the terms of the [Creative Commons Attribution-NonCommercial](https://creativecommons.org/licenses/by-nc/4.0/) License, which permits use, distribution and reproduction in any medium, provided the original work is properly cited and is not used for commercial purposes.

© 2022 The Authors. *GLIA* published by Wiley Periodicals LLC.



KEYWORDS

acute brain injury, Olig2, oligodendrocyte precursor cells, platelet derived growth factor receptor alpha, proliferation

1 | INTRODUCTION

Oligodendrocyte precursor cells (OPCs) are widely distributed within the central nervous system (CNS), however they are rather a heterogeneous population regarding to their location, origin, age and function (Marisca et al., 2020; Marques et al., 2016; Marques et al., 2018; Spitzer et al., 2019; Viganò et al., 2013). A conserved feature of OPCs is the capability to give rise to oligodendrocytes throughout the life (Trotter et al., 2010). OPC differentiation is tightly regulated by intrinsic and extrinsic factors (Rowitch & Kriegstein, 2010). The basic helix-loop-helix transcription factor Olig2, is one of the pivotal intrinsic determinants for oligodendrocyte specification (Liu et al., 2007; Lu et al., 2000; Lu et al., 2002; Maire et al., 2010; Zhou et al., 2000; Zhou & Anderson, 2002). In Olig2 null mice, OPC formation fails at embryonic and perinatal stages (Ligon et al., 2006; Mei et al., 2013), while overexpression of Olig2 triggers OPC differentiation and precocious myelination (Maire et al., 2010; Wegener et al., 2015). Although Olig2 is widely expressed throughout the oligodendroglial development, its function is rather specific to the cell stage (Mei et al., 2013). For instance, Olig2 expression in OPCs promotes cell differentiation and subsequent myelination, while in newly formed oligodendrocytes Olig2 seems to suppress maturation and myelination. Apart from lineage commitment, Olig2 exerts function in OPC migration. Overexpression of Olig2 accelerates OPC migration, differentiation and subsequently promoted remyelination in the lysoclethrin model of multiple sclerosis (Wegener et al., 2015).

Despite of the importance and abundance of Olig2 for the lineage of oligodendrocytes, a proportion of NG2^{pos} cells could not be detected for Olig2 expression in the healthy perinatal (about 1%) and adult cortex (8–30%) (Buffo et al., 2005; Ligon et al., 2006). This NG2^{pos}Olig2^{neg} population was even larger after a stab wound injury (Buffo et al., 2005). These NG2^{pos}Olig2^{neg} cells were defined according to their immunoreactivity to NG2 antibody. Of note, NG2 is also expressed by pericytes under physiological conditions and by a small population of microglia triggered by acute brain injuries (Huang et al., 2014; Huang et al., 2020). In addition, due to the cleavage of the extracellular domain of NG2 protein under pathological conditions, NG2 immunoreactivity per se cannot be referred as NG2 expression. Therefore, it is yet elusive whether or not Olig2^{neg} OPCs exist in the brain. If yes, how does the population develop with age? Are they functionally different to the Olig2^{pos} OPCs?

To address these open questions, we distinguished OPCs from other NG2 expressing cells with immunostaining of platelet derived growth factor receptor α (PDGFR α), a well-established marker of OPCs (Nishiyama et al., 1996). We analyzed different brain regions, for example, cortex, corpus callosum, CA1 and dentate gyrus, at different ages ranging from postnatal day (p) 5–44 weeks. PDGFR α ^{pos}Olig2^{neg} population was progressively increased at the first

two postnatal weeks, followed by a consistent decline. Derived from Olig2^{pos} cells, Olig2^{neg} cells were never expressing Ki67 and exhibited a less complex morphology. Complex motor learning or acute brain injuries, which are known to stimulate brain activity change, triggered increased the population of Olig2^{neg} OPCs in the adult hippocampus and cortex, respectively. In summary, our study demonstrates that OPCs suppress Olig2 expression upon the change of brain activity.

2 | RESULTS

2.1 | A subset of OPCs does not express Olig2

To investigate whether Olig2-non-expressing OPCs exist or not, we performed immunostaining of PDGFR α (P α) and Olig2 in coronal section of healthy mouse brain (Figure 1a). At postnatal day (p) 14, we observed a small population of P α ^{pos} cells expressing low level or no Olig2 in various brain regions, including primary motor cortex (MOp, Figure 1b–d), corpus callosum (CC, Figure 1e), CA1 (Figure 1f) and in the dentate gyrus region (DG, Figure 1g). To further characterize these cell subtypes, we classified P α ^{pos} cells into Olig2^{pos} cells with high immunoreactivity (fluorescence intensity [FI] > 10³, 96.52%) and Olig2^{neg} cells with no Olig2 expression (FI < 10³, 3.48%) (Supplementary Figure 1 A, B). To minimize misinterpretations attributable to potential masking of antigenic sites of Olig2 by formalin fixation, we compared the density of P α ^{pos}Olig2^{neg} cells by performing immunostaining with antigen retrieval. Employing three different methods, including 10 min incubation in 1% SDS solution, heat treatment in Tris-EDTA buffer (pH 9.0) or citrate buffer (pH 6.0) at 95°C for 30 min, we observed comparable amounts of P α ^{pos}Olig2^{neg} cells in all brain regions (Supplementary Figure 1 C–F). These results indicate that indeed a subset of OPCs do not express Olig2 in several brain regions.

To confirm these P α ^{pos}Olig2^{neg} cells are OPCs, we further performed immunostainings by combining P α and Olig2 with various cell type specific markers at p14, when the population peaks. All P α ^{pos}Olig2^{neg} cells were immunopositive for NG2 with bona fide OPC morphology (Figure 2a, Supplementary Figure 2 A). However, the majority (about 98%) of P α ^{pos}Olig2^{neg} cells were also negative for Sox10 (transcription factor, another lineage marker of oligodendrocytes) (Figure 2b, Supplementary Figure 2 B). In addition, these cells never expressed markers of mature oligodendrocytes (e.g., APC CC1, Figure 2c, Supplementary Figure 2 C), astrocytes (GFAP, Figure 2d, Supplementary Figure 2 D; GS, Supplementary Figure 2 E), neurons (NeuN, Figure 2e, Supplementary Figure 2 G), microglia (Iba1, Figure 2f, Supplementary Figure 2 F), or precursors (DCX, Figure 2g; Sox2, Figure 2h; Supplementary Figure 2 H). Therefore, our results suggest that P α ^{pos}Olig2^{neg} cells are OPCs/NG2 glia.

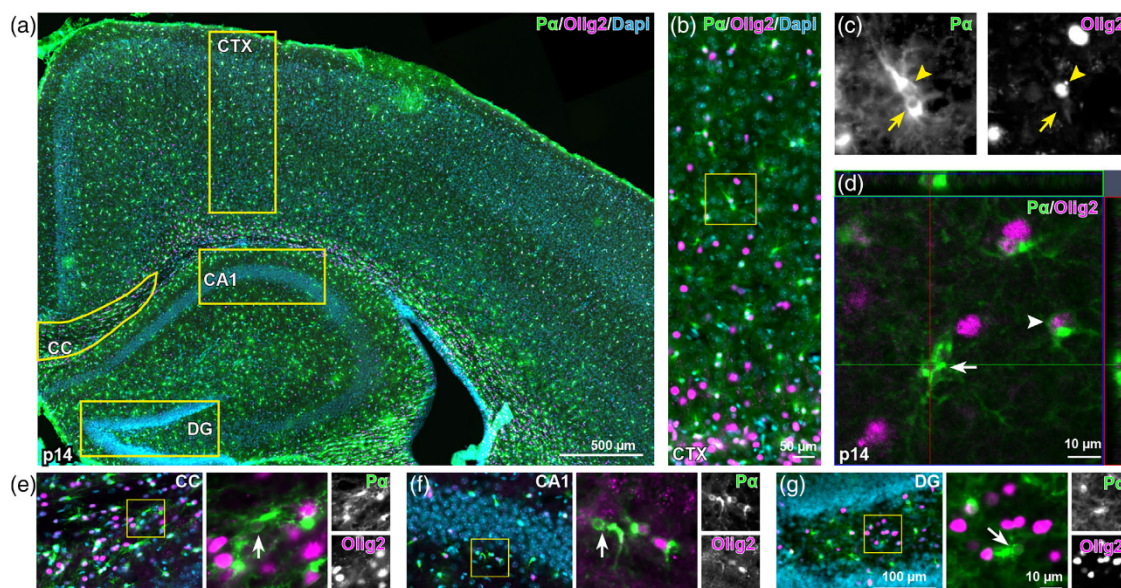


FIGURE 1 A subset of PDGFR α -positive cells do not express Olig2. (a) Overview of PDGFR α (P α , green) and Olig2 (magenta) immunostaining of coronal brain slices from p14 mice. (b and e–g) Representative images of cortex (CTX), corpus callosum (CC), CA1, and dentate gyrus (DG) stained with P α and Olig2. (c) Magnified views of P α ^{pos}Olig2^{neg} cells from b (boxed area). (d) Confocal images showing P α ^{pos} cells without Olig2 expression in cortex. Arrowheads: Olig2^{pos} OPCs, arrows: Olig2^{neg} OPCs.

To further substantiate the lack of Olig2 in a subset of OPCs, we took advantage of NG2-CreER^{T2} × R26-*lsl*-tdTomato mice, in which OPCs, their descendent oligodendrocytes as well as pericytes express tdTomato (tdT) after tamoxifen induced recombination. Tamoxifen was administered at p7 and 8 (Figure 2i), inducing tdT expression in about 80% of OPCs at p14 (Fang et al., 2022). Again, we observed a small population (about 3%) of P α ^{pos}tdT^{pos} cells expressing no Olig2 (Figure 2j,k), confirming that a subset of OPCs do not express Olig2.

2.2 | Olig2^{neg} OPCs are enriched in the juvenile brain

To elucidate whether this cell population exists temporarily or over all ages under physiological conditions, we further analyzed the mice at p5, p9, p14/2 week, 4, 9, 11, 22, and 44 week of age. In MOP, we observed about 1.3 ± 0.2 Olig2^{neg} cells/ 1×10^{-3} mm³ at p5 (Figure 3a,g), that is, about 2% of all OPCs (Figure 3h). Progressively, this P α ^{pos}Olig2^{neg} cell population increased reaching 3.1 ± 0.8 cells/ 1×10^{-3} mm³ (accounting for 7% of all OPCs) at p14 (Figure 3g,h). The same increase was observed in other brain regions (Figure 3g, Supplementary Figure 1 G–J) where P α ^{pos}Olig2^{neg} cells were covering 9%, 11%, 13%, and 26% of all OPCs in CC, mPFC, DG, and CA1, respectively (Figure 3h). After p14, the density of P α ^{pos}Olig2^{neg} cells continuously decreased. It became rarely detectable in the adult cortex (MOP and mPFC), but it still remained at a rather high level in CC (Figure 3d–f,g,h). Please note, the proportion

of P α ^{pos}Olig2^{neg} cells among all P α ^{pos} cells increased till the fourth postnatal week (Figure 3h), likely due to the reduced pool of P α ^{pos}Olig2^{pos} cells during development as observed by us and others (Figure 3i) (Kessar et al., 2006). Overall, our results indicate that Olig2^{neg} OPCs are present in the brain throughout life, with higher population during the development.

2.3 | Olig2^{neg} OPCs exhibit low proliferative activity

To understand whether the dynamic of the population size was attributed to cell proliferation, cell death or to a transient regulation of Olig2 gene expression, we firstly analyzed apoptosis and phagocytosis of these cells by performing immunostaining of cleaved caspase 3 (CC-3, a well-established marker for apoptosis) (Figure 4a) and CD68 (phagocytic marker, Figure 4b) at p14. Notably, Olig2^{neg} OPCs were neither positive for CC-3 nor for CD68 (Figure 4a,b, Supplementary Figure 3), largely excluding apoptotic loss or microglia mediated elimination of Olig2^{neg} OPCs.

Then, we assessed the proliferation by BrdU incorporation. To distinguish the fast and slowly dividing cells, BrdU was administered at 2 h prior to the analysis at p14 or for consecutive 3 days from p12 till p14 (Figure 4c). With the short pulse of BrdU administration, none of the Olig2^{neg} OPCs showed BrdU immunoreactivity in contrast to about 7% of Olig2^{pos} OPCs (Figure 4d,e). Nevertheless, a long-term administration of BrdU labeled about 10% of Olig2^{neg} OPCs with

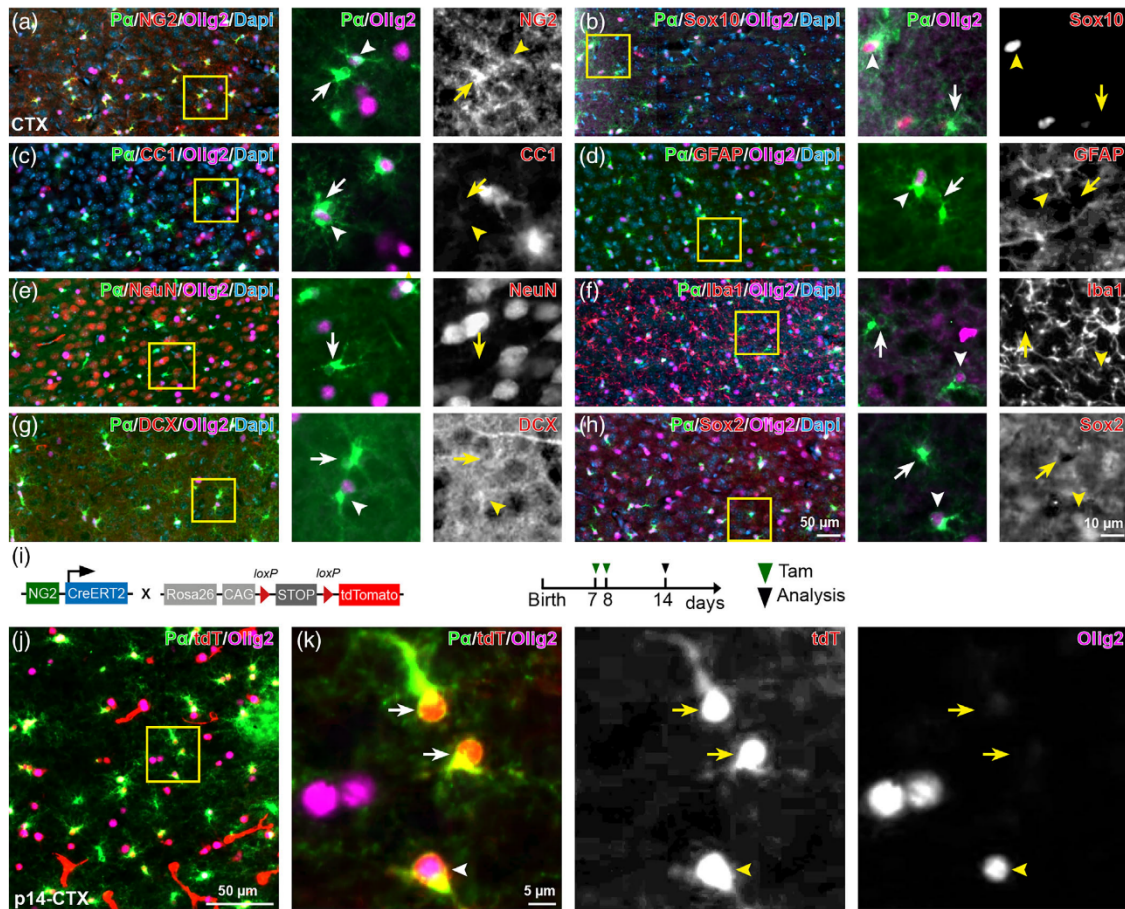


FIGURE 2 PDGFR α^{pos} Olig2 neg cells are bona fide OPCs. (a and b) P α^{pos} Olig2 neg cells are immunopositive for NG2 (a), but rarely express Sox10 (b). (c–h) P α^{pos} Olig2 neg cells are not oligodendrocytes (c), astrocytes (d), neuron (e), microglia (f), or neural precursors (g and h). (i) Scheme of transgene construct and experimental schedule. (j) Immunostaining of P α and Olig2 in the cortex of NG2-CreERT T2 x R26-tdTomato mice at p14. (k) Magnified views of P α^{pos} Olig2 neg cells expressing tdTomato (tdT) from the area indicated in (j). Arrowheads: Olig2 pos OPCs, arrows: Olig2 neg OPCs.

BrdU, which was still less than Olig2 pos OPCs (29%) (Figure 4d,e), suggesting that Olig2 neg OPCs divide very slowly if at all, and are likely derived from Olig2 pos OPCs.

To further clarify a potential proliferation capacity of Olig2 neg cells, we performed an immunostaining against the mitotic marker Ki67 on these cells at p14 brain (Figure 4f). About 7%–9% of Olig2 pos OPCs in the gray matter (MOp, CA1, and DG) and about 28% in the white matter (corpus callosum) (Figure 4g) (arrowheads in Figure 4f) were positive for Ki67, whereas 1.9% of P α^{pos} Olig2 neg cells in MOp (only one cell from a total of 160 cells from 10 mice) and none in CC, CA1 or DG showed immunoreactivity to Ki67 (Figure 4g, Supplementary Figure 4 A) both with or without antigen retrieval (Figure 4g, Supplementary Figure 4 C and D). To substantiate that Olig2 neg cells are not proliferative, we applied the same immunohistochemical protocol in the forebrain of embryos at embryonic day (E) 15.5, when the cells are more actively dividing. At E15.5, the first and second wave of

OPCs are already generated (Kessaris et al., 2006). We still could detect about 7% of OPCs being Olig2 neg (Figure 4h), suggesting Olig2 neg is not limited to the third wave of OPCs generated at perinatal days. While the majority of Olig2 pos OPCs expressed Ki67, none of the Olig2 neg cells expressed Ki67, thereby strongly suggesting a very low-proliferative property of Olig2 neg OPCs.

Taken together, our data suggest that Olig2 neg cells persist in the adult brain as a distinct subpopulation of oligodendrocyte lineage cells derived from Olig2 pos OPCs.

2.4 | Olig2 neg cells exhibit a simplified morphology

Since Olig2 is critical for OPC differentiation and subsequent myelination, we asked whether these Olig2 neg cells still could generate oligodendrocytes. OPCs increase branching of processes as they

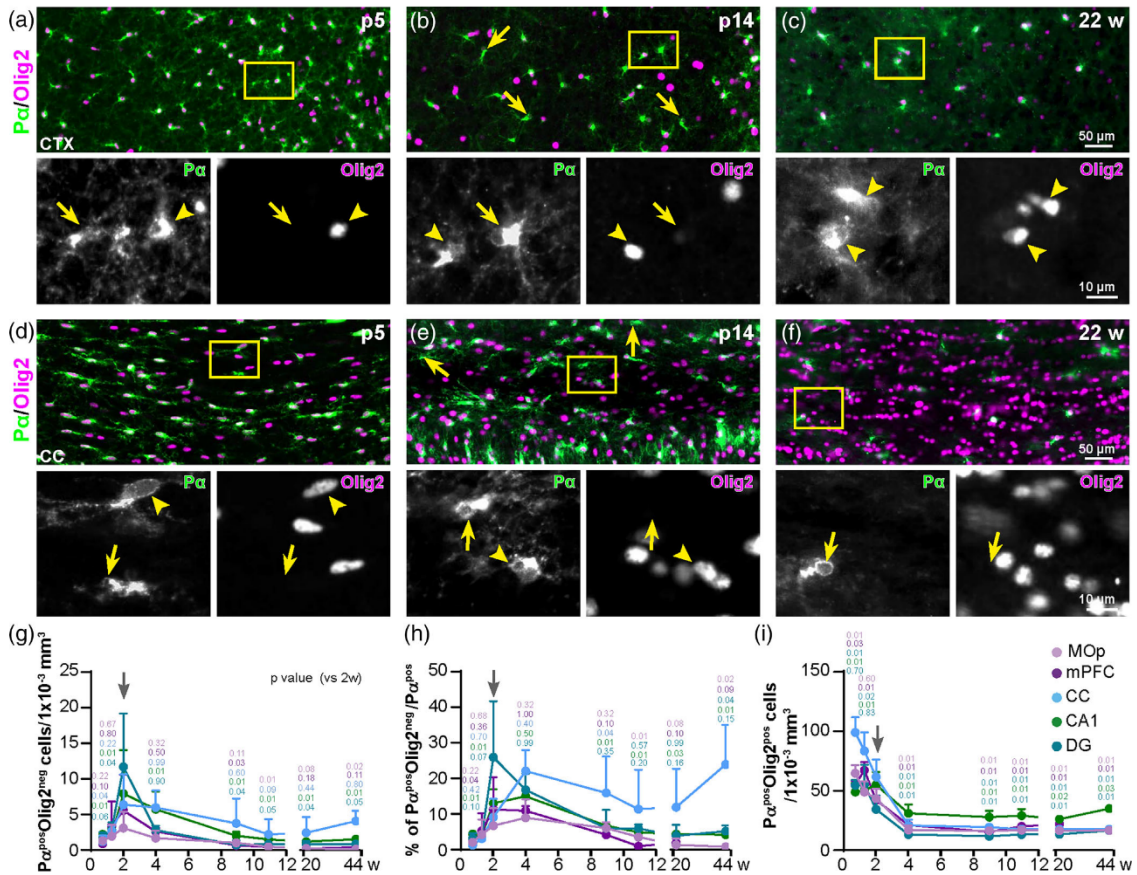


FIGURE 3 Olig2^{neg} OPCs are enriched in the juvenile brain. (a–c) Immunostaining of Pα and Olig2 in the cortex of mice at the age of p5 (a), p14 (b), and 22 weeks (c). (d–f) Immunostaining of Pα and Olig2 in the corpus callosum of mice at the age of p5 (d), p14 (e), and 22 week (f). (g–i) Quantification of density and proportion of Pα^{pos}Olig2^{neg} (g, i) and Pα^{pos}Olig2^{pos} cells (h) reveals maximal population of Pα^{pos}Olig2^{neg} cells in the juvenile brain (primary motor cortex, MOp; medial prefrontal cortex, mPFC; Corpus callosum, CC, CA1, and DG). (p5: N = 4 mice (all regions); p9: N = 4 mice (all regions); p14: N = 9 mice (MOp, CC, CA1, mPFC) and N = 7 mice (DG); 4 weeks: N = 4 mice (MOp), N = 5 mice (CA1), N = 3 mice (DG); 9 weeks: N = 4 mice (MOp, CC, CA1, DG), N = 6 mice (mPFC); 11 weeks: N = 5 mice (MOp and CA1), N = 2 mice (CC and mPFC), N = 3 mice (DG); 22 week: N = 2 mice (MOp, CC and CA1), N = 3 mice (DG and mPFC); 44 weeks: N = 3 (MOp, CC, CA1 and DG), N = 0 (mPFC). (within the same brain region, ordinary one-way ANOVA was used for statistical analysis between different time points. Similarly, different brain regions were compared using ordinary one-way ANOVA.) Arrowheads: Olig2^{pos} OPCs, arrows: Olig2^{neg} OPCs.

differentiate into oligodendrocytes (Pfeiffer et al., 1993). Therefore, we compared the morphology of these cells from the p14 cortex using a Sholl analysis based on Pα immunostaining (Figure 5a). We found that Olig2^{neg} OPCs displayed less process branches and shorter total filament length compared to the Olig2^{pos} cells (Figure 5b–d). These data indicate that Olig2^{neg} cells might remain in a precursor stage rather than differentiating into oligodendrocytes.

Studies have suggested that perivascular OPCs exhibit simpler morphologies in comparison to parenchymal ones (Kishida et al., 2019). To understand whether these Olig2^{neg} cells are perivascular OPCs, we labeled endothelial cells of the brain vasculature by PECAM-1/CD31 immunostaining in the p14 brain (Figure 6a, Supplementary Figure 4 B). About 40% of Olig2^{neg} OPCs in CC and 30% in

CA1 were located at blood vessels (Figure 6b). However, we also observed a rather low percentage of total Olig2^{pos} OPCs situated perivascular (18.5 ± 8.2% in CC; 16.7 ± 2.7% in CA1). In addition, in cortex and DG, the percentages of these two subtypes at blood vessels were similar (27.7 ± 8.4% [Olig2^{neg}] vs. 25.9 ± 7.0% [Olig2^{pos}] in MOp; 21.3 ± 2.1% [Olig2^{neg}] vs. 15.9 ± 2.8% [Olig2^{pos}] in DG) (Figure 6b). Hence, our results indicate that Olig2^{neg} cells are not necessarily perivascular OPCs, and vice versa. Interestingly, at E15.5 forebrain (about 7% of OPCs were Olig2^{neg}), almost 80% of Olig2^{neg} cells were situated perivascular (Figure 6c–e). This number was 2–3 folds higher than those observed in the adult brain (Figure 6b).

These results indicate that OPCs can down regulate Olig2 and stay in their precursor phase during brain development.

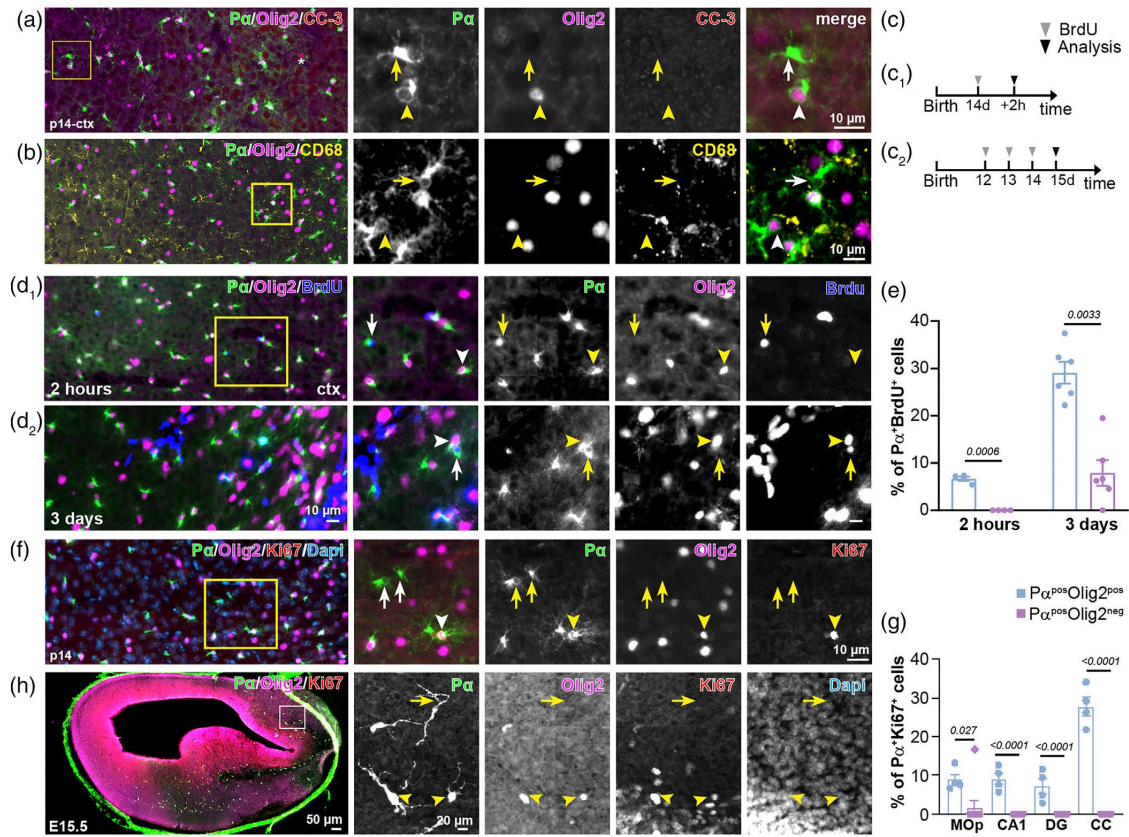


FIGURE 4 Olig2^{neg} cells proliferate less than Olig2^{pos} OPCs. (a) Pα^{pos}Olig2^{neg} cells lacked immunolabeling by apoptotic markers. (b) Pα^{pos}Olig2^{neg} cells are not phagocytosed by microglia. Arrowheads: Olig2^{pos} OPCs, arrows: Olig2^{neg} OPCs. (c) Experimental schedule for BrdU assay (c₁ and c₂) in d₁ and d₂, respectively. (d) Immunostaining of Pα and Olig2 in the cortex of p14 mice after 2 h (c₁, d₁) or 3 days (c₂, d₂) of BrdU administration. (e) Quantification of proliferating Olig2^{pos} and Olig2^{neg} OPCs by BrdU labeling (N = 4 mice (2 h), N = 6 mice (3 days); two tailed paired t-test). (f and g) Unlike Olig2^{pos} OPCs, Olig2^{neg} OPCs rarely expressed the proliferation marker Ki67 (primary motor cortex, MOP; CA1; dentate gyrus, DG; corpus callosum, CC). (N = 10 mice for all brain regions; two-tailed paired t-tests for each brain region). (h) Pα^{pos}Olig2^{neg} cells did not exhibit Ki67 immunoreactivity in the forebrain at embryonic day 15.5. Arrowheads: Olig2^{pos} OPCs, arrows: Olig2^{neg} OPCs.

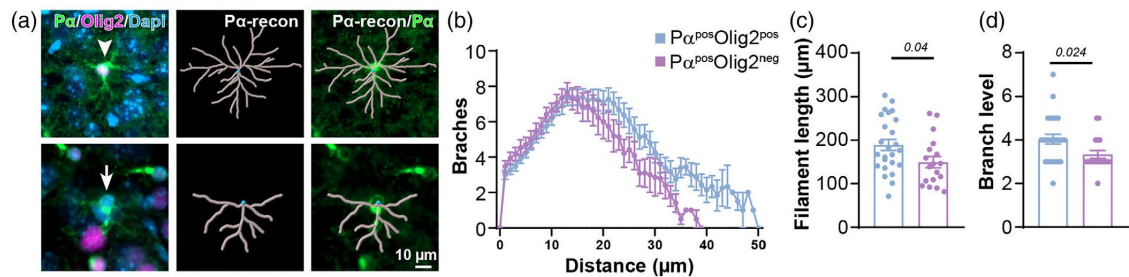


FIGURE 5 Pα^{pos}Olig2^{neg} cells are morphologically less complex than Olig2^{pos} OPCs. (a) Morphological analysis of Olig2^{pos} and Olig2^{neg} OPCs based on Pα immunostaining using Imaris software. (b-d) Sholl analysis showed shorter filament length (b and c) and less branches (b and d) of Olig2^{neg} OPCs. (b): Olig2^{pos} n = 26 cells from 4 mice, Olig2^{neg} n = 23 cells from 4 mice; c and d: Olig2^{pos} n = 25 cells from 4 mice, Olig2^{neg} n = 23 cells from 4 mice; two-tailed unpaired t-test)

10891136, 2023, 2, Downloaded from https://onlinelibrary.wiley.com/doi/10.1002/glia.24284 by Universitat Des Saarlandes, Wiley Online Library on [03/06/2023]. See the Terms and Conditions (https://onlinelibrary.wiley.com/terms-and-conditions) on Wiley Online Library for rules of use; OA articles are governed by the applicable Creative Commons License

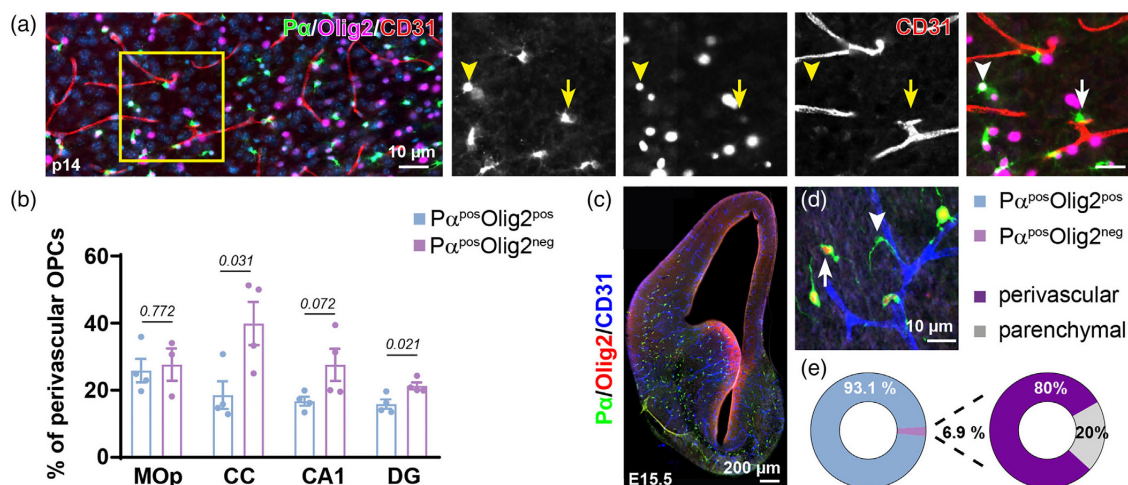


FIGURE 6 In dentate gyrus and corpus callosum P α ^{pos}Olig2^{neg} cells are preferentially located along the blood vessels in comparison to Olig2^{pos} OPCs. (a) Immunostaining of P α , Olig2, and CD31 at the p14 cortex showed OPCs with or without Olig2 expression adjacent to the blood vessels. (b) Percentage of perivascular OPCs with or without Olig2 from total P α ^{pos}Olig2^{pos} or P α ^{pos}Olig2^{neg} cells in p14 brain, respectively. (MOP: $N = 4$ (Olig2^{pos}) versus 3 (Olig2^{neg}) mice; CC: $N = 4$ mice; CA1: $N = 4$ mice; DG: $N = 4$ mice; two-tailed unpaired t-test). (c and d) Immunostaining of P α , Olig2, and CD31 in the E15.5 forebrain. (e) Population of Olig2^{neg} OPCs among all OPCs and the percentage of perivascular Olig2^{neg} OPCs from all Olig2^{neg} OPCs at E15.5. ($N = 4$ mice). Arrowheads: Olig2^{pos} OPCs, arrows: Olig2^{neg} OPCs.

2.5 | Increase of Olig2^{neg} OPCs in the adult brain after acute brain injuries

The main establishment of neural networks occurs between birth and p30, which parallels with the emergence of Olig2^{neg} OPCs. OPCs shape neural circuits by participating in synaptic transmission already from p5 and forming connections after differentiation (Bergles et al., 2000; Lin & Bergles, 2004; Orduz et al., 2015). Therefore, we asked whether there could be a causal link between the brain activity status and the formation of Olig2^{neg} OPCs. Therefore, we performed three different types of acute brain injuries in adult mice, when the Olig2^{neg} cell population is rather low. We used stab wound injuries (SWI), kainic acid (KA)-evoked seizures or middle cerebral artery occlusion (MCAO). SWI was induced to 9-week-old mice and analyzed at 3, 7, or 10 days post injury (Figure 7a,b). Already at 3 days post injury (dpi), the density of P α ^{pos}Olig2^{neg} cells in the ipsilateral side, especially at the lesion site (50 μ m aside from the lesion), increased 10-fold compared to the contralateral side (34.1 ± 6 vs. 3.5 ± 1 cells/ 1×10^{-2} mm³, Figure 7c). This number increased further at 7 dpi (75.8 ± 17.5 cells/ 1×10^{-2} mm³), while returned to the level as 3 dpi at 10 dpi (28.6 ± 1.8 cells/ 1×10^{-2} mm³) (Figure 7c). KA injection and MCAO also triggered the increase of P α ^{pos}Olig2^{neg} OPC population at the ipsilateral cortex 2 wp KA injection (Figure 7d-f and Supplementary Figure 5 A-C) or in the most affected region (according to the GFAP and Iba1 expression) of the MCAO stroke model (Supplementary Figure 5 D-G). All these data indicate that the formation of Olig2^{neg} cells can be triggered in the adult brain by modifying the brain activity.

To investigate whether these P α ^{pos}Olig2^{neg} cells were derived from pre-existing OPCs or from other precursors, we took advantage of NG2-CreER^{T2} \times R26-lsl-GCaMP3 mice where the OPCs can be assessed by evaluating the reporter gene GCaMP3 using GFP antibodies. In addition, compared to the R26-lsl-tdTomato reporter line, GCaMP3 mouse line labels less pericytes after fixation and immunostaining, facilitating a less complex system for OPC visualization among intensive glial and blood cell reaction at the lesion site. Recombination was induced by injection of tamoxifen at the age of 4 weeks. An SWI was performed at the age of 9 weeks (Figure 8a). About 90% OPCs were recombined at the age of 9 weeks (Fang et al., 2022). Analyzed at 3 dpi, all the P α ^{pos}Olig2^{neg} cells in both ipsilateral and contralateral sides were GFP^{pos} (Figure 8b,c), indicating that P α ^{pos}Olig2^{neg} cells were originating from pre-existing GFP^{pos} OPCs, not from other precursor cells. To confirm these hypothesis, we administered BrdU in the drinking water of NG2-CreER^{T2} \times R26-lsl-GCaMP3 mice for two consecutive weeks prior to the SWI to label dividing OPCs (Figure 8a). In the contralateral side of 3 dpi cortex, about 47.5% of Olig2^{pos} OPCs were BrdU⁺, but none of the Olig2^{neg} cells, again excluding a proliferative capacity of Olig2^{neg} cells. However, at the lesion site, 7% of P α ^{pos}GFP^{pos}Olig2^{neg} OPCs had incorporated BrdU (Figure 8b,c). Further immunostaining showed that Olig2^{neg} OPCs did not express Ki67 at 3 dpi (Figure 8c), as observed under physiological conditions, suggesting their origin from pre-existing OPCs after acute brain injuries.

Taken together, our data demonstrate that acute brain injuries can induce the generation of Olig2^{neg} OPCs from Olig2^{pos} OPCs.

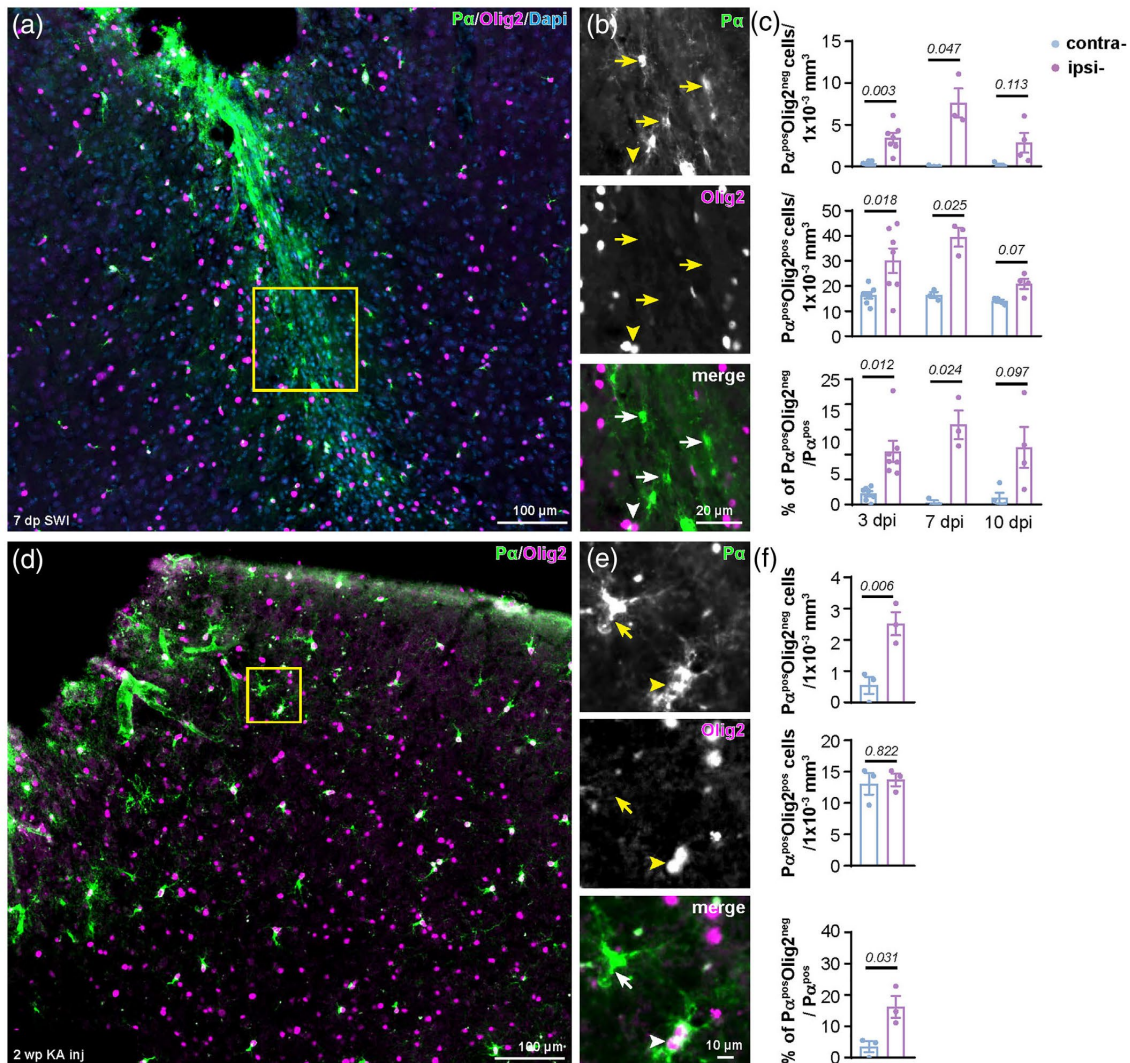


FIGURE 7 Cortical brain injuries trigger the new formation of P α^{pos} Olig2^{neg} OPCs at the lesion site. (a and b) Immunostaining of P α and Olig2 at the ipsilateral side after 7 days of stab wound injury (SWI) shows numerous P α^{pos} Olig2^{neg} OPCs at the lesion site. (c) Quantification of Olig2^{neg} and Olig2^{pos} OPCS cell density, as well as the proportion of P α^{pos} Olig2^{neg} cells among all OPCs in the contralateral and ipsilateral side at 3, 7, and 10 days post SWI. (3 dpi: $N = 7$, 7 dpi = 3, 10 dpi = 4 mice; two-tailed paired t-test). (d and e) Immunostaining of P α and Olig2 at the ipsilateral side of kainate injected cortex 2wpi. (f) Cell densities of Olig2^{neg} and Olig2^{pos} OPCS, and the percentage of Olig2^{neg} cells in the contralateral and ipsilateral side at 2 wpi of kainate. ($N = 3$ mice, two-tailed paired t-test). Arrowheads: Olig2^{pos} OPCS, arrows: Olig2^{neg} OPCS.

2.6 | The formation of Olig2^{neg} OPCs is related to the establishment of neural networks

To substantiate that Olig2^{neg} OPCs are required for the plastic formation of functional neural networks, we challenged mice with a 3-week complex running program on the Erasmus Ladder (Van Der Giessen et al., 2008). After 5 days of habituation, mice at 8 or 19 weeks of age had to run the ladder with random cues and obstacles for consecutive

16 days (Figure 9a). To correlate the learning and the appearance of Olig2^{neg} OPCs, immunostaining was performed at three different time points: before learning (right after habituation, day 5), middle of learning (day 13) and end of learning (day 21) (Figure 9a, Supplementary Figure 6 A). Quantification of missteps showed that the mice could run properly only at the last few days of the learning (Supplementary Figure 6 B). Learning a complex running program combines basic motor activity and learning. Therefore, motor cortex and hippocampus

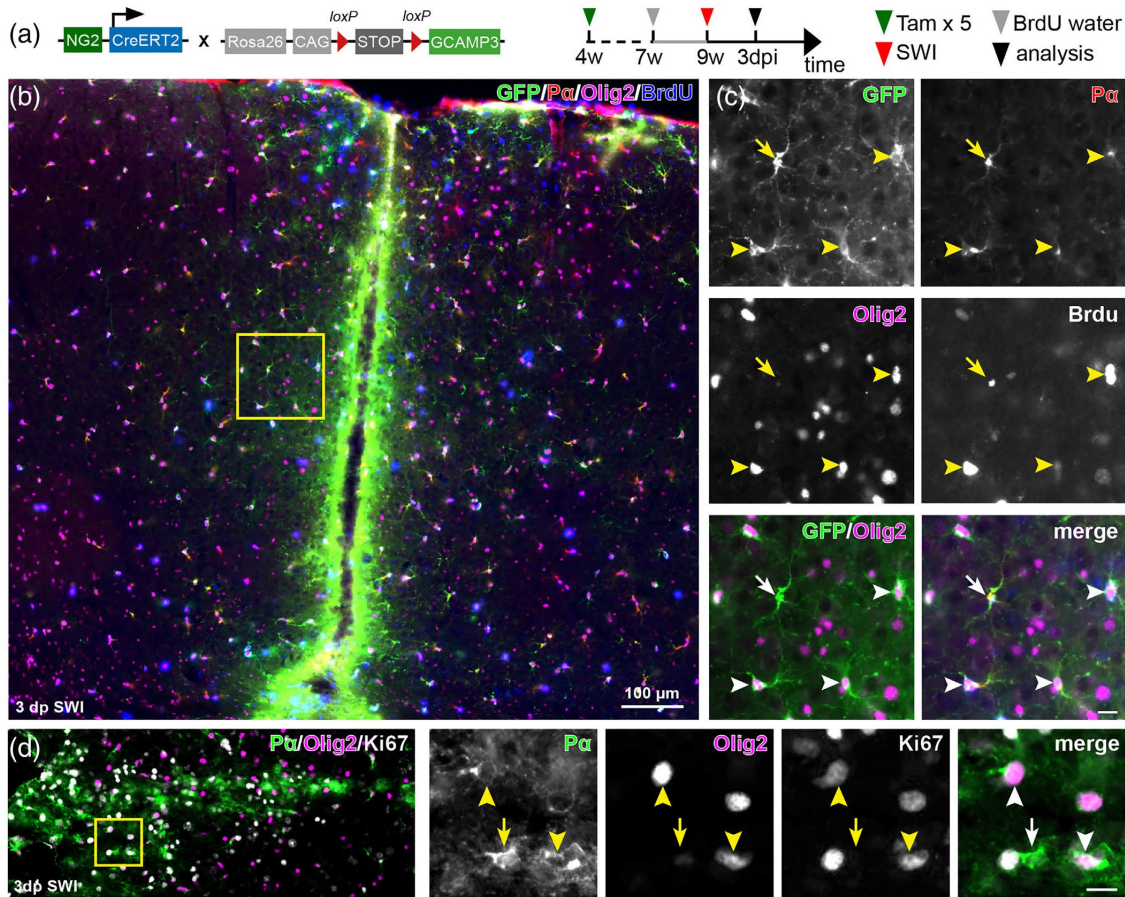


FIGURE 8 OPCs transiently suppress Olig2 after acute brain injury. (a) Scheme of transgene structure and experimental design for b and c. (b) Immunostaining of GFP, P α , Olig2, and BrdU at the lesion site 3 dpi. (c) Representative images showing that GFP^{POS}P α ^{POS} OPCs with (arrowhead) or without Olig2 (arrow) expression incorporated with BrdU. (d) Immunostaining of P α ^{POS}Olig2^{NEG} OPCs by the mitotic marker Ki67 in the lesion site at 3 days post stab wound injury (dpi SWI). Arrowheads: Olig2^{POS} OPCs, arrows: Olig2^{NEG} OPCs.

were primarily analyzed for the P α ^{POS}Olig2^{NEG} cell population, both brain regions closely related to motor activity and learning in the forebrain (Burman, 2019; Jacobacci et al., 2020). In the hippocampus, while the density of P α ^{POS}Olig2^{NEG} cells increased 2–4 times in both DG and CA1 region compared to control animal after complete learning session (Figure 9a–d), no change was observed before or during the early learning period (Supplementary Figure 6 C–E). In addition, the population of Olig2^{NEG} OPCs remained stable in the motor cortex, somatosensory cortex or CC (Supplementary Figure 6 F–J). These results suggest that the formation of Olig2^{NEG} OPCs in the hippocampus is likely related to learning induced novel neural networks.

In summary, our results indicate that a subset of OPCs transiently downregulate Olig2 upon micro-environmental changes, contributing further to OPCs heterogeneity.

3 | DISCUSSION

Olig2, a basic helix loop helix transcription factor, is a critical determinant for oligodendrocyte lineage function, specification, and differentiation. However, here, we observed a subset of OPCs that lack Olig2 throughout life in the brain, in gray as well as in white matter regions such as cortex, hippocampus or corpus callosum. Emergence of this population coincided with brain activity changes. Unlike Olig2^{POS} OPCs, Olig2^{NEG} cells exhibited very low (if any) self-renewing activity and a simplified morphology in the developing brain, suggesting a putative functional difference between these two subpopulations. Overall, our study demonstrated that upon the change of brain activity, a subset of OPCs transiently shutdown Olig2 expression.

OPCs receive glutamatergic and GABAergic input from neurons and differentiate into oligodendrocytes (Bergles et al., 2000; Gautier

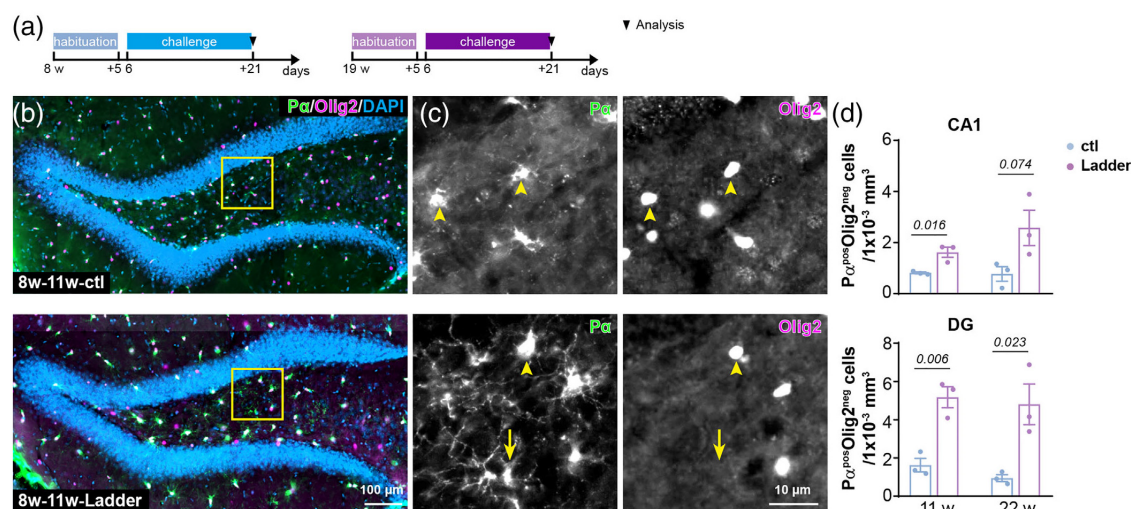


FIGURE 9 Complex motor learning increases the formation of Pα^{pos}Olig2^{neg} OPCs in the adult hippocampus. (a) Experimental schedule. (b) Overview of hippocampus immunostained with Pα and Olig2 in the control and trained mice. (c) Magnified views of the area indicated in (b) show OPCs (Pα^{pos}) with (arrowhead) or without (arrow) Olig2 expression. (d) Quantification of Pα^{pos}Olig2^{neg} cell density in the CA1 and DG region in the control and Erasmus ladder trained mice at 11 or 22 weeks. ($N = 3$ mice, two-tailed unpaired t -test). Arrowheads: Olig2^{neg} OPCs, arrows: Olig2^{pos} OPCs.

et al., 2015; Orduz et al., 2015; Serrano-Regal et al., 2020). Not only, OPCs also shape neural circuits (Fang et al., 2022; Xiao et al., 2022; Zhang et al., 2021). For instance, prior to myelin onset, the large population of OPCs in mouse medial prefrontal cortex release TNF like weak inducer of apoptosis (TWEAK) to optimize interneuron population which is pivotal for proper neural network activity (Fang et al., 2022). In addition, as seen in zebrafish optic tectum, a subtype of OPCs remain precursors throughout life and control axonal remodeling, never differentiating into myelinating oligodendrocytes (Xiao et al., 2022). A recent study has demonstrated that a set of genes, involved in pathways including neuronal differentiation and brain development, are repressed by Olig2 to ensure OPC differentiation into oligodendrocytes (Zhang et al., 2022). Therefore, it is tempting to speculate that OPCs switch off Olig2 expression and remain as precursors or NG2 glia upon the change of brain activity. Indeed, we observed a less complex morphology of Olig2^{neg} cells in comparison to Olig2^{pos} cells, suggesting Olig2^{neg} OPCs yet exhibit less potential to commit the differentiation.

In general, neural plasticity is greater in the developing brain than in the adult, and learning a new skill or brain injuries could boost neural circuit reorganization (Galván, 2010; Su et al., 2016). The appearance of Olig2^{neg} OPCs in the postnatal brain coincided with the development of neuron-OPCs connectivity starting from postnatal day 4–5 and reaching a peak at p10 for cortical interneurons (Orduz et al., 2015). Complex motor learning processes as well as acute brain injuries evoked novel formation of Olig2^{neg} OPCs. Interestingly, BMP4, known to repress Olig2 expression, is essential for synapse plasticity and is upregulated during brain development and after

injuries (Bai et al., 2021; Higashi et al., 2018). Therefore, BMP4 might be involved in the downregulation of Olig2 in OPCs during neural circuit establishment and to keep OPCs in precursor stage and innervate into neural circuit. Nevertheless, Olig2^{neg} cells were more frequently observed in white matter areas such as corpus callosum than in the gray matter of cortex or hippocampus. This could be attributable to inherited intrinsic programs (Viganò et al., 2013; Viganò & Dimou, 2015) and/or microenvironmental variations. E.g., the corpus callosum exhibits higher stiffness than gray matter, and such high stiffness hinders OPCs proliferation and differentiation (Segel et al., 2019). However, the Olig2^{neg} OPC population wanes with age, albeit the brain stiffness increases with age (Segel et al., 2019). Hence, molecular mechanisms involved in the generation of Olig2^{neg} OPCs needs to be further studied.

Taking advantage of NG2-CreER^{T2} mice, we found that Olig2^{neg} OPCs were derived from pre-existing OPCs downregulating Olig2 upon acute brain injuries. Interestingly, different to the Olig2^{pos} cells, Olig2^{neg} OPCs were rarely recognized by Ki67 antibody at any brain region. Indeed, Olig2 directly activates cell proliferating pathways to facilitate tumor growth in proneural glioma (Lu et al., 2016). Single cell RNA sequencing database of zebrafish and mouse brain have also suggested a subgroup of PDGFRα^{pos} OPCs that apparently lack expression of Olig2 and the mitotic marker Ki67 (Figure 10a) (Marisca et al., 2020; Marques et al., 2016). By analyzing the published database (<https://mouse-oligo-het.cells.ucsc.edu>) (Marques et al., 2016), we identified slightly higher numbers of OPCs without Olig2 mRNA (31.6% (database) vs 10–25% (own data), Figure 10d) and also similarly large proportion of these cells not expressing Ki67 (91%

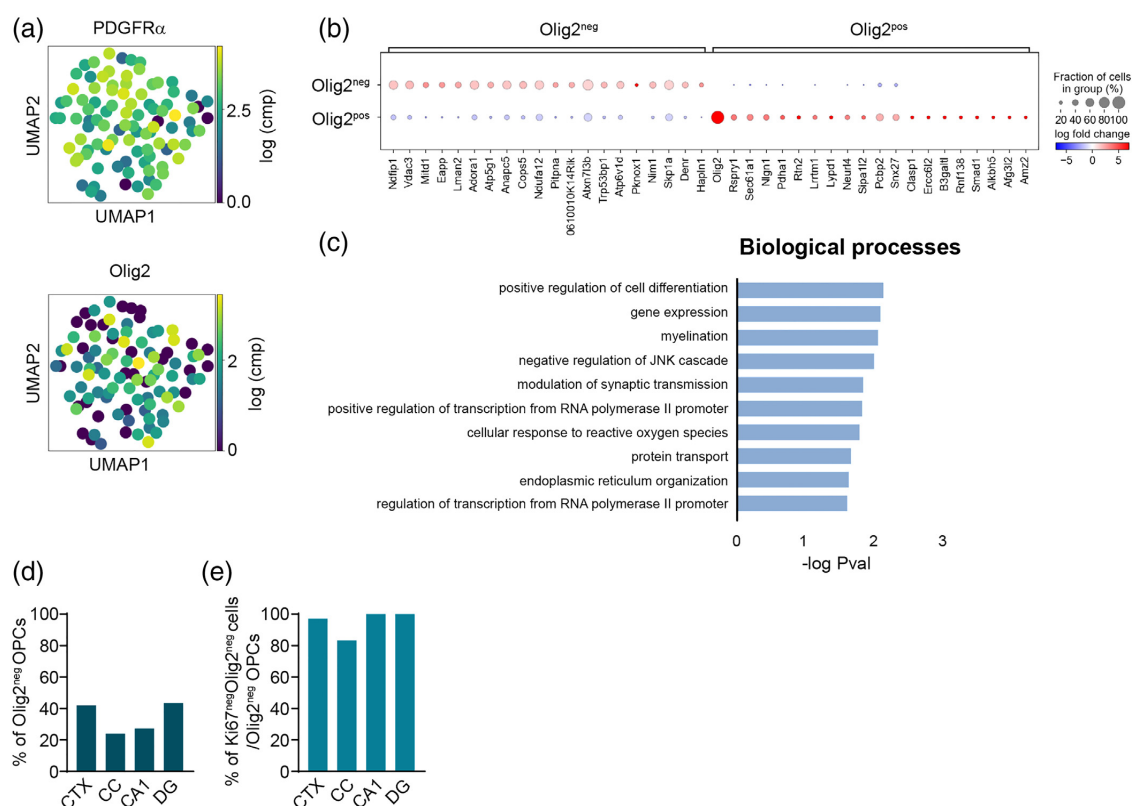


FIGURE 10 Cell differentiation and myelination is suppressed in Olig2^{neg} OPCs. (a) UMAP dimension reduction representation of single OPCs for PDGFR α and Olig2 expression from published database (Marques et al., 2016). (b) Dot plot visualizing differential gene expression between Olig2^{neg} and Olig2^{pos} OPCs. (c) Biological processes enriched for genes that are higher expressed in Olig2^{pos} OPCs. (d and e) Quantification of OPCs expressing no Olig2 (expression level = 0) (d) and Olig2^{neg} OPCs expressing no Ki67 (e) in cortex (CTX), corpus callosum (CC), CA1 and dentate gyrus (DG) from the data source of (Marques et al., 2016).

(database) vs 98–100% (own data), Figure 10e). In addition, in the zebra fish spinal cord, the “cluster #1” OPCs were also found to be negative for Ki67, considered as “quiescent” OPCs since they lacked proliferation and differentiation related markers (Marisca et al., 2020). Instead, these cells were enriched with mRNAs involved in axon guidance and synaptic communication (Marisca et al., 2020). Hence, if Olig2^{neg} OPCs represent similar “quiescent” OPC population in the mouse brain, these cells might be also well integrated into neural circuit. By comparing the genes differently expressed in Olig2^{pos} and Olig2^{neg} OPCs using published single cell transcriptomic data (Marques et al., 2016) (<https://mouse-oligo-het.cells.ucsc.edu>), we observed 59 genes enriched in Olig2^{neg} OPCs and 400 for Olig2^{pos} cells (Supplementary File S1, top 20 genes for each population are listed in Figure 10b). In Olig2^{neg} cells, for example, adenosine A1 receptor (A1AR, *Adora1*) was enriched compared to Olig2^{pos} cells, suggesting a potential purinergic signaling involved in suppression of Olig2 in OPCs. Shown by gene ontology (GO) analysis, genes positively regulating cell differentiation and myelination, eg. *Olig2*, *Mbp*,

Egr2 were highly enriched in the Olig2^{pos} cells (Figure 10c). Nevertheless, whether Olig2^{neg} OPCs are a functionally and physiologically different group of OPCs needs additional further characterization, for example, by electrophysiology or patch-sequencing. Developmentally, OPCs are generated in three waves: at E12.5 from Nkx2.1^{pos} precursors, at E14.5 from Gsx2^{pos} precursors and from Emx1^{pos} precursors at perinatal days (Kessaris et al., 2006). After birth, the first wave of OPCs, especially in the dorsal cortex, disappear within the first two postnatal weeks, matching to the time points when Olig2^{neg} OPCs start to appear. However, we did not observe Olig2^{neg} OPCs expressing cleaved caspase-3 or being phagocytosed by microglia. In addition, Olig2^{neg} OPCs can also exist in the embryonic brain (detected at E15.5), when yet no OPC death was reported. Nonetheless, we do not exclude other mechanisms eliminating OPCs thereby transiently becoming PDGFR α ^{pos}Olig2^{neg} cells, when PDGFR α is yet not fully degraded whereas Olig2 already is. However, the half-life of PDGFR α is 3 h in the absence of ligands and that of Olig2 is in the range of 4–8 h, at least *in vitro* (Coats et al., 1994; Kupp et al., 2016).



Unfortunately, these Olig2^{neG} OPCs are not able to be fate-tracked by live imaging techniques, since Olig2^{neG} OPCs can, so far, only be recognized by the immunostaining.

At the early postnatal brain Olig2 is mainly expressed by oligodendrocyte lineage cells and a subtype of astrocytes (Cai et al., 2007; Wang et al., 2021). Subsequently, astrocytes progressively downregulate Olig2 during their postnatal development, thereby Olig2 becomes restricted to the oligodendrocyte lineage (Lu et al., 2000; Takebayashi et al., 2002; Zhou et al., 2000). However, under pathological conditions, Olig2 expression alters and the expressing population even extends to other cell types, for example, astrocytes (Chen et al., 2008). Olig2 is essential for the astrogliosis after cortical injuries (Chen et al., 2008). Deletion of Olig2 specifically in OPCs induced the differentiation into astrocytes rather than into oligodendrocytes (Zhu et al., 2012). Several studies have indicated that OPCs differentiate into astrocytes upon acute brain injuries (Bai et al., 2021; Dimou et al., 2008; Komitova et al., 2011; Scheller et al., 2017; Tatsumi et al., 2008). Therefore, it is possible that these Olig2^{neG} OPCs switch their fate and give rise to astrocytes. However, fate mapping with NG2-CreER^{T2} mice did not show any reporter positive astrocytes in the physiological brain, also not after the peak of Olig2^{neG} OPCs appearance. Therefore, additional studies are necessary to investigate the function of Olig2^{neG} OPCs. This might provide a novel insight for the understanding of neuron-OPCs communication under physiological and pathological conditions.

4 | MATERIALS AND METHODS

4.1 | Ethics statement

All animal experiments were carried out at the University of Saarland in strict accordance with recommendations of European and German guidelines for the welfare of experimental animals. Animal experiments were approved by Saarland state's "Landesamt für Gesundheit und Verbraucherschutz" in Saarbrücken/Germany (animal license numbers: Perfusion 2020–2025, 36/2016, 03/2021, 08/2021).

4.2 | Animals

All mouse lines were maintained in C57BL/6N background and housed with a 12 hour (h) light/dark cycle at 20°C in the animal facility of the CIPMM. Mice were fed a breeding diet (V1125, Sniff) ad libitum. For the developmental study, C57BL/6N animals were analyzed at the age of postnatal day 5 (P5), P9, 2, 4, 9, 11, 22, and 44 weeks, while embryos were analyzed at E15.5. To follow the fate of OPCs, we took advantage of NG2-CreERT2 knock-in mice carrying CAG^{fl}-STOP^{fl}-tdTomato (TgH[ROSA26-CAG-fl-stop-fl-tdTomato]) or CAG^{fl}-STOP^{fl}-GCaMP3 (TgH[ROSA26-CAG-fl-stop-fl-GCaMP3]) reporter (W. Huang et al., 2014; Madisen et al., 2010; Paukert et al., 2014). Mice were always heterozygous for NG2-CreER^{T2} and homozygous for the floxed reporter loci. Data from both genders were pooled together without bias.

4.3 | Tamoxifen induced recombination

Tamoxifen (Carbolution, Neunkirchen, Germany) was dissolved in Miglyol[®]812 (Caesar & Lorentz GmbH, Hilden, Germany) to a final concentration of 10 mg/ml and administrated intraperitoneally for two consecutive days at postnatal day 7 and 8 or for five consecutive days at the age of 4 weeks (Fang et al., 2022; Jahn et al., 2018).

4.4 | Erasmus ladder

Complex motor learning was performed using the Erasmus Ladder (Noldus Technology) as previously described with modifications (Saab et al., 2012; Van Der Giessen et al., 2008). Individual test mice were placed in a dark shelter. With a light cue and 3 s delayed air cue, the animal was encouraged to run over the ladder and reach the shelter at the other side. One trial was defined as a single ladder crossing from one shelter to another, and one session was composed of 42 trials. Each mouse performed one session per day. The first 5 days were regarded as training sessions followed by 16 days of challenging sessions. At training sessions, mice were habituated with the ladder and the cues. From the sixth day, during ladder running mice were randomly perturbed by single sounds or obstacles, or combinations of sound and obstacles. Only one or no perturbation was added per trial. The duration time of steps per trial was automatically recorded.

4.5 | Stab wound injury

Stab wound injuries (SWI) were performed on 9–12 weeks old mice as described previously (Bai et al., 2021). Briefly, mice were anesthetized with a mixture of 2% Isoflurane and 49% O₂ and 49% N₂O via inhalation and the skull was thinned with a dental drill laterally 1.5 mm and longitudinally 2 mm from Bregma. A 1 mm deep stab wound was made by the insertion of surgical scalpel into the somatosensory cortex. The skin was sutured and buprenorphine/carprofen was intraperitoneally/subcutaneously given for three consecutive days. Tramadol (0.4 mg/ml) was administered in drinking water for seven consecutive days. Mice were analyzed at 3, 7, and 10 days post injury (dpi).

4.6 | Middle cerebral artery occlusion

MCAO was performed as previously described (W. Huang et al., 2020). Mice were anesthetized with inhalation anesthetics as described above. Briefly, the left common carotid artery (CCA) and the external carotid artery were ligated with silk sutures and an arteriotomy was performed on the CCA. Then a silicon-coated filament (Doccol Corp, CA) was inserted into the CCA and advanced through the internal carotid artery until it reached the origin of the middle cerebral artery. After 15 min of occlusion, reperfusion was obtained by withdrawal of the filament. Lastly, another suture was made around the CCA, to prevent back flow through the arteriotomy.

Mouse body temperature was continuously monitored using a rectal thermometer and an adjustable heat plate. Mice received buprenorphine/carprofen for pain relief and subcutaneous injection of 0.5 ml saline as fluid replacement for three consecutive days. Tramadol (0.4 mg/ml) was administered in drinking water for 7 consecutive days. Mice were analyzed at 3 dpi.

4.7 | Kainate injection

Cortical kainate injections were performed unilaterally as described previously (Bedner et al., 2015). Briefly, 70 nl of 20 mM kainic acid in saline was injected to the right hemisphere of anesthetized mice, at the position of AP:-1.92 mm, ML: 1.5 mm, DV: 1 mm referred to the bregma. Proper analgesic treatment was performed as ment Tramadol (0.4 mg/ml) was administered in drinking water for 7 consecutive days. Mice were analyzed at 1 and 14 dpi.

4.8 | Immunohistochemistry

Mice were perfused with PBS followed by 4% PFA. After post fixation, coronal vibratome slices in 40 μ m thickness were collected. After 1 h incubation with blocking buffer (5% horse serum with 0.5% Triton in PBS), free floating slices were incubated with primary antibodies at 4 °C overnight, followed by secondary antibody incubation. DAPI (25 ng/ml) was used to stain nuclei (A10010010, Biochimica). Primary and secondary antibodies are listed in the Supplementary Tables 1 and 2, respectively.

4.9 | Antigen retrieval treatment

Prior to the blocking step, the following treatments were performed:

SDS treatment: Slices were incubated with 1% SDS buffer (in 1x PBS) for 10 min and washed subsequently with 1x PBS for 5 min by three times (Q. Liu et al., 2022).

Heat treatment in Tris-EDTA buffer (pH = 9.0) or citrate buffer (pH = 6.0): Slices were attached to the slides in a proper sized slide container filled with 1 X Tris EDTA buffer (10 mM Tris base and 1 mM EDTA) or citrate buffer (10 mM citric acid and 0.05% Tween 20). The container was placed in water bath at temperature above 95°C for 30 min. After cooling to room temperature for 20 min, slices were blocked for primary antibody incubation. These two treatments were suggested by the website (Patel et al., 2020; Wimmer et al., 2019).

4.10 | Bromodeoxyuridine assay

For adult animals, 1 mg/ml BrdU was administered in the drinking water for 2 weeks before the surgery. For short pulse labeling, 10 mg/ml BrdU saline solution was intraperitoneally injected to the mice 2 h prior to the analysis. For BrdU immunostaining, after washing

off the secondary antibody, slices were fixed with 2% PFA at room temperature (RT) for 15 min, followed by washing with 1x PBS twice and once by distilled water. Slices were then incubated with 2 M HCl at 37°C for 45 min. After three times washing, slices were incubated with primary BrdU antibody and secondary antibodies as described above.

4.11 | Microscopic analysis and quantification

Two brain slices per mouse and at least three animals per group were analyzed. Images were obtained with an automated slide-scanning epifluorescence microscopy system (Zeiss AxioScan Z1, for overviews) or a confocal laser-scanning microscope (Zeiss LSM-710, for high-resolution and image stacks).

For quantification of fluorescence intensity of Olig2 and PDGFR α , slices scanned with the AxioScan Z1 were analyzed using ZEN 3.1 (blue edition, Zeiss) software. When the Olig2 fluorescence intensity was comparable to background value (between 1×10^2 and 1×10^3), it was considered as Olig2^{neg} OPC (Supplementary Figure 1 A). To account for variability in the staining from different animal, all values of Olig2 and PDGFR α were directly compared with values of the background in the same brain section.

4.12 | Single cell RNA sequencing analysis

Source data from (Marques et al., 2016) has been used for analysis. Read count data and meta data were downloaded from the USCS Cell Browser (<https://mouse-oligo-het.cells.ucsc.edu>). Counts were filtered and normalized using Scanpy (Wolf et al., 2018). Cells were identified as OPCs based on the “OPC” annotation in the meta data with high *Pdgfra* expression and no *Plp1* expression. Differential expression was identified by the *scanpy.tl.rank_genes_groups* command and genes with *p* value <.01 were subjected to DAVID online tool (Huang et al., 2009a, 2009b) to search for enriched GO terms. For Olig2^{neg} cells, only 7 genes (*p* <.01) were selected which were not adequate for GO analysis (Supplementary File S1).

4.13 | Statistical analysis

Data were analyzed with Graphpad Prism 9.0 and figures were generated with Adobe Indesign 2022. Animal numbers and the statistical parameters are indicated in the figure legends. Data were shown as mean \pm SEM and the means of each group were compared. Briefly, for the comparisons between two groups but from the same mice (e.g., the contra- and ipsilateral sides, or Olig2^{pos} and Olig2^{neg} cells with BrdU or Ki67 expression), we performed two-tailed paired t-tests. For the comparisons among more than two groups, we employed one-way ANOVA analysis. For two-group comparison between different mice, two-tailed unpaired t-tests were performed.

AUTHOR CONTRIBUTIONS

Li-Pao Fang and Xianshu Bai conceived and designed the experiments; Xianshu Bai and Li-Pao Fang performed surgeries and kainate injections; Erika Meyer performed MCAO experiments; Li-Pao Fang, Qing Liu and Wenhui Huang performed Erasmus Ladder experiments. Li-Pao Fang and Qing Liu carried out slice preparations, immunohistochemistry, confocal imaging, and data analysis. Anja Scheller performed AxioScan imaging. Anna Welle performed analysis of single cell RNA transcriptomic data. Xianshu Bai and Frank Kirchhoff supervised the project; Xianshu Bai wrote the manuscript with input from the other authors.

ACKNOWLEDGMENTS

The authors are grateful to Daniel Schauenburg and Frank Rhode for their excellent animal husbandry and technical assistance. We thank Prof. Dr. Mengsheng Qiu (Institute of Life Sciences, Hangzhou Normal University, Hangzhou, China) for providing feedback on the manuscript. We are grateful to Dr. Hongkui Zeng (Allen Institute for Brain Science, Seattle, Washington, USA) for providing Rosa26-tdTomato reporter mice, Dr. Amit Agarwal (Institute for Anatomy and Cell Biology, Heidelberg University, Heidelberg, Germany) for providing Rosa26-GCaMP3 mice and Prof. Dr. Jacqueline Trotter (Molecular Cell Biology, Johannes-Gutenberg University, Mainz, Germany) for providing AN2/NG2 antibodies. Qing Liu was supported by a PhD student stipend from the Chinese Scholarship Council. Open Access funding enabled and organized by Projekt DEAL.

FUNDING INFORMATION

This work was supported by grants from the DFG (SPP 1757 to Frank Kirchhoff and SPP1757 Young Investigator grant to Xianshu Bai; FOR 2289 to Frank Kirchhoff and Anja Scheller, Project 462650276 to Wenhui Huang), the Romanian UEFISCDI (PCE 227; PN-III-P4-ID-PCE-2020-2477 to Frank Kirchhoff) and the University of Saarland (NanoBioMed Young Investigator Grant to Xianshu Bai, HOMFORzellen2018 program to Xianshu Bai).

CONFLICT OF INTEREST

The authors declare no competing or financial interests.

DATA AVAILABILITY STATEMENT

The raw data are available from the corresponding authors upon reasonable request. Data of single cell RNA sequencing was submitted with the manuscript in Supplementary file.

ORCID

Li-Pao Fang  <https://orcid.org/0000-0002-7973-9523>
 Qing Liu  <https://orcid.org/0000-0002-5245-1474>
 Erika Meyer  <https://orcid.org/0000-0002-8425-6358>
 Anna Welle  <https://orcid.org/0000-0001-9915-2845>
 Wenhui Huang  <https://orcid.org/0000-0001-9865-0375>
 Anja Scheller  <https://orcid.org/0000-0001-8955-2634>
 Frank Kirchhoff  <https://orcid.org/0000-0002-2324-2761>
 Xianshu Bai  <https://orcid.org/0000-0002-4758-1645>

REFERENCES

- Bai, X., Zhao, N., Huang, W., Caudal, L., Zhao, R., Hirrlinger, J., Walz, W., Kirchhoff, F., & Scheller, A. (2021). After traumatic brain injury oligodendrocytes regain a plastic phenotype and can become astrocytes. *bioRxiv*, 2021.2006.2018.448919. <https://doi.org/10.1101/2021.06.18.448919>
- Bedner, P., Dupper, A., Hüttmann, K., Müller, J., Herde, M.K., Dublin, P., Deshpande, T., Schramm, J., Häussler, U., Haas, C.A., Henneberger, C., Theis, M., & Steinhäuser, C. (2015). Astrocyte uncoupling as a cause of human temporal lobe epilepsy. *Brain*, 138(Pt 5), 1208–1222. <https://doi.org/10.1093/brain/awv067>
- Bergles, D. E., Roberts, J. D., Somogyi, P., & Jahr, C. E. (2000). Glutamatergic synapses on oligodendrocyte precursor cells in the hippocampus. *Nature*, 405(6783), 187–191. <https://doi.org/10.1038/35012083>
- Buffo, A., Vosko, M. R., Ertürk, D., Hamann, G. F., Jucker, M., Rowitch, D., & Götz, M. (2005). Expression pattern of the transcription factor Olig2 in response to brain injuries: Implications for neuronal repair. *Proceedings of the National Academy of Sciences of the United States of America*, 102(50), 18183–18188. <https://doi.org/10.1073/pnas.0506535102>
- Burman, D. D. (2019). Hippocampal connectivity with sensorimotor cortex during volitional finger movements: Laterality and relationship to motor learning. *PLoS One*, 14(9), e0222064. <https://doi.org/10.1371/journal.pone.0222064>
- Cai, J., Chen, Y., Cai, W. H., Hurlock, E. C., Wu, H., Kernie, S. G., Parada, L. F., & Lu, Q. R. (2007). A crucial role for Olig2 in white matter astrocyte development. *Development*, 134(10), 1887–1899. <https://doi.org/10.1242/dev.02847>
- Chen, Y., Miles, D. K., Hoang, T., Shi, J., Hurlock, E., Kernie, S. G., & Lu, Q. R. (2008). The basic helix-loop-helix transcription factor olig2 is critical for reactive astrocyte proliferation after cortical injury. *The Journal of Neuroscience*, 28(43), 10983–10989. <https://doi.org/10.1523/JNEUROSCI.3545-08.2008>
- Coats, S. R., Olashaw, N. E., & Pledger, W. J. (1994). Characterization of platelet-derived growth factor alpha receptor synthesis and metabolic turnover. *Cell Growth & Differentiation*, 5(9), 937–942.
- Dimou, L., Simon, C., Kirchhoff, F., Takebayashi, H., & Goetz, M. (2008). Progeny of Olig2-expressing progenitors in the gray and white matter of the adult mouse cerebral cortex. *Journal of Neuroscience*, 28(41), 10434–10442. <https://doi.org/10.1523/jneurosci.2831-08.2008>
- Fang, L. P., Zhao, N., Caudal, L. C., Chang, H. F., Zhao, R., Lin, C. H., Hainz, N., Meier, C., Bettler, B., Huang, W., Scheller, A., Kirchhoff, F., & Bai, X. (2022). Impaired bidirectional communication between interneurons and oligodendrocyte precursor cells affects social cognitive behavior. *Nature Communications*, 13(1), 1394. <https://doi.org/10.1038/s41467-022-29020-1>
- Galván, A. (2010). Neural plasticity of development and learning. *Human Brain Mapping*, 31(6), 879–890. <https://doi.org/10.1002/hbm.21029>
- Gautier, H. O., Evans, K. A., Volbracht, K., James, R., Sitnikov, S., Lundgaard, I., James, F., Lao-Peregrin, C., Reynolds, R., Franklin, R.J.M., & Káradóttir, R. T. (2015). Neuronal activity regulates remyelination via glutamate signalling to oligodendrocyte progenitors. *Nature Communications*, 6, 8518. <https://doi.org/10.1038/ncomms9518>
- Higashi, T., Tanaka, S., Iida, T., & Okabe, S. (2018). Synapse elimination triggered by BMP4 exocytosis and presynaptic BMP receptor activation. *Cell Reports*, 22(4), 919–929. <https://doi.org/10.1016/j.celrep.2017.12.101>
- Huang, D. W., Sherman, B. T., & Lempicki, R. A. (2009a). Bioinformatics enrichment tools: Paths toward the comprehensive functional analysis of large gene lists. *Nucleic Acids Research*, 37(1), 1–13. <https://doi.org/10.1093/nar/gkn923>
- Huang, D. W., Sherman, B. T., & Lempicki, R. A. (2009b). Systematic and integrative analysis of large gene lists using DAVID bioinformatics resources. *Nature Protocols*, 4(1), 44–57. <https://doi.org/10.1038/nprot.2008.211>

- Huang, W., Bai, X., Meyer, E., & Scheller, A. (2020). Acute brain injuries trigger microglia as an additional source of the proteoglycan NG2. *Acta Neuropathologica Communications*, 8(1), 146. <https://doi.org/10.1186/s40478-020-01016-2>
- Huang, W., Zhao, N., Bai, X., Karram, K., Trotter, J., Goebels, S., Scheller, A., & Kirchhoff, F. (2014). Novel NG2-CreERT2 knock-in mice demonstrate heterogeneous differentiation potential of NG2 glia during development. *Glia*, 62(6), 896–913. <https://doi.org/10.1002/glia.22648>
- Jacobacci, F., Armony, J. L., Yeffal, A., Lerner, G., Amaro, E., Jovicich, J., Doyon, J., & Della-Maggiore, V. (2020). Rapid hippocampal plasticity supports motor sequence learning. *Proceedings of the National Academy of Sciences of the United States of America*, 117(38), 23898–23903. <https://doi.org/10.1073/pnas.2009576117>
- Jahn, H. M., Kasakow, C. V., Helfer, A., Michely, J., Verkhatsky, A., Maurer, H. H., Scheller, A., & Kirchhoff, F. (2018). Refined protocols of tamoxifen injection for inducible DNA recombination in mouse astroglia. *Scientific Reports*, 8(1), 5913. <https://doi.org/10.1038/s41598-018-24085-9>
- Kessarlis, N., Fogarty, M., Iannarelli, P., Grist, M., Wegner, M., & Richardson, W. D. (2006). Competing waves of oligodendrocytes in the forebrain and postnatal elimination of an embryonic lineage. *Nature Neuroscience*, 9(2), 173–179. <https://doi.org/10.1038/nn1620>
- Kishida, N., Maki, T., Takagi, Y., Yasuda, K., Kinoshita, H., Ayaki, T., Noro, T., Kinoshita, Y., Ono, Y., Kataoka, H., Yoshida, K., Lo, E.H., Arai, K., Miyamoto, S., & Takahashi, R. (2019). Role of perivascular oligodendrocyte precursor cells in angiogenesis after brain ischemia. *Journal of the American Heart Association*, 8(9), e011824. <https://doi.org/10.1161/JAHA.118.011824>
- Komitova, M., Serwanski, D. R., Lu, Q. R., & Nishiyama, A. (2011). NG2 cells are not a major source of reactive astrocytes after neocortical stab wound injury. *Glia*, 59(5), 800–809. <https://doi.org/10.1002/glia.21152>
- Kupp, R., Shtayer, L., Tien, A. C., Szeto, E., Sanai, N., Rowitch, D. H., & Mehta, S. (2016). Lineage-restricted OLIG2-RTK signaling governs the molecular subtype of glioma stem-like cells. *Cell Reports*, 16(11), 2838–2845. <https://doi.org/10.1016/j.celrep.2016.08.040>
- Ligon, K. L., Kesari, S., Kitada, M., Sun, T., Arnett, H. A., Alberta, J. A., Anderson, D.J., Stiles, C.D., & Rowitch, D. H. (2006). Development of NG2 neural progenitor cells requires Olig gene function. *Proceedings of the National Academy of Sciences of the United States of America*, 103(20), 7853–7858. <https://doi.org/10.1073/pnas.0511001103>
- Lin, S. C., & Bergles, D. E. (2004). Synaptic signaling between GABAergic interneurons and oligodendrocyte precursor cells in the hippocampus. *Nature Neuroscience*, 7(1), 24–32. <https://doi.org/10.1038/nn1162>
- Liu, Q., Guo, Q., Fang, L. P., Yao, H., Scheller, A., Kirchhoff, F., & Huang, W. (2022). Specific detection and deletion of the sigma-1 receptor widely expressed in neurons and glial cells in vivo. *J Neurochem*. <https://doi.org/10.1111/jnc.15693>
- Liu, Z., Hu, X., Cai, J., Liu, B., Peng, X., Wegner, M., & Qiu, M. (2007). Induction of oligodendrocyte differentiation by Olig2 and Sox10: Evidence for reciprocal interactions and dosage-dependent mechanisms. *Developmental Biology*, 302(2), 683–693. <https://doi.org/10.1016/j.ydbio.2006.10.007>
- Lu, F., Chen, Y., Zhao, C., Wang, H., He, D., Xu, L., Wang, J., He, X., Deng, Y., Lu, E.E., Liu, X., Verma, R., Bu, H., Drissi, R., Fouladi, M., Stemmer-Rachamimov, A.O., Burns, D., Xin, M., Rubin, J.B., & Lu, Q. R. (2016). Olig2-dependent reciprocal shift in PDGF and EGF receptor signaling regulates tumor phenotype and mitotic growth in malignant glioma. *Cancer Cell*, 29(5), 669–683. <https://doi.org/10.1016/j.ccell.2016.03.027>
- Lu, Q. R., Sun, T., Zhu, Z., Ma, N., Garcia, M., Stiles, C. D., & Rowitch, D. H. (2002). Common developmental requirement for Olig function indicates a motor neuron/oligodendrocyte connection. *Cell*, 109(1), 75–86. [https://doi.org/10.1016/s0092-8674\(02\)00678-5](https://doi.org/10.1016/s0092-8674(02)00678-5)
- Lu, Q. R., Yuk, D., Alberta, J. A., Zhu, Z., Pawlitzky, I., Chan, J., McMahon, A.P., Stiles, C.D., & Rowitch, D. H. (2000). Sonic hedgehog-regulated oligodendrocyte lineage genes encoding bHLH proteins in the mammalian central nervous system. *Neuron*, 25(2), 317–329.
- Madisen, L., Zwingman, T. A., Sunkin, S. M., Oh, S. W., Zariwala, H. A., Gu, H., Ng, L.L., Palmiter, R.D., Hawrylycz, M.J., Jones, A.R., Lein, E.S., & Zeng, H. (2010). A robust and high-throughput Cre reporting and characterization system for the whole mouse brain. *Nature Neuroscience*, 13(1), 133–140. <https://doi.org/10.1038/nn.2467>
- Maire, C. L., Wegener, A., Kerninon, C., & Nait Oumesmar, B. (2010). Gain-of-function of Olig transcription factors enhances oligodendrogenesis and myelination. *Stem Cells*, 28(9), 1611–1622. <https://doi.org/10.1002/stem.480>
- Marisica, R., Hoche, T., Agirre, E., Hoodless, L. J., Barkey, W., Auer, F., Castelo-Branco, G., & Czopka, T. (2020). Functionally distinct subgroups of oligodendrocyte precursor cells integrate neural activity and execute myelin formation. *Nature Neuroscience*, 23(3), 363–374. <https://doi.org/10.1038/s41593-019-0581-2>
- Marques, S., van Bruggen, D., Vanichkina, D. P., Floriddia, E. M., Munguba, H., Våremo, L., Giacomello, S., Falcão, A.M., Meijer, M., Björklund, Å.K., Hjerling-Leffler, J., Taft, R.J., & Castelo-Branco, G. (2018). Transcriptional convergence of oligodendrocyte lineage progenitors during development. *Developmental Cell*, 46(4), 504–517. <https://doi.org/10.1016/j.devcel.2018.07.005>
- Marques, S., Zeisel, A., Codeluppi, S., van Bruggen, D., Mendanha Falcão, A., Xiao, L., Li, H., Häring, M., Hochgerner, H., Romanov, R.A., Gyllborg, D., Muñoz Manchado, A., La Manno, G., Lönnnerberg, P., Floriddia, E.M., Rezayee, F., Ernfors, P., Arenas, E., Hjerling-Leffler, J., & Castelo-Branco, G. (2016). Oligodendrocyte heterogeneity in the mouse juvenile and adult central nervous system. *Science*, 352(6291), 1326–1329. <https://doi.org/10.1126/science.aaf6463>
- Mei, F., Wang, H., Liu, S., Niu, J., Wang, L., He, Y., Etxeberria, A., Chan, J.R., & Xiao, L. (2013). Stage-specific deletion of Olig2 conveys opposing functions on differentiation and maturation of oligodendrocytes. *The Journal of Neuroscience*, 33(19), 8454–8462. <https://doi.org/10.1523/JNEUROSCI.2453-12.2013>
- Nishiyama, A., Lin, X. H., Giese, N., Heldin, C. H., & Stallcup, W. B. (1996). Co-localization of NG2 proteoglycan and PDGF alpha-receptor on O2A progenitor cells in the developing rat brain. *Journal of Neuroscience Research*, 43(3), 299–314. [https://doi.org/10.1002/\(SICI\)1097-4547\(19960201\)43:3<299::AID-JNR5>3.0.CO;2-E](https://doi.org/10.1002/(SICI)1097-4547(19960201)43:3<299::AID-JNR5>3.0.CO;2-E)
- Orduz, D., Maldonado, P. P., Balia, M., Vélez-Fort, M., de Sars, V., Yanagawa, Y., Emiliani, V., & Angulo, M. C. (2015). Interneurons and oligodendrocyte progenitors form a structured synaptic network in the developing neocortex. *eLife*, 4, 1–20. <https://doi.org/10.7554/eLife.06953>
- Patel, C., Meadowcroft, M. D., Zagon, I. S., & McLaughlin, P. J. (2020). [Met5]-enkephalin preserves diffusion metrics in EAE mice. *Brain Research Bulletin*, 165, 246–252. <https://doi.org/10.1016/j.brainresbull.2020.10.015>
- Paukert, M., Agarwal, A., Cha, J., Doze, V. A., Kang, J. U., & Bergles, D. E. (2014). Norepinephrine controls astroglial responsiveness to local circuit activity. *Neuron*, 82(6), 1263–1270. <https://doi.org/10.1016/j.neuron.2014.04.038>
- Pfeiffer, S. E., Warrington, A. E., & Bansal, R. (1993). The oligodendrocyte and its many cellular processes. *Trends in Cell Biology*, 3(6), 191–197. [https://doi.org/10.1016/0962-8924\(93\)90213-k](https://doi.org/10.1016/0962-8924(93)90213-k)
- Rowitch, D. H., & Kriegstein, A. R. (2010). Developmental genetics of vertebrate glial-cell specification. *Nature*, 468(7321), 214–222. <https://doi.org/10.1038/nature09611>
- Saab, A. S., Neumeyer, A., Jahn, H. M., Cupido, A., Šimek, A. A., Boele, H. J., Scheller, A., Le Meur, K., Götz, M., Monyer, H., Sprengel, R., Rubio, M.E., Deitmer, J.W., De Zeeuw, C.I., & Kirchhoff, F. (2012). Bergmann glial AMPA receptors are required for fine motor



- coordination. *Science*, 337(6095), 749–753. <https://doi.org/10.1126/science.1221140>
- Scheller, A., Bai, X., & Kirchhoff, F. (2017). The role of the oligodendrocyte lineage in acute brain trauma. *Neurochemical Research*, 42(9), 2479–2489. <https://doi.org/10.1007/s11064-017-2343-4>
- Segel, M., Neumann, B., Hill, M. F. E., Weber, I. P., Viscomi, C., Zhao, C., Young, A., Agley, C.C., Thompson, A.J., Gonzalez, G.A., Sharma, A., Holmqvist, S., Rowitch, D.H., Franze, K., Franklin, R.J.M., & Chalut, K. J. (2019). Niche stiffness underlies the ageing of central nervous system progenitor cells. *Nature*, 573(7772), 130–134. <https://doi.org/10.1038/s41586-019-1484-9>
- Serrano-Regal, M. P., Luengas-Escuza, I., Bayón-Cordero, L., Ibarra-Aizpuru, N., Alberdi, E., Pérez-Samartín, A., Matute, C., & Sánchez-Gómez, M. V. (2020). Oligodendrocyte differentiation and myelination is potentiated via GABA. *Neuroscience*, 439, 163–180. <https://doi.org/10.1016/j.neuroscience.2019.07.014>
- Spitzer, S. O., Sitnikov, S., Kamen, Y., Evans, K. A., Kronenberg-Versteeg, D., Dietmann, S., de Faria, O. Jr., Agathou, S., & Kárádóttir, R. T. (2019). Oligodendrocyte progenitor cells become regionally diverse and heterogeneous with age. *Neuron*, 101(3), 459–471.e455. <https://doi.org/10.1016/j.neuron.2018.12.020>
- Su, Y. S., Veeravagu, A., & Gerald, G. (2016). Neuroplasticity after traumatic brain injury. In D. Laskowitz & G. Grant (Eds.), *Translational research in traumatic brain injury*. CRC Press/Taylor and Francis Group.
- Takebayashi, H., Nabeshima, Y., Yoshida, S., Chisaka, O., & Ikenaka, K. (2002). The basic helix-loop-helix factor olig2 is essential for the development of motoneuron and oligodendrocyte lineages. *Current Biology*, 12(13), 1157–1163.
- Tatsumi, K., Takebayashi, H., Manabe, T., Tanaka, K. F., Makinodan, M., Yamauchi, T., Makinodan, E., Matsuyoshi, H., Okuda, H., Ikenaka, K., & Wanaka, A. (2008). Genetic fate mapping of Olig2 progenitors in the injured adult cerebral cortex reveals preferential differentiation into astrocytes. *Journal of Neuroscience Research*, 86(16), 3494–3502. <https://doi.org/10.1002/jnr.21862>
- Trotter, J., Karram, K., & Nishiyama, A. (2010). NG2 cells: Properties, progeny and origin. *Brain Research Reviews*, 63(1–2), 72–82. <https://doi.org/10.1016/j.brainresrev.2009.12.006>
- Van Der Giessen, R. S., Koekkoek, S. K., van Dorp, S., De Gruilj, J. R., Cupido, A., Khosrovani, S., Dortland, B., Wellershaus, K., Degen, J., Deuchars, J., Fuchs, E.C., Monyer, H., Willecke, K., De Jeu, M.T., & De Zeeuw, C. I. (2008). Role of olivary electrical coupling in cerebellar motor learning. *Neuron*, 58(4), 599–612. [S0896-6273\(08\)00262-6 \[pii\] 10.1016/j.neuron.2008.03.016](https://doi.org/10.1016/j.neuron.2008.03.016)
- Viganò, F., & Dimou, L. (2015). The heterogeneous nature of NG2-glia. *Brain Research*, 1638, 129–137. <https://doi.org/10.1016/j.brainres.2015.09.012>
- Viganò, F., Möbius, W., Götz, M., & Dimou, L. (2013). Transplantation reveals regional differences in oligodendrocyte differentiation in the adult brain. *Nature Neuroscience*, 16(10), 1370–1372. <https://doi.org/10.1038/nn.3503>
- Wang, H., Xu, L., Lai, C., Hou, K., Chen, J., Guo, Y., Sambangi, A., Swaminathan, S., Xie, C., Wu, Z., & Sambangi, A., Swaminathan, S., Xie, C., Wu, Z., & Chen, G. (2021). Region-specific distribution of Olig2-expressing astrocytes in adult mouse brain and spinal cord. *Molecular Brain*, 14(1), 36. <https://doi.org/10.1186/s13041-021-00747-0>
- Wegener, A., Deboux, C., Bachelin, C., Frah, M., Kerninon, C., Seilhean, D., Wieder, M., Wegner, M., & Nait-Oumesmar, B. (2015). Gain of Olig2 function in oligodendrocyte progenitors promotes remyelination. *Brain*, 138(Pt 1), 120–135. <https://doi.org/10.1093/brain/awu375>
- Wimmer, I., Scharler, C., Zrzavy, T., Kadowaki, T., Mödgl, V., Rojc, K., Tröschler, A.R., Kitić, M., Ueda, S., Bradl, M., & Lassmann, H. (2019). Microglia pre-activation and neurodegeneration precipitate neuroinflammation without exacerbating tissue injury in experimental autoimmune encephalomyelitis. *Acta Neuropathologica Communications*, 7(1), 14. <https://doi.org/10.1186/s40478-019-0667-9>
- Wolf, F. A., Angerer, P., & Theis, F. J. (2018). SCANPY: large-scale single-cell gene expression data analysis. *Genome Biology*, 19(1), 15. <https://doi.org/10.1186/s13059-017-1382-0>
- Xiao, Y., Petrucco, L., Hoodless, L. J., Portugues, R., & Czopka, T. (2022). Oligodendrocyte precursor cells sculpt the visual system by regulating axonal remodeling. *Nature Neuroscience*, 25, 280–284. <https://doi.org/10.1038/s41593-022-01023-7>
- Zhang, K., Chen, S., Yang, Q., Guo, S., Chen, Q., Liu, Z., Li, L., Jiang, M., Li, H., Hu, J., Pan, X., Deng, W., Xiao, N., Wang, B., Wang, Z.X., Zhang, L., & Mo, W. (2022). The oligodendrocyte transcription factor 2 OLIG2 regulates transcriptional repression during myelinogenesis in rodents. *Nature Communications*, 13(1), 1423. <https://doi.org/10.1038/s41467-022-29068-z>
- Zhang, X., Liu, Y., Hong, X., Li, X., Meshul, C. K., Moore, C., Yang, Y., Han, Y., Li, W.G., Qi, X., Lou, H., Duan, S., Xu, T.L., & Tong, X. (2021). NG2 glia-derived GABA release tunes inhibitory synapses and contributes to stress-induced anxiety. *Nature Communications*, 12(1), 5740. <https://doi.org/10.1038/s41467-021-25956-y>
- Zhou, Q., & Anderson, D. J. (2002). The bHLH transcription factors OLIG2 and OLIG1 couple neuronal and glial subtype specification. *Cell*, 109(1), 61–73. [https://doi.org/10.1016/s0092-8674\(02\)00677-3](https://doi.org/10.1016/s0092-8674(02)00677-3)
- Zhou, Q., Wang, S., & Anderson, D. J. (2000). Identification of a novel family of oligodendrocyte lineage-specific basic helix-loop-helix transcription factors. *Neuron*, 25(2), 331–343.
- Zhu, X., Zuo, H., Maher, B. J., Serwanski, D. R., LoTurco, J. J., Lu, Q. R., & Nishiyama, A. (2012). Olig2-dependent developmental fate switch of NG2 cells. *Development*, 139(13), 2299–2307. <https://doi.org/10.1242/dev.078873>

SUPPORTING INFORMATION

Additional supporting information can be found online in the Supporting Information section at the end of this article.

How to cite this article: Fang, L.-P., Liu, Q., Meyer, E., Welle, A., Huang, W., Scheller, A., Kirchhoff, F., & Bai, X. (2023). A subset of OPCs do not express Olig2 during development which can be increased in the adult by brain injuries and complex motor learning. *Glia*, 71(2), 415–430. <https://doi.org/10.1002/glia.24284>



Application of Fused Organoid Models to Study Human Brain Development and Neural Disorders

Augustin Chen^{1,2,3†}, Zhenming Guo^{1,2,4†}, Lipao Fang^{1,2,3†} and Shan Bian^{1,2,*}

¹Institute for Regenerative Medicine, Shanghai East Hospital, School of Life Sciences and Technology, Tongji University, Shanghai, China, ²Frontier Science Center for Stem Cell Research, Tongji University, Shanghai, China, ³Molecular Physiology, Center for Integrative Physiology and Molecular Medicine (CIPMM), University of Saarland, Homburg, Germany, ⁴Bio-X Institute, Shanghai Jiao Tong University, Shanghai, China

Human brain organoids cultured from human pluripotent stem cells provide a promising platform to recapitulate histological features of the human brain and model neural disorders. However, unlike animal models, brain organoids lack a reproducible topographic organization, which limits their application in modeling intricate biology, such as the interaction between different brain regions. To overcome these drawbacks, brain organoids have been pre-patterned into specific brain regions and fused to form an assembloid that represents reproducible models recapitulating more complex biological processes of human brain development and neurological diseases. This approach has been applied to model interneuron migration, neuronal projections, tumor invasion, oligodendrogenesis, forebrain axis establishment, and brain vascularization. In this review article, we will summarize the usage of this technology to understand the fundamental biology underpinning human brain development and disorders.

Keywords: brain organoid, fusion models, stem cells, brain development, neural disorder

OPEN ACCESS

Edited by:

Cristina Cereda,
National Institute of Casimiro
Mondino Neurological Institute
(IRCCS), Italy

Reviewed by:

James P. Kesby,
University of Queensland, Australia
Jinchong Xu,
Johns Hopkins University,
United States

*Correspondence:

Shan Bian
shan_bian@tongji.edu.cn

[†]These authors have contributed
equally to this work

Specialty section:

This article was submitted to *Cellular
Neurophysiology*, a section of the
journal *Frontiers in Cellular
Neuroscience*

Received: 15 February 2020

Accepted: 21 April 2020

Published: 15 May 2020

Citation:

Chen A, Guo Z, Fang L and Bian S
(2020) Application of Fused Organoid
Models to Study Human Brain
Development and Neural Disorders.
Front. Cell. Neurosci. 14:133.
doi: 10.3389/fncel.2020.00133

INTRODUCTION

The human central nervous system (CNS) develops from several distinct vesicles into multiple intertwined regions. During this process, a range of migratory streams arise where progenitors generated in one place migrate and integrate into other areas (Marín et al., 2001; Kwan et al., 2012; Clowry et al., 2018; Molnár et al., 2019), and complex networks emerge, neurons branching and projecting across multiple regions (López-Bendito and Molnár, 2003). Besides, the colonization of the embryonic brain by mesodermal derivatives, namely microglia progenitors from the yolk-sac (Rezaie et al., 2005; Monier et al., 2007), and capillaries from the meningeal inner pial lamella (Marín-Padilla, 2012) adds complexity to the development of the human brain. Yet convoluted, the mechanism underpinning the formation of the human CNS is a highly ordered process that needs to be understood.

Human brain organoids are self-organizing three-dimensional stem cell cultures that recapitulate many aspects of the early developing human brain. These organoids include the formation of cortical progenitors with *in vivo*-like morphology and spatiotemporal organization (Eiraku et al., 2008; Kadoshima et al., 2013; Lancaster et al., 2013, 2017; Pasca et al., 2015; Renner et al., 2017) as well as faithful gene expression and epigenome compared to human fetal brains (Camp et al., 2015; Luo et al., 2016; Quadrato et al., 2017; Amiri et al., 2018; Velasco et al., 2019; Trevino et al., 2020). To recapitulate the first developmental stages of the human CNS, human brain

organoids overcome many limitations imposed by animal models, providing a unique tool to study early stages of the human brain development under both physiological and pathological conditions (Lancaster and Knoblich, 2014b; Fatehullah et al., 2016). Although there are still many limitations, brain organoids have been applied to model human brain development and disorders since the milestone publication by Eiraku et al. (2008) introducing the model for the very first time.

By comparing the cerebral organoids derived from humans and non-human primates, this technology led to the discovery of human-specific developmental features (Mora-Bermúdez et al., 2016; Otani et al., 2016; Kanton et al., 2019; Pollen et al., 2019). Results from clonal analysis and live-imaging experiments converged on the finding that human cortical progenitors spend more time in a proliferative state (Mora-Bermúdez et al., 2016; Otani et al., 2016). This has been supported by the description of a higher activity of the PI3K-AKT-mTOR pathway—involved in the maintenance of pluripotency—specific to human radial glia from outer subventricular zones (Pollen et al., 2019). These studies provide possible developmental mechanisms to the higher number of neurons observed in the human cortex. When grown from patient-derived induced pluripotent stem cell (iPSC), brain organoids can model some aspects of developmental diseases (Amin and Pasca, 2018), such as microcephaly (Lancaster et al., 2013; Omer Javed et al., 2018; Zhang et al., 2019), macrocephaly (Li et al., 2017), lissencephaly (Bershteyn et al., 2017; Iefremova et al., 2017), autism (Mariani et al., 2015), schizophrenia (Ye et al., 2017), Down syndrome (Xu et al., 2019), and neuronal heterotopia (Klaus et al., 2019). When exposed to viral loads, brain organoids provide new insights into prenatal infections like ZIKV (Cugola et al., 2016; Garcez et al., 2016; Qian et al., 2016). Moreover, brain organoids could be used as *in vitro* screening platform for potential therapeutics and gene editing technologies for the introduction or the suppression of oncogene mutations (Bian et al., 2018). In a nutshell, by reproducing many aspects of the intricate development of the CNS, human brain organoids are used to study the impact of genomic and transcriptomic modifications as well as the exposition to various stress factors on the early development of the human CNS (Schwartz et al., 2015; Lee et al., 2017; Zhu Y. et al., 2017; Belair et al., 2018; Wang et al., 2018).

Throughout the embryonic brain, neural progenitors progressively acquire their spatial identities, a process regulated by the successive actions of patterning centers and transcriptional frameworks (Molnár et al., 2019). When grown without additional patterning molecules, one single organoid can differentiate into various brain regions, including dorsal and ventral forebrain, choroid plexus, hippocampus, and retina (Lancaster et al., 2013). Although some organizing centers were observed in brain organoids (Renner et al., 2017), which are critical for regional brain patterning, most of the spatial identities in organoids appeared in an uncontrolled manner, thereby limiting the study of complex interregional interactions. Application of patterning factors and/or chemicals allows us to pattern brain organoids into different brain regions (Eiraku et al., 2008, 2011; Muguruma et al., 2010, 2015; Nakano et al., 2012;

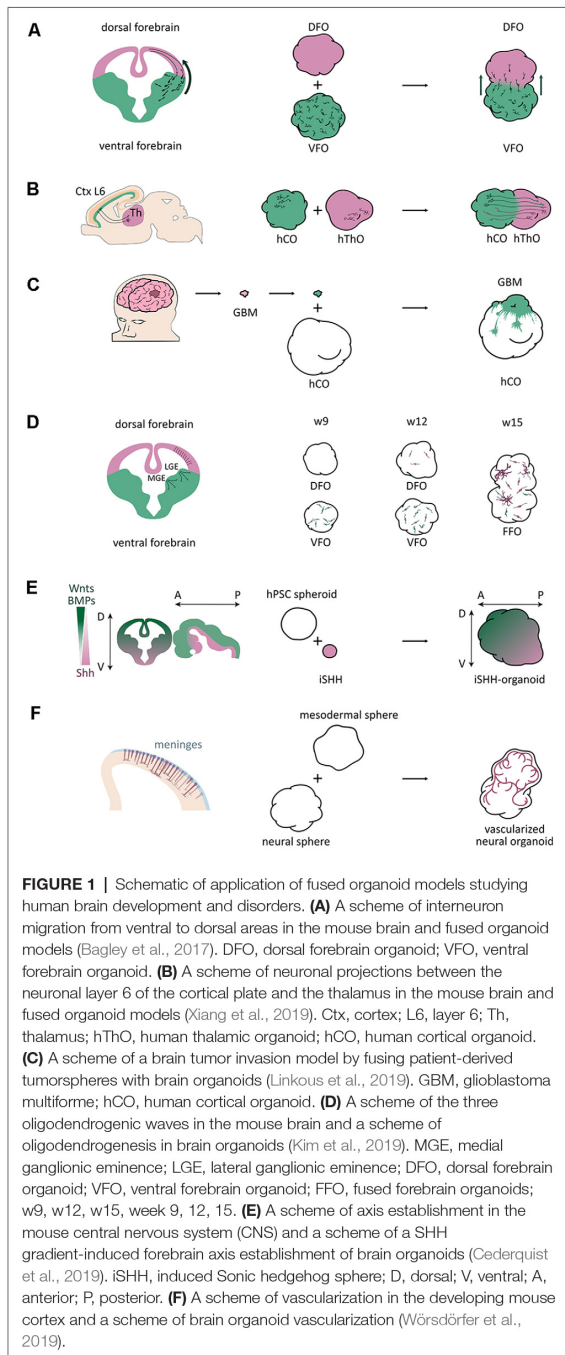
Kadoshima et al., 2013; Sakaguchi et al., 2015; Jo et al., 2016; Qian et al., 2016; Xiang et al., 2019), which provides researchers “LEGO blocks” to establish fused organoid approaches. The development of fused organoids, also called assembloids (Marton and Pasca, 2019), opens a new avenue to investigate interregional dynamics in the embryonic brain. Fusing two brain organoids pre-patterned into different regional identities enables the study of interregional interactions. This organoid fusion technology has already been applied for the study of interneuron migration (Bagley et al., 2017; Birey et al., 2017; Xiang et al., 2017), brain circuits (Giandomenico et al., 2019; Xiang et al., 2019), oligodendrogenesis (Xiang et al., 2017; Kim et al., 2019), and to establish the dorsoventral and anteroposterior axes within forebrain organoids (Cederquist et al., 2019). Organoids made by the fusion approach can help to deconstruct organogenesis by reconstructing the brain piece by piece.

The fusion paradigm should not be limited to the interaction of different brain regions. Any 3D co-culture system involving the assembly of brain organoids with a different tissue can be encompassed in the fusion approaches. This extended definition includes the co-culture of organoids with other cell types, such as endothelial cells (Song et al., 2019; Wörsdörfer et al., 2019) and tumor cells (Ogawa et al., 2018; Linkous et al., 2019; Bhaduri et al., 2020; Zhu et al., 2020). In this review article, we summarize the potential and great diversity of brain organoid fusion and co-culture models in studying human brain development and neural disorders.

INTERNEURON MIGRATION

Inhibitory interneurons, mostly GABAergic cells, are mainly derived from two areas of the human embryonic subpallium (ventral forebrain): the medial ganglionic eminence (MGE) and the caudal ganglionic eminence (CGE; Yuste, 2005; Wonders and Anderson, 2006; Bartolini et al., 2013). After production, post-mitotic interneurons migrate tangentially towards the dorsal forebrain, where, they wire and form functional circuits with locally born excitatory neurons. Defects in interneuron proliferation or impeded migration would disrupt the balance between these two types of neurons and are thought to contribute to many neurological and psychiatric disorders, such as schizophrenia, Down syndrome and autism (Wonders and Anderson, 2006; Bartolini et al., 2013; Bagley et al., 2017; Xu et al., 2019).

Studying interneurons, especially their interaction with excitatory neurons in organoids, would expand our view of these diseases, which are mainly studied using animal models. Although different brain regions, including dorsal and ventral forebrain, can be found in cerebral organoids, they appear in random locations without a stereotyped arrangement (Lancaster et al., 2013, 2017; Lancaster and Knoblich, 2014a), which make it challenging to model interneuron migration in organoids. However, the organoid fusion technique overcame this issue thereby allowing the modeling of human interneuron migration. In 2017, three independent groups generated interneuron migration models using fused organoid approaches (Figure 1A; Bagley et al., 2017; Birey et al., 2017; Xiang et al., 2017).



Interneurons were produced in the ventral organoids, and migrated into the dorsal regions after fusion.

The first study using brain organoids to model interneuron migration has been reported by Birey et al. (2017). Based

on a cortical spheroid (hCS) protocol (Pasca et al., 2015), Birey et al. (2017) patterned their organoids into ventral forebrain or subpallium identities by adding WNT inhibitor and Sonic Hedgehog (SHH) agonist during early stages of the differentiation protocol. The results of immunostaining and single-cell RNA sequencing (scRNA-seq) revealed that human subpallium spheroids (hSSs) were composed of various ventral progenitors and GABAergic interneurons, which were also found to be functionally active by patch clamping. After fusing hCSs with hSSs, Dlx1/2b::eGFP labeled hSS cells were found crossing the fusion boundary, moving further into hCSs, generating elaborated branched morphologies, and forming functional synapses with hCS glutamic neurons. FACS followed by scRNA-seq analysis revealed interneuron transcriptional signatures in eGFP⁺ cells isolated from the hCSs, following previous findings (Zechel et al., 2014). This migration in hSS-hCS fused organoids is consistent with human cortical development. Also, they combined patient-derived iPSCs and the organoid fusion approach to study Timothy syndrome, an L-type calcium channel (LTCCs)-related disorder affecting many organs of the human body including the nervous system. A previous study in mice indicated that LTCCs are associated with interneuron migration (Bortone and Polleux, 2009). Impaired interneuron migration was observed in patient-iPSC derived hSS-hCS, and was rescued by administration of an LTCC blocker.

Bagley et al. (2017) also established a fusion method, but modified from Lancaster's protocol (Lancaster and Knoblich, 2014a). The WNT inhibitor IWP2 and SHH agonist SAG were applied for organoid ventralization, while CycA, an SHH receptor antagonist, was used to dorsalize organoids (Vazin et al., 2014). In GFP⁺ ventral and dTomato⁺ dorsal fused organoids, a uni-directional cell migration from ventral into dorsal regions was observed. Rarely, migration was observed within the dorso-dorsal fused organoids. The largest proportion of migrated cells was SOX6⁺ MGE cells. Also, COUP-TFII⁺/NR2F2⁺ and SP8⁺ lateral ganglionic eminence (LGE)/CGE cells were observed to migrate into dorsal regions. Slice culture of dorso-ventral fusion organoids and time-lapse imaging analysis revealed characteristic interneuron migratory dynamics. Administration of the CXCR4 antagonist AMD3100 onto organoid slice cultures perturbed the migration, supporting a potential application of the fusion platform for drug screening.

Further, Xiang et al. (2017) generated human MGE organoids (hMGEOs) using an *NKX2-1::GFP* reporter human embryonic stem cell (hESC) line. RNA-seq, scRNA-seq, and chromatin accessibility analysis revealed that hMGEOs exhibited a strong correlation with the transcriptional signature of the MGE tissues from of human fetal brain. By fusing human cortical organoids (hCOs) and hMGEOs, they established hMGEOs-hCOs fusion organoids, named hFMCOs. GFP⁺ but RFP⁺ interneuron progenitors migrated into the neuronal layer of hCOs. Their migration can be inhibited by the application of blebbistatin, a myosin II inhibitor. Besides, functional synapses in hFMCOs were also observed by calcium imaging analysis.

Furthermore, using a dorsoventral organoid fusion model, Yuan et al. (2020) showed that LHX6 is essential for

GABAergic interneuron migration. Another study implanted patient iPSC-derived ventralized organoids into the mouse brain to investigate the role of OLIG2 in Down syndrome etiology (Xu et al., 2019). All these studies highlight the great potential of using the organoid fusion approaches to investigate the role of interneuron migration during human brain development and neural disorders.

NEURONAL PROJECTIONS

Long distance-projections play essential roles in brain functions. According to recent reports, corticothalamic interactions are relevant for sensorimotor interplay, selective attention, and arousal behaviors (López-Bendito and Molnár, 2003). Recently, Xiang et al. (2019) developed a method to form human thalamic organoids (hThOs) and created a model for corticothalamic projection by merging cortical and thalamic organoids (Figure 1B). The expression of the caudal forebrain marker OTX2, ventral thalamic marker DBX1, thalamic marginal zone marker of GBX2, and thalamic marker TCF7L2 significantly increased in the hThOs. Furthermore, scRNA-seq analysis identified specific cell types also found in the human fetal thalamus. After fusing hThOs and hCOs, they found that the axons from both cortex and thalamus reach the other side within 6 days. They also performed whole-cell patch-clamp recordings to examine the functional properties of thalamic neurons. The results revealed that cortico-thalamic neuronal projections might affect the maturation of thalamic neurons. The finding of this study provides a prospect to explore thalamic development and disorders associated with thalamic anomalies, for example, schizophrenia, epilepsy, and autism spectrum disorder.

Another study described the successful formation of neuronal projections between cerebral organoids and the mouse spinal cord (Giandomenico et al., 2019). Giandomenico et al. (2019) applied the air-liquid interface cerebral organoid (ALI-CO) method, which can improve oxygen supply compared to the standard approach, to promote the survival and maturation of brain cells, such as more complex dendrites and dendritic spines. ScRNA-seq indicated that ALI-COs exhibit various neuronal identities correlated with diverse axon morphologies. Interestingly, three-dimensional multi-electrode arrays revealed the highest correlated activity occurred over long distances, suggesting neurons were not limited to nearest-neighbor connections. Using this slice culture approach, they assessed the functionality of subcortically projecting tracts by co-culturing ALI-COs with the spinal cord sections from embryonic mice. Bundles of axon tracts connected to the spinal cord after around 2–3 weeks. Synapses could also be detected between ALI-CO projecting axons and spinal cord neurons. Strikingly, axon tracts could guide mouse muscle contraction when innervated, showing that organoid-derived projections can stimulate spinal cord/muscle explants. This study provides a way to explore neuronal connectivity with both input and output and can be used to study some aspects of neuronal circuit imbalances, degenerative conditions, or spinal cord injury.

Also, Mansour et al. (2018) transplanted human brain organoids into the adult mouse brain. In the chimeric brains, the grafted organoids displayed continuous differentiation and maturation. Moreover, they discovered an extension of axons into various regions of the host brain. Most axon tracts projected out of human organoids into the cortical layers and the corpus callosum. Axons with lower fiber density were observed in the deeper tissues of the host brain, such as the hippocampus and the thalamus, and even the contralateral areas. Furthermore, *in vivo* extracellular recording revealed synaptic connections and neuronal activity within the graft. This study supports the development of cell replacement therapy using brain organoids.

BRAIN TUMOR

Brain tumors are among the most lethal cancers and are the leading cause of cancer deaths in children under the age of 14 (Ostrom et al., 2016a,b). Their study is limited because of the incompleteness of available laboratory models. Brain organoids provide a novel platform to study brain tumor biology. Brain tumor organoid models were established by genetically introducing clinically relevant mutations into cerebral organoids to mimic brain tumor initiation (Bian et al., 2018; Ogawa et al., 2018). However, some studies implanted or fused patient-derived tumor cells into brain organoids to study brain tumor invasion (Figure 1C; Ogawa et al., 2018; Linkous et al., 2019; Bhaduri et al., 2020) or therapy (Zhu et al., 2020).

Because of its aggressiveness and invasiveness, glioblastoma multiforme (GBM) is the deadliest and most widespread primary brain tumor in adults. Their property to spread through infiltration in the host brain tissue is associated with high resistance and recurrence rate. To understand the mechanism underpinning this invasive phenotype, organoid-GBM fusion models are particularly appropriate. Ogawa et al. (2018) fused tumorspheres from one patient-derived GBM cell line SK2176 with cerebral organoids and found that SK2176 cells invaded and proliferated within the organoid parenchyma rapidly (Ogawa et al., 2018). In another study, Linkous et al. (2019) used brain organoids to provide a “normal” human brain microenvironment for tumors. They introduced cerebral organoid glioma (GLICO) as a model for tumor infiltration by co-culturing glioblastoma stem cells (GSCs) with cerebral organoids. The GLICO model showed that tumor cells deeply invaded the organoid parenchyma, and proliferated within the host tissues. They also observed the formation of an interconnected network of tumor microtubules, which is critical for tumor invasion. Moreover, in the most recent research, Bhaduri et al. (2020) identified an invasive tumor population similar to outer radial glial (oRG) cells using scRNA-seq analysis of patient specimens. They found that PTPRZ1⁺ cells expanded and invaded into the cerebral organoids after engraftment, and showed that PTPRZ1 plays a crucial role in tumor invasion.

Tumor-organoid fusion models have been used for preclinical therapeutic studies. Previously, the Zika virus (ZIKV) has been proven to be a potential oncolytic virus for brain tumor therapy

because of its tropism towards tumor cells (Zhu Z. et al., 2017). In further investigation, Zhu et al. (2020) used GBM-brain cerebral organoid (GBM-BCO) models to identify the SOX2-integrin $\alpha_v\beta_5$ axis as a potential mechanism for ZIKV tropism. Thus, organoid-GSC fusion models could be used as *in vitro* platforms to characterize GBM invasiveness and screen for potential therapeutics.

OLIGODENDROGENESIS

Oligodendrocytes (OLs) are the myelinating glial cells of the brain and the last type of neural cells to be generated after neurons and astroglial cells during mammalian brain development (Goldman and Kuypers, 2015). Based on the research using animal models, especially rodents, there are three major waves of oligodendrogenesis during forebrain development that have been described. Around embryonic day 12.5 (E12.5) and E15.5 in mice, oligodendrogenesis occurs in the ventral forebrain (Tekki-Kessaris et al., 2001; Kessaris et al., 2006; Chapman et al., 2013). After birth, oligodendrocyte precursors (OPCs) migrate tangentially to the cortex and spread throughout the forebrain. The third wave arises around birth date from the EMX1-expressing precursors in the dorsal forebrain (Kessaris et al., 2006). The dorsally born OPCs migrate locally and replace the OPCs generated from the first two waves. Although oligodendrogenesis has been well studied in animal brains, it remains unclear whether human oligodendrogenesis has any unique features because of the lack of human brain experimental models. The establishment of brain organoids provides a new platform to study human-specific oligodendrogenesis.

In one of the interneuron migration studies, Xiang et al. (2017) observed oligodendrogenesis in hMGEO cultures. They performed chromatin accessibility analysis of hMGEOs by ATAC-seq and found hMGEOs and human MGE shared similar open chromatin regions. Specifically, in ventral organoids, regions of oligodendrocyte-expressing genes were exclusively open. ScRNA-seq analysis showed OLIG1⁺ cells could be found in hMGEOs at day 80, suggesting an earlier oligodendrocyte generation in human MGE than in the cortex.

Another study used dorsoventral fused organoids to study human developmental processes, particularly the dorsally derived oligodendrogenesis (Kim et al., 2019). They generated an OLIG2-GFP knockin hPSC reporter line to visualize OPC generation, and cultured organoids as dorsal forebrain organoids (DFOs), ventral forebrain organoids (VFOs), or fused forebrain organoids (FFOs) to study oligodendrogenesis. Similar to the first two oligodendrogenic waves in the mouse brain, OPCs first appeared in VFO culture. From week 5 to 7, intensive GFP⁺ cells were observed in VFOs. In week 9, a big portion of OLIG2-GFP⁺ OPCs were observed within VFOs (Figure 1D). Only until week 12, the GFP⁺ OPCs were remarkably generated in DFOs, mimicking the third wave of oligodendrogenesis in the mouse brain (Figure 1D). More interestingly, when fusing VFO and DFO into FFO, they found that dorsally born OLs outnumber ventral-derived OLs and become dominant in FFOs after long-term culture,

which is also comparable to the oligodendrogenesis in mouse cortex (Figure 1D). Although this study did not find human-specific features, it introduced a novel model to study oligodendrogenesis and myelination-related diseases in a human genetic background.

FOREBRAIN AXIS ESTABLISHMENT

During brain development, topographic structures are generated by gradients of various signaling activities, such as WNT, SHH, and BMP (Petros et al., 2011), that regulate cell fate determination and regional identities. Brain organoids can recapitulate histological features of the human brain, but lack reproducible topographic organization. To overcome this drawback, a recent study established a self-organized dorsoventral and anteroposterior axes in forebrain organoids through an SHH protein gradient (Cederquist et al., 2019). By fusing the forebrain organoid with an inducible SHH-expressing hPSC-derived spheroid, Cederquist et al. (2019) introduced a SHH protein gradient into forebrain organoids (Figure 1E). SHH-patterned brain organoids exhibited *in vivo*-like topography of major forebrain subdivisions. This study opens the possibility to investigate more subtle neurodevelopmental mechanisms and region-specific neural disorders in a single organoid system.

BRAIN ORGANOID VASCULARIZATION

During brain development, the vasculature is one of the important niche components for neural stem cells and plays critical roles in neurogenesis (Bjornsson et al., 2015). However, due to a lack of cells from the mesodermal lineage during the brain organoid culture procedure, the absence of vascularization represents one of the major limitations of brain organoid models. There were several attempts to vascularize brain organoids using different approaches. Wörsdörfer et al. (2019) fused mesodermal precursor cell (MPC) aggregates with brain organoids for vascularization (Figure 1F). They found blood vessel-like structures in the brain organoids. Interestingly, these blood vessel-like tissues exhibited typical blood vessel ultrastructures, such as basement membranes, endothelial cell-cell junctions, and microvesicles. Also, they found IBA1⁺ microglia-like cells, which are delivered from MPCs, infiltrating the brain organoids. Another study established hybrid neurovascular spheroids by fusing cortical neural precursor cell (iNSC) spheroids, endothelial cell (iEC) spheroids, and mesenchymal stem cells (MSCs; Song et al., 2019). Furthermore, Cakir et al. (2019) mixed wildtype hESCs with engineered hESCs that ectopically express ETS variant 2 (ETV2) to grow brain organoid. During the culture, vascular-like networks were generated within cortical organoids as ETV2 induces differentiation of hESCs into endothelial cells. All these studies open new doors to improve vascularization of brain organoids. However, it is still far from mimic the *in vivo* vascularization during brain development, and significant improvements still need to be done before obtaining functional vascular networks in organoid cultures.

CONCLUDING REMARKS

Brain organoid fusion technology allows us to study more complicated biology during human brain development and neural disorders using hESCs or patient-derived iPSCs, including interneuron migration, and neuronal projections. Using the same technique, researchers can also study other pathological processes and potential mechanisms, such as corpus callosum deformity. Assembling multiple different brain regions would be the next step towards a more complete human “mini-brain,” which could then be used to study biological mechanisms requiring the interaction of several brain regions *in vitro*. The fusion strategy should not be limited to the fusion of brain tissues as it can be applied to assemble brain organoids with other types of organoids to study the interaction between different organs. For instance, hepato-biliary-pancreatic organogenesis has been modeled using a multi-organoid fusion approach (Koike et al., 2019). In future studies, investigating the interaction between brain organoids and retinal organoids, inner ear organoids, or even intestinal organoids would be of particular interest.

REFERENCES

- Amin, N. D., and Pasca, S. P. (2018). Building models of brain disorders with three-dimensional organoids. *Neuron* 100, 389–405. doi: 10.1016/j.neuron.2018.10.007
- Amiri, A., Coppola, G., Scuderi, S., Wu, F., Roychowdhury, T., Liu, F., et al. (2018). Transcriptome and epigenome landscape of human cortical development modeled in organoids. *Science* 362:eaat6720. doi: 10.1126/science.aat6720
- Bagley, J. A., Reumann, D., Bian, S., Lévi-Strauss, J., and Knoblich, J. A. (2017). Fused cerebral organoids model interactions between brain regions. *Nat. Methods* 14, 743–751. doi: 10.1038/nmeth.4304
- Bartolini, G., Cicceri, G., and Marin, O. (2013). Integration of GABAergic interneurons into cortical cell assemblies: lessons from embryos and adults. *Neuron* 79, 849–864. doi: 10.1016/j.neuron.2013.08.014
- Belair, D. G., Wolf, C. J., Moorefield, S. D., Wood, C., Becker, C., and Abbott, B. D. (2018). A three-dimensional organoid culture model to assess the influence of chemicals on morphogenetic fusion. *Toxicol. Sci.* 166, 394–408. doi: 10.1093/toxsci/kfy207
- Bershteyn, M., Nowakowski, T. J., Pollen, A. A., Di Lullo, E., Nene, A., Wynshaw-Boris, A., et al. (2017). Human iPSC-derived cerebral organoids model cellular features of lissencephaly and reveal prolonged mitosis of outer radial glia. *Cell Stem Cell* 20, 435.e4–449.e4. doi: 10.1016/j.stem.2016.12.007
- Bhaduri, A., Di Lullo, E., Jung, D., Müller, S., Crouch, E. E., Espinosa, C. S., et al. (2020). Outer radial glia-like cancer stem cells contribute to heterogeneity of glioblastoma. *Cell Stem Cell* 26, 48.e6–63.e6. doi: 10.1016/j.stem.2019.11.015
- Bian, S., Repic, M., Guo, Z., Kavirayani, A., Burkard, T., Bagley, J. A., et al. (2018). Genetically engineered cerebral organoids model brain tumor formation. *Nat. Methods* 15, 631–639. doi: 10.1038/s41592-018-0070-7
- Birey, F., Andersen, J., Makinson, C. D., Islam, S., Wei, W., Huber, N., et al. (2017). Assembly of functionally integrated human forebrain spheroids. *Nature* 545, 54–59. doi: 10.1038/nature22330
- Bjornsson, C. S., Apostolopoulou, M., Tian, Y., and Temple, S. (2015). It takes a village: constructing the neurogenic niche. *Dev. Cell* 32, 435–446. doi: 10.1016/j.devcel.2015.01.010
- Bortone, D., and Polleux, F. (2009). KCC2 expression promotes the termination of cortical interneuron migration in a voltage-sensitive calcium-dependent manner. *Neuron* 62, 53–71. doi: 10.1016/j.neuron.2009.01.034
- Cakir, B., Xiang, Y., Tanaka, Y., Kural, M. H., Parent, M., Kang, Y.-J., et al. (2019). Engineering of human brain organoids with a functional vascular-like system. *Nat. Methods* 16, 1169–1175. doi: 10.1038/s41592-019-0586-5
- Camp, J. G., Badsha, F., Florio, M., Kanton, S., Gerber, T., Wilsch-Bräuninger, M., et al. (2015). Human cerebral organoids recapitulate gene expression programs

AUTHOR CONTRIBUTIONS

AC, ZG, and LF wrote the manuscript. AC and ZG prepared the figures. SB directed the manuscript preparation and wrote the manuscript.

FUNDING

This work is supported by Shanghai Pujiang Program (19PJ1410200), Key Project of the Science and Technology Commission of Shanghai Municipality (19JC1415300), Fundamental Research Funds for the Central Universities (22120190150), and Major Program of Development Fund for Shanghai Zhangjiang National Innovation Demonstration Zone (ZJ2018-ZD-004).

ACKNOWLEDGMENTS

We are grateful to J. Bagley for his great help with the language editing and comments on the manuscript.

of fetal neocortex development. *Proc. Natl. Acad. Sci. U S A* 112, 15672–15677. doi: 10.1073/pnas.1520760112

- Cederquist, G. Y., Asciolla, J. J., Tchiew, J., Walsh, R. M., Cornacchia, D., Resh, M. D., et al. (2019). Specification of positional identity in forebrain organoids. *Nat. Biotechnol.* 37, 436–444. doi: 10.1038/s41587-019-0085-3
- Chapman, H., Waclaw, R. R., Pei, Z., Nakafuku, M., and Campbell, K. (2013). The homeobox gene *Gsx2* controls the timing of oligodendroglial fate specification in mouse lateral ganglionic eminence progenitors. *Development* 140, 2289–2298. doi: 10.1242/dev.091090
- Clowry, G. J., Alzu'bi, A., Harkin, L. F., Sarma, S., Kerwin, J., and Lindsay, S. J. (2018). Charting the protomap of the human telencephalon. *Semin. Cell Dev. Biol.* 76, 3–14. doi: 10.1016/j.semcdb.2017.08.033
- Cugola, F. R., Fernandes, I. R., Russo, F. B., Freitas, B. C., Dias, J. L. M., Guimarães, K. P., et al. (2016). The Brazilian Zika virus strain causes birth defects in experimental models. *Nature* 534, 267–271. doi: 10.1038/nature18296
- Eiraku, M., Takata, N., Ishibashi, H., Kawada, M., Sakakura, E., Okuda, S., et al. (2011). Self-organizing optic-cup morphogenesis in three-dimensional culture. *Nature* 472, 51–56. doi: 10.1038/nature09941
- Eiraku, M., Watanabe, K., Matsuo-Takasaki, M., Kawada, M., Yonemura, S., Matsumura, M., et al. (2008). Self-organized formation of polarized cortical tissues from ESCs and its active manipulation by extrinsic signals. *Cell Stem Cell* 3, 519–532. doi: 10.1016/j.stem.2008.09.002
- Fatehullah, A., Tan, S. H., and Barker, N. (2016). Organoids as an *in vitro* model of human development and disease. *Nat. Cell Biol.* 18, 246–254. doi: 10.1038/ncb3312
- Garcez, P. P., Loiola, E. C., Madeiro da Costa, R., Higa, L. M., Trindade, P., Delvecchio, R., et al. (2016). Zika virus impairs growth in human neurospheres and brain organoids. *Science* 352, 816–818. doi: 10.1126/science.aaf6116
- Giandomenico, S. L., Mierau, S. B., Gibbons, G. M., Wenger, L. M. D., Masullo, L., Sit, T., et al. (2019). Cerebral organoids at the air-liquid interface generate diverse nerve tracts with functional output. *Nat. Neurosci.* 22, 669–679. doi: 10.1038/s41593-019-0350-2
- Goldman, S. A., and Kuypers, N. J. (2015). How to make an oligodendrocyte. *Development* 142, 3983–3995. doi: 10.1242/dev.126409
- Iefremova, V., Manikakis, G., Krefft, O., Jabali, A., Weynans, K., Wilkens, R., et al. (2017). An organoid-based model of cortical development identifies non-cell-autonomous defects in wnt signaling contributing to miller-dieker syndrome. *Cell Rep.* 19, 50–59. doi: 10.1016/j.celrep.2017.03.047
- Jo, J., Xiao, Y., Sun, A. X., Cukuroglu, E., Tran, H.-D., Göke, J., et al. (2016). Midbrain-like organoids from human pluripotent stem cells contain functional dopaminergic and neuromelanin-producing neurons. *Cell Stem Cell* 19, 248–257. doi: 10.1016/j.stem.2016.07.005

- Kadoshima, T., Sakaguchi, H., Nakano, T., Soen, M., Ando, S., Eiraku, M., et al. (2013). Self-organization of axial polarity, inside-out layer pattern, and species-specific progenitor dynamics in human ES cell-derived neocortex. *Proc. Natl. Acad. Sci. U S A* 110, 20284–20289. doi: 10.1073/pnas.1315710110
- Kanton, S., Boyle, M. J., He, Z., Santel, M., Weigert, A., Sanchís-Calleja, F., et al. (2019). Organoid single-cell genomic atlas uncovers human-specific features of brain development. *Nature* 574, 418–422. doi: 10.1038/s41586-019-1654-9
- Kessarlis, N., Fogarty, M., Iannarelli, P., Grist, M., Wegner, M., and Richardson, W. D. (2006). Competing waves of oligodendrocytes in the forebrain and postnatal elimination of an embryonic lineage. *Nat. Neurosci.* 9, 173–179. doi: 10.1038/nn1620
- Kim, H., Xu, R., Padmashri, R., Dunaevsky, A., Liu, Y., Dreyfus, C. F., et al. (2019). Pluripotent stem cell-derived cerebral organoids reveal human oligodendrogenesis with dorsal and ventral origins. *Stem Cell Reports* 12, 890–905. doi: 10.1016/j.stemcr.2019.04.011
- Klaus, J., Kanton, S., Kyrousi, C., Ayo-Martin, A. C., Di Giaimo, R., Riesenberger, S., et al. (2019). Altered neuronal migratory trajectories in human cerebral organoids derived from individuals with neuronal heterotopia. *Nat. Med.* 25, 561–568. doi: 10.1038/s41591-019-0371-0
- Koike, H., Iwasawa, K., Ouchi, R., Maezawa, M., Giesbrecht, K., Saiki, N., et al. (2019). Modelling human hepato-biliary-pancreatic organogenesis from the foregut-midgut boundary. *Nature* 574, 112–116. doi: 10.1038/s41586-019-1598-0
- Kwan, K. Y., Šestan, N., and Anton, E. S. (2012). Transcriptional co-regulation of neuronal migration and laminar identity in the neocortex. *Development* 139, 1535–1546. doi: 10.1242/dev.069963
- Lancaster, M. A., Corsini, N. S., Wolfinger, S., Gustafson, E. H., Phillips, A. W., Burkard, T. R., et al. (2017). Guided self-organization and cortical plate formation in human brain organoids. *Nat. Biotechnol.* 35, 659–666. doi: 10.1038/nbt.3906
- Lancaster, M. A., and Knoblich, J. A. (2014a). Generation of cerebral organoids from human pluripotent stem cells. *Nat. Protoc.* 9, 2329–2340. doi: 10.1038/nprot.2014.158
- Lancaster, M. A., and Knoblich, J. A. (2014b). Organogenesis in a dish: modeling development and disease using organoid technologies. *Science* 345, 1247125–1247125. doi: 10.1126/science.1247125
- Lancaster, M. A., Renner, M., Martin, C.-A., Wenzel, D., Bicknell, L. S., Hurles, M. E., et al. (2013). Cerebral organoids model human brain development and microcephaly. *Nature* 501, 373–379. doi: 10.1038/nature12517
- Lee, C.-T., Chen, J., Kindberg, A. A., Bendriem, R. M., Spivak, C. E., Williams, M. P., et al. (2017). CYP3A5 mediates effects of cocaine on human neocorticalgenesis: studies using an *in vitro* 3D self-organized hPSC model with a single cortex-like unit. *Neuropsychopharmacology* 42, 774–784. doi: 10.1038/npp.2016.156
- Li, Y., Muffat, J., Omer, A., Bosch, I., Lancaster, M. A., Sur, M., et al. (2017). Induction of expansion and folding in human cerebral organoids. *Cell Stem Cell* 20, 385.e3–396.e3. doi: 10.1016/j.stem.2016.11.017
- Linkous, A., Balamatsias, D., Snuderl, M., Edwards, L., Miyaguchi, K., Milner, T., et al. (2019). Modeling patient-derived glioblastoma with cerebral organoids. *Cell Rep.* 26, 3203.e5–3211.e5. doi: 10.1016/j.celrep.2019.02.063
- López-Bendito, G., and Molnár, Z. (2003). Thalamocortical development: how are we going to get there? *Nat. Rev. Neurosci.* 4, 276–289. doi: 10.1038/nrn1075
- Luo, C., Lancaster, M. A., Castanon, R., Nery, J. R., Knoblich, J. A., and Ecker, J. R. (2016). Cerebral organoids recapitulate epigenomic signatures of the human fetal brain. *Cell Rep.* 17, 3369–3384. doi: 10.1016/j.celrep.2016.12.001
- Mansour, A. A., Gonçalves, J. T., Bloyd, C. W., Li, H., Fernandes, S., Quang, D., et al. (2018). An *in vivo* model of functional and vascularized human brain organoids. *Nat. Biotechnol.* 36, 432–441. doi: 10.1038/nbt.4127
- Mariani, J., Coppola, G., Zhang, P., Abyzov, A., Provini, L., Tomasini, L., et al. (2015). FOXP1-dependent dysregulation of GABA/glutamate neuron differentiation in autism spectrum disorders. *Cell* 162, 375–390. doi: 10.1016/j.cell.2015.06.034
- Marín-Padilla, M. (2012). The human brain intracerebral microvascular system: development and structure. *Front. Neuroanat.* 6:38. doi: 10.3389/fnana.2012.00038
- Marín, O., Yaron, A., Bagri, A., Tessier-Lavigne, M., and Rubenstein, J. L. (2001). Sorting of striatal and cortical interneurons regulated by semaphorin-neuropilin interactions. *Science* 293, 872–875. doi: 10.1126/science.1061891
- Marton, R. M., and Pasca, S. P. (2019). Organoid and assembloid technologies for investigating cellular crosstalk in human brain development and disease. *Trends Cell Biol.* 30, 133–143. doi: 10.1016/j.tcb.2019.11.004
- Molnár, Z., Clowry, G. J., Šestan, N., Alzu'bi, A., Bakken, T., Hevner, R. F., et al. (2019). New insights into the development of the human cerebral cortex. *J. Anat.* 235, 432–451. doi: 10.1111/joa.13055
- Monier, A., Adle-Biasette, H., Delezoide, A.-L., Evrard, P., Gressens, P., and Verney, C. (2007). Entry and distribution of microglial cells in human embryonic and fetal cerebral cortex. *J. Neuropathol. Exp. Neurol.* 66, 372–382. doi: 10.1097/nen.0b013e3180517b46
- Mora-Bermúdez, F., Badsha, F., Kanton, S., Camp, J. G., Vernot, B., Köhler, K., et al. (2016). Differences and similarities between human and chimpanzee neural progenitors during cerebral cortex development. *Elife* 5:e18683. doi: 10.7554/eLife.18683
- Muguruma, K., Nishiyama, A., Kawakami, H., Hashimoto, K., and Sasai, Y. (2015). Self-organization of polarized cerebellar tissue in 3D culture of human pluripotent stem cells. *Cell Rep* 10, 537–550. doi: 10.1016/j.celrep.2014.12.051
- Muguruma, K., Nishiyama, A., Ono, Y., Miyawaki, H., Mizuhara, E., Hori, S., et al. (2010). Ontogeny-recapitulating generation and tissue integration of ES cell-derived Purkinje cells. *Nat. Neurosci.* 13, 1171–1180. doi: 10.1038/nn.2638
- Nakano, T., Ando, S., Takata, N., Kawada, M., Muguruma, K., Sekiguchi, K., et al. (2012). Self-formation of optic cups and storable stratified neural retina from human ESCs. *Cell Stem Cell* 10, 771–785. doi: 10.1016/j.stem.2012.05.009
- Ogawa, J., Pao, G. M., Shokhirev, M. N., and Verma, I. M. (2018). Glioblastoma model using human cerebral organoids. *Cell Rep.* 23, 1220–1229. doi: 10.1016/j.celrep.2018.03.105
- Omer Javed, A., Li, Y., Muffat, J., Su, K.-C., Cohen, M. A., Lungjangwa, T., et al. (2018). Microcephaly modeling of kinetochore mutation reveals a brain-specific phenotype. *Cell Rep.* 25, 368.e5–382.e5. doi: 10.1016/j.celrep.2018.09.032
- Ostrom, Q. T., Gittleman, H., de Blank, P. M., Finlay, J. L., Gurney, J. G., McKean-Cowdin, R., et al. (2016a). American brain tumor association adolescent and young adult primary brain and central nervous system tumors diagnosed in the united states in 2008–2012. *Neurooncology* 18, ii–i50. doi: 10.1093/neuonc/nov297
- Ostrom, Q. T., Gittleman, H., Xu, J., Kromer, C., Wolinsky, Y., Kruchko, C., et al. (2016b). CBTRUS statistical report: primary brain and other central nervous system tumors diagnosed in the united states in 2009–2013. *Neurooncology* 18, v1–v75. doi: 10.1093/neuonc/nov207
- Otani, T., Marchetto, M. C., Gage, F. H., Simons, B. D., and Livesey, F. J. (2016). 2D and 3D stem cell models of primate cortical development identify species-specific differences in progenitor behavior contributing to brain size. *Cell Stem Cell* 18, 467–480. doi: 10.1016/j.stem.2016.03.003
- Pasca, A. M., Sloan, S. A., Clarke, L. E., Tian, Y., Makinson, C. D., Huber, N., et al. (2015). Functional cortical neurons and astrocytes from human pluripotent stem cells in 3D culture. *Nat. Methods* 12, 671–678. doi: 10.1038/nmeth.3415
- Petros, T. J., Tyson, J. A., and Anderson, S. A. (2011). Pluripotent stem cells for the study of CNS development. *Front. Mol. Neurosci.* 4:30. doi: 10.3389/fnfmol.2011.00030
- Pollen, A. A., Bhaduri, A., Andrews, M. G., Nowakowski, T. J., Meyerson, O. S., Mostajo-Radji, M. A., et al. (2019). Establishing cerebral organoids as models of human-specific brain evolution. *Cell* 176, 743.e17–756.e17. doi: 10.1016/j.cell.2019.01.017
- Qian, X., Nguyen, H. N., Song, M. M., Hadiono, C., Ogden, S. C., Hammack, C., et al. (2016). Brain-region-specific organoids using mini-bioreactors for modeling ZIKV exposure. *Cell* 165, 1238–1254. doi: 10.1016/j.cell.2016.04.032
- Quadrato, G., Nguyen, T., Macosko, E. Z., Sherwood, J. L., Min Yang, S., Berger, D. R., et al. (2017). Cell diversity and network dynamics in photosensitive human brain organoids. *Nature* 545, 48–53. doi: 10.1038/nature22047
- Renner, M., Lancaster, M. A., Bian, S., Choi, H., Ku, T., Peer, A., et al. (2017). Self-organized developmental patterning and differentiation in cerebral organoids. *EMBO J.* 36, 1316–1329. doi: 10.15252/embj.201694700

- Rezaie, P., Dean, A., Male, D., and Ulfig, N. (2005). Microglia in the cerebral wall of the human telencephalon at second trimester. *Cereb. Cortex* 15, 938–949. doi: 10.1093/cercor/bhh194
- Sakaguchi, H., Kadoshima, T., Soen, M., Narii, N., Ishida, Y., Ohgushi, M., et al. (2015). Generation of functional hippocampal neurons from self-organizing human embryonic stem cell-derived dorsomedial telencephalic tissue. *Nat. Commun.* 6:8896. doi: 10.1038/ncomms9896
- Schwartz, M. P., Hou, Z., Propson, N. E., Zhang, J., Engstrom, C. J., Santos Costa, V., et al. (2015). Human pluripotent stem cell-derived neural constructs for predicting neural toxicity. *Proc. Natl. Acad. Sci. U S A* 112, 12516–12521. doi: 10.1073/pnas.1516645112
- Song, L., Yuan, X., Jones, Z., Griffin, K., Zhou, Y., Ma, T., et al. (2019). Assembly of human stem cell-derived cortical spheroids and vascular spheroids to model 3-D brain-like tissues. *Sci. Rep.* 9:5977. doi: 10.1038/s41598-019-42439-9
- Tekki-Kessar, N., Woodruff, R., Hall, A. C., Gaffield, W., Kimura, S., Stiles, C. D., et al. (2001). Hedgehog-dependent oligodendrocyte lineage specification in the telencephalon. *Development* 128, 2545–2554.
- Trevino, A. E., Sinnott-Armstrong, N., Andersen, J., Yoon, S.-J., Huber, N., Pritchard, J. K., et al. (2020). Chromatin accessibility dynamics in a model of human forebrain development. *Science* 367:eaay1645. doi: 10.1126/science.aay1645
- Vazin, T., Ball, K. A., Lu, H., Park, H., Ataeijannati, Y., Head-Gordon, T., et al. (2014). Efficient derivation of cortical glutamatergic neurons from human pluripotent stem cells: a model system to study neurotoxicity in Alzheimer's disease. *Neurobiol. Dis.* 62, 62–72. doi: 10.1016/j.nbd.2013.09.005
- Velasco, S., Kedaigle, A. J., Simmons, S. K., Nash, A., Rocha, M., Quadrato, G., et al. (2019). Individual brain organoids reproducibly form cell diversity of the human cerebral cortex. *Nature* 570, 523–527. doi: 10.1038/s41586-019-1289-x
- Wang, Y., Wang, L., Zhu, Y., and Qin, J. (2018). Human brain organoid-on-a-chip to model prenatal nicotine exposure. *Lab Chip* 18, 851–860. doi: 10.1039/c7lc01084b
- Wonders, C. P., and Anderson, S. A. (2006). The origin and specification of cortical interneurons. *Nat. Rev. Neurosci.* 7, 687–696. doi: 10.1038/nrn1954
- Wörsdörfer, P., Dalda, N., Kern, A., Krüger, S., Wagner, N., Kwok, C. K., et al. (2019). Generation of complex human organoid models including vascular networks by incorporation of mesodermal progenitor cells. *Sci. Rep.* 9:15663. doi: 10.1038/s41598-019-52204-7
- Xiang, Y., Tanaka, Y., Cakir, B., Patterson, B., Kim, K.-Y., Sun, P., et al. (2019). hESC-derived thalamic organoids form reciprocal projections when fused with cortical organoids. *Cell Stem Cell* 24, 487.e7–497.e7. doi: 10.1016/j.stem.2018.12.015
- Xiang, Y., Tanaka, Y., Patterson, B., Kang, Y.-J., Govindaiah, G., Roselaar, N., et al. (2017). Fusion of regionally specified hPSC-derived organoids models human brain development and interneuron migration. *Cell Stem Cell* 21, 383.e7–398.e7. doi: 10.1016/j.stem.2017.07.007
- Xu, R., Brawner, A. T., Li, S., Liu, J.-J., Kim, H., Xue, H., et al. (2019). OLIG2 drives abnormal neurodevelopmental phenotypes in human iPSC-Based organoid and chimeric mouse models of down syndrome. *Cell Stem Cell* 24, 908.e8–926.e8. doi: 10.1016/j.stem.2019.04.014
- Ye, F., Kang, E., Yu, C., Qian, X., Jacob, F., Yu, C., et al. (2017). DISC1 regulates neurogenesis via modulating kinetochore attachment of Ndel1/Nde1 during mitosis. *Neuron* 96, 1041.e5–1054.e5. doi: 10.1016/j.neuron.2017.10.010
- Yuan, F., Fang, K.-H., Hong, Y., Xu, S.-B., Xu, M., Pan, Y., et al. (2020). LHX6 is essential for the migration of human pluripotent stem cell-derived GABAergic interneurons. *Protein Cell* 11, 286–291. doi: 10.1007/s13238-019-00686-6
- Yuste, R. (2005). Origin and classification of neocortical interneurons. *Neuron* 48, 524–527. doi: 10.1016/j.neuron.2005.11.012
- Zechel, S., Zajac, P., Lönnerberg, P., Ibáñez, C. F., and Linnarsson, S. (2014). Topographical transcriptome mapping of the mouse medial ganglionic eminence by spatially resolved RNA-seq. *Genome Biol.* 15:486. doi: 10.1186/s13059-014-0486-z
- Zhang, W., Yang, S.-L., Yang, M., Herrlinger, S., Shao, Q., Collar, J. L., et al. (2019). Modeling microcephaly with cerebral organoids reveals a WDR62-CEP170-KIF2A pathway promoting cilium disassembly in neural progenitors. *Nat. Commun.* 10, 2612–2614. doi: 10.1038/s41467-019-10497-2
- Zhu, Z., Gorman, M. J., McKenzie, L. D., Chai, J. N., Hubert, C. G., Prager, B. C., et al. (2017). Correction: zika virus has oncolytic activity against glioblastoma stem cells. *J. Exp. Med.* 214:3145. doi: 10.1084/jem.2017109309122017c
- Zhu, Y., Wang, L., Yin, F., Yu, Y., Wang, Y., Shepard, M. J., et al. (2017). Probing impaired neurogenesis in human brain organoids exposed to alcohol. *Integr. Biol.* 9, 968–978. doi: 10.1039/c7ib00105c
- Zhu, Z., Mesci, P., Bernatchez, J. A., Gimple, R. C., Wang, X., Schafer, S. T., et al. (2020). Zika virus targets glioblastoma stem cells through a SOX2-integrin $\alpha\beta 5$ axis. *Cell Stem Cell* 26, 187.e10–204.e10. doi: 10.1016/j.stem.2019.11.016

Conflict of Interest: The authors declare that the research was conducted in the absence of any commercial or financial relationships that could be construed as a potential conflict of interest.

Copyright © 2020 Chen, Guo, Fang and Bian. This is an open-access article distributed under the terms of the Creative Commons Attribution License (CC BY). The use, distribution or reproduction in other forums is permitted, provided the original author(s) and the copyright owner(s) are credited and that the original publication in this journal is cited, in accordance with accepted academic practice. No use, distribution or reproduction is permitted which does not comply with these terms.

11. Reference

- Arancibia-Carcamo, I. L., and D. Attwell. 2014. 'The node of Ranvier in CNS pathology', *Acta Neuropathol*, 128: 161-75.
- Arancibia-Carcamo, I. L., M. C. Ford, L. Cossell, K. Ishida, K. Tohyama, and D. Attwell. 2017. 'Node of Ranvier length as a potential regulator of myelinated axon conduction speed', *Elife*, 6.
- Arnsten, A. F. 2009. 'Stress signalling pathways that impair prefrontal cortex structure and function', *Nat Rev Neurosci*, 10: 410-22.
- Auguste, Y. S. S., A. Ferro, J. A. Kahng, A. M. Xavier, J. R. Dixon, U. Vrudhula, A. S. Nichitiu, D. Rosado, T. L. Wee, U. V. Pedmale, and L. Cheadle. 2022. 'Oligodendrocyte precursor cells engulf synapses during circuit remodeling in mice', *Nat Neurosci*, 25: 1273-78.
- Bai, X., F. Kirchhoff, and A. Scheller. 2021. 'Oligodendroglial GABAergic Signaling: More Than Inhibition!', *Neurosci Bull*, 37: 1039-50.
- Balia, M., N. Benamer, and M. C. Angulo. 2017. 'A specific GABAergic synapse onto oligodendrocyte precursors does not regulate cortical oligodendrogenesis', *Glia*, 65: 1821-32.
- Balia, M., M. Velez-Fort, S. Passlick, C. Schafer, E. Audinat, C. Steinhauser, G. Seifert, and M. C. Angulo. 2015. 'Postnatal down-regulation of the GABAA receptor gamma2 subunit in neocortical NG2 cells accompanies synaptic-to-extrasynaptic switch in the GABAergic transmission mode', *Cereb Cortex*, 25: 1114-23.
- Baracska, K. L., C. S. Duchala, R. H. Miller, W. B. Macklin, and B. D. Trapp. 2002. 'Oligodendrogenesis is differentially regulated in gray and white matter of jimpy mice', *J Neurosci Res*, 70: 645-54.
- Bedner, P., A. Dupper, K. Hüttmann, J. Müller, M. K. Herde, P. Dublin, T. Deshpande, J. Schramm, U. Häussler, C. A. Haas, C. Henneberger, M. Theis, and C. Steinhäuser. 2015. 'Astrocyte uncoupling as a cause of human temporal lobe epilepsy', *Brain*, 138: 1208-22.
- Benamer, N., M. Vidal, M. Balia, and M. C. Angulo. 2020. 'Myelination of parvalbumin interneurons shapes the function of cortical sensory inhibitory circuits', *Nat Commun*, 11: 5151.
- Bergles, D. E., J. D. Roberts, P. Somogyi, and C. E. Jahr. 2000. 'Glutamatergic synapses on oligodendrocyte precursor cells in the hippocampus', *Nature*, 405: 187-91.
- Bettler, B., K. Kaupmann, J. Mosbacher, and M. Gassmann. 2004. 'Molecular structure and physiological functions of GABA(B) receptors', *Physiol Rev*, 84: 835-67.
- Bicks, L. K., H. Koike, S. Akbarian, and H. Morishita. 2015. 'Prefrontal Cortex and Social Cognition in Mouse and Man', *Front Psychol*, 6: 1805.
- Birey, F., M. Kloc, M. Chavali, I. Hussein, M. Wilson, D. J. Christoffel, T. Chen, M. A. Frohman, J. K. Robinson, S. J. Russo, A. Maffei, and A. Aguirre. 2015. 'Genetic and Stress-Induced Loss of NG2 Glia Triggers Emergence of Depressive-like Behaviors through Reduced Secretion of FGF2', *Neuron*, 88: 941-56.
- Bitzenhofer, S. H., J. A. Popplau, M. Chini, A. Marquardt, and I. L. Hanganu-Opatz. 2021. 'A transient developmental increase in prefrontal activity alters network maturation and causes cognitive dysfunction in adult mice', *Neuron*, 109: 1350-64 e6.
- Bolino, A. 2021. 'Myelin Biology', *Neurotherapeutics*, 18: 2169-84.
- Buchanan, J., L. Elabbady, F. Collman, N. L. Jorstad, T. E. Bakken, C. Ott, J. Glatzer, A. A. Bleckert, A. L. Bodor, D. Brittain, D. J. Bumbarger, G. Mahalingam, S. Seshamani, C. Schneider-Mizell, M. M. Takeno, R. Torres, W. Yin, R. D. Hodge, M. Castro, S. Dorckenwald, D. Ih, C. S. Jordan, N. Kemnitz, K. Lee, R. Lu, T. Macrina, S. Mu, S. Popovych, W. M. Silversmith, I. Tartavull, N. L. Turner, A. M. Wilson, W. Wong, J. Wu, A. Zlateski, J. Zung, J. Lippincott-Schwartz, E. S. Lein, H. S. Seung, D. E. Bergles, R. C. Reid, and N. M. da Costa. 2022. 'Oligodendrocyte precursor cells ingest axons in the mouse neocortex', *Proc Natl Acad Sci U S A*, 119: e2202580119.

Reference

- Butt, A. M., A. Duncan, M. F. Hornby, S. L. Kirvell, A. Hunter, J. M. Levine, and M. Berry. 1999. 'Cells expressing the NG2 antigen contact nodes of Ranvier in adult CNS white matter', *Glia*, 26: 84-91.
- Cheadle, L., S. A. Rivera, J. S. Phelps, K. A. Ennis, B. Stevens, L. C. Burkly, W. A. Lee, and M. E. Greenberg. 2020. 'Sensory Experience Engages Microglia to Shape Neural Connectivity through a Non-Phagocytic Mechanism', *Neuron*, 108: 451-68 e9.
- Chicheportiche, Y., P. R. Bourdon, H. Xu, Y. M. Hsu, H. Scott, C. Hession, I. Garcia, and J. L. Browning. 1997. 'TWEAK, a new secreted ligand in the tumor necrosis factor family that weakly induces apoptosis', *J Biol Chem*, 272: 32401-10.
- Crosby, K. C., S. E. Gookin, J. D. Garcia, K. M. Hahm, M. L. Dell'Acqua, and K. R. Smith. 2019. 'Nanoscale Subsynaptic Domains Underlie the Organization of the Inhibitory Synapse', *Cell Rep*, 26: 3284-97 e3.
- Cserep, C., B. Posfai, N. Lenart, R. Fekete, Z. I. Laszlo, Z. Lele, B. Orsolits, G. Molnar, S. Heindl, A. D. Schwarcz, K. Ujvari, Z. Kornyei, K. Toth, E. Szabadits, B. Sperlagh, M. Baranyi, L. Csiba, T. Hortobagyi, Z. Magloczky, B. Martinecz, G. Szabo, F. Erdelyi, R. Szipocs, M. M. Tamkun, B. Gesierich, M. Duering, I. Katona, A. Liesz, G. Tamas, and A. Denes. 2020. 'Microglia monitor and protect neuronal function through specialized somatic purinergic junctions', *Science*, 367: 528-37.
- Daroische, R., M. S. Hemminghyth, T. H. Eilertsen, M. H. Breivte, and L. J. Chwyszczuk. 2021. 'Cognitive Impairment After COVID-19-A Review on Objective Test Data', *Front Neurol*, 12: 699582.
- Davalos, D., J. Grutzendler, G. Yang, J. V. Kim, Y. Zuo, S. Jung, D. R. Littman, M. L. Dustin, and W. B. Gan. 2005. 'ATP mediates rapid microglial response to local brain injury in vivo', *Nat Neurosci*, 8: 752-8.
- Davies, A. M. 2003. 'Regulation of neuronal survival and death by extracellular signals during development', *EMBO J*, 22: 2537-45.
- Deacon, R. M. 2006. 'Assessing nest building in mice', *Nat Protoc*, 1: 1117-9.
- Deidda, G., I. F. Bozarth, and L. Cancedda. 2014. 'Modulation of GABAergic transmission in development and neurodevelopmental disorders: investigating physiology and pathology to gain therapeutic perspectives', *Front Cell Neurosci*, 8: 119.
- Denaxa, M., G. Neves, A. Rabinowitz, S. Kemlo, P. Liodis, J. Burrone, and V. Pachnis. 2018. 'Modulation of Apoptosis Controls Inhibitory Interneuron Number in the Cortex', *Cell Rep*, 22: 1710-21.
- Duan, Z. R. S., A. Che, P. Chu, L. Modol, Y. Bollmann, R. Babij, R. N. Fetcho, T. Otsuka, M. V. Fuccillo, C. Liston, D. J. Pisapia, R. Cossart, and N. V. De Marco Garcia. 2020. 'GABAergic Restriction of Network Dynamics Regulates Interneuron Survival in the Developing Cortex', *Neuron*, 105: 75-92 e5.
- Dubey, M., M. Pascual-Garcia, K. Helmes, D. D. Wever, M. S. Hamada, S. A. Kushner, and M. H. P. Kole. 2022. 'Myelination synchronizes cortical oscillations by consolidating parvalbumin-mediated phasic inhibition', *Elife*, 11.
- Eshkoo, S. A., T. A. Hamid, C. Y. Mun, and C. K. Ng. 2015. 'Mild cognitive impairment and its management in older people', *Clin Interv Aging*, 10: 687-93.
- Essrich, C., M. Lorez, J. A. Benson, J. M. Fritschy, and B. Luscher. 1998. 'Postsynaptic clustering of major GABAA receptor subtypes requires the gamma 2 subunit and gephyrin', *Nat Neurosci*, 1: 563-71.
- Fame, R. M., J. L. MacDonald, and J. D. Macklis. 2011. 'Development, specification, and diversity of callosal projection neurons', *Trends Neurosci*, 34: 41-50.
- Fernandez-Castaneda, A., and A. Gaultier. 2016. 'Adult oligodendrocyte progenitor cells - Multifaceted regulators of the CNS in health and disease', *Brain Behav Immun*, 57: 1-7.
- Fields, R. D. 2015. 'A new mechanism of nervous system plasticity: activity-dependent myelination', *Nat Rev Neurosci*, 16: 756-67.

Reference

- Franklin, Keith, and George Paxinos. 2007. *The mouse brain in stereotaxic coordinate* (Academic press).
- Freund, T. F., and G. Buzsaki. 1996. 'Interneurons of the hippocampus', *Hippocampus*, 6: 347-470.
- Glauert, A.M. 1975. *Fixation, Dehydration and Embedding of Biological Specimens. Practical methods in electron microscopy*. (North - Holland Publishing Company).
- Gonchar, Y., Q. Wang, and A. Burkhalter. 2007. 'Multiple distinct subtypes of GABAergic neurons in mouse visual cortex identified by triple immunostaining', *Front Neuroanat*, 1: 3.
- Grossmann, T. 2013. 'The role of medial prefrontal cortex in early social cognition', *Front Hum Neurosci*, 7: 340.
- Haller, C., E. Casanova, M. Müller, C. M. Vacher, R. Vigot, T. Doll, S. Barbieri, M. Gassmann, and B. Bettler. 2004. 'Floxed allele for conditional inactivation of the GABAB(1) gene', *Genesis*, 40: 125-30.
- Hill, R. A., A. M. Li, and J. Grutzendler. 2018. 'Lifelong cortical myelin plasticity and age-related degeneration in the live mammalian brain', *Nat Neurosci*, 21: 683-95.
- Hines, J. H., A. M. Ravanelli, R. Schwandt, E. K. Scott, and B. Appel. 2015. 'Neuronal activity biases axon selection for myelination in vivo', *Nat Neurosci*, 18: 683-9.
- Hu, H., J. Gan, and P. Jonas. 2014. 'Interneurons. Fast-spiking, parvalbumin(+) GABAergic interneurons: from cellular design to microcircuit function', *Science*, 345: 1255263.
- Huang, W., X. Bai, L. Stopper, B. Catalin, L. P. Cartarozzi, A. Scheller, and F. Kirchhoff. 2018. 'During Development NG2 Glial Cells of the Spinal Cord are Restricted to the Oligodendrocyte Lineage, but Generate Astrocytes upon Acute Injury', *Neuroscience*, 385: 154-65.
- Huang, W., N. Zhao, X. Bai, K. Karram, J. Trotter, S. Goebbels, A. Scheller, and F. Kirchhoff. 2014. 'Novel NG2-CreERT2 knock-in mice demonstrate heterogeneous differentiation potential of NG2 glia during development', *Glia*, 62: 896-913.
- Hughes, E. G., and M. E. Stockton. 2021. 'Premyelinating Oligodendrocytes: Mechanisms Underlying Cell Survival and Integration', *Front Cell Dev Biol*, 9: 714169.
- Jahn, H. M., C. V. Kasakow, A. Helfer, J. Michely, A. Verkhatsky, H. H. Maurer, A. Scheller, and F. Kirchhoff. 2018. 'Refined protocols of tamoxifen injection for inducible DNA recombination in mouse astroglia', *Sci Rep*, 8: 5913.
- Jung, M., E. Krämer, M. Grzenkowski, K. Tang, W. Blakemore, A. Aguzzi, K. Khazaie, K. Chlichlia, G. von Blankenfeld, and H. Kettenmann. 1995. 'Lines of murine oligodendroglial precursor cells immortalized by an activated neu tyrosine kinase show distinct degrees of interaction with axons in vitro and in vivo', *Eur J Neurosci*, 7: 1245-65.
- Kaidanovich-Beilin, O., T. Lipina, I. Vukobradovic, J. Roder, and J. R. Woodgett. 2011. 'Assessment of social interaction behaviors', *J Vis Exp*.
- Kang, S. H., M. Fukaya, J. K. Yang, J. D. Rothstein, and D. E. Bergles. 2010. 'NG2+ CNS glial progenitors remain committed to the oligodendrocyte lineage in postnatal life and following neurodegeneration', *Neuron*, 68: 668-81.
- Klausberger, T., and P. Somogyi. 2008. 'Neuronal diversity and temporal dynamics: the unity of hippocampal circuit operations', *Science*, 321: 53-7.
- Kukley, M., M. Kiladze, R. Tognatta, M. Hans, D. Swandulla, J. Schramm, and D. Dietrich. 2008. 'Glial cells are born with synapses', *FASEB J*, 22: 2957-69.
- La Manno, G., K. Siletti, A. Furlan, D. Gyllborg, E. Vinsland, A. Mossi Albiach, C. Mattsson Langseth, I. Khven, A. R. Lederer, L. M. Dratva, A. Johnsson, M. Nilsson, P. Lonnerberg, and S. Linnarsson. 2021. 'Molecular architecture of the developing mouse brain', *Nature*, 596: 92-96.

Reference

- Leone, D. P., S. Genoud, S. Atanasoski, R. Grausenburger, P. Berger, D. Metzger, W. B. Macklin, P. Chambon, and U. Suter. 2003. 'Tamoxifen-inducible glia-specific Cre mice for somatic mutagenesis in oligodendrocytes and Schwann cells', *Mol Cell Neurosci*, 22: 430-40.
- Lepiemme, F., J. Stoufflet, M. Javier-Torrent, G. Mazzucchelli, C. G. Silva, and L. Nguyen. 2022. 'Oligodendrocyte precursors guide interneuron migration by unidirectional contact repulsion', *Science*, 376: eabn6204.
- Levine, J. M., R. Reynolds, and J. W. Fawcett. 2001. 'The oligodendrocyte precursor cell in health and disease', *Trends Neurosci*, 24: 39-47.
- Lewis, D. A., T. Hashimoto, and D. W. Volk. 2005. 'Cortical inhibitory neurons and schizophrenia', *Nat Rev Neurosci*, 6: 312-24.
- Lin, A. W., D. Siscovick, B. Sternfeld, P. Schreiner, C. E. Lewis, E. T. Wang, S. S. Merkin, M. Wellons, L. Steffen, R. Calderon-Margalit, P. A. Cassano, and M. E. Lujan. 2021. 'Associations of diet, physical activity and polycystic ovary syndrome in the Coronary Artery Risk Development in Young Adults Women's Study', *BMC Public Health*, 21: 35.
- Lin, S. C., and D. E. Bergles. 2004. 'Synaptic signaling between GABAergic interneurons and oligodendrocyte precursor cells in the hippocampus', *Nat Neurosci*, 7: 24-32.
- Luyt, K., T. P. Slade, J. J. Dorward, C. F. Durant, Y. Wu, R. Shigemoto, S. J. Mundell, A. Varadi, and E. Molnar. 2007. 'Developing oligodendrocytes express functional GABA(B) receptors that stimulate cell proliferation and migration', *J Neurochem*, 100: 822-40.
- Maas, D. A., V. D. Eijnsink, M. Spoelder, J. A. van Hulten, P. De Weerd, J. R. Homberg, A. Valles, B. Nait-Oumesmar, and G. J. M. Martens. 2020. 'Interneuron hypomyelination is associated with cognitive inflexibility in a rat model of schizophrenia', *Nat Commun*, 11: 2329.
- Madisen, L., T. A. Zwingman, S. M. Sunkin, S. W. Oh, H. A. Zariwala, H. Gu, L. L. Ng, R. D. Palmiter, M. J. Hawrylycz, A. R. Jones, E. S. Lein, and H. Zeng. 2010. 'A robust and high-throughput Cre reporting and characterization system for the whole mouse brain', *Nat Neurosci*, 13: 133-40.
- Makinodan, M., K. M. Rosen, S. Ito, and G. Corfas. 2012. 'A critical period for social experience-dependent oligodendrocyte maturation and myelination', *Science*, 337: 1357-60.
- Maldonado, P. P., M. Velez-Fort, F. Levavasseur, and M. C. Angulo. 2013. 'Oligodendrocyte precursor cells are accurate sensors of local K⁺ in mature gray matter', *J Neurosci*, 33: 2432-42.
- Mangin, J. M., A. Kunze, R. Chittajallu, and V. Gallo. 2008. 'Satellite NG2 progenitor cells share common glutamatergic inputs with associated interneurons in the mouse dentate gyrus', *J Neurosci*, 28: 7610-23.
- Marisca, R., T. Hoche, E. Agirre, L. J. Hoodless, W. Barkey, F. Auer, G. Castelo-Branco, and T. Czopka. 2020. 'Functionally distinct subgroups of oligodendrocyte precursor cells integrate neural activity and execute myelin formation', *Nat Neurosci*, 23: 363-74.
- Marshall, F. H., K. A. Jones, K. Kaupmann, and B. Bettler. 1999. 'GABAB receptors - the first 7TM heterodimers', *Trends Pharmacol Sci*, 20: 396-9.
- Meldrum, B. 1982. 'Pharmacology of GABA', *Clin Neuropharmacol*, 5: 293-316.
- Mercau, M. E., S. Patwa, K. P. L. Bhat, S. Ghosh, and C. V. Rothlin. 2022. 'Cell death in development, maintenance, and diseases of the nervous system', *Semin Immunopathol*, 44: 725-38.
- Micheva, K. D., D. Wolman, B. D. Mensh, E. Pax, J. Buchanan, S. J. Smith, and D. D. Bock. 2016. 'A large fraction of neocortical myelin ensheathes axons of local inhibitory neurons', *Elife*, 5.
- Middei, S., G. Houeland, V. Cavallucci, M. Ammassari-Teule, M. D'Amelio, and H. Marie. 2013. 'CREB is necessary for synaptic maintenance and learning-induced changes of the AMPA receptor GluA1 subunit', *Hippocampus*, 23: 488-99.
- Minocha, S., D. Valloton, I. Brunet, A. Eichmann, J. P. Hornung, and C. Lebrand. 2015. 'NG2 glia are required for vessel network formation during embryonic development', *Elife*, 4.

Reference

- Miyamae, T., K. Chen, D. A. Lewis, and G. Gonzalez-Burgos. 2017. 'Distinct Physiological Maturation of Parvalbumin-Positive Neuron Subtypes in Mouse Prefrontal Cortex', *J Neurosci*, 37: 4883-902.
- Morley, J. E. 2018. 'An Overview of Cognitive Impairment', *Clin Geriatr Med*, 34: 505-13.
- Nagy, C., M. Maitra, A. Tanti, M. Suderman, J. F. Theroux, M. A. Davoli, K. Perlman, V. Yerko, Y. C. Wang, S. J. Tripathy, P. Pavlidis, N. Mechawar, J. Ragoussis, and G. Turecki. 2020. 'Single-nucleus transcriptomics of the prefrontal cortex in major depressive disorder implicates oligodendrocyte precursor cells and excitatory neurons', *Nat Neurosci*, 23: 771-81.
- Neely, C. L. C., K. A. Pedemonte, K. N. Boggs, and J. M. Flinn. 2019. 'Nest Building Behavior as an Early Indicator of Behavioral Deficits in Mice', *J Vis Exp*.
- Nimmerjahn, A., F. Kirchhoff, and F. Helmchen. 2005. 'Resting microglial cells are highly dynamic surveillants of brain parenchyma in vivo', *Science*, 308: 1314-8.
- Olsen, R. W., and W. Sieghart. 2008. 'International Union of Pharmacology. LXX. Subtypes of gamma-aminobutyric acid(A) receptors: classification on the basis of subunit composition, pharmacology, and function. Update', *Pharmacol Rev*, 60: 243-60.
- Ong, W. Y., and J. M. Levine. 1999. 'A light and electron microscopic study of NG2 chondroitin sulfate proteoglycan-positive oligodendrocyte precursor cells in the normal and kainate-lesioned rat hippocampus', *Neuroscience*, 92: 83-95.
- Orduz, D., N. Benamer, D. Ortolani, E. Coppola, L. Vigier, A. Pierani, and M. C. Angulo. 2019. 'Developmental cell death regulates lineage-related interneuron-oligodendroglia functional clusters and oligodendrocyte homeostasis', *Nat Commun*, 10: 4249.
- Orduz, D., P. P. Maldonado, M. Balia, M. Velez-Fort, V. de Sars, Y. Yanagawa, V. Emiliani, and M. C. Angulo. 2015. 'Interneurons and oligodendrocyte progenitors form a structured synaptic network in the developing neocortex', *Elife*, 4.
- Pais, R., L. Ruano, C. Moreira, O. P. Carvalho, and H. Barros. 2020. 'Prevalence and incidence of cognitive impairment in an elder Portuguese population (65-85 years old)', *BMC Geriatr*, 20: 470.
- Pan-Vazquez, A., W. Wefelmeyer, V. Gonzalez Sabater, G. Neves, and J. Burrone. 2020. 'Activity-Dependent Plasticity of Axo-axonic Synapses at the Axon Initial Segment', *Neuron*, 106: 265-76 e6.
- Pinal, C. S., and A. J. Tobin. 1998. 'Uniqueness and redundancy in GABA production', *Perspect Dev Neurobiol*, 5: 109-18.
- Priya, R., M. F. Paredes, T. Karayannis, N. Yusuf, X. Liu, X. Jaglin, I. Graef, A. Alvarez-Buylla, and G. Fishell. 2018. 'Activity Regulates Cell Death within Cortical Interneurons through a Calcineurin-Dependent Mechanism', *Cell Rep*, 22: 1695-709.
- Pudasaini, S., V. Friedrich, C. Buhner, S. Endesfelder, T. Scheuer, and T. Schmitz. 2022. 'Postnatal myelination of the immature rat cingulum is regulated by GABA(B) receptor activity', *Dev Neurobiol*, 82: 16-28.
- Saab, A. S., I. D. Tzvetavona, A. Trevisiol, S. Baltan, P. Dibaj, K. Kusch, W. Mobius, B. Goetze, H. M. Jahn, W. Huang, H. Steffens, E. D. Schomburg, A. Perez-Samartin, F. Perez-Cerda, D. Bakhtiari, C. Matute, S. Lowel, C. Griesinger, J. Hirrlinger, F. Kirchhoff, and K. A. Nave. 2016. 'Oligodendroglial NMDA Receptors Regulate Glucose Import and Axonal Energy Metabolism', *Neuron*, 91: 119-32.
- Sakry, D., and J. Trotter. 2016. 'The role of the NG2 proteoglycan in OPC and CNS network function', *Brain Res*, 1638: 161-66.
- Saul, M. L., D. L. Helmreich, S. Rehman, and J. L. Fudge. 2015. 'Proliferating cells in the adolescent rat amygdala: Characterization and response to stress', *Neuroscience*, 311: 105-17.
- Scala, F., D. Kobak, S. Shan, Y. Bernaerts, S. Laturnus, C. R. Cadwell, L. Hartmanis, E. Froudarakis, J. R. Castro, Z. H. Tan, S. Papadopoulos, S. S. Patel, R. Sandberg, P. Berens, X. Jiang, and A. S. Tolias. 2019. 'Layer 4 of mouse neocortex differs in cell types and circuit organization between sensory areas', *Nat Commun*, 10: 4174.

Reference

- Seibenhener, M. L., and M. C. Wooten. 2015. 'Use of the Open Field Maze to measure locomotor and anxiety-like behavior in mice', *J Vis Exp*: e52434.
- Seifi, M., N. L. Corteen, J. J. van der Want, F. Metzger, and J. D. Swinny. 2014. 'Localization of NG2 immunoreactive neuroglia cells in the rat locus coeruleus and their plasticity in response to stress', *Front Neuroanat*, 8: 31.
- Seo, J. H., T. Maki, M. Maeda, N. Miyamoto, A. C. Liang, K. Hayakawa, L. D. Pham, F. Suwa, A. Taguchi, T. Matsuyama, M. Ihara, K. W. Kim, E. H. Lo, and K. Arai. 2014. 'Oligodendrocyte precursor cells support blood-brain barrier integrity via TGF- β signaling', *PLoS One*, 9: e103174.
- Serrano-Regal, M. P., L. Bayon-Cordero, J. C. Chara Ventura, B. I. Ochoa-Bueno, V. Tepavcevic, C. Matute, and M. V. Sanchez-Gomez. 2022. 'GABA(B) receptor agonist baclofen promotes central nervous system remyelination', *Glia*, 70: 2426-40.
- Serrano-Regal, M. P., I. Luengas-Escuza, L. Bayon-Cordero, N. Ibarra-Aizpurua, E. Alberdi, A. Perez-Samartin, C. Matute, and M. V. Sanchez-Gomez. 2020. 'Oligodendrocyte Differentiation and Myelination Is Potentiated via GABA(B) Receptor Activation', *Neuroscience*, 439: 163-80.
- Sohal, V. S., and J. L. R. Rubenstein. 2019. 'Excitation-inhibition balance as a framework for investigating mechanisms in neuropsychiatric disorders', *Mol Psychiatry*, 24: 1248-57.
- Sohal, V. S., F. Zhang, O. Yizhar, and K. Deisseroth. 2009. 'Parvalbumin neurons and gamma rhythms enhance cortical circuit performance', *Nature*, 459: 698-702.
- Somogyi, P., and I. Soltesz. 1986. 'Immunogold demonstration of GABA in synaptic terminals of intracellularly recorded, horseradish peroxidase-filled basket cells and clutch cells in the cat's visual cortex', *Neuroscience*, 19: 1051-65.
- Southwell, D. G., M. F. Paredes, R. P. Galvao, D. L. Jones, R. C. Froemke, J. Y. Sebe, C. Alfaro-Cervello, Y. Tang, J. M. Garcia-Verdugo, J. L. Rubenstein, S. C. Baraban, and A. Alvarez-Buylla. 2012. 'Intrinsically determined cell death of developing cortical interneurons', *Nature*, 491: 109-13.
- Soysal, P., L. Smith, M. Trott, P. Alexopoulos, M. Barbagallo, S. G. Tan, A. Koyanagi, S. Shenkin, N. Veronese, Dementia European Society of Geriatric Medicine Special Interest Group in, Reviews Systematic, and Analyses Meta. 2022. 'The Effects of COVID-19 lockdown on neuropsychiatric symptoms in patients with dementia or mild cognitive impairment: A systematic review and meta-analysis', *Psychogeriatrics*, 22: 402-12.
- Spitzer, S. O., S. Sitnikov, Y. Kamen, K. A. Evans, D. Kronenberg-Versteeg, S. Dietmann, O. de Faria, Jr., S. Agathou, and R. T. Karadottir. 2019. 'Oligodendrocyte Progenitor Cells Become Regionally Diverse and Heterogeneous with Age', *Neuron*, 101: 459-71 e5.
- Stedehouder, J., J. J. Couey, D. Brizee, B. Hosseini, J. A. Slotman, C. M. F. Dirven, G. Shpak, A. B. Houtsmuller, and S. A. Kushner. 2017. 'Fast-spiking Parvalbumin Interneurons are Frequently Myelinated in the Cerebral Cortex of Mice and Humans', *Cereb Cortex*, 27: 5001-13.
- Tabata, H. 2015. 'Diverse subtypes of astrocytes and their development during corticogenesis', *Front Neurosci*, 9: 114.
- Tao, X., S. Finkbeiner, D. B. Arnold, A. J. Shaywitz, and M. E. Greenberg. 1998. 'Ca²⁺ influx regulates BDNF transcription by a CREB family transcription factor-dependent mechanism', *Neuron*, 20: 709-26.
- Timmermann, Aline, Ronald Jabs, Anne Boehlen, Catia Domingos, Magdalena Skubal, Wenhui Huang, Frank Kirchhoff, Christian Henneberger, Andras Bilkei-Gorzo, Gerald Seifert, and Christian Steinhäuser. 2021. 'Dysfunction of grey matter NG2 glial cells affects neuronal plasticity and behavior', *bioRxiv*: 2021.08.20.457086.
- Trapp, B. D., A. Nishiyama, D. Cheng, and W. Macklin. 1997. 'Differentiation and death of premyelinating oligodendrocytes in developing rodent brain', *J Cell Biol*, 137: 459-68.
- Tricoire, L., K. A. Pelkey, B. E. Erkkila, B. W. Jeffries, X. Yuan, and C. J. McBain. 2011. 'A blueprint for the spatiotemporal origins of mouse hippocampal interneuron diversity', *J Neurosci*, 31: 10948-70.

-
-
- Tsai, H. H., J. Niu, R. Munji, D. Davalos, J. Chang, H. Zhang, A. C. Tien, C. J. Kuo, J. R. Chan, R. Daneman, and S. P. Fancy. 2016. 'Oligodendrocyte precursors migrate along vasculature in the developing nervous system', *Science*, 351: 379-84.
- Velez-Fort, M., P. P. Maldonado, A. M. Butt, E. Audinat, and M. C. Angulo. 2010. 'Postnatal switch from synaptic to extrasynaptic transmission between interneurons and NG2 cells', *J Neurosci*, 30: 6921-9.
- Velmeshev, D., L. Schirmer, D. Jung, M. Haeussler, Y. Perez, S. Mayer, A. Bhaduri, N. Goyal, D. H. Rowitch, and A. R. Kriegstein. 2019. 'Single-cell genomics identifies cell type-specific molecular changes in autism', *Science*, 364: 685-89.
- Wang, B. S., M. S. Bernardez Sarria, X. An, M. He, N. M. Alam, G. T. Prusky, M. C. Crair, and Z. J. Huang. 2021. 'Retinal and Callosal Activity-Dependent Chandelier Cell Elimination Shapes Binocularity in Primary Visual Cortex', *Neuron*, 109: 502-15 e7.
- Wang, L. P., J. Pan, Y. Li, J. Geng, C. Liu, L. Y. Zhang, P. Zhou, Y. H. Tang, Y. Wang, Z. Zhang, and G. Y. Yang. 2022. 'Oligodendrocyte precursor cell transplantation promotes angiogenesis and remyelination via Wnt', *J Cereb Blood Flow Metab*, 42: 757-70.
- Wong, F. K., K. Bercsenyi, V. Sreenivasan, A. Portales, M. Fernandez-Otero, and O. Marin. 2018. 'Pyramidal cell regulation of interneuron survival sculpts cortical networks', *Nature*, 557: 668-73.
- Zawadzka, M., L. E. Rivers, S. P. Fancy, C. Zhao, R. Tripathi, F. Jamen, K. Young, A. Goncharevich, H. Pohl, M. Rizzi, D. H. Rowitch, N. Kessaris, U. Suter, W. D. Richardson, and R. J. Franklin. 2010. 'CNS-resident glial progenitor/stem cells produce Schwann cells as well as oligodendrocytes during repair of CNS demyelination', *Cell Stem Cell*, 6: 578-90.
- Zhang, Y., K. Chen, S. A. Sloan, M. L. Bennett, A. R. Scholze, S. O'Keeffe, H. P. Phatnani, P. Guarnieri, C. Caneda, N. Ruderisch, S. Deng, S. A. Liddelow, C. Zhang, R. Daneman, T. Maniatis, B. A. Barres, and J. Q. Wu. 2014. 'An RNA-sequencing transcriptome and splicing database of glia, neurons, and vascular cells of the cerebral cortex', *J Neurosci*, 34: 11929-47.
- Zhu, X., R. A. Hill, D. Dietrich, M. Komitova, R. Suzuki, and A. Nishiyama. 2011. 'Age-dependent fate and lineage restriction of single NG2 cells', *Development*, 138: 745-53.
- Zonouzi, M., J. Scafidi, P. Li, B. McEllin, J. Edwards, J. L. Dupree, L. Harvey, D. Sun, C. A. Hubner, S. G. Cull-Candy, M. Farrant, and V. Gallo. 2015. 'GABAergic regulation of cerebellar NG2 cell development is altered in perinatal white matter injury', *Nat Neurosci*, 18: 674-82.

12. ACKNOWLEDGEMENT

This thesis would not have been possible without the support, guidance, and encouragement of many individuals. I would like to express my heartfelt gratitude to all those who have contributed to my academic journey.

First and foremost, I would like to extend my heartfelt appreciation to Prof. Frank Kirchhoff, my mentor, for his support, guidance, and inspiration. Your wisdom, experience, and vision have been a constant source of motivation and inspiration throughout my academic journey.

I am deeply grateful to my supervisor, Dr. XianShu Bai, for providing me with guidance, encouragement, and invaluable feedback throughout the entire research process. Your expertise and support have been instrumental in shaping this thesis into its final form. Your guidance and encouragement have challenged me to grow both personally and professionally, and I am deeply grateful for your mentorship.

I am also indebted to my colleagues. Thanks Dr. Na Zhao for Patching clamp; thanks Dr. Laura Christel Caudal for EEG recording; thanks Dr. Hsin-Fang Chang and Ching-Hsin Lin for primary cell culture; thanks Prof. Carola Meier and Dr. Nadine Hainz for electron microscope; thanks for Prof. Bian for brain organoid teaching and special thanks for Dr. Wenhui Huang and Dr. Anja Scheller, for their support and stimulating discussions. Many thanks to Davide Gobbo, Phillip Rider, Seth Rhea, Buttigieg Emeline, Frank Rhode, Daniel Schauenburg, Erika Meyer, Mariza Bortolanza, Naielly Rodrigues da Silva, Ting Zhang, Nana-Oye Awuku and Paula Gelonch-Capell, your insights, critiques, and enthusiasm have been invaluable in sharpening my ideas and pushing me to think more deeply about my research. Your friendship and encouragement have made my academic journey more fulfilling and enjoyable.

To my friends, Qilin Guo, Qing Liu, and Paula Gelonch-Capell, thank you for your unwavering support, encouragement, and understanding during this demanding period of my life. Your presence has helped me keep my sanity and balance my academic pursuits with my personal life. Your unwavering belief in me has been a constant source of motivation, and I am deeply grateful for your friendship.

Finally, to my family and my girlfriend, thank you for your love, encouragement, and unwavering support. Your sacrifices and support have made it possible for me to pursue my academic dreams, and I am forever grateful for your unwavering belief in me. Your support has been the foundation of my academic journey, and I am blessed to have you in my life.

In conclusion, I would like to express my heartfelt gratitude to all those who have supported and encouraged me throughout this journey. Your unwavering belief in me has been the driving force behind my success, and I am deeply grateful for your support. This thesis represents the culmination of years of hard work, dedication, and support, and I am honored to share this achievement with you all.

13. CURRICULUM VITAE AND LIST OF PUBLICATIONS

The curriculum vitae was removed from the electronic version of the doctoral thesis for reasons of data protection.

Oral presentations (International)

1. Impaired bidirectional communication between interneurons and oligodendrocyte precursor cells affects cognitive behavior. 4th DAAD-CAPES workshop. Campinas, Brazil (2022)
2. Impaired bidirectional communication between interneurons and oligodendrocyte precursor cells affects cognitive behavior. International Astrocyte School. Bertinoro, Italy (2021)

Poster presentations (first author)

1. **Fang** et al., 2022. Oligodendrocyte precursor cells shape inhibition in medial prefrontal cortex. 3rd FALAN Congress. Belem, Brazil.
2. **Fang** et al., 2021. Impaired bidirectional communication between interneurons and oligodendrocyte precursor cells affects cognitive behavior. 15th EuroGlia Meeting. Marseille, France.
3. **Fang** et al., 2023. OPCs shape the medial prefrontal cortical inhibition by regulating interneuron apoptosis and myelination employing GABA_B receptor. 15th Göttingen Meeting of the German Neuroscience Society

Others

1. 15th Opel Haerberlen Halbmarathon Füssen, Germany, 01:52:52 h, 21.09 km
2. 11th RAGhartfüssler Trail 2022, Saarbrücken, Germany, 01:11:05 h, 14 km
3. Ruprecht Trail 2022, Niederlosheim, Germany, 03:20:30, 29,5 km
4. 2023 Schneider Electric Marathon de Paris, France, 03:49:10 h, 42.195 km

Publications (<https://orcid.org/0000-0002-7973-9523>)

1. **Fang LP**, Zhao N, Caudal LC, Chang HF, Zhao R, Lin CH, Hainz N, Meier C, Bettler B, Huang W, Scheller A, Kirchhoff F, Bai X. (2022). Impaired bidirectional communication between interneurons and oligodendrocyte precursor cells affects social cognitive behavior. **Nat Commun** 13 (1):1394. **Selected as editor's highlights in 'From brain to behavior' section.**
2. **Fang LP**, Liu Q, Meyer E, Huang W, Scheller A, Kirchhoff F*, Bai X. (2023). A subset of OPCs do not express Olig2 during development which can be increased in the adult by brain injuries and complex motor learning. **Glia**. 71(2):415-430
3. **Fang LP**, Bai X. (2023). Implications of Olig2 silencing in oligodendrocyte precursor cells. **Neural Regen Res**.18 (12):p 2649-2650.
4. **Fang LP**, Bai X. (2023). Oligodendrocyte precursor cells: Multitasker in brain function. **Pflügers Arch** (Invited review, in press).
5. Bai X, Zhao N, **Fang LP**, Caudal LC, Zhao R, Hirrlinger J, Walz W, Bian S, Huang W, Kirchhoff F, Scheller A. (2023). In the mouse cortex, oligodendrocytes regain a plastic capacity, transforming into astrocytes after acute injury. **Dev Cell** S1534-5807(23)00192-2.
6. Liu Q, Guo Q, **Fang LP**, Yao H, Scheller A, Kirchhoff F, Huang W. (2023). Specific detection and deletion of the sigma-1 receptor widely expressed in neurons and glial cells in vivo. **J Neurochem** 164: 764-785.
7. Chen A, Guo Z, **Fang L**, Bian S. (2020). Application of Fused Organoid Models to Study Human Brain Development and Neural Disorders. **Frontiers in Cellular Neuroscience**. 15;14:133.
8. Zhu JW, Zou MM, Li YF, Chen WJ, Liu JC, Chen H, **Fang LP**, Zhang Y, Wang ZT, Chen JB, Huang W, Li S, Jia WQ, Wang QQ, Zhen XC, Liu CF, Li S, Xiao ZC, Xu GQ, Schwamborn JC, Schachner M, Ma QH, Xu RX. (2020). Absence of Tripartite Motif Protein 32 Leads to Autism-like Behaviors in Mice via enhancing mTOR-mediated Macroautophagy. **Cerebral cortex**;14;30(5):3240-3258.
9. Lu MH, Ji WL, Xu DE, Yao PP, Zhao XY, Wang ZT, **Fang LP**, Huang R, Lan LJ, Chen JB, Wang TH, Cheng LH, Xu RX, Liu CF, Puglielli L, Ma QH. (2019). Inhibition of sphingomyelin synthase 1 ameliorates alzheimer-like pathology in APP/PS1 transgenic mice through promoting lysosomal degradation of BACE1. **Experimental Neurology** 311, 67-79
10. Wang ZT, Lu MH, Zhang Y, Ji WL, Lei L, Wang W, **Fang LP**, Wang LW, Yu F, Wang J, Li ZY, Wang JR, Wang TH, Dou F, Wang QW, Wang XL, Li S, Ma QH, Xu RX. (2018). Disrupted-in-schizophrenia-1 protects synaptic plasticity in a transgenic mouse model of Alzheimer's disease as a mitophagy receptor. **Aging Cell** 18 e12860
11. Yan Q, **Fang L**, Wei J, Xiao G, Lv M, Ma Q, Liu C, Wang W. (2017). Silicon nanowires enhanced proliferation and neuronal differentiation of neural stem cell with vertically surface microenvironment. **Journal of Biomaterials Science**, Polymer Edition 28, 1394-1407.